TIME AND RATE DEPENDENT EXTENSIONS TO THE PROGRESSIVELY FRACTURING SOLIDS THEORY

A thesis submitted to the

University of London

for

the degree

of

Doctor of Philosophy

and

Diploma of Imperial College

by

Hatem Khodr Abdih

University of London, Imperial College, 1990

ABSTRACT

The work presented reviews the theory of the progressively fracturing solid which describes the behaviour of an ideal material that fractures in a stable fashion with consequential stiffness loss.

In order to develop the original theory, physical models have been used by previous researchers. These models simulate the response of a progressively fracturing solid to loading. The adoption of these models enables tests to be performed computationally rather than physically. Similar models are used in the present work. Several tests on a "network model", a planar frame of pin–jointed bar elements having different lengths and material properties, are performed. Computer analysis allows the model to be tested under various loading conditions of controlled deformations, temperature, lack of fit,..., or a combination of these. Results of these tests are discussed and compared qualitatively to those of physical materials.

In order to extend the theory into the time domain, additional assumptions on the material behaviour were required. These assumptions are discussed, and a general multi–dimensional continuum theory is developed to describe the behaviour of an ideal time–dependent progressively fracturing solid.

Both a "network model" and a "fibre bundle model", a system of parallel elastic fibres having different strengths, are used to describe the behaviour of solids that exhibit time–dependent fracture. Computer programs are used to describe the response of the models to loading under various strain rates and to conditions of constant stress and strain. Stability under such conditions is considered.

Results of the tests illustrate the models' potential in describing aspects of material behaviour related to time, history, and rate dependence.

ACKNOWLEDGEMENT

I am very grateful to Dr John Dougill, my supervisor, for his continuous help, support, and encouragement. I wish also to thank Dr C.J. Burgoyne of Cambridge University and Professor J. Burland of Imperial College for their guidance and help during the course of my research. I wish to acknowledge the Advisory Staff of the computer centre at Imperial College for their assistance and their efficient service.

My thanks are due to my father and the committees of the Overseas Research Students Awards and the University of London Studentships for their financial support without which this research would have never been undertaken.

I extend my thanks to Alcina Tatsis and Mrs. M.J. Treadaway , at Imperial College, for their help which contributed to the final production of this book.

I wish also to thank my friends, namely Carla, Emilia, Shawki, Reza, and Ziad for their inspiring friendship and love which have contributed much to this thesis.

Finally, I am indebted to my parents, my brothers, and my wife Raida, who helped me type this thesis, for their support and patience.

TABLE OF CONTENTS

LIST OF FIGURES

CHAPTER I

INTRODUCTION

1–1 Introduction

The response of materials to applied forces and displacements is of prime concern to engineers. An understanding of the mechanical behaviour of engineering materials under loads is necessary if structures are to be analysed properly and designed safely and economically.

Several approaches have been used to describe the behaviour of materials such as concrete and rocks. On one hand, development of particular rules of material behaviour based on experimental results of testing under specified conditions has been found to be extremely useful. This empirical approach is practical but lacks generality. In particular, there is no basis for the application of such rules to circumstances other than those covered by the original tests. On the other hand, general theories that describe the behaviour of materials under various loading conditions are sought. These theories describe the behaviour of ideal rather than real physical materials. The behaviour of an ideal material follows from a set of initially assumed postulates, rendering the analysis of the behaviour analytically possible. The applicability of such theories to physical materials is dependent on how closely the ideal material resembles a real one. The more general the theory is, the more complex it becomes.

The recent advances in numerical and computational techniques have made analysis using complicated theories possible.

These two extremes in approaches do not exclude each other. When a test is performed, it is useful to know the basic laws of mechanics governing material behaviour so that the experimental setup and data analysis are done properly with a minimum number of variables. Also, in choosing the postulates to define the behaviour of an ideal material, knowledge of actual material behaviour is essential. Moreover, the application of a general theory to real problems requires assigning numerical values to some parameters. This can only be achieved by the quantitative comparison to experimental results.

1–2 Aims and scope of the work

The aim of the work presented in this thesis is to explore further the behaviour of a class of ideal materials termed progressively fracturing solids. Upon loading such a solid, its stiffness is reduced due to stable progressive fracture. The solid is always in a linear elastic state in the sense that, upon unloading, the stress and strain are linearly related with a constant stiffness, the value of which depends on the extent of damage inflicted on the solid prior to unloading. This progressively fracturing solid has the property that it may always be returned to a state of zero stress and zero strain upon unloading. A theory for the time–independent behaviour of this class of materials was originally developed by Dougill [1–6].

There is no real physical material that behaves exactly like the ideal progressively fracturing solid described above. Similarly, there is no physical material that behaves exactly like any other ideal solid described by alternative continuum theories. Nevertheless, an ideal progressively fracturing solid exhibits some modes of behaviour that are common in engineering materials such as rocks, concrete, and overconsolidated clays.

Cracks induced in concrete–like solids upon loading result in degradation of material stiffness. Strain softening is observed in these materials under strain controlled testing. Thus, the above theory can be (and has been) used alone or in conjunction with other theories (such as plasticity theories) to describe a more general behaviour of concrete–like materials.

Materials such as concrete and rocks are time–dependent and also are affected by internal stressing due to thermal and other induced deformations. This, therefore, provides the motivation to attempt to extend the theory of the progressively fracturing solids to include a description of time and rate dependence and to study the behaviour of such solids under conditions of internally induced stresses.

Accordingly, the aims of the work were to

(i) explore further the behaviour of a time–independent progressively fracturing solid,

(ii) develop a general multi–dimensional time–dependent progressively fracturing solids theory that describes the behaviour of a class of ideal solids,

(iii) study the response to loading of some ideal model materials that fail progressively under loads,

(iv) and study the scope of application of such theory by a qualitative comparison with the behaviour of real materials.

Further work is done in this thesis on the time–independent progressively fracturing solids theory to study the behaviour of such solids under a variety of loading. The behaviour of such a solid under loading conditions other than controlled deformations, which was studied by earlier researchers, is looked upon.

Attention is then focused on the exploration of the behaviour of such a solid when time induced damage is superimposed on fracture inflicted by loading. An extension of the above theory to include the time domain is sought. This general theory reduces to the already established time–independent theory under certain loading conditions.

The theory, together with the results of tests performed on model materials, will present a basic step towards a more profound understanding of the behaviour of an ideal progressively fracturing solid. Thus, more complex situations of physical materials' behaviour, incorporating both progressive fracture and load history dependence, can be analysed and simulated by the use of this theory in conjunction with other established theories.

1–3 Contents of the thesis

This section describes briefly the contents of the remaining chapters of the thesis.

Chapter II describes the time–independent behaviour of concrete and rock–like materials under loading as observed from experimentally controlled tests. A review of some aspects of concrete behaviour in response to loading is presented.

An explanation of some modes of behaviour that concrete–like materials exhibit, which cannot normally be explained by the traditional theories, is presented from the fracture and damage mechanics points of view.

This chapter also includes a literature review of the theoretical and experimental work that has lead to the formulation of the time–independent progressively fracturing solids theory. A summary of the theory is then presented.

In order to develop this theory, ideal model materials, the behaviour of which describes the response to loading of a progressively fracturing solid, have been used earlier. Some of these models are discussed in this chapter and a general approach to their analysis is mentioned.

In chapter III attention is focused on the rate and load history sensitivity of concrete–like materials and the effects of such variables on their behaviour. Some experimental results showing the behaviour under varying strain rates is presented. Also a description of concrete behaviour under creep and relaxation experimental tests is given.

A summary of some of the theoretical work done in simulating concrete behaviour with regard to strain rate sensitivity is presented. This is followed by a review of some theories that incorporate viscosity to provide time–dependent behaviour under loading conditions such as creep and relaxation.

In chapter IV the effects of progressive degradation are studied using a structural model comprising discrete brittle elements. A "network model" is introduced and is tested under various loading conditions of controlled deformations simulating uniaxial tensile tests, controlled deformations with an initial lack of fit, increasing temperature or equivalently increasing the lack of fit, and controlled deformations on initially damaged networks. Tests demonstrating

the path dependence of the network model are also presented.

Results from an analytical study of fibrous systems (elastic fibres in series or in parallel) under increasing temperature are discussed in conjunction with those obtained for the network model.

A theoretical development of a time–dependent progressively fracturing solids theory is presented in chapter V. The basic requirements behind this theory, as well as the time–independent simplification, are the convexity of the fracture surface defined in strain space and the normality of the defined fracture stress decrement to this fracture surface. These two criteria are discussed in detail and found to be valid for the model if certain assumptions are followed.

Based on the normality and convexity criteria, a general multi–dimensional time–dependent theory is devised and then simplified to give a revised model suitable for analysis.

The remaining chapters are dedicated to study the behaviour of some model materials that exhibit time–dependent progressive fracture. The effects of time–dependent degradation are studied using the "network model" (extended to incorporate time effects). Tests on a continuum time–dependent fracturing model, termed the "fibre bundle model", are also performed. The results of these tests are discussed and compared qualitatively to those of physical materials.

Refinements to the theory and its applications, so that the behaviour attained becomes more realistic, are discussed. Possible linkage of the theory to already existing theories is discussed so that a more general description of material behaviour becomes possible.

CHAPTER II

TIME–INDEPENDENT PROGRESSIVELY FRACTURING SOLIDS

2–1 The mechanical behaviour of some engineering materials

Until comparatively recently, strain softening and material degradation were excluded from theoretical models of material behaviour. Accordingly, additional theories were necessary to deal with a class of materials exhibiting these phenomena. This group of materials includes concrete, rocks, over–consolidated clays, and some fibre composites. These materials exhibit strain softening under strain controlled testing conditions. Deformation of such solids is accompanied by the formation and grouping of cracks resulting in the reduction of stiffness. They have the ability to undergo large deformations without total failure and can sustain relatively large strains at a fraction of their maximum attainable stress.

Progressive failure is observed in carbon/epoxy laminates [7]. Failure of a layer does not necessarily result in the complete failure of the entire laminate. Upon loading, cracks occur in different plies. This results in the reduction of the stiffness of individual plies, the overall laminate stiffness, and in progressive failure accompanied by softening of the stress–strain response of the laminate [7,8].

Under imposed deformations, rocks tend to crack. Initially, cracks are of a small scale. With increasing imposed deformations, larger cracks are formed. This process results in progressive failure of rocks with consequential strain softening and loss of stiffness. Figure 2.1(a,b) depicts the above modes of behaviour in granite [9]. Similar results were observed for other types of rocks. Tests on sandstone [10], basalt, and cemented fill [11], show similar mechanical behaviour.

Strain softening is observed in some clays. These clays tend to sustain large strains at stress levels below the peak stress after this peak stress is attained. It was argued [12] that this behaviour is the result of progressive failure of bonds between clay particles. As over–consolidated clays are strained, they build up an increasing resistance up to a certain limit. Beyond this limit there is a decrease in the resistance with increasing strain. This mode of strain softening eventually reaches a level of residual strength which is maintained by the clay. Fissured or jointed clays have potential points of stress concentration. Strength

at an imperfection is normally low. Thus if the peak strength is reached at a certain point in the clay, consequential loss of strength is observed. This in turn passes the stress to other points which in turn may soften, resulting in progressive failure down to a residual stress value. Tests on samples of Kaolin clay have shown strain softening behaviour [13] (figure 2.2(a)). Recent tests [14] showed that sand in direct shear exhibits reduction of strength in the post peak portion of it stress–strain curve (figure 2.2(b)). Interesting results have been obtained from delicate testing on some lunar sand [15]. Figure 2.3 shows some of these results. Similar modes of softening behaviour on other types of clays were also observed [16,17].

Stable direct tensile tests performed on concrete have shown that strain softening occurs [18]. This phenomenon has also been detected for concrete and microconcrete tested in controlled compression [18]. Results of tensile testing on concrete [19] (figure 2.4 – 2.5) show the post peak strain softening behaviour and the subsequent reduction of the elasticity modulus with deformation. Concrete was found to undergo large deformations without total failure at stress levels lower than the maximum stress. Progressive damage was observed in concrete in uniaxial compression tests [20,21]. Specimens were subjected to a series of cycles of loading and unloading (increasing and decreasing strains) and were found to fail progressively with strain softening and the resulting decrease of unloading moduli (figure 2.6). Progressive reduction in the initial elastic moduli (tangents to the loading portions of loading–unloading cycles), with increasing the maximum applied strain, was reported. Reduction of these moduli varies considerably in the region of the stress strain curve following the peak stress, but is always apparent in all regions of the curve (figure 2.6).

Interesting tests have been performed to examine the post peak cyclic behaviour of concrete in uniaxial tensile conditions [22]. Figure 2.7 depicts the results of these tests showing the post peak behaviour of concrete following monotonic tensile loading, cyclic tensile loading and alternating loading. The progressive post–peak failure of concrete and the reduction of its stiffness with increasing applied maximum stress are observed. Similar results were obtained recently [23] from tests performed on concrete, mortar, and cement paste, in direct tension. Strain softening and stiffness loss were also apparent for cement paste and mortar under uniaxial compression as well as for steel fibre reinforced concrete [24,25].

It should be noted that the above mentioned modes of behaviour are localized. Figure 2.8 shows the load of deflection curves of samples of concrete

specimens with waisted profiles tested in uniaxial tension [26]. It shows an initial linear behaviour up to peak stress followed by a sharp decrease of stress as a result of softening with a highly localized response. Deformations on one surface of the specimen were measured to give displacement contours which in turn are interpreted to give local strains. The results in figure 2.9, with contours of direct strain in the direction of the applied load, show the regions of high strain intensity.

At early stages of loading, several regions of high strain intensity may be detected showing that damage is of a contained distributed nature. At later stages, damage becomes localized and these regions cluster in a narrow band. This results in the occurrence of all deformations in this band with the rest of the specimen being unloaded. This localization was initiated even before the peak stress was attained.

2–2 Modelling of some engineering materials

In this section attention is turned to some material models that have been developed and used for the simulation of the behaviour of concrete–like materials.

Continuum theories, describing the behaviour of some ideal materials, have been used in modelling the response of real materials by averaging microscopic quantities over a representative volume with macroscopic dimensions. In other words, homogenization of a heterogeneous solid is an essential feature of any continuum description.

Elastic models describe the material behaviour by assuming that the work done upon loading depends only on the initial and final states of the material. In its simplest form, linear elasticity, stress and strain are related by a constant modulus.

The theory of elasticity describes deformations that are path independent and fully recoverable. This behaviour may apply to concrete and rocks at low strains but not near failure.

Idealizations of material behaviour, based on plasticity assumptions have been used. Materials are assumed to achieve irrecoverable time–independent strains at a constant or increasing stress (perfect or hardening plasticity). The material is thus path dependent and can be described by relations between increments of stress and strain (incremental theories). Alternatively, in flow theories, total stress and strain are used during loading with linear elastic unloading.

Both elasticity and plasticity based theories are generally inadequate in describing softening behaviour observed in some engineering materials. Recent work has been directed towards a revision of some of the basic concepts of plasticity, originally developed for metals, so that applicability to soils, rocks, granular earth materials, and concrete becomes possible.

Incremental elasto–plastic relations, in which changing elastic moduli with plastic deformations are allowed for, were studied [27]. By adopting a stability criteria other than that of Drucker [28] and assuming, according to Hill [29], that the second order work performed along any proportional path is non–negative for all strain increments, possibilities of the existence and

uniqueness of strain softening emerge. This continuum model [27] was based on the following assumptions:

(a) The plastic strain rate vector has a direction different from the outward normal to the yield surface in the stress space, and is related to the plastic dilatancy.

(b) The elastic moduli, followed upon unloading, change as plastic deformations develop. Irreversible strains include those due to moduli changes.

(c) The yield surface has the ability to expand, contract, or remain unaltered upon an increment of stress causing yield. This allows the model to cater for hardening, softening, or perfect plasticity.

The traditional formulation of plasticity theories employs yield surfaces in stress space, in conjunction with loading criteria which involve the increments of stress. Il'ushin [30,31] suggested the use of strain space. This is valid for the full range of elastic–plastic deformations (in particular perfectly plastic behaviour, and strain softening).

Casey and Naghdi [32], used both strain and stress spaces together. The yield surface in strain space, defined as the states of strain that will initiate yield for given values of plastic strains and hardening parameters, always moves outward during loading. On the other hand, the yield surface in stress space, defined as the states of stress corresponding to strain states that will initiate yield for given fixed values of plastic strains and hardening parameters, may be moving outwards, inwards, or may be stationary as a result of the material exhibiting hardening, softening, or perfectly plastic behaviour. These three types of behaviour may thus be defined by a dimensionless quotient of derivatives deduced from the loading functions in both spaces. This quotient measures the ratio of the outward velocities with which the yield surfaces in the two spaces move during loading.

Reference [33] presents a review of soil and rock modelling based on the concept of plasticity and its variations.

From the continuum mechanics point of view, one particularly important feature of strain softening is that of instability [34–37]. Bazant [34] argues that strain softening in a continuum causes instability. In a real physical material, small strain softening regions, whose size is greater than a lower limit

dictated by the material itself, absorb strain energy stored in the material structure. Ductility is thus determined from stability conditions by introducing the effects of size, heterogeneity, and stored energy into the stability analysis. If these are taken into account, then instability or failure on the strain softening branch of the stress–strain curve occurs only when the downward slope reaches a certain critical value. Stability in the strain softening portion of the stress strain curve is further increased by using stiff elastic rods in parallel with test specimens and by taking into account the reduction of the unloading stiffness modulus with increasing deformations [34,35]. Stress–displacement rather than stress–strain analysis of a continuum with size effects taken into account was found to be more plausible [37]. This is similar to the analysis of crack growth in the material rather than defining a region of high strains. In addition to the mechanical stability criteria normally used, similar arguments follow if thermodynamic stability is studied in conjunction with mechanical stability [38].

Damage theories have been used to describe fracture in engineering materials. Two different approaches are normally followed. In the first one, fracture is based on the growth and propagation of a single crack (Griffith's theory), thus there is the disadvantage of initially having to assume the existence of a crack. Energy put into the material during crack growth is considered to be partly stored as strain energy and partly absorbed to cause crack propagation [40].

Alternatively, damage may be considered to be distributed over a volume of the material and thus can be measured by some internal variables that affect the response to loading (Kachanov [41]). A limited review of some of these theories can be found in reference [42]. This idea of uniformly distributed damage over a volume of the material allows the definition of an effective cross–sectional area, A_e, for a damaged material [41]. This area is equal to the original area, A_o, for an undamaged state of the material and reduces with increasing damage. Assuming that at complete failure A_e becomes zero, then a damage variable D can be defined to measure this load bearing area (or the increase in the relative void area or crack intensity) such that

$$\begin{aligned} &D = 0 \text{ for } A_e = A_o \\ &\qquad \text{and} \qquad\qquad (2.2.1) \\ &D = 1 \text{ for } A_e = 0 \end{aligned}$$

This approach suggests the definition of a pseudo stress or effective stress [41,43]. This stress is associated with the effective area determined by the distribution of

cracks over a volume of the material. The actual stress of the material can be determined from the effective stress by assuming a damage evolution law incorporating the damage variable D [41,43,44].

Krajcinovic [42,45–47] presented a general theory for the description of damaging materials. According to this theory, these solids will exhibit damage when loaded, but remain unchanged (in the sense of internal damage variables) upon unloading. Total free energy for the solid is considered to be a scalar function of a damage vector as well as the strain tensor. Through this energy function stress increments will result for a change of strain, damage, or both. The damage is described as a function of a void density vector, which in turn is defined by means of a damage law defining a surface in strain space which divides states of strain between those that will and will not cause damage. A very similar model is given in [48].

Theories based on the assumption of uniformly distributed damage have the disadvantage of excluding any description of localization observed in real material fracture. On the other hand, their formulation does not require the initial assumption of the existence of a crack.

For heterogeneous materials, fracture may be considered as a general process because the material may contain cracks, or even potential fracture sites, that propagate at different rates. At high levels of imposed deformations, fracture becomes contained in localized zones. The disadvantage of having to assume the existence and/or distribution of cracks, in fracture and damage based theories, motivates the attempt to describe materials as a continuum. In a continuum approach, constitutive relations are described at a point or a volume small enough to be taken as a point. Thus the detailed structure of the material and any discontinuities in the displacement field, over that volume, can be ignored. This concept lies behind the formulation of all continuum theories. The theory of progressively fracturing solids follows this continuum approach and is presented in the next section.

2–3 The theory of progressively fracturing solids

Strain softening may be assumed to be a result of progressive fracture, accompanied by stiffness degradation, at a point in a continuum. The behaviour of a material volume, comprising progressively fracturing material points, will contain, under loads, failure points (or failure sites) that are distributed or localized in a small region. Failure at a point is considered to occur when the stiffness, at that point, degrades completely to zero. A failed point or group of points resembles a crack in a real material.

The idea of considering an ideal heterogeneous model material that fails progressively originated from work done on mathematical modelling for the failure of cement paste and mortar (Dougill [49,50]). The work was based on an assumed distribution of the micro–stress components. The manner in which failure occurs is by progressive propagation of fracture or yield at the microscopic level. Some statistical rules of stress redistribution at the microscopic scale were used. Stability of the behaviour was found to be dependent on the energy required to fracture the material after the peak stress. Fracture propagation occurs in a more stable fashion for higher values of this energy.

Later, some physical tests on concrete [20,21] proved to be highly supportive of the idea that softening behaviour in concrete is accompanied by a degradation of stiffness (also observed in other tests, section 2.1). Spooner and Dougill [21] focused their concern on energy considerations during compressive loading of concrete. They observed that during first loading on concrete, damage is initiated and energy is released by fracture. During unloading and reloading fracture process ceases and no damage is inflicted but energy is still released due to damping process. This suggested the use of the variation of the components of energy, released in first loading, with strain as a measure of damage.

In what follows the theory of progressively fracturing solids is described. Details of how it was developed and implemented can be found in references [1–6].

The ideal material, described by this theory, loses its stiffness due to stable progressive fracture during loading. The value of the stiffness, during unloading and reloading, is dependent on the extent of fracture prior to unloading. This means that, if the sense of deformation is reversed, the material behaves in a linear elastic manner. The material, thus, has the property of always being unstressed when its original dimensions are recovered. Stress and strain are

considered to be averages taken for a representative volume which corresponds to a point in a continuum. The mechanism of fracture and its resultant discontinuities are ignored, since description of the behaviour is assumed to apply at a point.

Keeping in mind the above assumptions on the ideal material behaviour, the stress tensor σ_{ij} and the strain tensor ϵ_{ij} can at any time be related using a generalized Hooke's law

$$\sigma_{ij} = S_{ijkm}\,\epsilon_{km} \qquad (2.3.1)$$

where S_{ijkm} is a symmetric tensor representing the current stiffness moduli of the material.

During progressive fracture these moduli change so that

$$d\sigma_{ij} = S_{ijkm}\,d\epsilon_{km} + dS_{ijkm}\,\epsilon_{km} \qquad (2.3.2)$$

represents the increment of stress for a change in strain, $d\epsilon_{ij}$, and/or stiffness, dS_{ijkm}.

This allows the definition of an elastic component of the stress increment and a fracture component, $d\sigma'_{ij}$ and $d\sigma''_{ij}$ respectively (figure 2.10). Thus

$$d\sigma'_{ij} = S_{ijkm}\,d\epsilon_{km} \qquad (2.3.3)$$

and

$$d\sigma''_{ij} = dS_{ijkm}\,\epsilon_{km} \qquad (2.3.4)$$

so that (2.3.2) becomes

$$d\sigma_{ij} = d\sigma'_{ij} + d\sigma''_{ij} \qquad (2.3.5)$$

The fracture component of the stress increment is absent during unloading or reloading.

To distinguish between the different modes of behaviour some loading criteria are needed. Deformation paths in strain space are used to describe deformation sequences. The existence of a "fracture surface" is postulated. This surface in strain space contains all strain states that can be obtained through a purely elastic deformation path without changing the stiffness of the material and consequently the fracture surface itself. The fracture surface is in analogy to the yield surface used in hardening plasticity theories.

The surface is assumed to be regular and of the form

$$F(\epsilon_{ij}, H_k) = 0 \qquad (2.3.6)$$

where H_k is a vector of k parameters describing the history of progressive fracture. H_k remains unchanged during elastic unloading or reloading. The sign of the loading function F is chosen so that

$$\frac{\partial F}{\partial H_k} dH_k < 0 \qquad (2.3.7)$$

during progressive failure. Naturally

$$\frac{\partial F}{\partial H_k} dH_k = 0 \qquad (2.3.8)$$

during elastic behaviour. Noting that dF is given by

$$dF = \frac{\partial F}{\partial \epsilon_{ij}} d\epsilon_{ij} + \frac{\partial F}{\partial H_k} dH_k \qquad (2.3.9)$$

and taking F to be negative for strain states within the fracture surface, the loading criteria become

(a) $F=0$ and $\frac{\partial F}{\partial \epsilon_{ij}} d\epsilon_{ij} > 0$ during progressive fracture

(b) $F=0$ and $\frac{\partial F}{\partial \epsilon_{ij}} d\epsilon_{ij} = 0$ during neutral loading

(c) $F \leq 0$ and $\frac{\partial F}{\partial \epsilon_{ij}} d\epsilon_{ij} < 0$ during elastic unloading

(d) $F<0$ and $\frac{\partial F}{\partial \epsilon_{ij}} d\epsilon_{ij} > 0$ during elastic reloading

(2.3.10)

The loading conditions (2.3.10) allow the fracture stress increment to be expressed as

$$d\sigma''_{ij} = g_{ij} \frac{\partial F}{\partial \epsilon_{km}} d\epsilon_{km} \qquad (2.3.11)$$

with g_{ij} being a symmetric tensor.

The material is further restricted to conform with Il'ushin's [31] postulate of plasticity that the total work done during the application and removal of a small increment of deformation should be non–negative.

Il'ushin's postulate requires that

$$-\frac{1}{2} d\sigma''_{ij} d\epsilon_{ij} \geq 0 \qquad (2.3.12)$$

the left hand side being the work done upon the application and removal of a

strain increment (figure 2.10). Substituting 2.3.11 into 2.3.12 gives

$$-g_{ij}\, d\epsilon_{ij} \frac{\partial F}{\partial \epsilon_{km}} d\epsilon_{km} \geq 0 \qquad (2.3.13)$$

Noting that $\frac{\partial F}{\partial \epsilon_{km}} \epsilon_{km}$ is positive during progressive fracture, the quantity $(-g_{ij}\, d\epsilon_{ij})$ should also be always non–negative. Hence,

$$-g_{ij}\, d\epsilon_{ij} \geq 0 \qquad (2.3.14)$$

If the material is further considered to be linear in the small, so that g_{ij} is independent of $d\epsilon_{ij}$, then 2.3.14 can be satisfied for any choice of $d\epsilon_{ij}$ if and only if g_{ij} lies on the inward normal to the fracture surface. Thus

$$g_{ij} = -K \frac{\partial F}{\partial \epsilon_{ij}} \qquad (2.3.15)$$

and the flow rule (2.3.11) becomes

$$d\sigma''_{ij} = -K \frac{\partial F}{\partial \epsilon_{ij}} \frac{\partial F}{\partial \epsilon_{km}} d\epsilon_{km} \qquad (2.3.16)$$

where K is a positive function which may depend on strain and strain history but not on the current strain increment.

To calculate the scalar K we consider the energy dissipated per unit volume, D, during loading

$$D = \int_0^{\epsilon_{ij}} \sigma_{ij}\, d\epsilon_{ij} - \frac{1}{2} \sigma_{ij}\, \epsilon_{ij} \qquad (2.3.17)$$

The differential form of D, representing the rate of energy dissipated per unit volume, becomes

$$dD = \frac{1}{2} (\sigma_{ij}\, d\epsilon_{ij} - d\sigma_{ij}\, \epsilon_{ij}) \qquad (2.3.18)$$

The above, together with 2.3.1–2.3.5, will give

$$dD = -\frac{1}{2} d\sigma''_{ij}\, \epsilon_{ij} \qquad (2.3.19)$$

During progressive fracture $dF = 0$ so that

$$\frac{\partial F}{\partial \epsilon_{ij}} d\epsilon_{ij} + \frac{\partial F}{\partial H_k} dH_k = 0 \qquad (2.3.20)$$

Multiplying both sides of the flow rule (2.3.16) by ϵ_{ij} we get

$$d\sigma''_{ij}\,\epsilon_{ij} = -K\,\frac{\partial F}{\partial \epsilon_{ij}}\,\epsilon_{ij}\,\frac{\partial F}{\partial \epsilon_{km}}\,d\epsilon_{km} \tag{2.3.21}$$

Equations 2.3.19–2.3.21 give

$$K = -\frac{2\,dD}{\dfrac{\partial F}{\partial \epsilon_{ij}}\,\epsilon_{ij}\;\dfrac{\partial F}{\partial H_k}\,dH_k} \tag{2.3.22}$$

The flow rule (2.3.16) may be rewritten as

$$d\sigma''_{ij} = -K\,\frac{\dfrac{\partial F}{\partial \epsilon_{ij}}\,\dfrac{\partial F}{\partial \epsilon_{km}}\,\dfrac{\partial F}{\partial \epsilon_{rs}}\,d\epsilon_{rs}}{\dfrac{\partial F}{\partial \epsilon_{pq}}\,\epsilon_{pq}}\,\epsilon_{km} \tag{2.3.23}$$

so that the change in the elastic moduli becomes

$$dS_{ijkm} = -K\,\frac{\dfrac{\partial F}{\partial \epsilon_{ij}}\,\dfrac{\partial F}{\partial \epsilon_{km}}}{\dfrac{\partial F}{\partial \epsilon_{pq}}\,\epsilon_{pq}}\,\frac{\partial F}{\partial \epsilon_{rs}}\,d\epsilon_{rs} + R_{ijkm} \tag{2.3.24}$$

where the tensor R_{ijkm} must be symmetric and

$$R_{ijkm}\,\epsilon_{km} = 0 \tag{2.3.25}$$

Further restrictions on the material are needed to find the components of R_{ijkm}. Examples of these restrictions are given in the papers referenced in the beginning of this section. The simplest of these is taking R_{ijkm} to be zero which satisfies 2.3.25 for all ϵ_{km}. If the material is considered to be path independent in the small in the sense that the change in stiffness caused by the increment of strain is independent of the path used in applying the increment [2], then

$$R_{ijkm} = -\left(K\,\frac{\partial^2 F}{\partial \epsilon_{ij}\,\partial \epsilon_{km}} + \frac{\partial F}{\partial \epsilon_{ij}}\,\frac{\partial K}{\partial \epsilon_{km}}\right)\frac{\partial F}{\partial \epsilon_{rs}}\,d\epsilon_{rs} \tag{2.3.26}$$

The flow rule (2.3.23) together with the expression for the elastic moduli (2.3.24) are enough to describe the material behaviour as given by the constitutive law (2.3.2) and governed by the loading criteria (2.3.10).

2–4 Application to a linear loading function – The fibre bundle model

The theory presented in the previous section has been adopted [31] to describe the behaviour of a two–dimensional physical model consisting of fibre bundles assembled together. Within each bundle an individual fibre is assumed to be elastic/brittle. It breaks under tension only when its axial strain reaches its limiting tensile strain f_t. These limiting strains are continuously distributed between zero and infinity within a bundle.

It is noted that for a bundle at an angle θ ($0 \leq \theta \leq \pi$) with the '1' axis, the axial strain is the same for all fibres and, if shear strain is neglected, is given by

$$\epsilon = \epsilon_{11} \cos^2\theta + \epsilon_{22} \sin^2\theta \qquad (2.4.1)$$

Equation 2.4.1 can be rewritten as

$$\epsilon = \lambda_{ij} \epsilon_{ij} \qquad (2.4.2)$$

with

$$\lambda_{11} = \cos^2\theta ,$$
$$\lambda_{22} = \sin^2\theta ,$$
$$\lambda_{12} = \lambda_{21} = \sin\theta \cos\theta ,$$
$$\text{and } \epsilon_{12} = \epsilon_{21} = 0 \qquad (2.4.3)$$

A parameter h is defined to be equal to the current limiting strain value f_t, where all fibres with limiting strains less than f_t have been broken. It measures the history of fracture within the bundle.

The fracture surface in strain space (figure 2.11) is thus a straight line given by

$$F = \lambda_{ij} \epsilon_{ij} - h = 0 \qquad (2.4.4)$$

where h(D) is a function of damage in the bundle.

The fracture lines for all fibres lie parallel to each other and the current fracture surface for the bundle is the line of the last fibre broken thus defined by (2.4.4).

A loading path in strain space will result in fibres breaking and will thus move the fracture surface outwards resulting in progressive fracture (path OP in figure 2.11(a)). Unloading does not alter the current fracture surface; no

fibres break, and behaviour is linear elastic (path PQ in figure 2.11(a)).

2–5 Understanding progressive fracture by the use of the network model

A discrete simple model [3] was devised and found to exhibit the properties of progressive breakdown and softening in a stable manner similar to that observed in real materials and that described by the continuum theory presented in section 2–3.

The model, termed the "network model", is a plane pin–jointed frame that is produced in the memory of the computer in a random but reproducible manner. The members of the frame are taken to be linear elastic and brittle with the failure stress and stiffness of each member allocated to give independent normal distributions of these quantities. Means and standard deviations are specified and the distributions are truncated so that only positive values are assigned.

The failure of a member results in its stiffness being reduced to zero and thus the overall stiffness matrix of the model is modified.

With increasing deformations, defined by prescribed boundary displacements, the model exhibits progressive loss in stiffness and demonstrates the effects of heterogeneity. As a result, stable strain softening is possible and the model retains its linear elastic behaviour upon unloading which results in a stress free network at the initial strain free state.

The model has the advantages of reproducibility, ease of analysis, and the vast range of information that can be extracted from it at any stage of deformation. Truly identical specimens can be tested under various conditions. The structure of the material and its properties can be examined at any stage.

Tests done on the network model help to extend the range of behaviour described, and thus refinements of the continuum model and increasing its range of applicability become possible.

(a) Load–Deflection curve for Charcoal granite

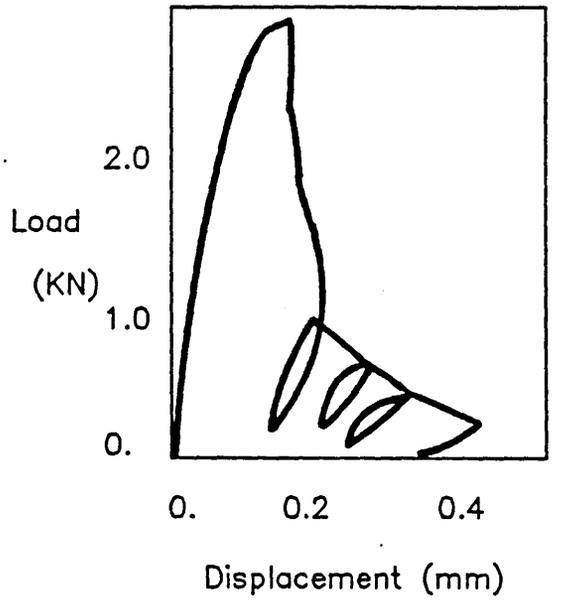

(b) Load–Deflection curve for Rockville granite

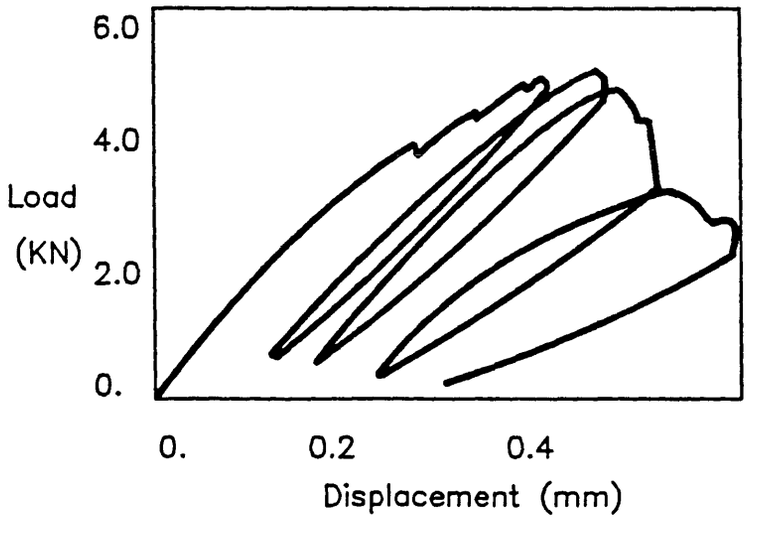

Fig. 2.1 Load–deflection curves for rock [9]

(a) Stress–Strain responses for Kaolin clay [13]

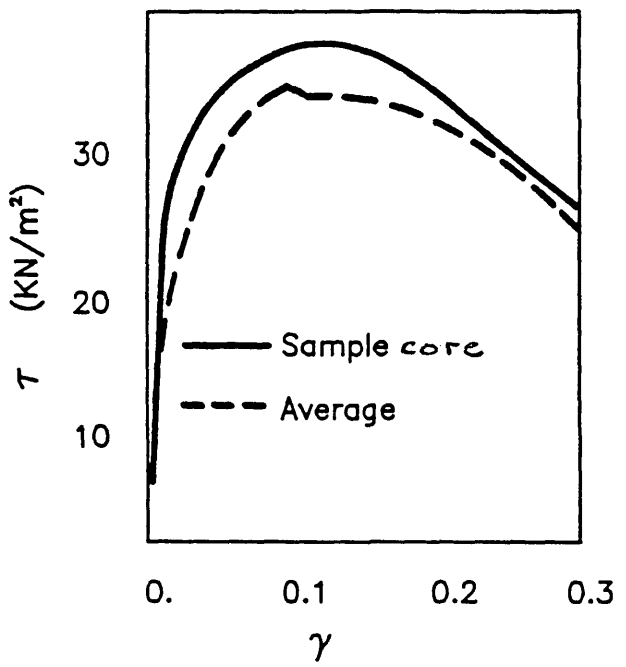

(b) Results of direct shear tests on sand with extensible and very stiff reinforcement at an angle with the shear plane [14]

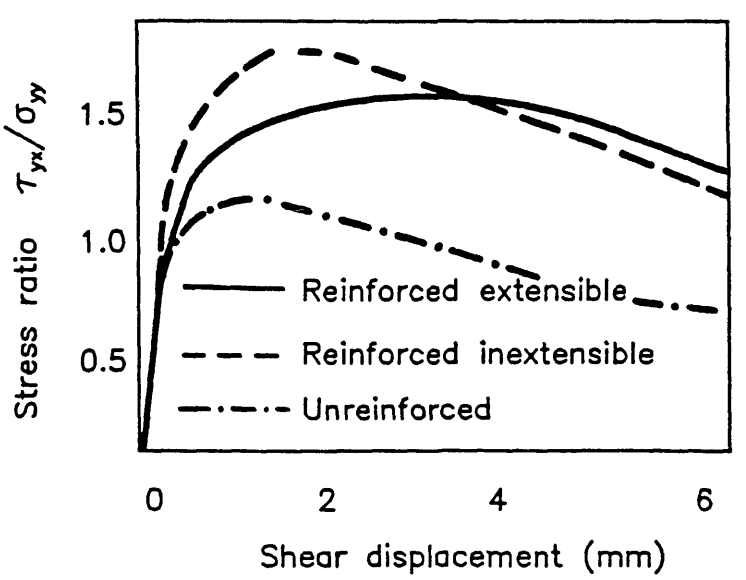

Fig. 2.2 Behaviour of clays and sand under applied deformations

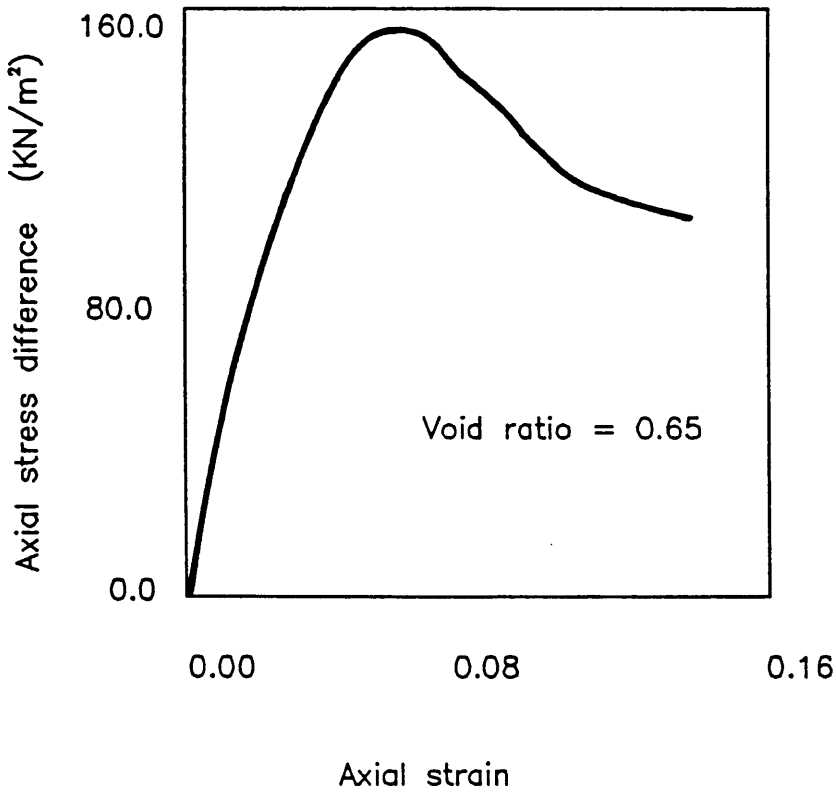

Fig. 2.3 Test results on lunar soil : confining pressure of 26 KN/m² [15]

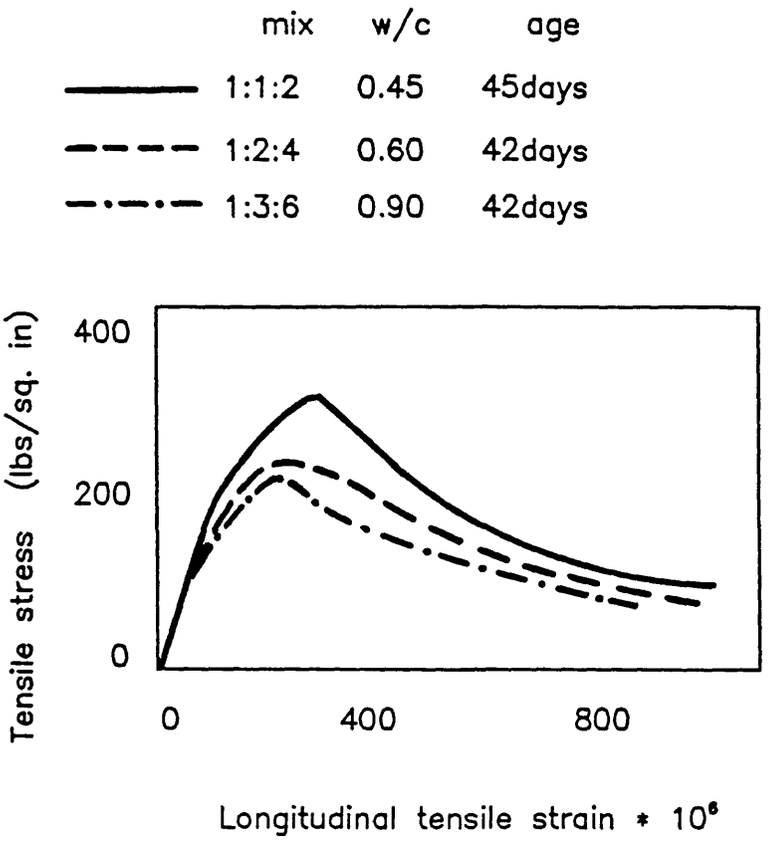

Fig. 2.4 Complete stress strain curves in direct tension for concrete [19]

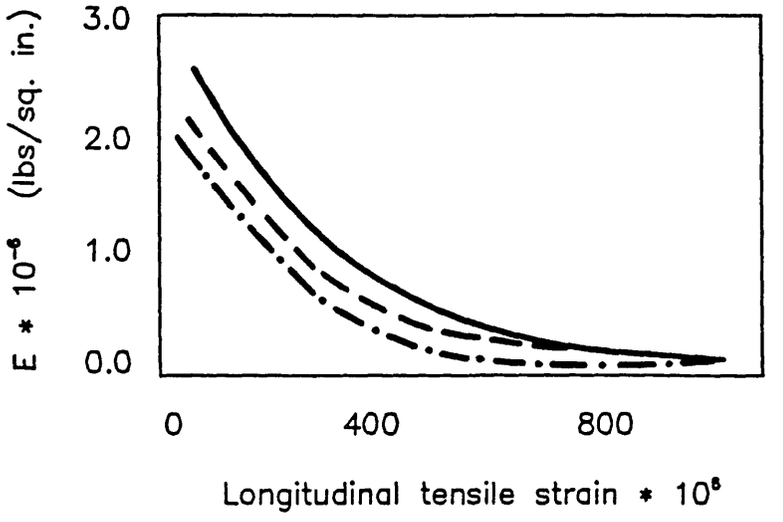

Fig. 2.5 Variation of E with strain for concrete [19]

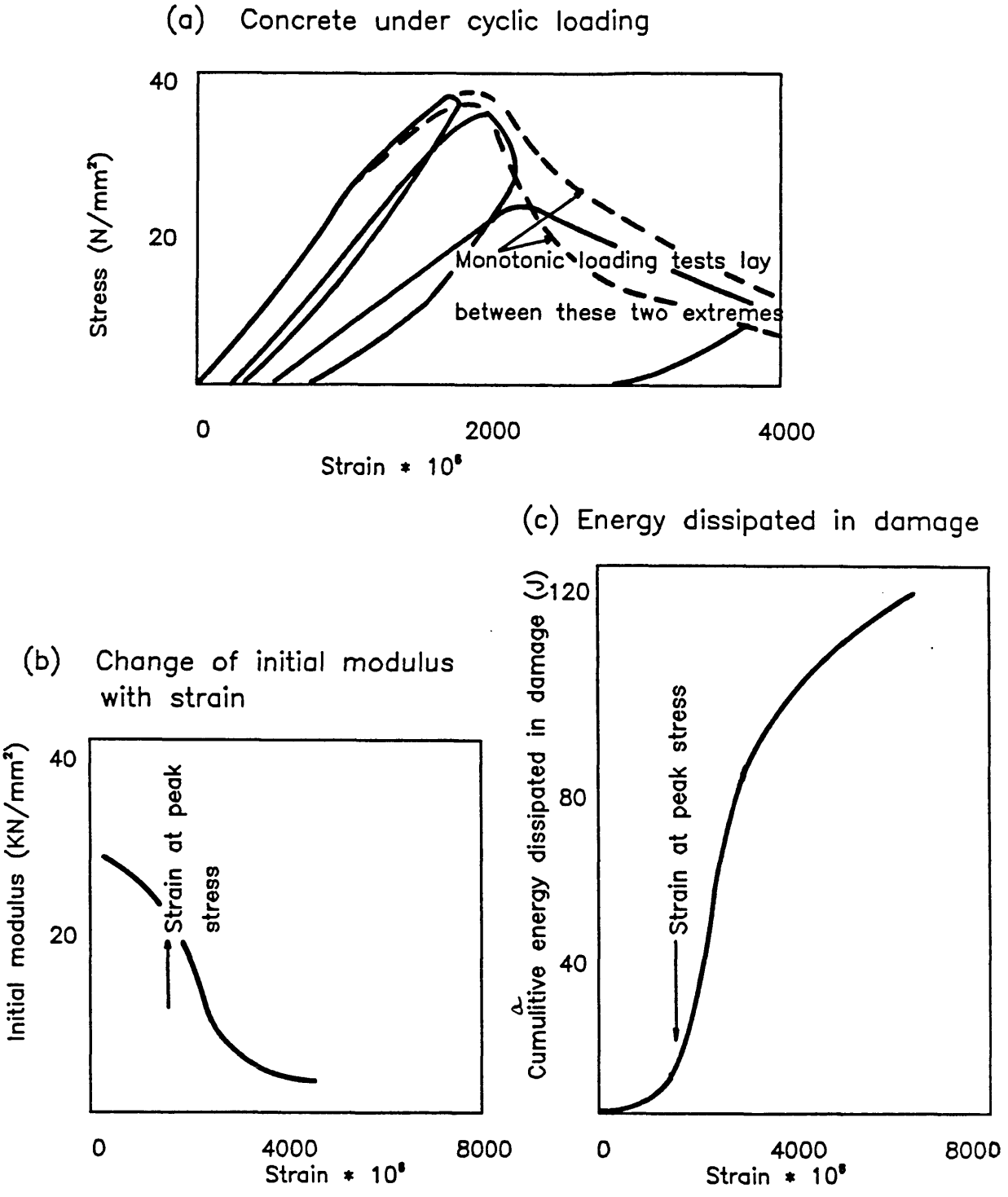

Fig. 2.6 Concrete under strain controlled tests [20] [21]

(a) Stress–Deformation curve at constant rate of deformation

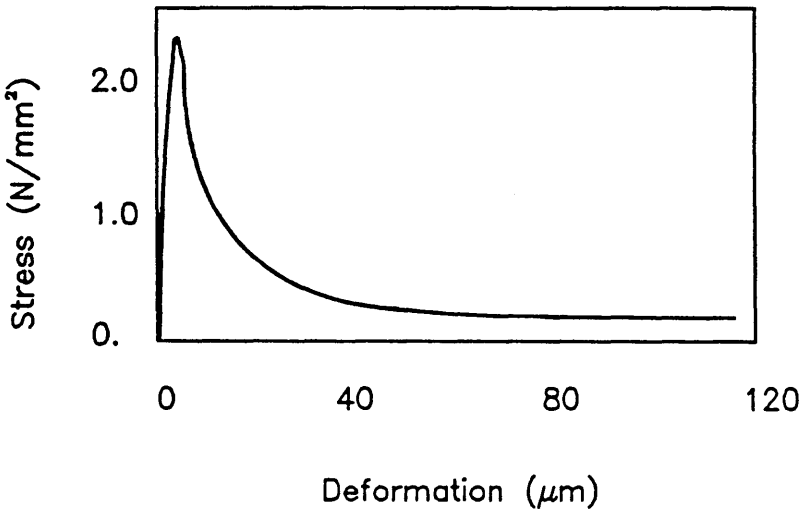

(b) Stress–Deformation curve under cyclic tensile loading

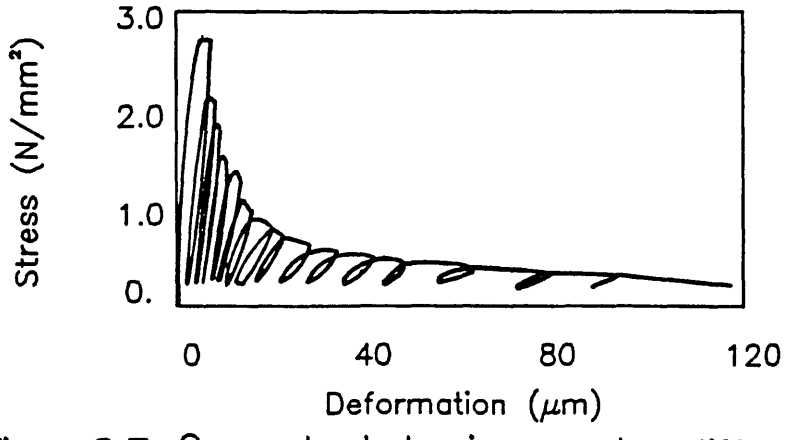

Fig. 2.7 Concrete behaviour under different strain histories [22]

(c) Stress–Deformation curve under alternating loading (small compressive stress)

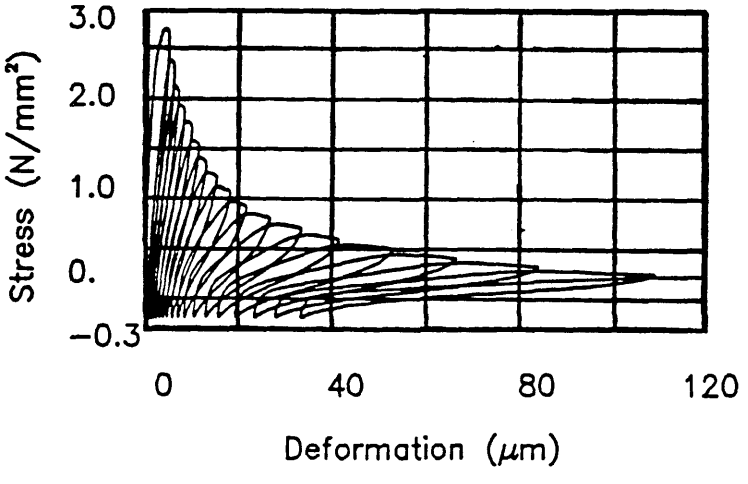

(d) Stress–Deformation curve under alternating loading (large compressive stress)

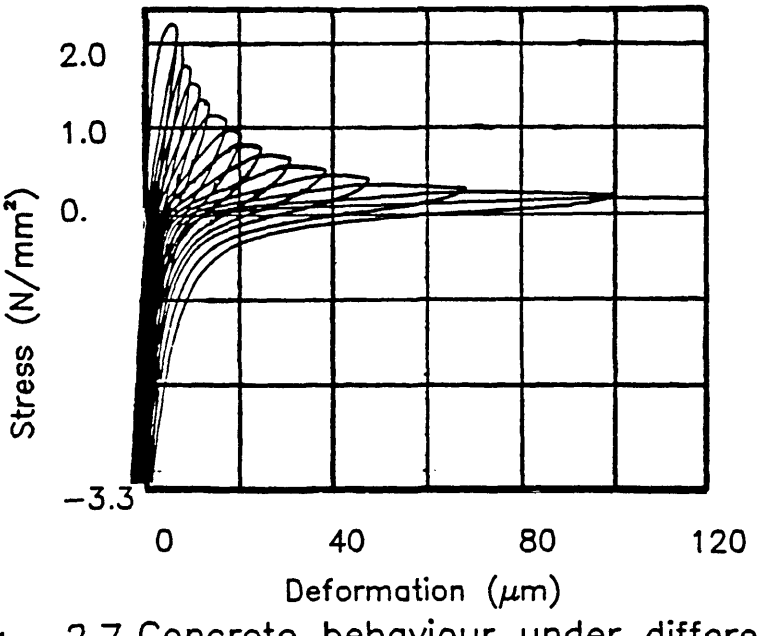

Fig. 2.7 Concrete behaviour under different strain histories (cont'd) [22]

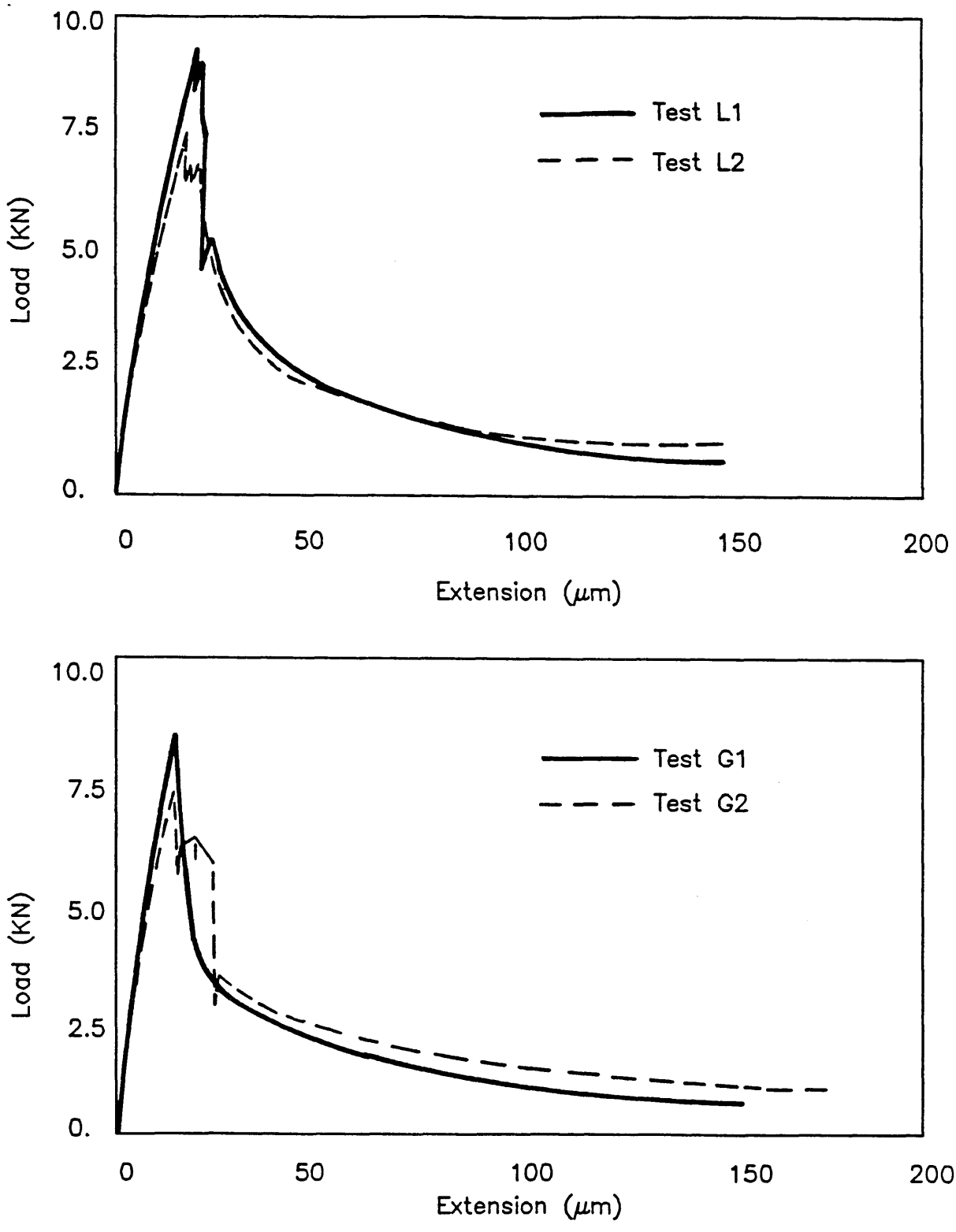

Fig. 2.8 Load–Extension curves for waisted concrete specimens [26]

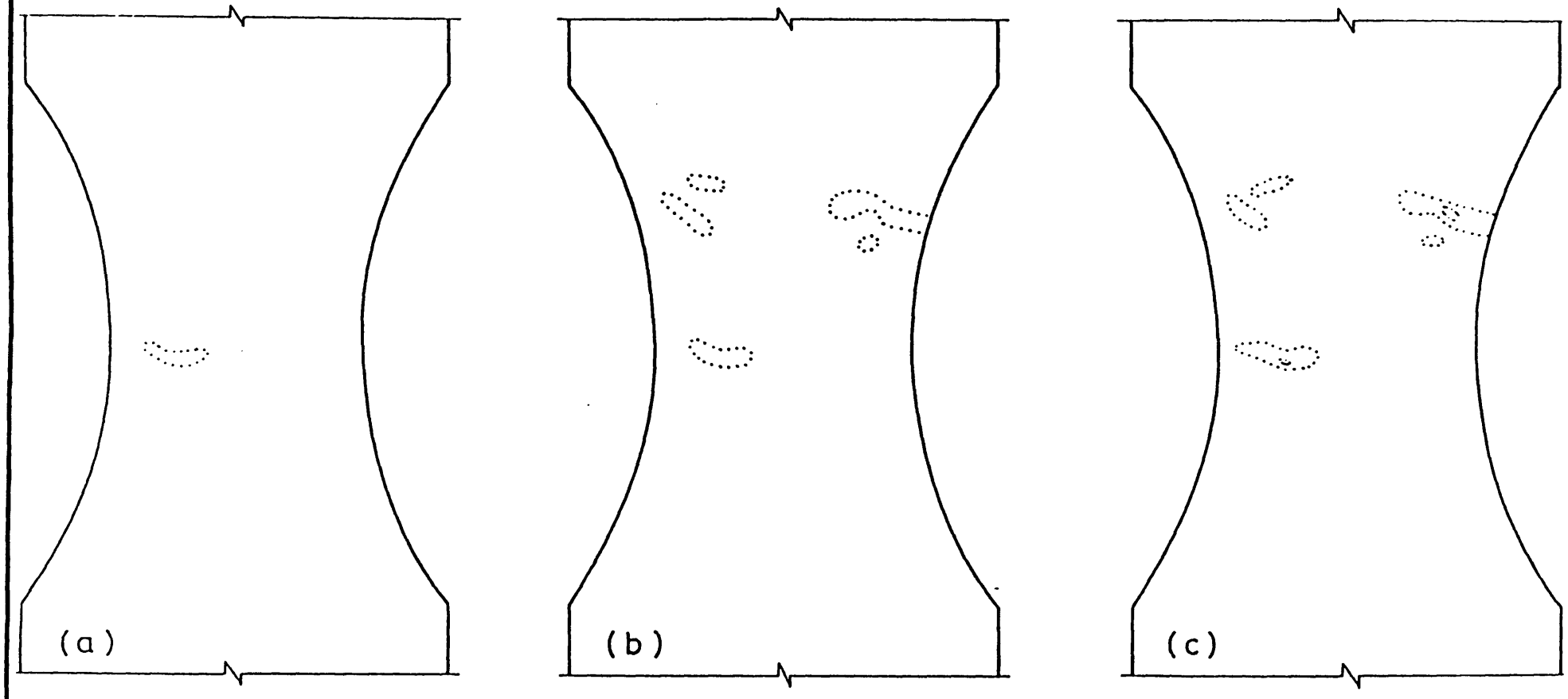

Fig. 2.9 Development of localisation zones before achievment of peak stress –sample L2 [26]

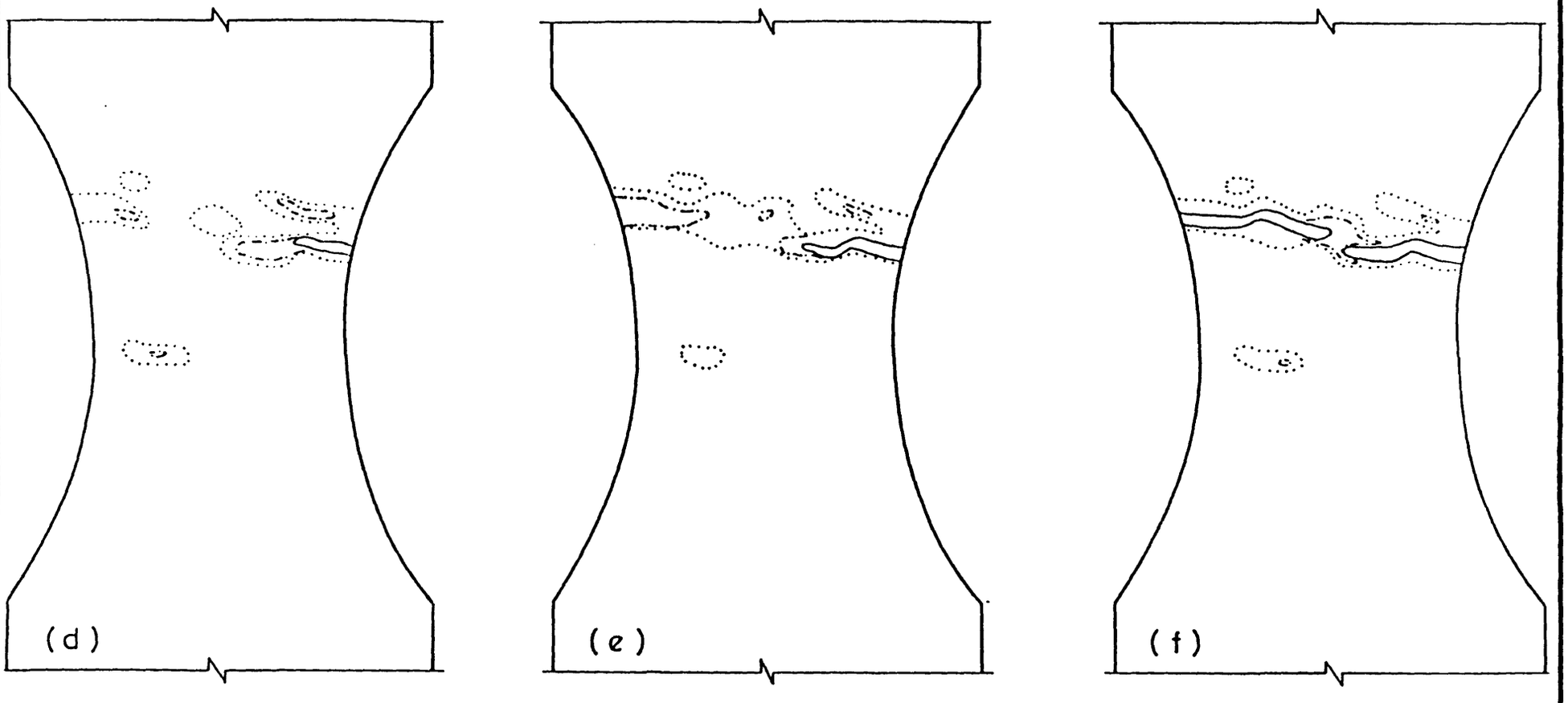

Fig. 2.9(cont'd)Development of localisation zones in the post peak region –sample L2 [26]

(a) Typical stress strain curve for the progressively fracturing solid

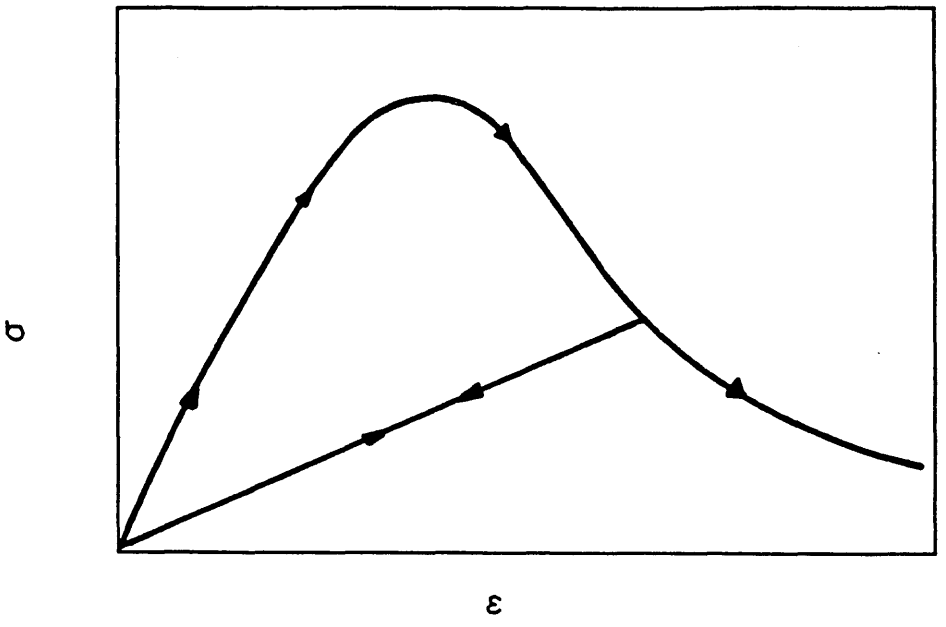

(b) Components of the stress increment tensor

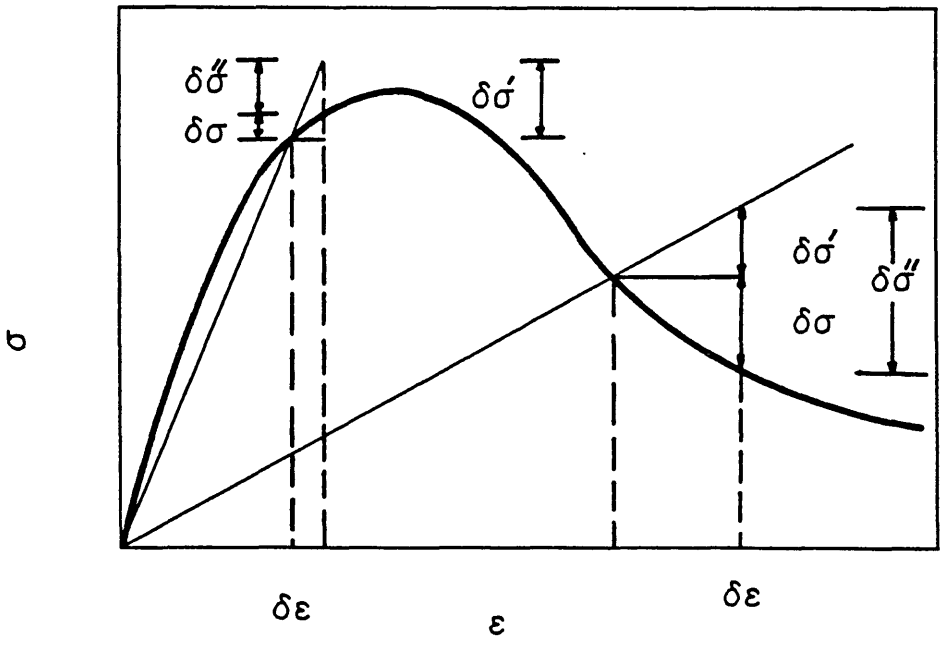

Fig. 2.10 Behaviour of an ideal progressively fracturing solid

(a) Current fracture surface for a typical fibre bundle

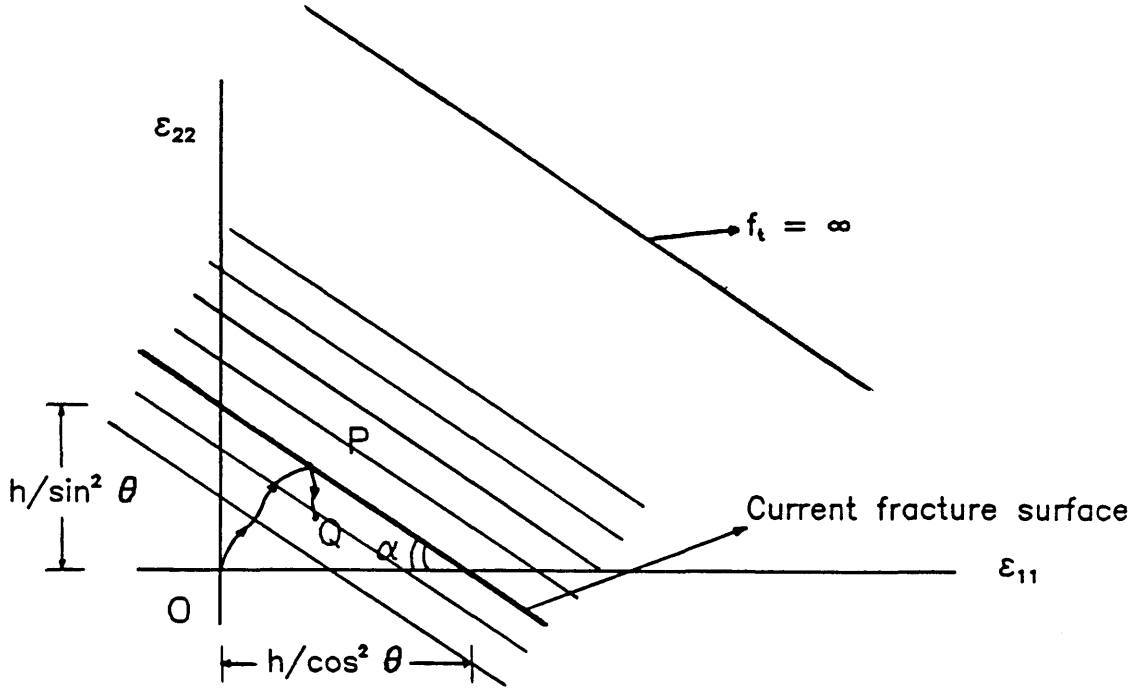

(b) A typical linear loading surface in strain space

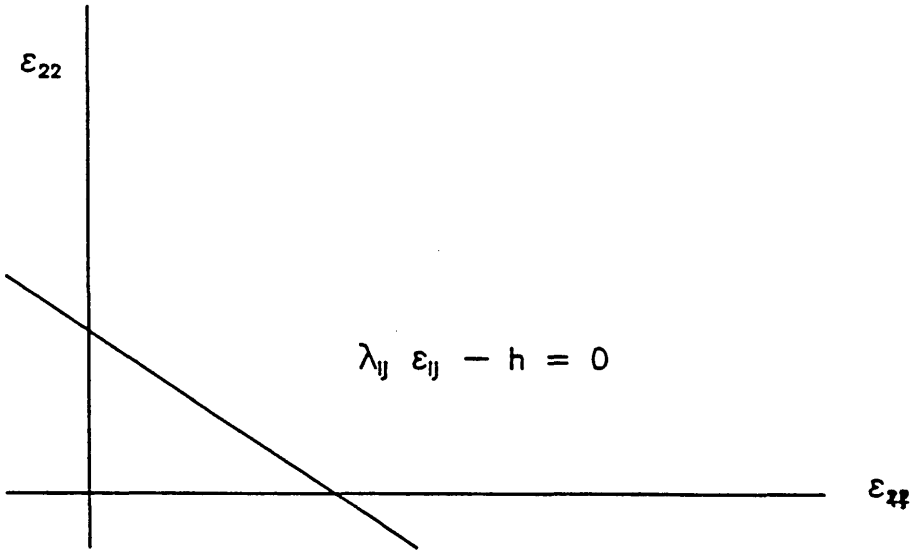

Fig. 2.11 Fracture surfaces of a fibre bundle using linear loading functions

CHAPTER III

TIME–DEPENDENT MATERIAL BEHAVIOUR AND RELEVANT THEORETICAL MODELLING

3–1 Introduction

Almost all engineering materials used in structures are significantly stronger and some are stiffer when strained or loaded at high rates than when tested at normal working rates or subjected to long duration loads in service. This response should be taken into account while interpreting results of high rate testing and when analysing data obtained under such conditions. Similar considerations apply when attempting to predict the response of rate sensitive materials.

Care should be taken when analysing material behaviour at very high rates of loading from some external structural effects that are introduced into the response at these levels of rates. For example, inertia forces become significant at very high rates of deformations and, although these should normally be considered as forces applied to the material, they can have a great influence on the material's response.

The response of some of these materials is not only dependent on the rate of application of the load but also on the history of loading. In other words, the material response, at a particular time, is determined by the complete time history of loading up to that instant of time. Even when applied loads are removed or kept unchanged the time–dependent characteristics of the material will enforce a response in a manner dependent on all prior loading. For example, engineering materials will normally deform or creep at a constant load and relax at a constant deformation. These phenomena are time–dependent and their prediction can only be achieved if the time–dependent characteristics of the materials are taken into account.

There will be situations when the rate sensitivity and time–dependence might result into undesirable effects in the response of engineering structural materials. Engineering design, whether based on empirical or theoretical approaches, should thus be capable of taking these modes of behaviour into consideration.

3–2 Sensitivity of concrete to rate of loading

In this section the effects of the rate of loading or straining on the response of concrete are investigated, and the resulting changes in the material properties (ultimate strength, stiffness, strain at peak stress,...) are discussed. Care should be taken when comparing quantitatively results of different tests because of the variations in the quality of concretes used, moisture content, age at test, size, shape, confinement conditions, techniques used to load the specimens, methods of data analysis and interpretations, assumed reference rates (static rates), etc.

When tested under uniaxial tensile conditions, concrete behaves as a stronger and stiffer material if the rate of loading is increased [52–54]. Figure 3.1 depicts results of experiments on the tensile strength related to the loading rate. When stress reaches its maximum value, higher values of strain are normally observed under rapid testing conditions than the corresponding values resulting from static tests (figure 3.2). A stress–strain curve of plain concrete subjected to high loading rates (30 $N/mm^2/ms$) is compared to that at a static rate (10^{-4} $N/mm^2/ms$) (figure 3.3). This diagram shows the increase of concrete resistance, as measured by its stiffness, with increasing loading rate. The secant modulus, and less clearly the initial tangent modulus, are found to increase with increasing loading rates. Figure 3.3 suggests that under direct tensile loading, more energy is required to fracture the material at higher loading rates than under quasi static conditions. This energy can be assessed by measuring the area contained within the stress strain curve.

In some recent tests [55], it was possible to obtain the post peak region of the stress–displacement curves under impact loading (figure 3.4). These results confirm that the energy absorbed up to total failure is larger for higher strain rates.

It has also been observed [56] that similar increases in strength due to high rates of loading occur for concrete subjected to uniaxial tension and for concrete subjected to the same conditions with additional lateral compression. This suggests that the rate effects determined in uniaxial tests will also be found under various multiaxial loading conditions.

Besides rate dependence observed under tensile loading, the behaviour of concrete is also rate dependent under uniaxial compressive loading.

A significant increase in the ultimate compressive strength of concrete will occur as the strain rate increases above the level of normal static loading [57–65]. Figure 3.5 depicts the increase in the ultimate strength of concrete with increasing applied strain rate. No attempt is made here to study the factors that affect strain rate sensitivity and a detailed investigation can be found elsewhere [65]. Most of the tests were intended to determine the load capacity of concrete at high rates of loading, but other properties can be deduced and measured especially if stress– strain curves are available. Figures 3.6–3.9 give some stress–strain curves obtained by different researchers.

Stiffness of concrete and its resistance to cracking, as measured by the secant modulus up to a predefined compressive strain level, show definite enhancement with increasing strain rate [58,61,63–65,69,70]. It is still, though, uncertain whether the initial tangent modulus is actually rate dependent. It is difficult normally to identify any significant changes in the initial tangent modulus because of the irregularity of the stress–strain curves at early stages of high rates loading. Researchers have reported that the initial tangent modulus either increases [58,61,67] or remains unchanged [63–65,70] with increasing strain rates.

Strain at ultimate strength is another area where conflicting results have been obtained. With an increase in the loading rate, tests have shown an increase [58,59,63,65,70] or a decrease [61,64,69] in the ultimate compressive strain corresponding to the peak stress.

The energy absorption capacity of concrete increases with increasing loading rate [58,65,71]. This energy can be measured by calculating the area under the stress–strain curve up to the peak stress (or sometimes up to complete failure). Figure 3.10 shows a comparison of static energy absorption with impact response for two concrete mixes [65].

Similar strain rate sensitivity have been observed in mortar and microconcrete [53] (figure 3.11), fibre reinforced mortar [71,72], and for confined concrete [63,64,70,73] where the confinement, in the form of steel stirrups, simulates uniform lateral pressure and stabilizes the post peak behaviour at static and impact loading (figure 3.12). Flexural response in mortar and concrete also showed similar rate dependence [71].

Reference [66] reviews some properties of engineering materials, including concrete, at high rates of straining or loading. Materials like steel,

aluminum, brick, glass, plastics, wood and concrete were all found to be rate–sensitive although not much data is available on high rates of loading on some of them.

When tested under increasing rates of deformation, rocks are found to exhibit changes in their material properties similar to those detected for concrete. Sandstone exhibits an increase in the compressive strength and the modulus of elasticity with a decrease in strain at peak stress (figure 3.13) [74]. Increasing the strain rate results in decreased stability of rock as manifested by a steepening of the negative slope of stress–strain curves (figures 3.13 and 3.14). Tests on the resistance of sandstone, and low and high porosity green shale [75], have shown an increase in the resistance to the penetration of projectiles with increasing projectile velocity.

Tests on various types of clays have also shown strain rate sensitivity [76–79]. Figure 3.15 shows the stress–strain curves for an overconsolidated clay at three different constant strain rates. Similar results were observed in [77] and are depicted in figure 3.16. Triaxial compression loading of saturated soils [79] have shown an increase in the resistance of clays to deformations with increasing strain rates (figure 3.17).

3–3 Effects of loading history on the mechanical behaviour of engineering materials

The time–dependent properties of concrete may be studied in terms of two special situations: creep (deformation at sustained loads) and relaxation (stress reduction at constant strains). These two situations represent extremes in loading conditions, and, although can be monitored in detail under controlled tests in laboratories, are practically non–existent as such in real situations. Still, results of controlled creep or relaxation tests can be used in predicting behaviour of engineering materials under complex strain and stress conditions.

When a compressive load is sustained, concrete specimens will deform to a strain much larger than the value initially obtained at the time of load application [80–86]. Similar qualitative behaviour is observed under axially sustained tensile loads [87–89] and under more complex stress conditions such as equal biaxial compression [82], combined axial compression and tension [83], hydrostatic stress situations [82], and flexure [90]. Several material factors affect the creep behaviour of concrete. The mix proportions, cement content, volumetric aggregate content, and water–cement ratio are all factors that affect creep [87,88,91].

One of the major factors affecting creep behaviour is the level of stress applied. At low levels of stress/strength ratio, concrete apparently creeps for ever but at a decreasing rate ($\dot{\epsilon}$ decreases with time). Creep, as indicated by creep strain, seems to be directly proportional to the applied stress. This linearity between creep strain and the stress/strength ratio does not apply at higher levels of stress. At high values of stress/strength ratios (above 0.8 for compression and 0.6–0.8 for tension) concrete creeps in a different fashion. After an initial period of decreasing creep rate, strain increase rapidly with time leading to material instability and complete failure.

This variation in creep behaviour at different stress levels is observed for both compressive and tensile stresses (figure 3.18 and 3.19). It is shown that the ultimate tensile strain tends to increase as the applied stress is decreased. Figure 3.20 shows how the time to rupture increases rapidly as the value of the tensile sustained load is reduced.

Creep is observed in concretes of all strength as well in cementatious composites. Typical creep curves for high–, medium– and low–strength concretes under sustained compressive stresses are shown in figure 3.21. Figure 3.22 shows

similar curves for fibre reinforced cement composites.

The ambient conditions also affect creep behaviour. Temperature and relative humidity are among the major factors influencing the rate of creep and its ultimate strain value [80,83,87]. Other time–dependent properties of concrete, which are not load induced, are a direct result of cement time–dependent hydration as well as ambient conditions and their changes. These properties include shrinkage, under no applied stress, and age dependence of the mechanical properties. The interaction between shrinkage, and age of concrete is quite complex and no attempt is made here to simulate such behaviour. Attention is focused only on time–dependent behaviour that is load induced.

Figure 3.23 shows the short term relaxation behaviour for high–strength dry concrete when strain is kept constant [93]. Relaxation is affected by more or less the same factors influencing creep such as stress/strength ratio, concrete strength, ambient conditions, specimen mix, and age of concrete. It should be noted that the procedure of applying constant strain on a specimen and measuring the residual stress is much more difficult than that encountered when applying constant stress and measuring deformations. Data on the stress relaxation of concrete is sparse compared to that on creep. Figure 3.24 shows typical stress relaxation curves [94] for concrete in compression.

The history of loading influences the subsequent mechanical properties of concrete [95–97]. Experiments have shown that sustained compressive loads, at a stress/strength ratio less than that that will cause failure, produces a consolidation process. As a result, the initial modulus of elasticity and the compressive strength are increased, while the strain at ultimate load is reduced [96]. At higher stress/strength ratios, damage inflicted by load application outweighs consolidation effects and both strength and stiffness are reduced. Sustained tensile loading results in microcracking and damage. Both the ultimate strength and the initial tangent modulus are reduced [97].

Time–dependent deformations are also observed in rocks [98]. Tests on shale, sandstone, and coal have shown that these materials will deform with time under constant compressive stress [99]. Creep curves of shale specimens tested in compression are shown in figure 3.25. Constant load tests on some clays [100] also show an increase of the axial deformation with time.

It is thus concluded that concrete and concrete–like materials behave in a manner dependent on time. This behaviour should be modelled if a proper

prediction of the material response is sought. Time–dependence is observed, and hence should be catered for in both analysis and design, when the material is subjected to high rates of loading or other complex loading histories.

3–4 Time–dependent material modelling

Several approaches have been followed to model the mechanical behaviour of concrete under high rates or impulsive loading. These range from empirical modelling, where the behaviour is assumed to follow laws that are numerically derived from experimental data, to mechanical modelling, where a mechanism of fracture or damage, at high strain rates, is postulated and used to derive stress strain laws for the material. The same approaches have been followed to describe other time–dependent behaviour of materials including the dependence on past time history of loads.

3–4–1 Empirical approach

(a) Rate sensitivity

Empirical equations, relating the change of compressive strength, strain at maximum stress, the secant modulus (at 0.45 of peak stress for example), and the initial tangent modulus to strain rate can be found in [101] together with an empirical formulation for the complete stress–strain curve which takes into account the rate of straining, confinement, and concrete strength. These equations are of the form

$$\frac{P_d}{P_s} = A + B \log_{10} \dot{\epsilon} + C (\log_{10} \dot{\epsilon})^2 \qquad (3.4.1)$$

where A, B, and C are material constants, P_d and P_s are the dynamic and static material properties respectively, and $\dot{\epsilon}$ is the strain rate ($\geq$ the static strain rate).

Other researchers [102] have proposed a power law, to predict strength of concrete at high rates, of the form

$$\frac{\sigma_d}{\sigma_s} = \left[\frac{\dot{\sigma}_d}{\dot{\sigma}_s} \right]^{\frac{1}{1+x}} \qquad (3.4.2)$$

where x is a material property, $\dot{\sigma}_d$ and $\dot{\sigma}_s$ are the dynamic and the quasi static stress rates, and σ_d and σ_s are the dynamic and the quasi static ultimate stresses respectively.

While equations represented by 3.4.1 were derived by curve fitting of data from compression tests from several researchers [101], equation 3.4.2 was

derived using a stochastic theory of fracture [102] with crack growth being dependent on stress, temperature, and material defects, and can be applied for both compression and tension.

It was suggested [65] that the use of static constitutive relationships to model impact behaviour is reasonable provided that the concrete under dynamic load is replaced by a stronger concrete under static load. Indeed, similar results can be obtained when comparing a strong concrete to a weaker one, as when comparing the behaviour of the same concrete under impact and static loading. This approach was also used [103] to describe the triaxial behaviour of concrete subjected to high rates of loading by using some previously established theories that describe the static behaviour with modifications of material parameters (peak strength, strain at peak, initial elastic module) to accommodate strain rate changes.

Inherent in all these formulations is the dependence of the expressions obtained on the range of experimental tests from which they were derived. Still, empirical and semi–empirical models have been successfully used to predict the behaviour of materials expected to undergo loading that is similar to that performed in controlled experiments.

(b) Creep and relaxation

Creep is normally expressed as a strain–time relationship applicable under a constant stress state and specified material and environmental conditions. Various forms of this relationship have been suggested on purely empirical bases. Semi–empirical formulas, based on some concepts thought to govern creep behaviour are also used. The most commonly used formulas are of hyperbolic, logarithmic, power law, or exponential form [91,92,104]. These expressions are calibrated (their constants calculated) by appropriate methods of data fitting. These formulas are normally adapted, by the use of parameters or parametric expressions, to include the effects of age, shrinkage, stress level, and environmental conditions such as temperature and humidity.

For example, in [105] a power function was used in conjunction with exponential expressions (proposed to describe shrinkage). The total time–dependent strain was assumed to be a function of time, age of concrete, stress level, and some parameters that can be calculated by curve fitting. In references [104–107] a double power law for basic creep of concrete was used. Creep was assumed to be fully described by a creep function $J(t,t')$ which represents strain ϵ

(elastic + creep) at time t caused by a constant unit stress acting since time t'. The form of $J(t,t')$ was taken as

$$J(t,t') = \frac{1}{E_0} + \frac{\varphi_1}{E_0} t'^{-m} (t-t')^n \qquad (3.4.3)$$

The above creep law has four material parameters E_0, φ_1, m, and n and it takes into account the age of concrete. In order to include creep of infinitely old concrete, t'^{-m} can be replaced by $c + t'^{-m}$. The above law showed very good agreement with a range of experimental data on basic creep (with no moisture exchange). It also gives good prediction of the change of the elastic modulus with age [104,105]. Additional terms in expression 3.4.3 can be used to account for drying (and wetting) as well as stress/ultimate stress ratio. Corrections to the parameters in 3.4.3 and/or the actual creep duration $(t-t')$ can be used to predict creep at different levels of temperature and relative humidity. In reference [106] recommendations for the values of these parameters in terms of other known material properties are given.

A combination of a double power and a logarithmic law [107] gave a better fit to test results for the long–term creep behaviour. Results from relaxation tests [94] have also shown that inverting a double power law gives good fit to experiments.

Tests on the creep behaviour of steel fibre reinforced cement composites [85] have shown that the results can be satisfactorily represented by hyperbolic and logarithmic expressions.

As mentioned earlier, information on the stress relaxation of concrete is very sparse. In many instances relaxation is viewed as restrained creep so that all theoretical and analytical expressions relating creep strains to time should, if possible, be used to relate stress relaxation to time. Rather than finding relaxation functions that fit experimental data, researchers tend to use creep laws either by inverting them to get relaxation laws or by discretizing creep laws so that stress history can be found numerically from a given strain history [94,108].

3–4–2 Modelling based on the mechanism of the time–dependent response

(a) Rate sensitivity

In this approach modelling is based on a certain mechanism assumed to

govern material time–dependent behaviour. Based on the postulated mechanism, mechanical laws can be derived and used to describe the material behaviour. This approach is semi–empirical in the sense that often a mechanism of material behaviour is postulated after observations made in real material testing.

By noting the different mechanisms of tensile fracture encountered in concrete under static and dynamic loads, Zielinski [109] developed a fracture mechanics model for this behaviour. The model is based on observations that cracks, under slowly increasing tensile loading, will grow along relatively weak interfaces between aggregate particles and the cement matrix and will then penetrate through the matrix. Under impact loading conditions, a great number of microcracks can be driven into extension simultaneously and will be forced to develop along shorter paths of higher resistance.

In this model, the energy absorbed during fracture is expressed as the sum of energies associated with crack extension in the matrix, aggregates, and interfacial bond between the two. The possibilities of multiple cracking is also taken into account. This absorbed energy increases with increasing stress rate. The tensile strength is then expressed in terms of the calculated fracture energy and an assumed shape factor of the stress strain curve.

(b) Creep

Whatever the form of the viscous creep law used to describe the relationship between time and strain, it can by no means be comprehensive. The range of mathematical expressions used to describe creep is a direct reflection of the variety of factors that influence creep and hence the long lasting controversy upon the physical nature of creep.

Creep is thought of by some researchers as being the direct result of the internal movement of water in the cement gel [110]. Others [111] have argued that creep is a shear process of crystal surfaces sliding one over the other with internal water acting as a lubricant. Indeed, both mechanisms are quite influential and tests show that creep might be a result of a combination of both [81,91]. Tensile testing of creep [87] and direct measurements of the physical changes (length, weight, solid volume) of cement paste with changes in conditions of exposure [80], suggest that time–dependent microcracking and slippage due to the reduction of surface energy are produced by the absorption of liquids into the developing cracks. Water movement, although existing, is not a mechanism but a catalyst. Slippage of particles and microcracking are enhanced by liquid motion.

Creep failure in tension can be a progressive process resulting in large cracks, or a sudden brittle mechanism. At low stress levels, cracks do form under a sustained tensile force but they eventually become contained and stabilized. Above a certain level of stress, the initially more or less homogeneously spread microcracks grow with time and eventually macroscopic cracks are formed resulting in failure [89]. The rate of formation of these cracks can be slow resulting in progressive rupture, or sudden inducing brittle failure.

Compressive testing of creep in various concretes [86] indicates that under compressive loads, the time–dependent load–induced deformation is due to water movement within the solid, water movement to and from the environment, and the development and propagation of internal microcracks. The rate and magnitude of creep are dependent on the contribution of each of the above mechanisms.

Recently, a new approach has been proposed where creep was thought to be the result of time–dependent movement of water from micropores and microcracks initially present in the solid to the load induced microcracks [112]. If deformation is kept constant, as in the case of relaxation tests, this internal movement will result in a reduction of stress concentration and hence a gradual reduction of the stress is observed.

The fact that creep behaviour is a complex one and is dependent on many material and ambient factors makes it impossible to assume a mechanism of behaviour that is comprehensive. A comprehensive theoretical formulation, based on all possible mechanisms of creep, will be too difficult to implement. On the other hand, if a simple mechanism is postulated, it will automatically exclude many significant factors that influence creep behaviour. Another difficulty inherent in this approach is the fact that different creep mechanisms are not independent and may be influenced by the same factors in the same or opposite manner.

(c) Dependence on loading history

It was mentioned earlier (section 3–3) that sustained loading applied before the mechanical testing of concrete has an effect on the values of the ultimate strength and the initial modulus. Both the ultimate strength and the initial modulus are reduced as a result of microcracking inflicted by the application and removal of a sustained tensile load prior to a monotonic loading to failure. Although microcracking is induced if compressive stress is sustained,

the overall result is a slight increase in the compressive stress and the initial modulus if the applied stress/strength ratio is low. The damage caused by microcracking is counterbalanced by other non–mechanical processes such as accelerated hydration process, closure of some previously existing microcracks perpendicular to load direction, and increase of molecular attractive forces due to the decrease of distance between particles [96,113].

Neglecting these beneficial effects, it was possible to model the dependence of strength of concrete upon the history of loading [113]. Defining the potential strength of a loaded specimen as the strength that would be exhibited if, at a time t, the load is increased to failure at the rate normally used in standard short term testing, then the effects of hydration with time and those due to microcracking inflicted by sustained load are expressed as

$$f = C_a(t)\, C_s(t)\, f'_c \qquad (3.4.4)$$

where f is the potential strength, f' is the standard strength without any previously applied loading, C_a is an increasing function of time to cater for hydration, and C_s decreases below unity as a result of sustained loading and is a function of stress and time under load. With the use of some simplifying assumptions on the behaviour of loaded specimen, 3.4.4 can be used for constant stress or constant strain conditions. It can also be used to describe the behaviour of concrete under monotonically increasing loads. This was achieved [113] by taking the stress history to be a discrete history of small increments within which stress is held constant.

3–4–3 Continuum approach to time–dependent modelling

In continuum formulation, distinction is made between two terms, namely "path history" and "time history". In a strain space based description, path history is referred to as the sequence of strain states experienced by a material from the start of straining to a the current state. In contrast to this, "time history" comprises the sequence of deformation states coupled with the time at which these states occurred. Two points in strain space reached by the same deformation path history do not necessarily have the same time history although the converse is true. Identical time histories necessarily provide identical path histories for the same time sequence.

In this way path history merely gives details of the magnitude of each increment of deformation whilst time history indicates the duration and thus the rate of deformation.

The time sequence with which loading is applied influences the mechanical response of concrete as well as other solids. One effect of this is the dependence on the duration of the load increment or in other words the rate of load application as seen in section 3–2.

(a) Linear time–dependent formulation

Continuum theories that adopt viscosity of solids to describe the time–dependent behaviour are very common in engineering practice. In a viscoelastic solid, the stress scalar σ is normally assumed to be expressed by a relaxation law of the form

$$\sigma(t) = \epsilon(0)\, G(t) + \int_0^t G(t-\tau)\, d\epsilon(\tau) \qquad (3.4.5)$$

for a prescribed strain history $\epsilon(t)$ and a relaxation function $G(t)$ [114]. Alternatively, strain ϵ may be described by a creep law of the form

$$\epsilon(t) = \sigma(0)\, J(t) + \int_0^t J(t-\tau)\, d\sigma(\tau) \qquad (3.4.6)$$

with the creep function $J(t)$ being a function of time [114].

Indeed, in this simple linear approach, the resultant material behaviour is dependent on the past time history of applied strain (or stress). Any other nonlinearity in the behaviour is ignored.

(b) Path dependence – Plasticity formulations

In plasticity based theories, any dependence of the material response on the past time history is ignored. Nevertheless, the material is assumed to be path dependent and hence its behaviour becomes non–linear. In a stress space formulation, the existence of a yield surface is assumed. This surface separates stress states that can be attained elastically from those that can only be reached with consequential plastic deformations. The yield surface is defined by

$$F(\sigma_{ij}, H_k) = 0 \qquad (3.4.7)$$

where σ_{ij} is the stress tensor and H_k is a hardening vector of k parameters. At any stage of loading, the strain increment $d\epsilon_{ij}$, resulting from an applied stress increment $d\sigma_{ij}$, is expressed as

$$d\epsilon_{ij} = d\epsilon^e_{ij} + d\epsilon^p_{ij} \qquad (3.4.8)$$

where $d\epsilon^e_{ij}$ is the elastic strain increment and $d\epsilon^P_{ij}$ is the plastic strain increment.

If the behaviour is restricted to materials that follow Drucker's stability criterion [115], then it follows that all yield surfaces should be convex and that the plastic strain increment is always normal to the yield surface at the point of yield (provided the material is assumed to be linear in the small).

The form of the function F and its sign together with the normality argument allow the calculation of the plastic stress increment to be performed.

Such a material is path dependent. Its response is dependent, not only on the current stress state, as defined by σ_{ij} and $d\sigma_{ij}$, but also on the past sequence of stress states experienced by the material as measured by the hardening vector H_k.

Valanis [116] proposed endochronic plasticity as an alternative to classical plasticity for the description of a class of materials that are path and history dependent. The endochronic theory is based on the assumption that material behaviour can be described by internal variables that define the material memory. As an alternative to the concept of the yield surface, a material property, termed the intrinsic time, is defined.

For such a material [117,118], an intrinsic time scale Z, which is related to an intrinsic time measure z, is defined by

$$dZ = \frac{dz}{F(z)} \qquad (3.4.9)$$

where

$$dz = | \, d\epsilon^P_{ij} \, d\epsilon^P_{ij} \, | \qquad (3.4.10)$$

and F(z) is a function, a property of the material, that accounts for the dependence of the increment of the intrinsic time on the past history of deformations, and $d\epsilon^P_{ij}$ is the plastic increment of strain.

Stress is assumed to be related to strain by

$$\sigma_{ij} = \int_0^Z \varphi(Z-Z') \, d\epsilon^P_{ij}(Z') \qquad (3.4.11)$$

where $\varphi(Z)$ is an integrable function over the interval $0 \leq Z \leq \infty$. The strain increment is given by 3.4.8 with the elastic strain increment related to the stress increment by an elastic material stiffness tensor.

Noting the similarity between (3.4.11) and (3.4.5), it might seem that the material described is dependent on the past time history of deformation. This is not true. The endochronic theory describes a material that is dependent on the past path history of deformations. The intrinsic time measures the past history of plastic strains without any account for the duration and time at which these states occurred.

(c) Path and time dependence – Nonlinear continuum approach

A continuum damage theory for predicting the dynamic behaviour of concrete was developed by Suaris and Shah [68,119]. As in the case of other damage theories, failure was considered to be the result of the nucleation and growth of a number of microcracks. The total (Helmholtz) free energy, ψ, of the solid is considered to be a function of strain ϵ_{ij} and a damage vector ω_i which is normal to the plane of the crack field and whose magnitude is equal to the area density of the cracks. A consistent kinematic and thermodynamic approach leads to the constitutive equation

$$\sigma_{ij} = \frac{\partial \psi}{\partial \epsilon_{ij}} \tag{3.4.12}$$

and a damage evolution law,

$$\rho\, k\, \ddot{\omega}_i = g^D_i(\epsilon_{ij}, \omega_i, \dot{\omega}_i) - \rho \frac{\partial \psi}{\partial \omega_i} \tag{3.4.13}$$

where ρ, k are the density of the material and its inertial resistance to crack growth, and σ_{ij} and ϵ_{ij} are the stress and strain tensors respectively. With proper calibration and analytical expressions for ψ and g^D_i, the above incremental laws can be used to yield the stress–strain response for a particular state of the material.

Viscosity based formulations are commonly used in conjunction with elasto–plastic theories in a variety of forms. The mechanical behaviour of viscoelastic/plastic solids, as described by Naghdi and Murch [120], requires that the total strain ϵ_{ij} be composed of two parts, the viscoelastic component ϵ^{ve}_{ij} and the plastic component ϵ^{p}_{ij}. While ϵ^{ve}_{ij}, at time t, is determined by the past time history of stress (time history dependent), the plastic strain component ϵ^{p}_{ij} is dependent on the path followed by stress (path history dependent). This does not necessitate that each component is defined by time or path history alone but by an interaction of the time sequence and the path of the stress trajectory. The

existence, in stress space, of a surface, of the form

$$f = f(\sigma_{ij}, \epsilon^{P}_{ij}, \chi_{ij}, \kappa_{ij}) = 0 \qquad (3.4.14)$$

is postulated, where χ_{ij} is a measure of viscous effects and κ_{ij} is work hardening parameter and thus dependent on the path history. This yield surface, in contrast to that of the inviscid theory of plasticity, can change its shape continually because of its dependence on the time history of stress. The notation of a rapid stress path, a stress path traversed in a vanishingly small interval of time such that χ_{ij} remains unchanged, is introduced together with the notation of the instantaneous yield surface corresponding to a state in the stress space. This surface is defined as

$$f_{a} = f(\sigma_{ij}, \epsilon^{P}_{ij}{}^{(a)}, \chi_{ij}{}^{(a)}, \kappa_{ij}{}^{(a)}) = 0 \qquad (3.4.15)$$

It is a surface reached from a point in stress space by a rapid path so that neither the work–hardening parameter κ_{ij} nor the time–history measure parameter χ_{ij} are altered. The convexity of all yield surfaces (3.4.14) and the normality of the plastic strain increment $\dot{\epsilon}^{P}_{ij}$ to the instantaneous loading surface are essential concepts used to evaluate $\dot{\epsilon}^{P}_{ij}$. These concepts (convexity and normality) restrict the theory to those materials satisfying the stability criterion as defined by Drucker [28]. The viscoelastic strain, ϵ^{ve}_{ij}, is evaluated by using creep integral laws similar to 3.4.6. It should be noted that although the material is called viscoelastic/plastic, it exhibits time–dependent behaviour in both the elastic and plastic modes. The plastic component ϵ^{P}_{ij} is not independent of time history of stress.

As an alternative continuum formulation, solids can be assumed to be elastic/viscoplastic, in the sense that viscous properties are only shown in the plastic region. This approach has been suggested by Perzyna [121]. For such a solid the total strain rate $\dot{\epsilon}_{ij}$ is the sum of two components. Hence,

$$\dot{\epsilon}_{ij} = \dot{\epsilon}^{e}_{ij} + \dot{\epsilon}^{VP}_{ij} \qquad (3.4.16)$$

where $\dot{\epsilon}^{e}_{ij}$ and $\dot{\epsilon}^{VP}_{ij}$ are the elastic and the viscoplastic components of the strain increment respectively.

For such an idealization, the viscoplastic component of the strain increment is assumed to be a function of the "excess stress" above the initial yield condition termed the static yield criterion. The static yield criterion is

assumed to satisfy all the conditions of the inviscid theory of plasticity and is of the form

$$f = f(\sigma_{ij}, \kappa) = 0 \qquad (3.4.17)$$

where κ is a hardening parameter. Since the viscoplastic strain component is a function of the excess stress above the static yield criterion, a dynamic yield surface can be defined as

$$F = (\sigma_{ij}, \kappa, b) = \frac{f(\sigma, \kappa) - b}{B} = 0 \qquad (3.4.18)$$

where B is a scaling factor having the dimensions of stress, and b/B measures the rate of expansion of the yield surface.

The flow rule for work hardening and rate–sensitive plastic materials may thus be given as

$$\dot{\epsilon}^{VP}_{ij} = \begin{cases} \lambda\, g\left[\dfrac{f}{B}\right] \dfrac{\partial f}{\partial \sigma_{ij}} & \text{if } f > 0 \\ \\ 0 & \text{if } f \leq 0 \end{cases} \qquad (3.4.19)$$

The function $g\left[\dfrac{f}{B}\right]$ may be chosen from dynamic testing on the material, λ is a viscosity parameter associated with time. Expressions 3.4.18 and 3.4.19 give

$$\frac{b}{B} = g^{-1}\left[\frac{1}{\lambda}\,(I_2^{VP})^{\frac{1}{2}}\,\left(\frac{1}{2}\,\frac{\partial f}{\partial \sigma_{ij}}\,\frac{\partial f}{\partial \sigma_{ij}}\right)^{-\frac{1}{2}}\right] \qquad (3.4.20)$$

with $I_2^{VP} = \dot{\epsilon}^{VP}_{ij}\,\dot{\epsilon}^{VP}_{ij}$

The function b/B describes the rate dependence of the dynamic loading surface. With a proper choice of the functions f, g, and hence F the behaviour of such a solid can be analysed [121–123].

In a modified elastic/viscoplastic model [124] strain softening was assumed to occur when stress reaches a strength limit surface F_f. Softening is thus described by a surface

$$F_f = F_f(\sigma_{ij}, \kappa, \epsilon^{VP}_{ij}) \qquad (3.4.21)$$

that initiates degradation of the static yield surface f.

An interesting one–dimensional model presented by Browing, Gurtin,

and Williams [125], assumed that the time–dependent stress is related to a constitutive quantity π, called the pseudo stress, which is in turn related to strain through an elastic/plastic stress–strain law. The entire time and rate dependent mode of the response is described by a relaxation function (relating σ to π) superimposed over a time–independent plastic behaviour. In other words,

$$\pi = F(\epsilon, \epsilon_m) \tag{3.4.22}$$

where π, ϵ are the pseudo stress and the strain at time t, and ϵ_m is the past maximum of strain, and

$$\sigma(t) = \int_0^t G(t-\tau)\ \dot{\pi}(\tau)dt \tag{3.4.23}$$

where G(t) is a stress relaxation function. Redefining all relationships in stress space gives

$$\pi(t) = \int_0^t J(t-\tau)\ \dot{\sigma}(\tau)dt \tag{3.4.24}$$

and

$$\epsilon = K(\pi, \pi_m) \tag{3.4.25}$$

where J(t) is a creep function and π_m is the past maximum of π. Appropriate expressions of the function F (or K) and G (or J) are needed to fully describe the material behaviour. Damage in this model is only measured as a function of the past maximum of strain (or past maximum of pseudo stress).

The idea of describing path and time dependence of material behaviour by combining plastic behaviour (path dependent) and viscous response (time dependent) enlightens the way of combining different path and time dependent formulations.

If time, in the viscous response, is replaced by the equivalent deformations occurring, then the overall response obtained is merely path dependent (endochronic theory). Alternatively, path and time dependent descriptions can be achieved (elastic/ viscoplastic, viscoelastic/ plastic).

This motivates the attempt to describe a class of engineering materials that fail in a time–dependent progressively fracturing manner as a result of stiffness degradation. This can, in theory, be achieved by combining viscoelasticity with the time–independent theory of progressively fracturing solids. This approach has been followed in this thesis to formulate the general time–dependent progressively fracturing solids theory presented in chapter V.

Before this is attempted, the general behaviour of a progressively fracturing solid is investigated through tests performed on a model material simulated by random networks.

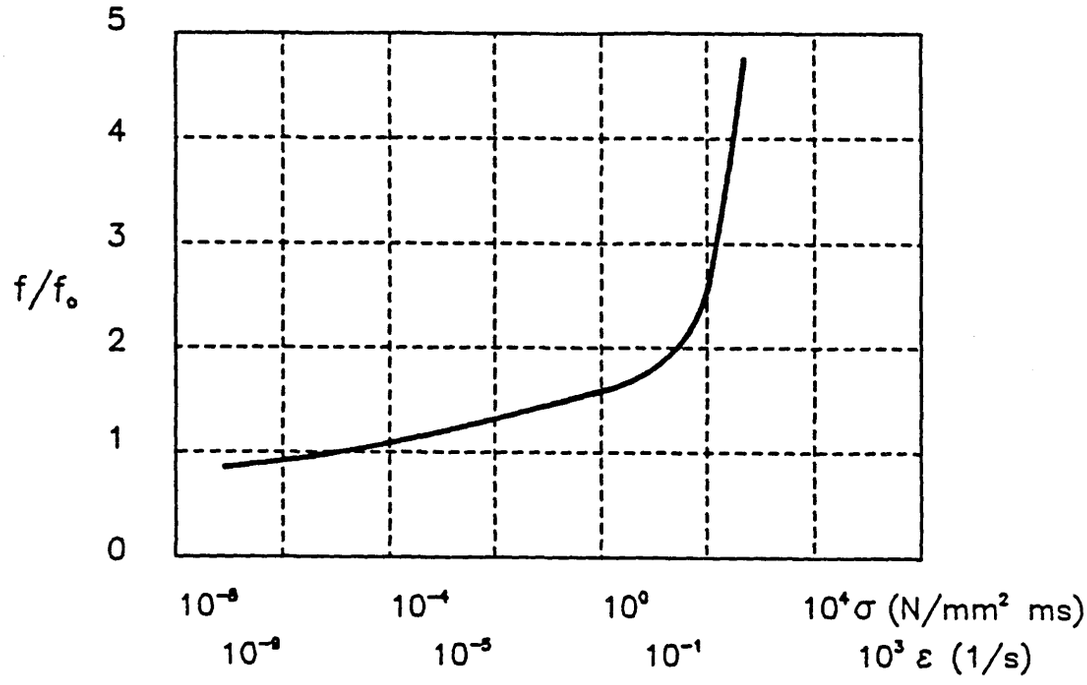

Fig. 3.1 Influence of strain rate upon the uniaxial tensile strength [54]

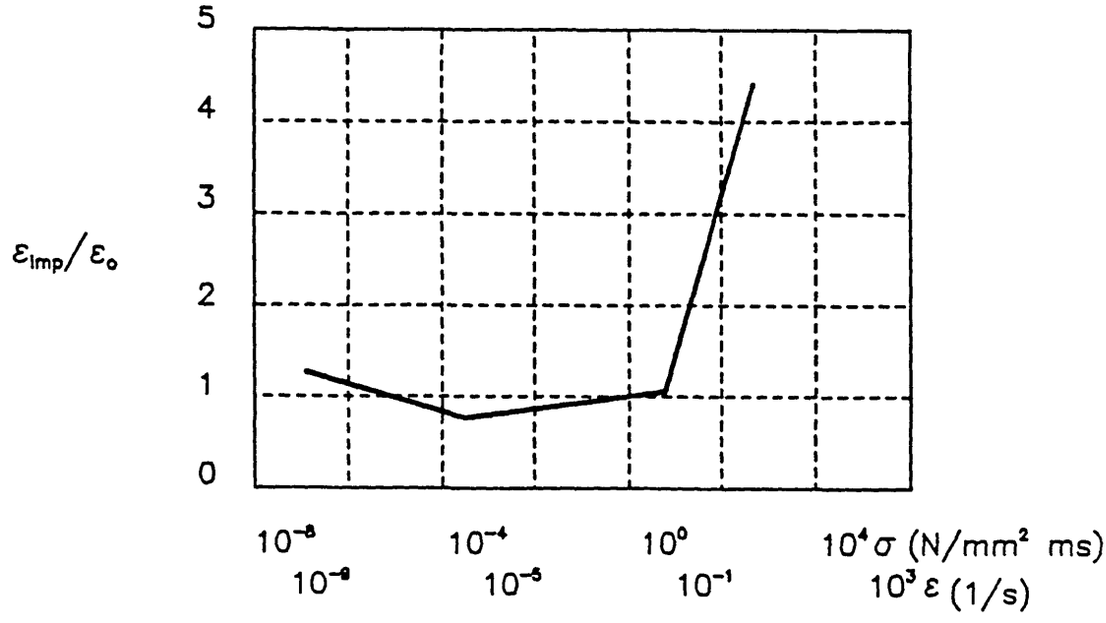

Fig. 3.2 Influence of strain rate upon the relative tensile strain [54]

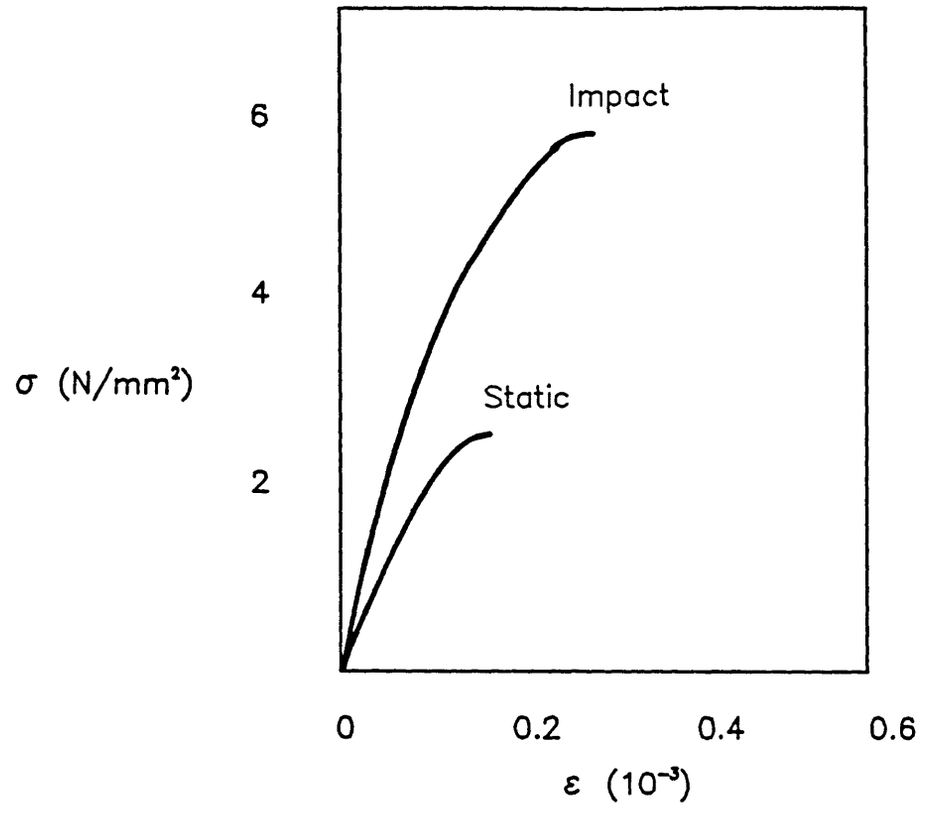

Fig. 3.3 Uniaxial tensile stress strain response of concrete [53]

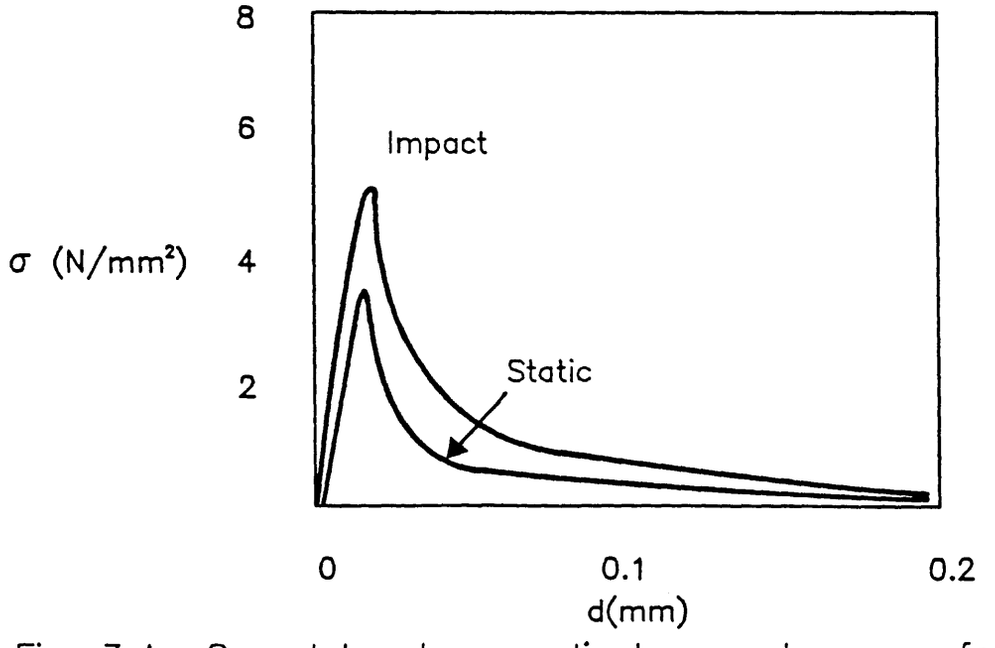

Fig. 3.4 Complete stress– displacement curves for concrete in uniaxial tension [55]

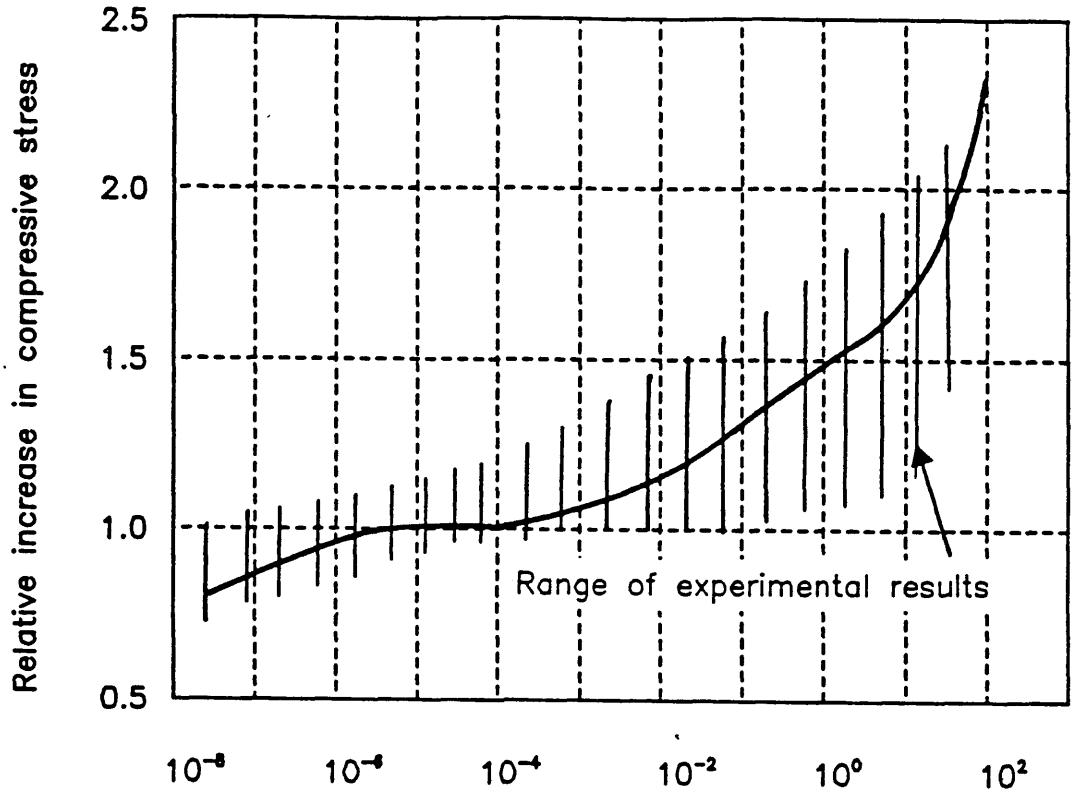

Fig. 3.5 Compressive strength increase of concrete at different strain rates [65]

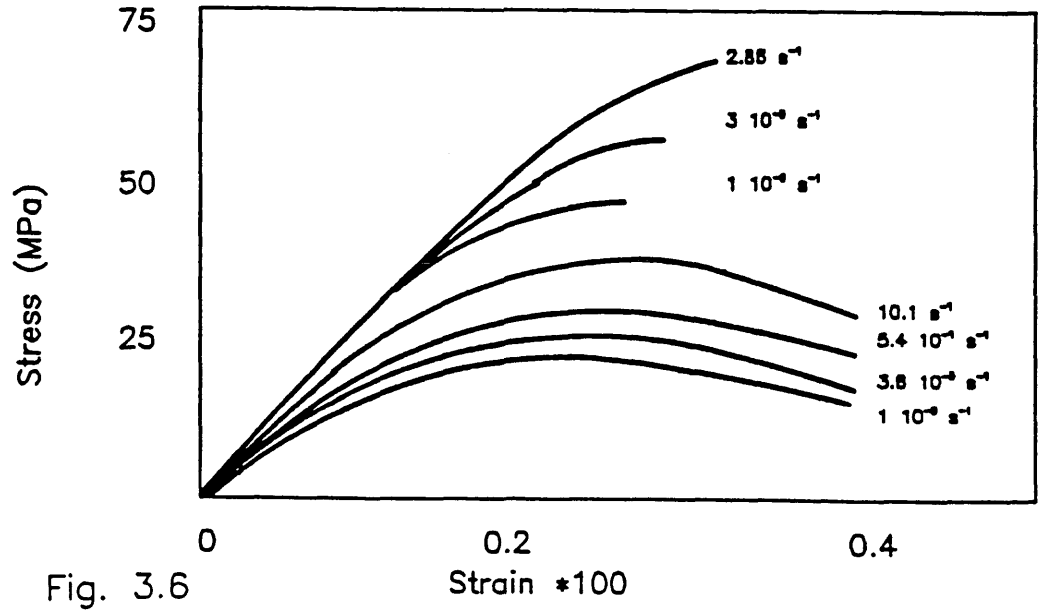

Fig. 3.6 Stress–strain response for two concretes in compression at different strain rates [66]

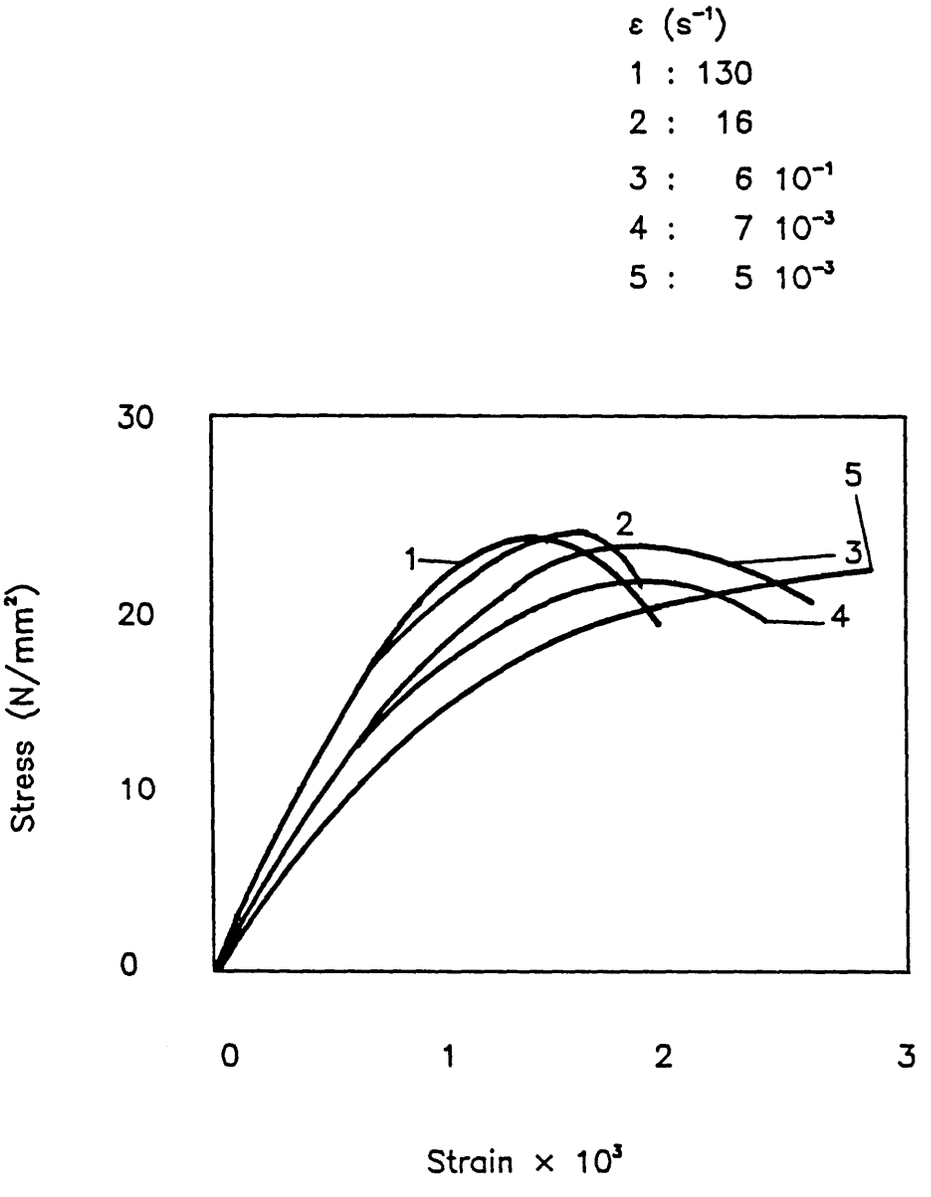

Fig. 3.7 Stress–strain curves for concrete in compression loaded at different strain rates [67]

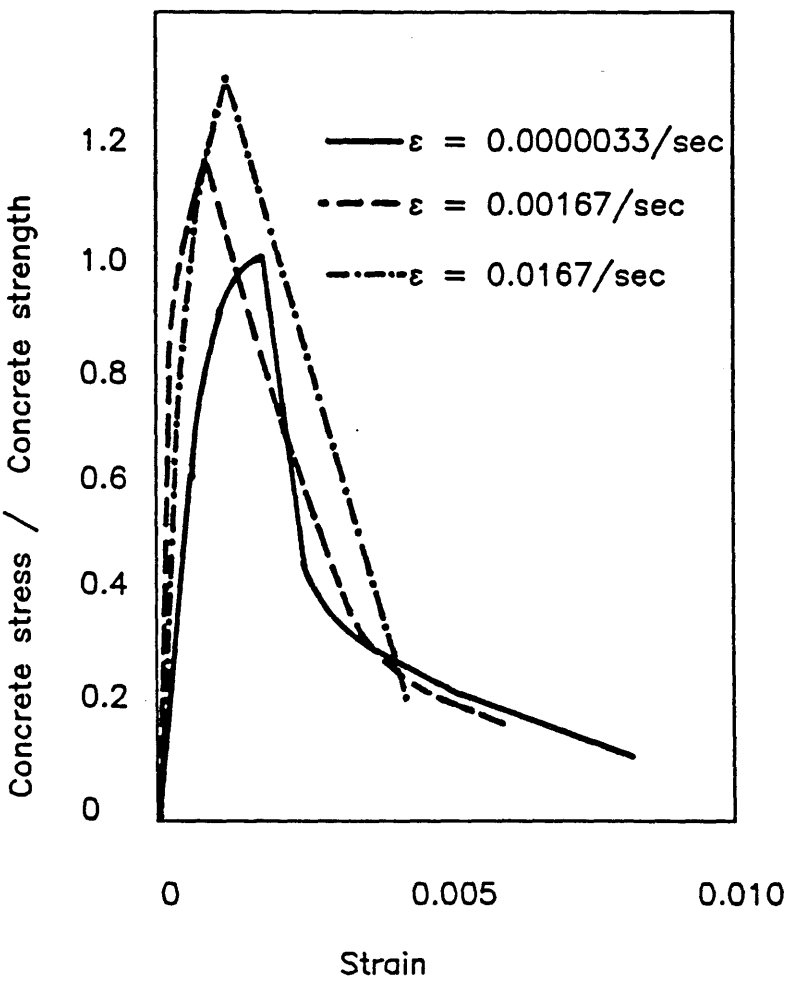

Fig. 3.8 Stress–strain curves for unreinforced concrete loaded at different strain rates in uniaxial compression [64]

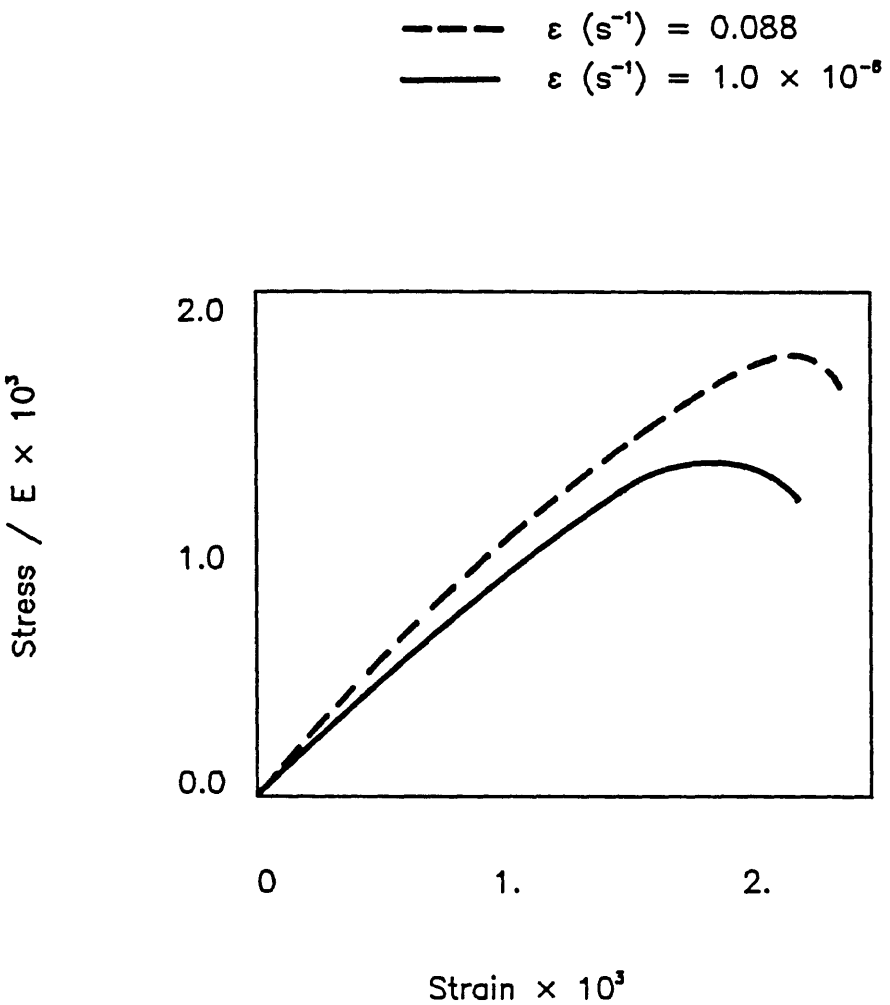

Fig. 3.9 Stress–strain curves for concrete in compression [68]

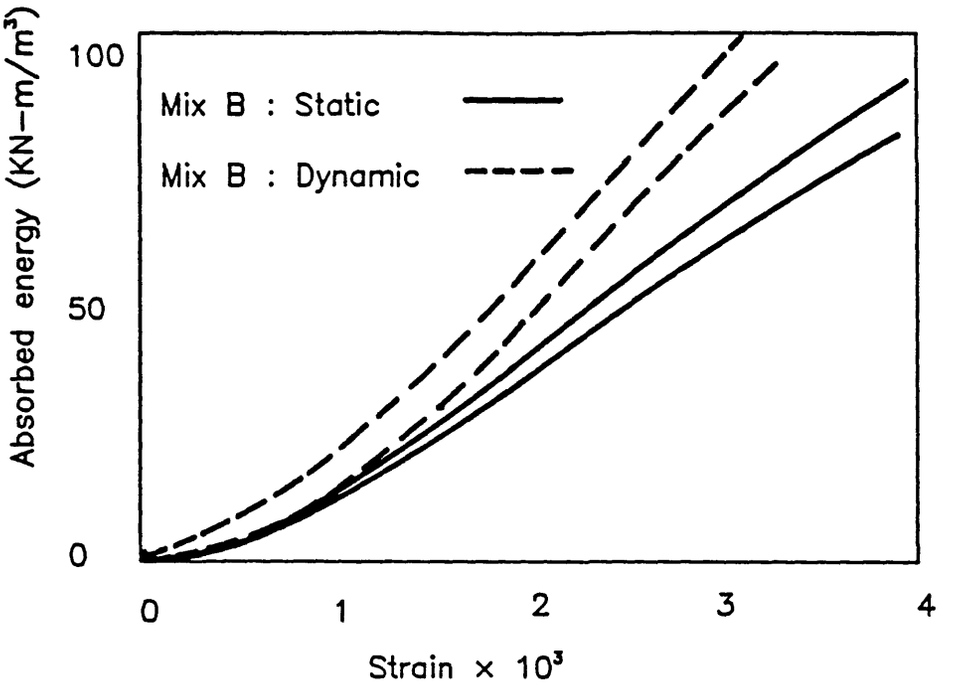

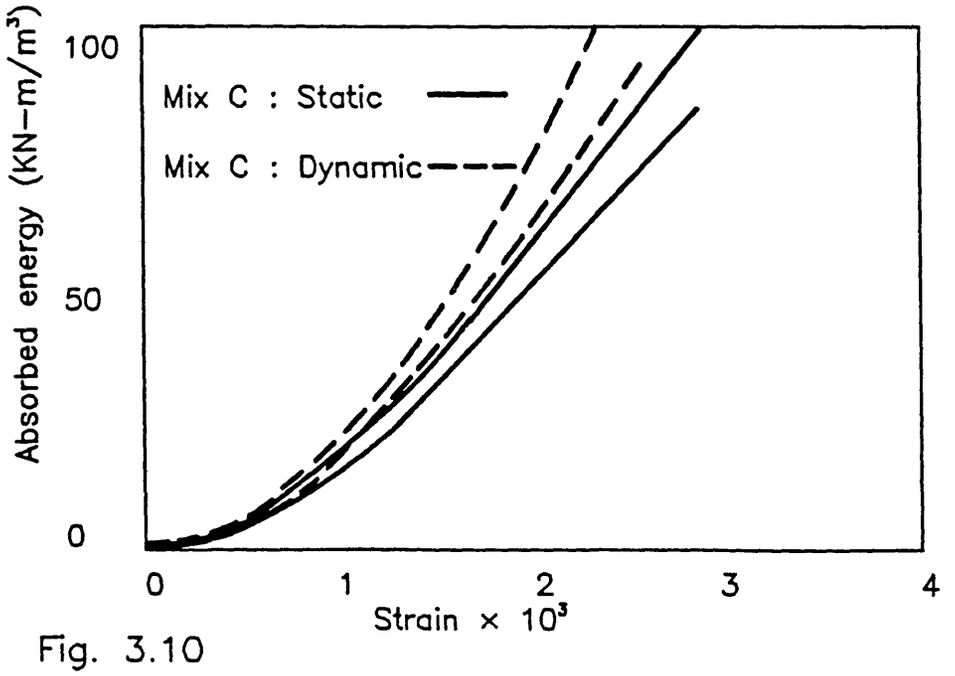

Fig. 3.10

Comparison of static energy absorption response with impact response in compression for two concrete mixes [65]

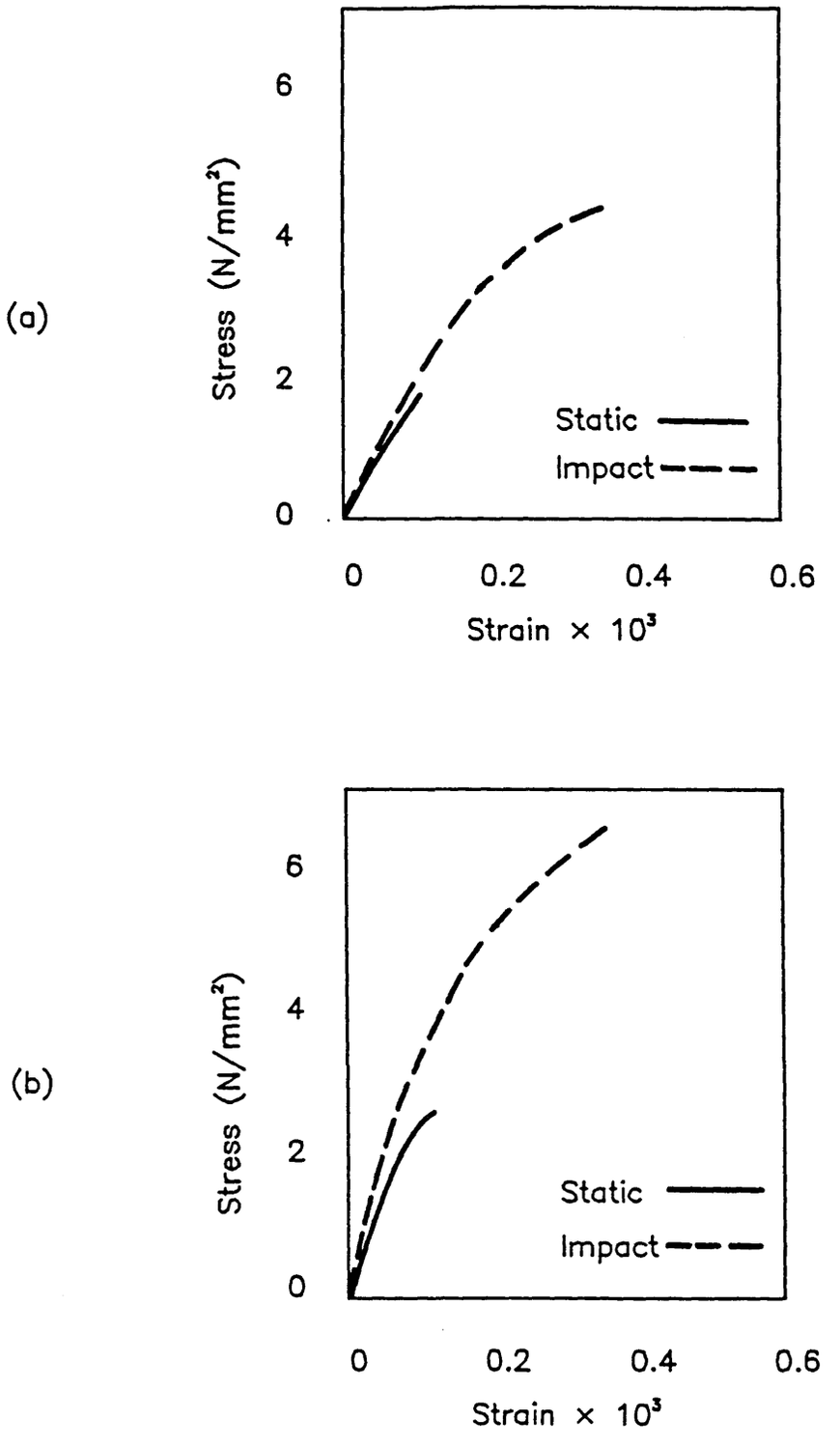

Fig. 3.11 Uniaxial tensile stress–strain response of
(a) mortar
(b) micro–concrete [53]

(a) 8 longitudinal bar units with transverse hoops

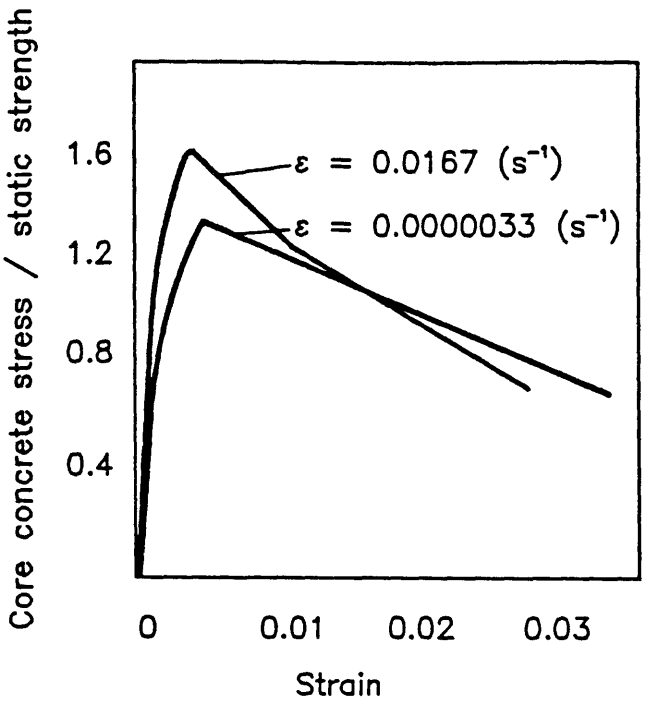

(b) 12 longitudinal bar units with transverse hoops

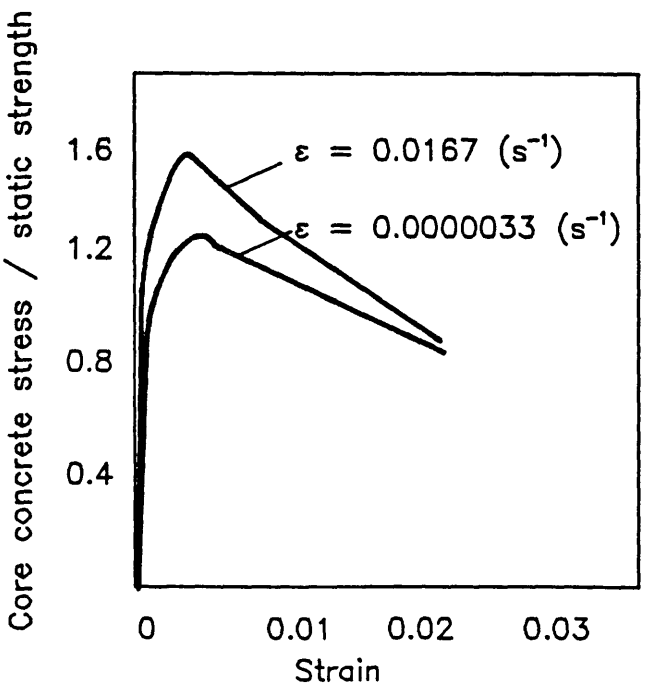

Fig. 3.12 Stress–strain curves for concrete units loaded at different strain rates [64]

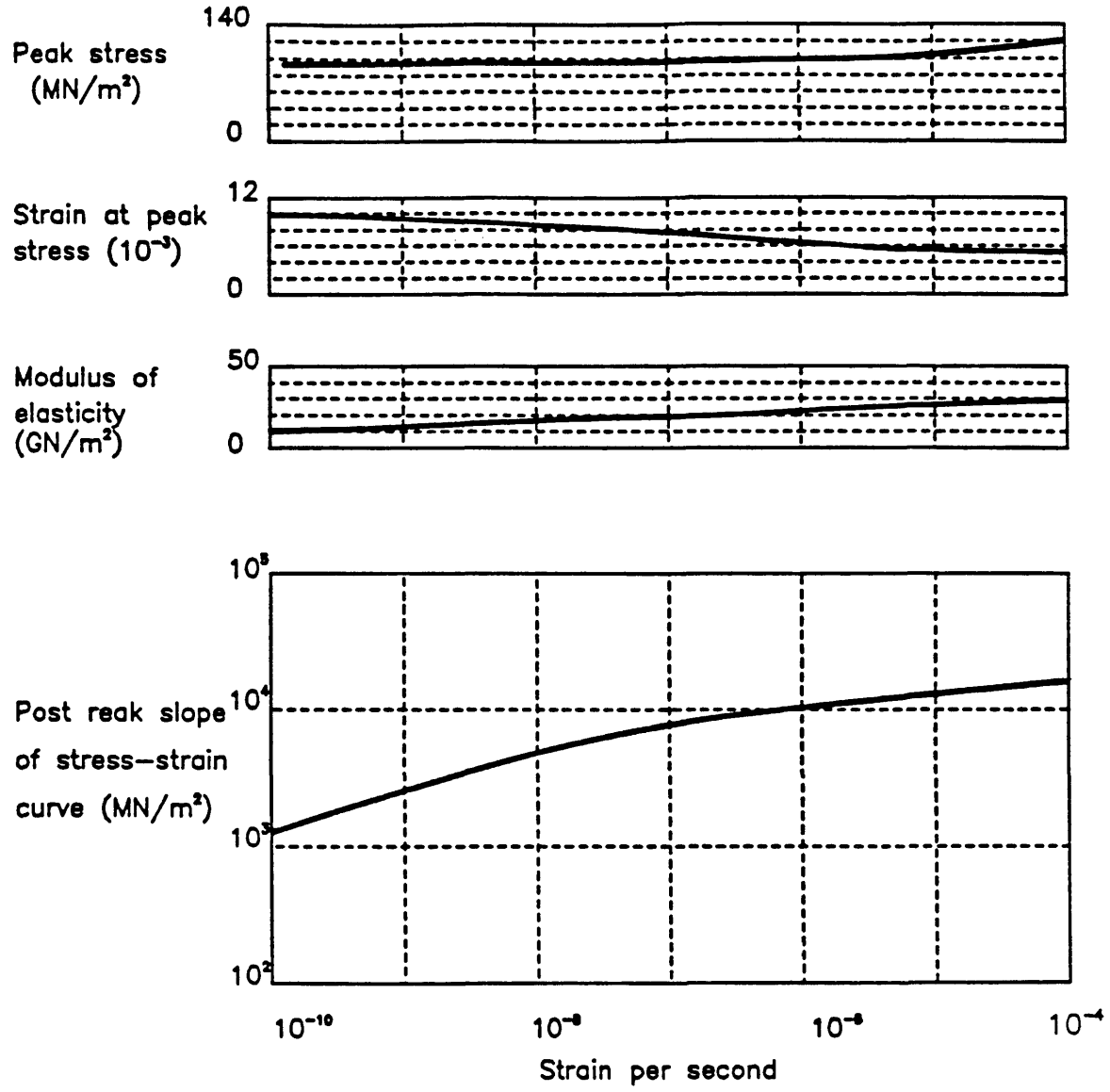

Fig. 3.13 Influence of strain rate on strength failure,strain at strength failure, modulus of elasticity, and post–peak slope for sandstone under uniaxial compression [74]

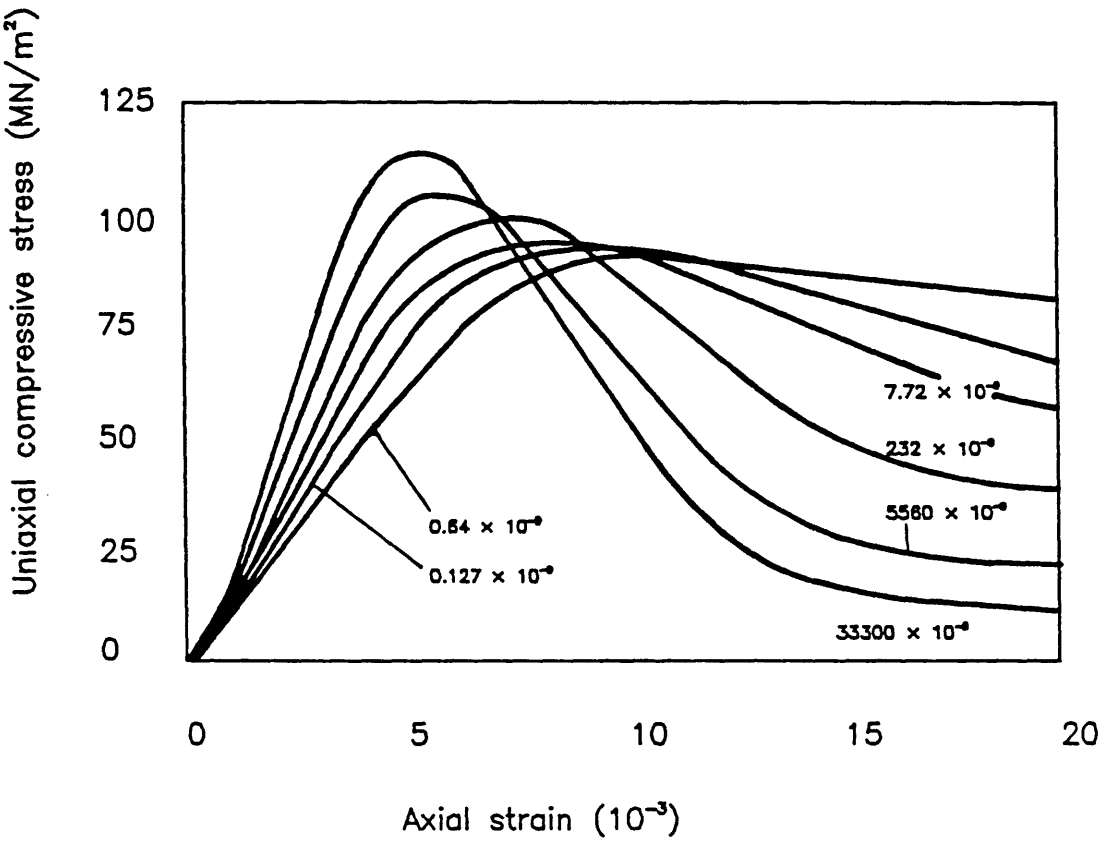

Fig. 3.14 Stress–strain curves for sandstone at various strain rates [74]

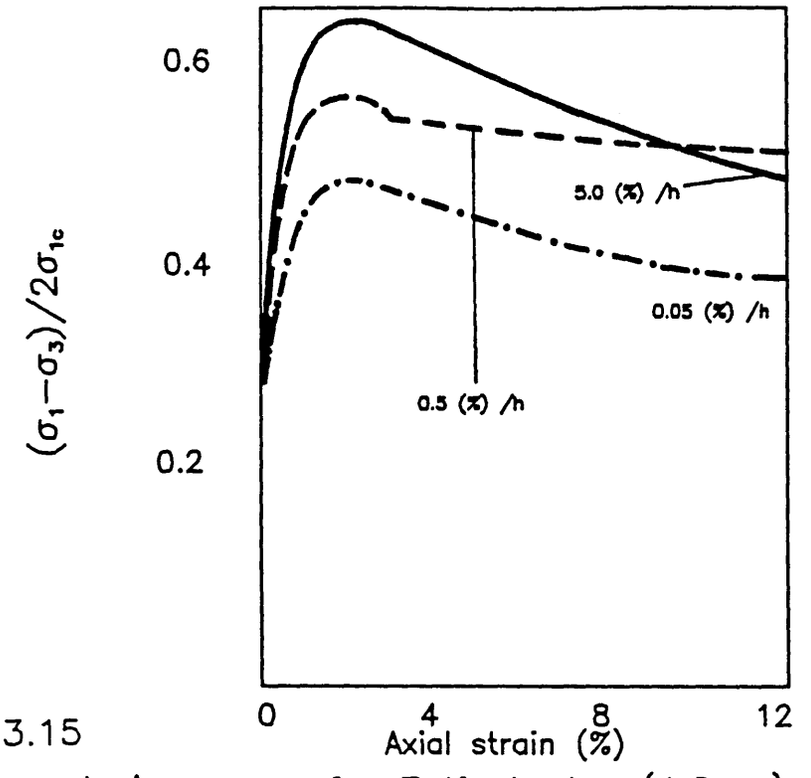

Fig. 3.15 Stress–strain curves for Belfast clay (4.0 m) under triaxial compression tests for various strain rates [76]

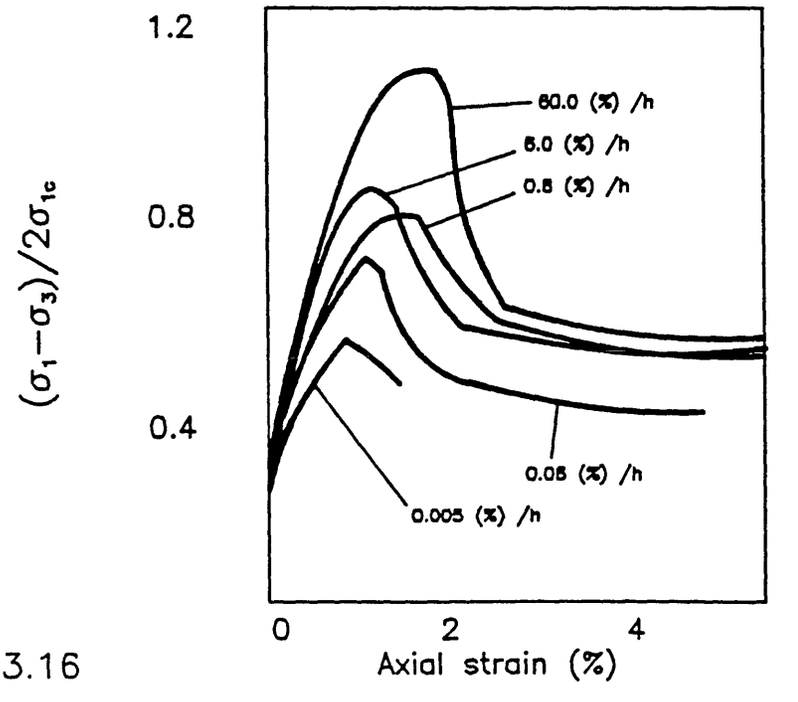

Fig. 3.16 Stress–strain curves for Rangsit clay (4.0 m) under triaxial compression tests for various strain rates [77]

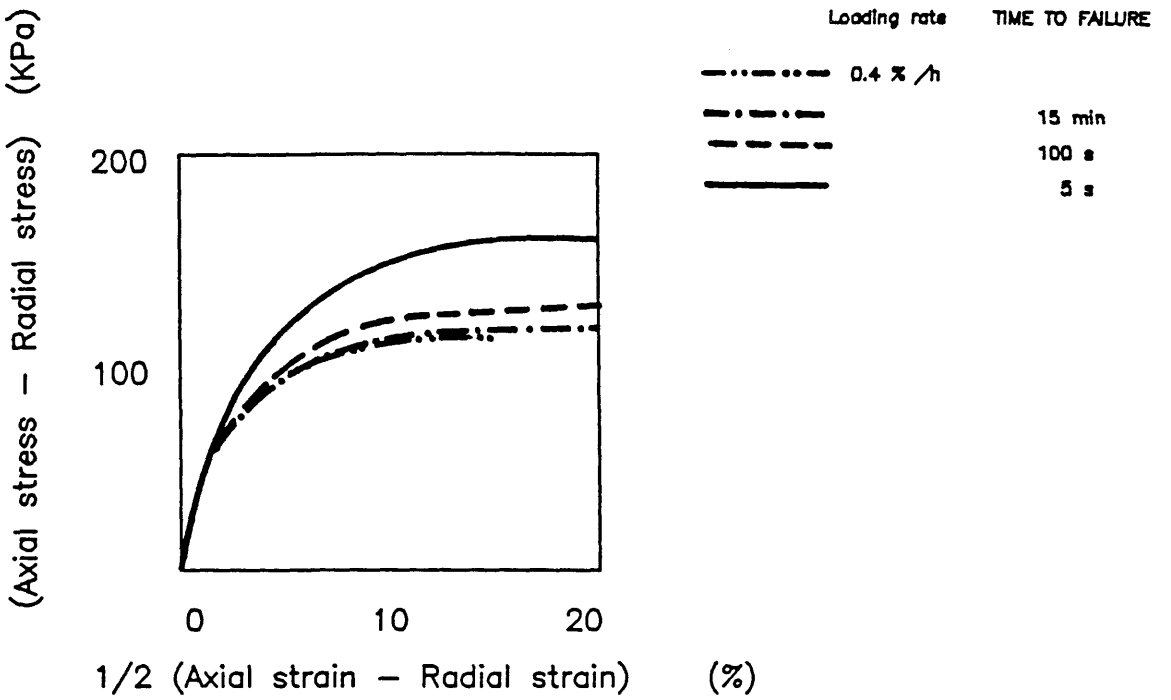

(a) Stress–strain curves for undrained overconsolidated clays

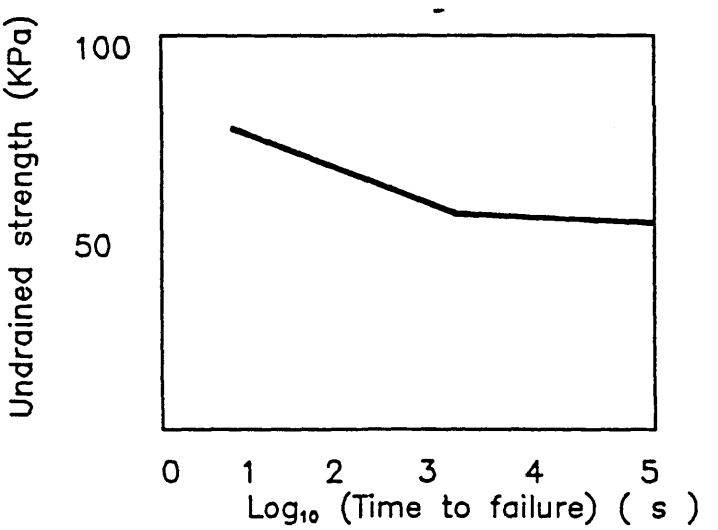

(b) Variation in undrained strength with time to failure

Fig. 3.17 Effect of loading rate on the behaviour of clays [79]

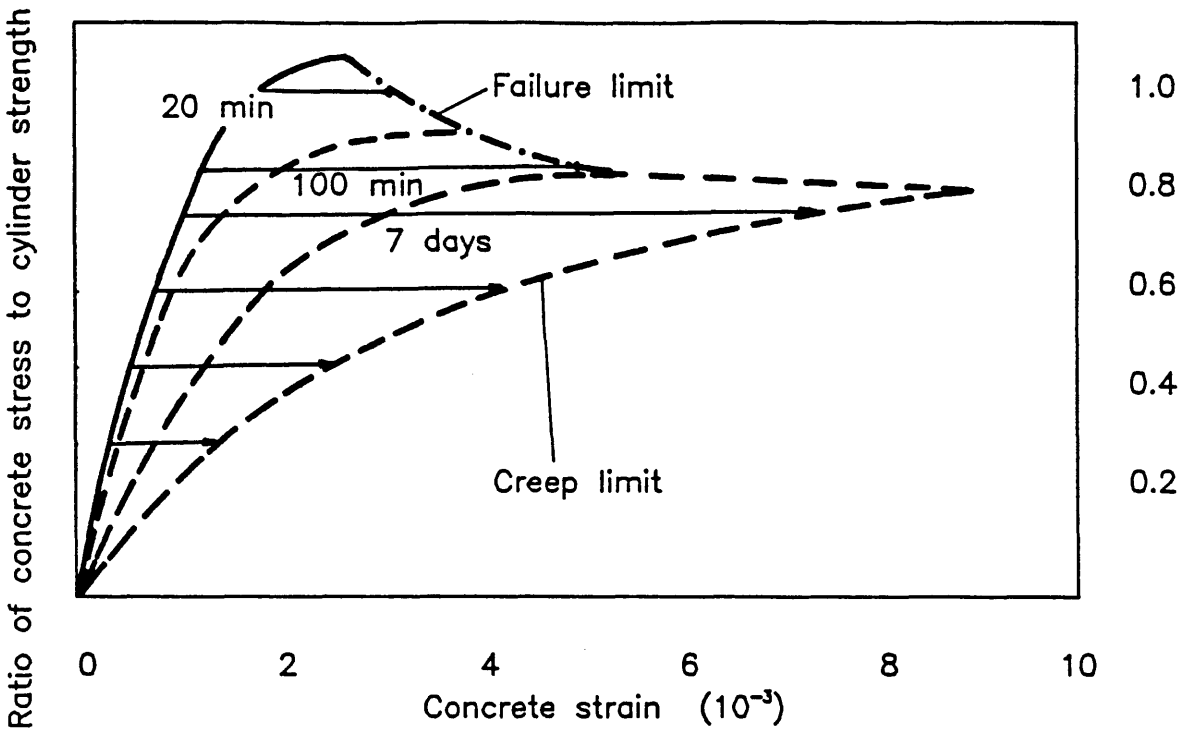

Fig. 3.18 Stress–strain curves for concrete subjected to various levels of compressive stress [92]

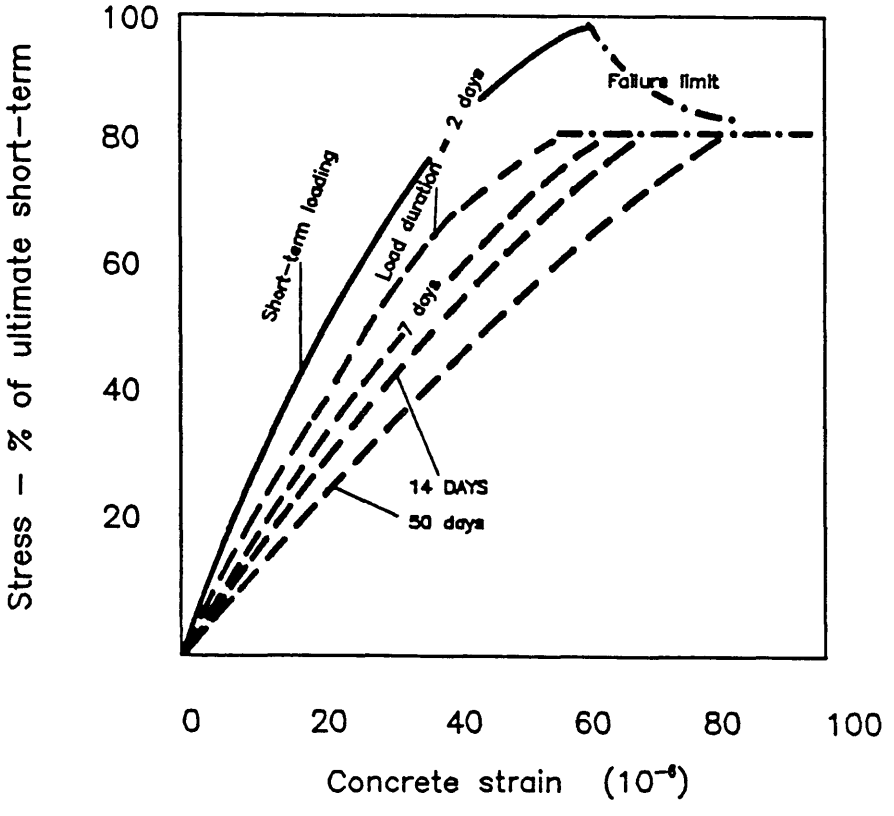

Fig. 3.19 Stress–strain curves for concrete subjected to various levels of tensile stress [88]

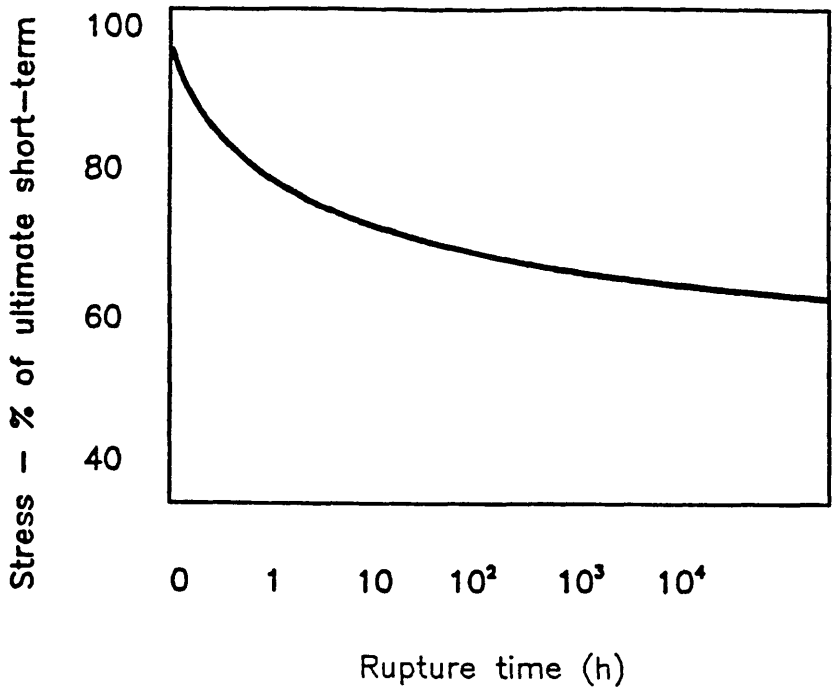

(a) Influence of sustained tensile load upon time to rupture

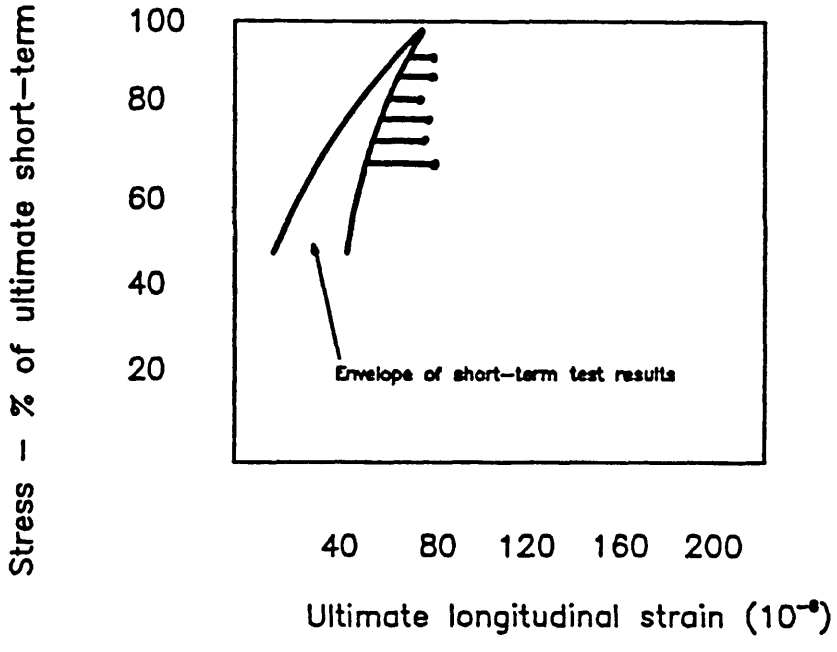

(b) Influence of sustained tensile load upon ultimate strain

Fig. 3.20 Influence of sustained tensile load upon creep behaviour of concrete [89]

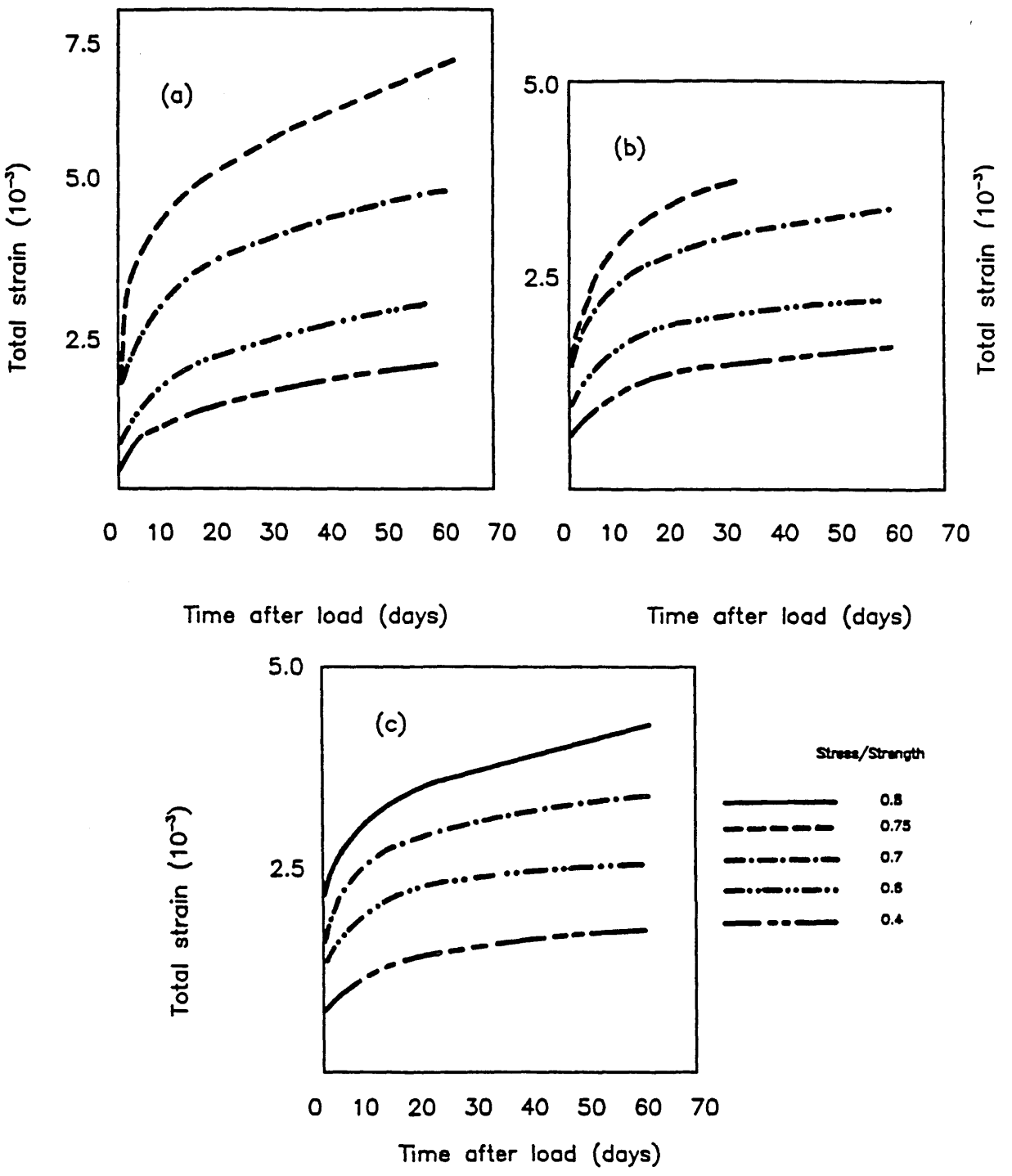

Fig. 3.21 Total strain versus time for (a) low, (b) medium, and (c) high strength concrete under sustained uniaxial compressive stresses [86]

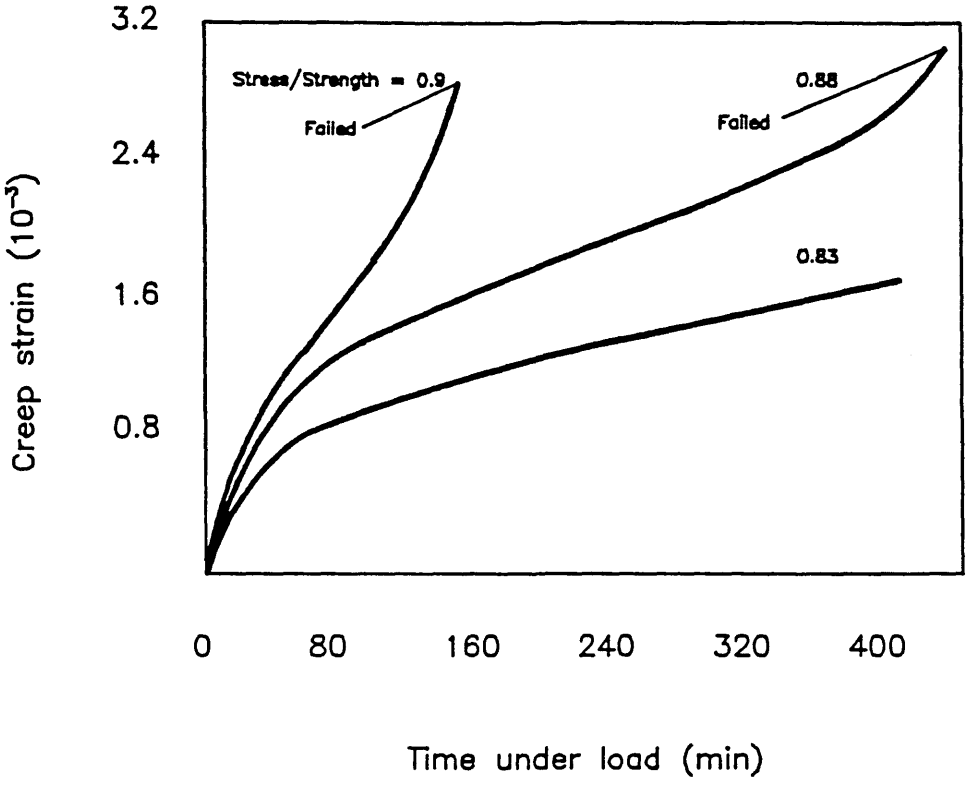

Fig. 3.22 Typical creep curves of steel fibre reinforced cement matrices at high stress–strength ratios [85]

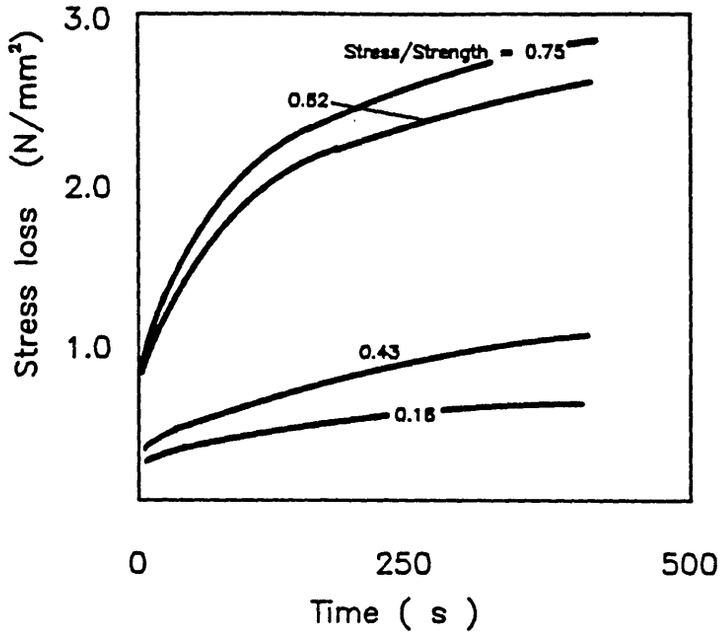

(a) Relaxation curves for high strength dry concrete

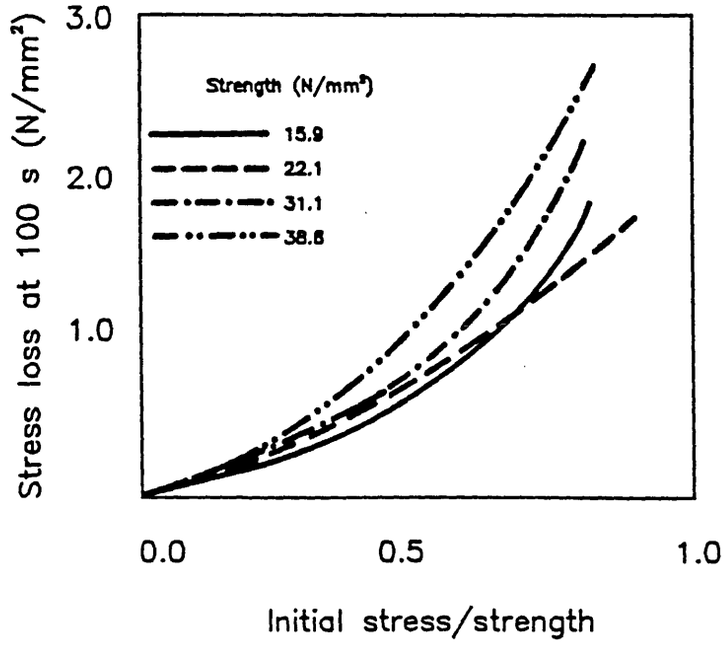

(b) Stress loss versus stress–strength ratio for dry concretes

Fig. 3.23 Variation of stress loss for dry concretes [93]

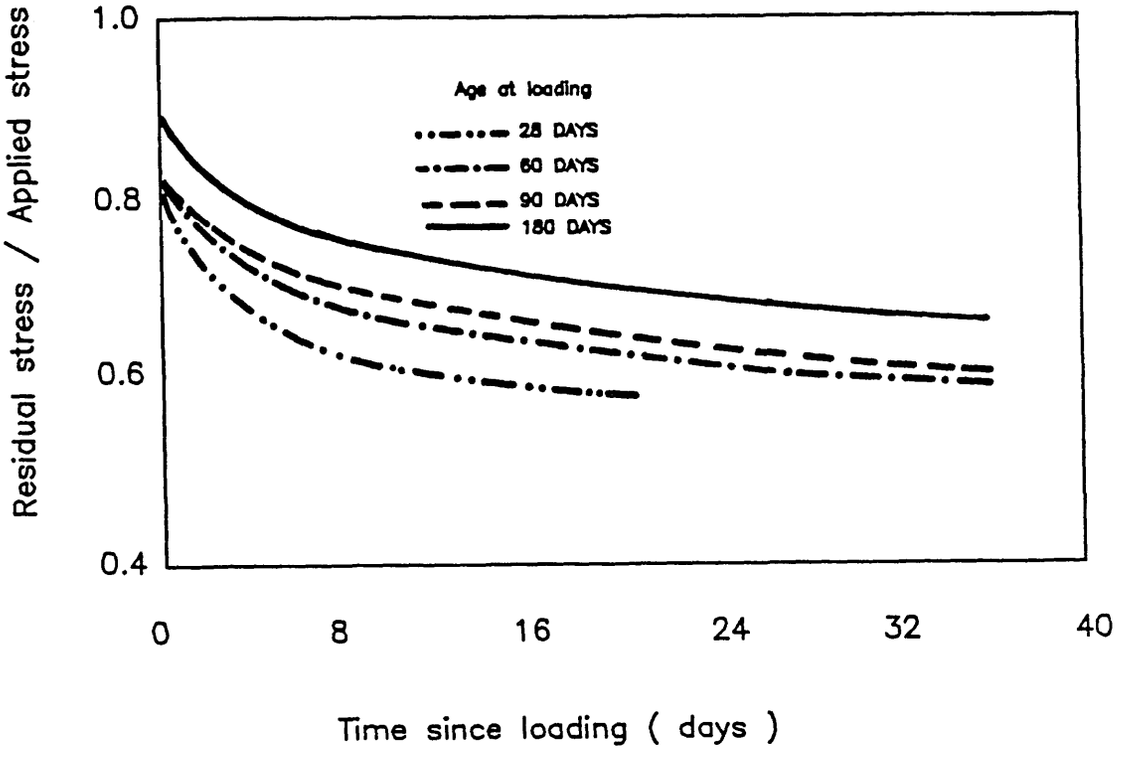

Fig. 3.24 Residual stress versus time for concrete specimens [94]

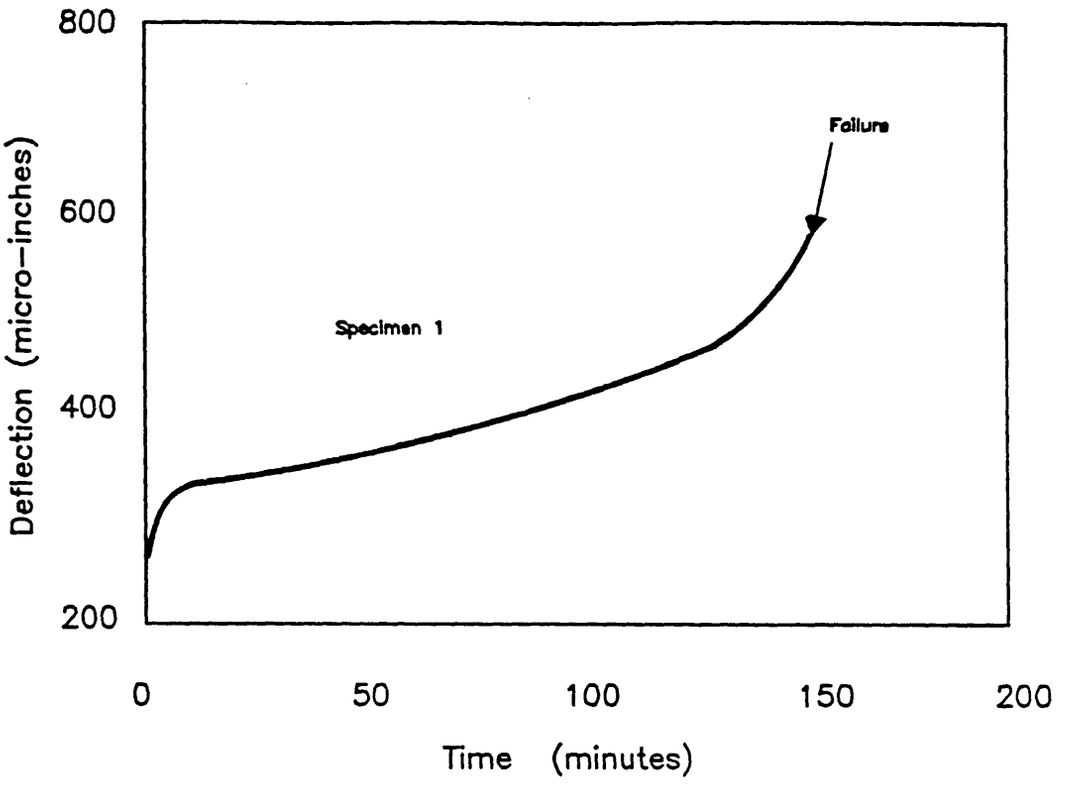

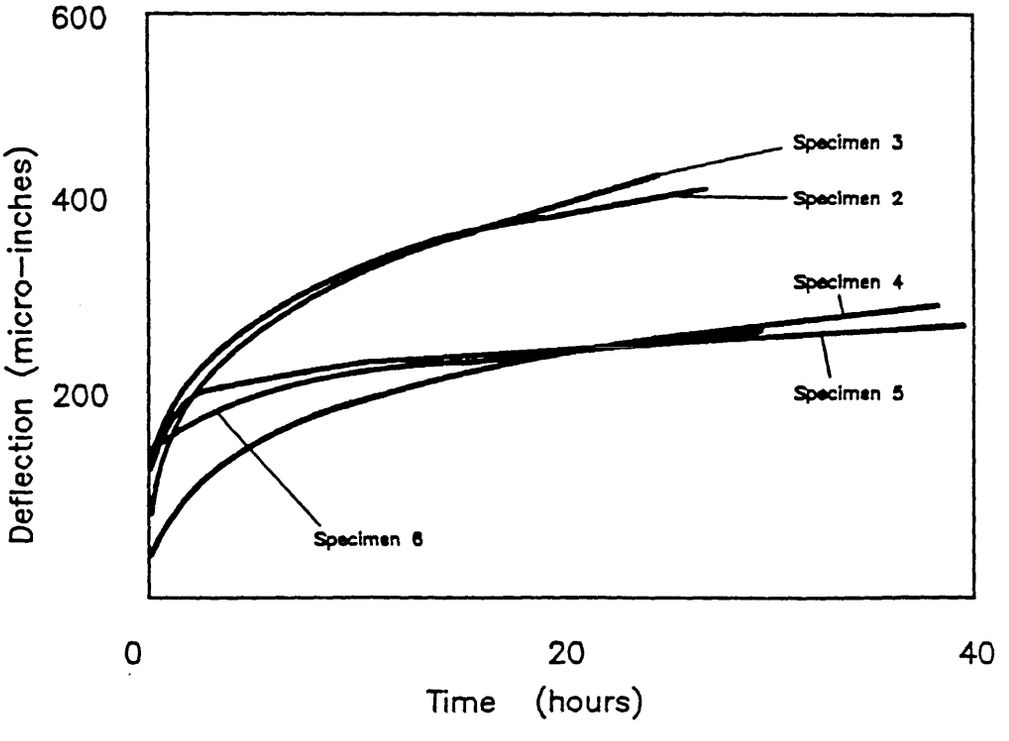

Fig. 3.25 Deflection under constant load for shale specimens [99]

CHAPTER IV

TIME–INDEPENDENT BEHAVIOUR OF A DISCRETE PROGRESSIVELY FRACTURING MODEL

4–1 The Model

A model material was devised and studied [3,126] in order to understand the behaviour of the ideal progressively fracturing solids (chapter II). Although the model material is discrete, and hence does not necessarily follow the continuum theory of progressively fracturing solids, its overall response to loading is very much similar to that expected for an ideal progressively fracturing solid.

The model material is taken to be a planar pin–jointed frame of bar elements capable of transmitting axial forces only. The structural behaviour of the truss is analysed by a simple finite element formulation. The structural geometry, member properties, and constitutive laws used to relate stresses and strains within the bars, are all stored in the computer memory for the analysis of the model under specific boundary and loading conditions.

The behaviour of the individual bar elements is taken to be linear elastic with failure occurring in a brittle fashion when stress within the member exceeds a specified value. Although the geometry is in the form of a simple braced network, the properties of the members are chosen to vary in a random manner with given means and standard deviations. This would result in an overall nonlinear response with accompanied strain softening even if the chosen network was of a regular geometry.

Essential to the formulation of this model is a random number generator routine. This computer routine will produce a random number (between zero and unity) such that if the routine is called n times then a set of n random numbers is obtained. The same set can be reproduced provided the routine is called with the same variable (initializing parameter). Different sets can be attained by assigning different values for the initializing parameter. Another routine was used which yields a set of random variables having a given mean and standard deviation from a normal distribution. Again an initializing parameter is used to insure reproducibility.

The feature of the approach is that, although the structure generated

by the various procedures is apparently random and properties vary from member to member in a random fashion, the description of the structure can be reproduced identically if so desired by merely restarting the process with the same initializing parameters. This has the advantage over physical testing in that different kinds of tests or loading sequences can be undertaken on samples which are truly identical even at the structural level.

Following generation of the model, the material sample is subjected to a prescribed sequence of boundary loading, imposed displacements, or thermal loads. The model is analysed in an incremental manner with member failure being recorded at each stage and with the appropriate modification of the material stiffness. In this way the behaviour of the material model is explored for a variety of loading.

The following paragraphs give details about the generation of the network model and the process of analysis. The methods used in generating the geometry, member properties, and loading and boundary conditions are described.

4–1–1 Geometry

A square matrix (42.0 × 42.0 units of length) is chosen to represent a sample of the model material. For N joints to be randomly dispersed in the matrix, a pair of random numbers, each between zero and one, is associated for each joint. Each pair of variables represents, after scaling to 42.0, the coordinates of the joint in the square with the lower left corner as the origin of the coordinate system.

With N joints, N(N–1)/2 potential members in the network exist. In order to reduce the density of the network, a control is imposed on members longer than a specified length L_c. The function

$$B_i = D_m (1.0 - L_i/L_c) \qquad (4.1.1)$$

where D_m is a parameter controlling members density, is calculated for each member of length L_i (i = 1, N(N–1)/2). For each member in turn, a random number R_i (between zero and one) is compared to B_i and the member is eliminated if R_i exceeds B_i. Thus, the complete geometry of the planar network can be generated and reproduced by specifying the network parameters N, D_m,

and L_c. Also, specifying the initial values of the random numbers generator routine is essential for the structure to be exactly reproducible.

4–1–2 Members

The structural members in the network are simple planar pin–jointed bars capable of sustaining axial loads only. Figure 4.1 depicts some typical networks used in the present work. The material properties and the constitutive laws for these bars are stored in the computer memory before analysis commences.

An elastic/brittle constitutive law for the members is used so that

$$F_i = \begin{cases} \dfrac{A_i E_i}{L_i} \Delta L_i & \text{for intact members.} \\ 0 & \text{for failed members.} \end{cases} \qquad (4.1.2)$$

where the stress and strain in the member are given by

$$\sigma_i = \frac{F_i}{A_i} \text{ and } \epsilon_i = \frac{\Delta L_i}{L_i} \qquad (4.1.3)$$

and where F_i is the force and ΔL_i the elongation within the i^{th} member. A_i, E_i, and L_i are the area, elastic modulus, and length of the i^{th} member. ΔL_i is its elongation.

If prescribed strains are imposed on the bars then expression 4.1.2 can be replaced by

$$F_i = \begin{cases} \dfrac{A_i E_i}{L_i} (\Delta L_i - \Delta L_i') & \text{for intact members.} \\ 0 & \text{for failed members.} \end{cases} \qquad (4.1.4)$$

so that the stress and strain within the member become related by

$$\sigma_i = \begin{cases} E_i(\epsilon_i - \epsilon_i') & \text{for intact members} \\ \\ 0 & \text{for failed members} \end{cases} \qquad (4.1.5)$$

where $\Delta L_i'$ is the prescribed deformation for the i^{th} member and $\epsilon_i' = \frac{\Delta L_i'}{L_i}$ is the corresponding prescribed strain.

For each of the member properties (area, elastic modulus) a set of values following a normal distribution is produced, with a specified mean and standard deviation. The distributions are truncated so that only positive values are assigned.

Since the network is tested by the computer, then any computationally measurable quantity can be used as a failure criterion, in the sense that a member is considered to have failed if this chosen variable exceeds a specified failure limit. In other words, the truss is built up such that quantities like stress, strain, stored energy, and others are monitored so that a member is disregarded in all subsequent steps of analysis if one of these quantities exceeds a critical value.

In the case of the network tested under controlled deformations or applied forces, the members behave in a linear elastic manner until failure (4.1.2, 4.1.3). Whether the failure criterion is taken as stress, strain, stored energy, or work done by the member is immaterial. Let σ_f, ϵ_f, and W_f denote the values of stress, strain, and work done per unit volume by a member at failure. Then

$$\sigma_f = E\,\epsilon_f \quad \text{or} \quad \epsilon_f = \frac{1}{E}\,\sigma_f \qquad (4.1.6)$$

and

$$W_f = \int_0^{\epsilon_f} \sigma\, d\epsilon = \frac{E}{2}\,\epsilon_f^2 = \frac{1}{2E}\,\sigma_f^2 \qquad (4.1.7).$$

Equations 4.1.6 and 4.1.7 show that fixing a critical limit of stress will result in fixed values of strain and work done at failure.

For the case of a fixed prescribed strain, ϵ', together with the applied

strain, equations 4.1.6 and 4.1.7 become

$$\sigma_f = E(\epsilon_f - \epsilon') \quad \text{or} \quad \epsilon_f = \frac{\sigma_f}{E} + \epsilon' \tag{4.1.8}$$

and

$$W_f = \int_{\epsilon'}^{\epsilon_f} \sigma \, d\epsilon = \frac{E}{2}(\epsilon_f - \epsilon')^2$$

$$= \frac{\sigma_f^2}{2E} \tag{4.1.9}.$$

Again in this case, all values at failure are uniquely determined since they can always be expressed in terms of the element parameters (A, E, and L) and of σ_f (for example). Thus the choice of a failure criterion is purely based on practicality and all potential criteria (stress, strain, and work done per unit volume to failure) are identical and interchangeable. It should be noted that for each element the strain, to be compared with the critical strain, is to be measured from the prescribed value ϵ' rather than from the state of zero strain.

For each of the bar elements a critical value of the stress σ_f is chosen so that if the tensile stress reaches a value σ_f or if the compressive stress reaches $-\beta\sigma_f$ then the member is considered to have failed. σ_f is chosen from a truncated normal distribution with only positive values assigned. β is the ratio of compressive to tensile strength.

4–1–3 Loading and boundary specifications

Tests simulating strain controlled uniaxial tensile conditions were performed. Because of the computational and geometric difficulties that arise if an exact line edge of the random network is used, boundary regions are defined. It is in these regions where the prescribed or suppressed displacements are imposed.

Figure 4.2 shows the "free end" boundary specifications used. It is equivalent to ideal frictionless loading conditions.

The two linear dimensions **a** and **b** in figure 4.2 are chosen for each network so that enough connectivity between boundaries of the network and its centre exist, without having the core too small. In zone (1), where vertical

displacements are prevented, one node was restrained from lateral motion. Otherwise the solution to the problem becomes computationally impossible.

Strain is defined as follows; let Y_1^0 and Y_2^0 be the initial averages of ordinates of all nodes in zones (1) and (2) respectively (figure 4.2). If at a certain stage of loading the above averages become Y_1 and Y_2 ($Y_1 = Y_1^0$ always), then the longitudinal strain ϵ_{yy} becomes

$$\epsilon_{yy} = \frac{(Y_2 - Y_1) - (Y_2^0 - Y_1^0)}{(Y_2^0 - Y_1^0)} \qquad (4.1.10).$$

The lateral strain is defined in a similar way. Two zones (4) and (5), that run along the edges x = 0 and x = 42, are chosen with widths **c** and **d** respectively. The lateral strain becomes

$$\epsilon_{xx} = \frac{(X_5 - X_4) - (X_5^0 - X_4^0)}{(X_5^0 - X_4^0)} \qquad (4.1.11)$$

where the terms X_5 and X_4 are the averages of the current abscissas of all nodes in zones (5) and (4) respectively. The terms X_5^0 and X_4^0 represent the initial averages of the abscissas of nodes in these two zones.

Stress σ_{yy} is calculated by computing the reactive force at the boundary zone (1) (by summing the resolved member forces) and dividing it by the width of the network (42.0 units).

If the network is tested under conditions simulating temperature controlled testing, then nodes in zone (2) are no longer given prescribed deformations. Loading is achieved by applying a constant temperature, at any time, to all members. For a member of length L_i, a temperature T will induce a thermal strain

$$\epsilon_i' = \alpha_i T \qquad (4.1.12)$$

in addition to strain due to stress in the member. Here, α_i is the thermal coefficient of linear expansion for the i^{th} member chosen from a truncated normal distribution with a given mean and standard deviation.

In undertaking the analysis, it is convenient to deal with thermal effects by using additional forces applied to the nodes in the direction of the

members. Thus, if temperature is imposed on the network model, analysis is dealt with by transforming the strains induced into equivalent nodal forces.

The term $\alpha_i T$ (equation 4.1.12) for each member can also be regarded as an alternative strain expression not determined by temperature if so required. Thus, problems of induced strains, members incompatibilities, and shrinkage can be eased. To study the response of the model to controlled deformations with initial incompatibilities each member is given an incipient deformation $\Delta L_i'$ prior to any loading. Equivalently, a constant temperature T can be imposed on the network at all stages of loading with $\Delta L_i'$ given by

$$\Delta L_i' = L_i \alpha_i T \qquad (4.1.13).$$

The problems of strain controlled tests on the network model with a constant imposed temperature T and that with an initial lack of fit $\Delta L_i'$ (members being too long or too short) are identical, provided the values of α_i are chosen so that (4.1.13) holds. Boundary specifications are the same as those leading to (4.1.10) and (4.1.11).

This completes the description of the model. In summary, the model is completely defined if its geometry, member properties, member stress strain laws, boundary and loading conditions are prescribed. These data are stored in the computer memory prior to the analysis phase.

4–2 Analysis of the network model

4–2–1 The network model under controlled deformations

For the analysis of the network model under controlled deformations, a linear elastic stiffness method is followed (figure 4.3). At any stage of loading the frame is analysed in a stiffness matrix form. The matrix is modified to accommodate boundary conditions. Imposed boundary displacements are transformed into nodal forces. The matrix form problem can then be solved for the unknown joint displacements.

For each member the stress σ can then be calculated and compared to its failure stress limits σ_f and $-\beta\sigma_f$. If σ lies outside these limits, the member is considered to have failed and its secant modulus of elasticity is set to zero in all subsequent steps of analysis.

Loading is discretized by applying the imposed boundary displacements in increments. If, during the analysis of an incremental boundary displacement, any member fails, the structure is reanalysed for the same boundary displacements with the elastic stiffness of the failed member set to zero. For situations in which more than one member would fail within a single increment, the increment of boundary displacements is reduced (halved) until only one member fails. This is normally possible unless the sample is behaving in an unstable fashion and failure is propagating rapidly throughout the sample.

At the end of each step of analysis the average stress in the sample as well as strains are calculated as indicated in section 4–1–3.

Networks with an initial lack of fit or with uniform constant temperature applied to all members throughout the test, are also analysed by the same method except that the strains imposed by these incompatibilities are also transformed into nodal forces before matrix analysis (figure 4.4).

4–2–2 The network model under temperature loading

Under temperature loading, no prescribed displacements are imposed. Instead, the structure is analysed for a sequence of temperatures. The analysis is very similar to that described in section 4–2–1. A simple stiffness matrix structural approach is followed (figure 4.5).

At any loading stage, corresponding to a temperature, the structural matrix is modified to accommodate boundary conditions. Member strains induced by temperature are transformed into nodal forces.

The stiffness matrix is then solved for the unknown nodal displacements. As before, stresses in members are calculated and compared to failure limits. If any member fails in the analysis step, then the network is reanalysed for the same temperature, with the modulus of elasticity of the failed member set to zero.

4–3 Tests and results

4–3–1 General behaviour

The first series of tests carried out on the network model (figure 4.1) were intended to review the general behaviour described earlier [3,126] under conditions simulating uniaxial tensile strain controlled tests. The stress–strain curves followed by a typical network (figure 4.1 (c)) are depicted in figure 4.6.

The network tested (figure 4.1 (c)) has 16 nodes connected by 83 members. The average values of the members elastic modulus E, area A, and failure stress σ_f are 60.0, 10.0, and 0.1 units respectively. The standard deviation of any distribution is taken to be 20% of its average value. The choice of relatively large standard deviations is necessary to provide a network with enough heterogeneity in material properties. Each side of the square matrix containing the network is 42.0 units with a, b, c, and d (dimensions defined in figure 4.2) being 4.6, 4.0, 5.0, and 5.5 respectively. This was found to ensure ample connectivity of the members with the boundary zones. The ratio of the compressive failure limit to the tensile limit, β, was taken as 100 so that the emphasis be on tensile failure.

Figure 4.6 presents the variation of the longitudinal stress σ_{yy} (or merely σ) with both the longitudinal and transverse strains ϵ_{yy} and ϵ_{xx}, under increasing longitudinal strain ϵ_{yy}. The plot of σ versus ϵ_{yy} presents a material with three modes of behaviour; an initially linear elastic response, degradation with an increase in stress (hardening), and degradation with stress reduction (strain softening).

Sharp vertical jumps in the stress strain curves are noted. These are due to the failure of members resulting in subsequent decrease of the overall stiffness of the network. As long as no members fail upon an increase of strain, stress increases linearly with strain even in the post peak portion of the behaviour. This is a characteristic of the network model.

At any stage of loading the model is linearly elastic such that upon reversal of the sense of applied deformations the network unloads in a linear elastic fashion to the state of zero stress and zero strain. Thus, the stress strain relationship of the model can be expressed by

$$\sigma = S_1 \epsilon_{yy} = -S_2 \epsilon_{xx} \qquad (4.3.1)$$

where S_1 and S_2 are the the reciprocals of the compliance moduli.

As the network is strained, more and more members fail resulting in the degradation of the overall stiffness. The decrease of the overall stiffness with increasing strain ϵ_{yy} is shown, by plotting the reciprocals of the compliance moduli, S_1 and S_2, with applied loading (figure 4.7). Upon unloading, both moduli remain unchanged until reloading to a strain ϵ_{yy} exceeding the maximum value attained prior to unloading.

Both the hardening and softening modes of behaviour of the network model are a direct result of the failure of members and the heterogeneous degradation of stiffness. The network is always stable even in the softening mode. If, at any stage, the strain is held unchanged then the stress also remains unvaried and no damage will be induced leaving the network in stable equilibrium.

The sequence of failed members is shown in figure 4.8, where the centroids of the failed members are plotted at various stages of loading. Failed members tend to be fairly well distributed through the network at early stages of loading but tend to cluster and fail in localized zones as strain is increased especially in the post peak portion of the stress strain curve. At or near complete failure, zones of failed members tend to be highly localized leaving the rest of the network fairly intact. A "tear" spreading across the network in the transverse direction is noted. This is shown in figure 4.9 which depicts the configuration of the network before and after loading.

It is interesting to note that, for the particular network of figure 4.1(c), localization is only observed at high strain levels in the post peak portion of the response. For some other networks tested (response not presented) localization was observed to start at or before the peak stress was attained but intensified in the softening mode.

This localization of failure in a limited zone leaves the rest of the network to unload elastically, and the combined behaviour of the two zones results in the overall strain softening of the network.

Figure 4.10 shows the strain path followed by the network model under

increasing longitudinal strain ϵ_{yy}. The transverse strain ϵ_{xx} starts to increase with ϵ_{yy}, reaches a maximum and then decreases again (in absolute value). At any stage of loading, if the sense of imposed deformation is reversed, the strain path follows a straight line passing through the origin of strain plane.

The response depicted by the σ–ϵ_{xx} curve (figure 4.6) suggests that instability in the post peak behaviour of the network model can occur if the loading conditions are such that transverse strain is increasing at a decreasing stress while the model can only unload (its strain). This behaviour is detected for real physical materials (section 2–1) and hence the instability in the post peak portion of the stress–strain curves can be thought of to be a result of damage that under certain loading conditions can only be stabilized by unloading.

The post peak portion of the σ–ϵ_{xx} curve (figure 4.6) is characterized by two modes of behaviour. A stable strain softening response, where ϵ_{xx} increases with decreasing stress σ, is noted after which ϵ_{xx} starts also to decrease. This "inelastic unloading" in the transverse direction can be understood to happen due to the formation of large transverse "tears" that leave the rest of the network to unload longitudinally. At failure, the network would have been split transversely into two fragments each of which has a state of zero stress and strain in all directions. Further increase in ϵ_{yy} is possible through rigid body displacement leaving the whole network in a state of zero stress and zero transverse strain ϵ_{xx}. Thus after a certain stage of loading and before complete failure, the network starts to unload in the transverse direction.

The failure of any member results in the decrease of the overall stiffness of the network and hence in the reciprocals of the compliance moduli S_1 and S_2 (equation 4.3.1). Very small unloading reloading cycles follow members failure in the σ–ϵ_{xx} curve as a result of the network unloading (in the transverse direction) with a decreasing modulus S_2 until failure. This unloading is not linearly elastic, but is composed of small steps (cycles) each of which is linear elastic with a constant value of the modulus S_2, which decreases from one cycle to another as members fail. At or near failure, ϵ_{xx} becomes close to zero and S_2 becomes undefined. This was also computationally detected and thus values of S_2 at high levels of ϵ_{yy} are not plotted (figure 4.7).

The behaviour of the network model may seem unusual or unrealistic because of its discrete nature and hence the discrete jumps observed in its response.

This phenomenon, resulting from the discrete nature of the model, can be reduced in its diversity if the network model is given larger number of nodes and members, and smaller dimensions. Jumps would still exist but their value would be small compared to the overall response. Figures 2.1 and 2.8 show that the response of rock and concrete to applied displacements does exhibit finite jumps in the load response.

Degradation of stiffness, progressive failure, hardening, and strain softening are all detected in the behaviour of physical materials (section 2–1). Materials like concrete and rocks do not normally unload to zero strains. Residual strains are detected upon the removal of stresses. These are attributed usually to plastic deformations associated with slip at the material level.

The network model, as well as the progressively fracturing solids continuum theory, ignore plastic slip and are incapable of describing the formation of residual strains. Hence, the degradation of stiffness is larger than that detected for real materials.

Real materials that do exhibit the modes of behaviour detected in the response of the network model (or predicted by the ideally progressively fracturing solids theory) can be considered as a transition between the two extremes of the fracturing and plastic idealizations.

Another significant phenomenon observed in real physical materials is that of localization of failure. This was found to be characteristic of the network model and might give an insight on the mechanisms of localized behaviour observed in real materials under loading. The mechanism of localization observed in the network model can be understood by studying the response of the network model to loading (figure 4.6) and the distribution of failed members at various stages of loading (figure 4.8). If the plot of the centroids of failed members is thought of as a plot of cracks in the sample material, then damage across the sample can be attributed to the formation and distribution of such cracks.

Initially, at low levels of loading, cracks are well distributed across the sample. With increasing applied displacements, a "tear" starts to develop at or near the peak stress. If loading is continued, the tear would develop and increase

in size with the rest of the sample developing little cracking. Near complete failure, applied displacements will result in widening of the tear until complete separation of the sample into parts that are left to unload elastically. The elastic unloading of the separate halves will result in the decrease of the overall transverse strain ϵ_{xx} down to zero at complete failure. At the same time, the formation of this "tear", results in the capability of the network to undergo large strains in the longitudinal direction before complete failure.

4–3–2 Dependence of the response on the strain path

The response of the network model is path dependent. The stress state of the material model is dependent on both the strain state and the strain path followed up to that state.

The stress σ, in the case of the uniaxial tensile tests, is defined by the strain ϵ_{yy} and the reciprocal of the compliance modulus S_1 which is a function of the maximum value of ϵ_{yy} the network has experienced.

Figure 4.11 shows three different paths followed, by a typical random network (figure 4.1 (c)), to the same strain state as defined by ϵ_{yy} and ϵ_{xx}. The first path corresponds to to a test simulating uniaxial tensile conditions. The second path comprises two portions. The network is strained first in the y–direction to a specified value of ϵ_{yy} with the strain ϵ_{xx} kept at zero. Then it is strained in the x–direction with ϵ_{yy} kept at the previously attained value. The third path is reciprocal to the second one with x and y–directions interchanged.

All the paths are distinct from each other but they all terminate at the same strain state. Figure 4.12 shows the corresponding stress paths followed. As seen in the figure, three different states of stress are attained by the three strain paths eventhough the strain states corresponding to these stress states are identical.

It should be pointed out that the above example of path dependence is conditioned by localization of failure. As the network is strained, tears perpendicular to the direction of straining start to occur and extend. This leaves the state of damage of the network dependent on the direction and magnitude of strains applied up to that state. It is thus logical to expect that the higher the level of the applied strains, the more the network becomes path dependent in the

sense that the states of stress, following different strain paths to the same strain states, become more different from each other.

4–3–3 Behaviour of the network model with initial incompatibilities

In this series of tests an additional heterogeneity is applied to the network initially before any loading. The members of the network are considered to be initially incompatible with nodal geometry prior to imposed deformations. This will cause initial internal strains in the members and in the network as a whole.

This can be achieved by applying a constant temperature T to all members throughout deformation history so that at any stage of loading each member has a constantly prescribed internal strain (equivalent to members being too long for a positive value of T). For each member this strain is given by equation 4.1.12. The values of the thermal coefficients of expansion were taken from a normal distribution with an average value of 10^{-4} and a standard deviation of 2×10^{-5} (20% of the average value). All other properties of the members, and the network's boundary specifications are identical to those used in the uniaxial tensile tests.

Figure 4.13 shows the behaviour of a typical network (figure 4.1 (c)) with an initial lack of fit imposed by a constant temperature T (T = 5.0 units of temperature). It is noted that the initial stress free state of the network no longer corresponds to a state of zero strain. A strain due to the initial lack of fit does exist. Upon loading, members break and the network degrades resulting in a decrease of its stiffness. If the sense of imposed deformations is reversed, the network unloads in a linear elastic fashion to a residual strain (over and above the initial non–zero strain).

At any level of damage following loading, the state of zero stress corresponds to a strain ϵ^{r}_{yy} given by

$$\epsilon^{r}_{yy} = \forall T \qquad (4.3.2)$$

where $\forall$ is the network's equivalent coefficient of thermal expansion.

Figure 4.14 depicts the variation of $\forall$ at constant values of T with increasing applied strain ϵ_{yy}. It is noted that the value of $\forall$, and consequently the value of the residual strain ϵ^{r}_{yy}, are functions of the temperature T and the

maximum strain applied to the network. In short, $\forall$ is a function of the damage caused by both the initial incompatibilities and the imposed deformations. An overall increase in $\forall$ was observed at high levels of imposed strain even though the value of $\forall$ was found to decrease at some instants with increasing ϵ_{yy}.

It should be noted that the initial state of zero stress not only corresponds to a state of non–zero strain but to a state of initial damage. This is due to the existence of failed members, the number of which is dependent on the degree of initial lack of fit (i.e. the imposed temperature T), and the distribution of which is dependent on the properties of the members. Figure 4.15 shows the behaviour of the network model under different imposed temperatures. The curves are all shifted to the point of stress free state which is taken as the datum of strain for all tests.

Initially, before any deformations are imposed on the network, the sample is already damaged due to strains resulting from the lack of fit. The initial slope of the stress–strain curve was found to decrease, indicating more broken members, with an increasing imposed temperature. The load bearing capacity of the network as measured by the peak stress was also found to decrease with an increasing applied temperature. The solid line curve of figure 4.16(a) show the decrease of peak stress with an increase in the initial incompatibilities as measured by the applied temperature T. No specific trend for the change of strain at peak stress was noted (solid line in figure 4.16(b)).

The mode of failure of the network changes with changes in the initial lack of fit or equivalently the applied temperature. As the applied temperature is increased, the network was found to fail progressively in a more ductile fashion with the softening branch of the stress–strain curve becoming less steep. Figure 4.18 shows the stress strain curves of a typical network (figure 4.1(c)) at three different levels of initial incompatibilities imposed by three different values of temperatures. The centroids of broken members at failure are also shown. At higher levels of temperatures, a more dispersed nature of the distribution of centroids of broken members is observed indicating distributed damage..

With an increasing initial degree of lack of fit, the network model tends to have a larger initial strain at the stress free state, a smaller initial stiffness when load is applied, a smaller portion of strain hardening behaviour, a smaller load bearing capacity (peak stress), and a more ductile mode of failure with a milder slope in the strain softening portion of the stress–strain curve. Plots of the

centroids of the broken members show that at higher values of applied temperatures "tears" tend to form at different, rather than localized, locations in the network.

Damage, resulting from members breakage, is a function of not only the applied deformations but also the degree of the lack of fit imposed on the network, which causes an increase in the heterogeneity of the model material.

A stationary initial incompatibility imposed on the behaviour of the network model is realistic. Both ambient conditions and internal reactions (for example shrinkage) will result in incompatibilities at the material level when concrete, for example, is tested in uniaxial tension.

These incompatibilities result , in the case of the network model, in the loss of memory of the initial state and hence in residual strains upon unloading. This can not be detected directly for physical materials because plastic deformations, occurring in materials like rock and concrete, will result in similar phenomena.

Nevertheless, the behaviour of the network model, if physical materials are assumed to behave as a result of both fracturing and plastic deformations, suggests that residual strains detected upon unloading of physical solids should not be completely attributed to plastic slip, but to the initial incompatibilities (inherent in solids like concrete) and damage caused by internal and imposed strains as well.

4–3–4–Behaviour of initially damaged networks

It is interesting to look at the effect of an initial damage on the behaviour of the network model. If, in figure 4.6, the network is deformed to a strain ϵ^m_{yy} (and the corresponding stress σ^m) and then the applied deformations are completely removed (elastic unloading), the network is then in a damaged state the value of which is dependent on ϵ^m_{yy}.

If this damaged network is loaded by applied controlled deformations, then stress will increase in a linear elastic fashion from the state of zero stress and zero strain up to the state of strain ϵ^m_{yy}. At ϵ^m_{yy} the stress state will be σ^m. Any further deformations, beyond ϵ^m_{yy}, will result in a stress–strain curve

identical to the portion of figure 4.6 starting from ϵ^{m}_{yy} to complete failure.

In another series of tests the network was heated up to a certain temperature T, cooled back to zero temperature, and then tested under conditions simulating uniaxial tensile testing. The tests are the same as those performed before on the network model (section 4–3–1) except that all elastic moduli of members broken due to heating–cooling prior to loading are set to zero.

Whatever the level of temperature applied to the network prior to loading, all members are fully compatible with nodal geometry in the sense that the state of stress free network corresponds to a state of zero strain (provided the applied temperature is removed). Nevertheless, the network is originally damaged prior to any deformation.

Figure 4.19 presents the behaviour of the network (figure 4.1(c)) under uniaxial strain controlled tensile loading, following a cycle of heating and cooling up to different maximum temperatures.

As the temperature T applied prior to (and not during) loading is increased, more damage is inflicted on the network model resulting in a decrease in the initial elastic modulus (figure 4.17 (b)), and the load bearing capacity. Figure 4.16(a) (dashed lines) shows the decrease in the value of peak stress with an increase in the initial damage as measured by the maximum applied temperature T prior to loading. Again, no trend for the strain at peak stress is noted (figure 4.16(b)).

Comparison of the results obtained in this series of tests and those obtained when the temperature was kept through deformation history (section 4–3–3) shows that for the same temperature the network has a higher value of peak stress when temperature was removed prior to loading (figure 4.16). The maximum temperature that can be applied to the network during deformation is much less than that that can be applied (and removed) prior to applied deformations. Any applied temperature above this limit renders the network unstable and uncapable to carry any additional deformations without instantaneous failure.

In figure 4.20 the centroids of broken members before and after loading to failure are plotted for three different temperatures applied and removed before straining. Damage, assessed by the intensity of broken members, before any

loading is larger for higher values of T. It tends to be fairly dispersed through the network with no large tears formed along any favourable direction.

After load is applied to the network, more members tend to fail and transverse tears tend to form. The diversity of such tears depends on the initial damage. The less the value of T, and thus the less the initial damage, failure tends to be more of a localized nature.

Damage can be thought to occur as a result of two factors: a well dispersed damage of a more or less homogeneous nature due to the temperature loading, and a localized damage caused by imposed deformations. The less the temperature applied, the more localized damage is allowed to occur when deformations are imposed. The network tends to behave in a less brittle fashion, with a milder softening slope when the initial applied temperature before loading is increased (figure 4.19).

The initial damage inflicted on the network model does not alter the qualitative behaviour upon deformation. The response is altered in terms of parameters like initial stiffness, peak stress, failure strain, and post peak softening slope in the stress–strain curve.

This suggests that the idea of path dependence (section 4–3–2) should be generalized into damage dependence. For this type of materials, the response is not affected by the path followed to a certain state as such, but actually is dependent on the damage inflicted while the material is following a certain path. This can be enhanced by factors other than deformation path, such as temperature, shrinkage, and lack of fit. The need to have a dimensional description of damage justifies the use of the strain path followed by such materials to measure the intensity of damage. If other factors are to be included, such as temperature, then equivalent damage parameters should be used.

4–3–5 Behaviour of the network model under temperature loading

Figure 4.21 shows the behaviour of a typical network (figure 4.1(c)) under an increasing temperature to failure with no applied deformations. Both the longitudinal and transverse strains ϵ_{yy} and ϵ_{xx} increase with increasing temperature. It should be noted that the terms transverse and longitudinal strains are merely used here for convenience and consistency with strain definitions in previous tests. Initially, the network behaves in an isotropic fashion

with both strains increasing linearly with temperature. Strains and temperature can be thus related by

$$\epsilon_{yy} = \forall_{yy} T \qquad (4.3.3)$$

$$\epsilon_{xx} = \forall_{xx} T \qquad (4.3.4)$$

where $\forall_{yy}$ and $\forall_{xx}$ are the equivalent thermal coefficients of the network in the y and x directions respectively. Initially both $\forall_{yy}$ and $\forall_{xx}$ are equal (provided the network is fairly randomly built up and thus initially isotropic). As the temperature increases, members start to fail causing possible changes in $\forall_{yy}$ and $\forall_{xx}$ and rendering them unequal.

At any level of temperature, if the network is cooled to zero temperature, it will return linearly to the state of zero strain.

Breakage of members results in possible changes in the values of $\forall_{xx}$ and $\forall_{yy}$. These changes cause discrete jumps in the temperature–strain curves. Jumps were found to occur both upward or downward meaning an increase or a decrease in the values of $\forall_{xx}$ and $\forall_{yy}$. Figures 4.22 and 4.23 show the variation of the coefficient of thermal expansion, $\forall_{yy}$, with the applied temperature T and the resulting strain ϵ_{yy}. The variation of $\forall_{yy}$ is somewhat arbitrary increasing or decreasing by vertical jumps (in temperature space) between which $\forall_{yy}$ remains constant. The initial value of $\forall_{yy}$ is very close to the average value (10^{-4}) of the coefficient of linear expansion of the members. Considering the number of failures that occur, it is certainly surprising that the changes in the values of $\forall_{xx}$ and $\forall_{yy}$ are not great.

Appendix A discusses the variation of the coefficient of thermal expansion of a system of elastic bars assembled in series or in parallel. It is seen that the coefficient of thermal expansion of a system of elastic fibres is a weighted average of the individual member coefficients. This average is insensitive to changes in the elastic moduli of the members in the case of a series assembly while it is sensitive in the case of a parallel assembly where a change in the stiffness of one or more members can result in an increase or a decrease in the overall thermal coefficient. Exceptionally, a change in stiffness could also leave the assembly's average coefficient unchanged.

The network model can be thought of as a combination of series and parallel assemblies or more realistically a random assembly between the two extremes.

The breakage of a member in the network results in a possible change in the overall coefficient of thermal expansion. The networks coefficient is thus a weighted average of the coefficients of the individual members. The weighting factors are related to members moduli, lengths, and orientations. Since the coefficients of linear expansion were taken from a set of normally distributed values with a specified mean, the averaging procedure suggests that even for a highly damaged network the overall coefficient of linear expansion will be close to the mean of this distribution. Hence the results obtained here are a consequence of the choice of allocation of member properties and would have been different if, for example, the coefficients of thermal expansion of the individual members were chosen from two (or more) sets of values having different means.

The overall structural stiffness of the network was measured at various levels of temperature by testing identical networks (with any failed member at the corresponding temperature given a zero elastic modulus) under uniaxial (temperature free) tensile conditions. The decrease of the reciprocal of the compliance modulus, S_1, with the applied temperature or its resulting strain are shown in figure 4.17 (initial slopes of the stress–strain curves in figure 4.19)

Plots of the centroids of failed members of the network model upon heating are shown in figure 4.24. Broken members are fairly well dispersed through the network at any stage of loading though they increase in intensity at high temperatures.

Localization is much less intense in the behaviour of the network model under temperature loading than under controlled deformations. This explains the small change in isotropy noted in the behaviour of the network model as seen in the strain path followed upon heating (figure 4.25). Figure 4.26 shows the configuration of the network near failure. Comparing figures 4.26 and 4.9 shows that under temperature loading failure is much less localized.

Temperature loading on materials like concrete results in complex effects on almost all material properties. The idealization presented here takes all temperature effects to be described by a single parameter $\forall$. Still the behaviour is capable of describing the degradation of stiffness with increasing temperature

detected for real materials [127].

For the changes in material behaviour due to thermal loading to be simulated by this model, a proper knowledge of the thermal effects on the material properties should be considered. No attempt is made here to achieve this. Temperature is merely considered to be an external variable other than strain that will cause damage in the model material. Hence it can be thought of as a damage parameter which in real terms can represent physical temperature, shrinkage, expansion, or changing internal incompatibilities.

The behaviour of real materials under applied temperatures does not fit the pattern of randomly distributed values of the coefficient of thermal expansion α_i in the present model. Concrete, for example, is a heterogeneous mixture of aggregates and cement and hence it would be more realistic to assume that the values of α_i belong to two randomly distributed sets each resembling one of these two constituents. With cracking in concrete occurring in the cement matrix, the overall coefficient of thermal expansion will eventually increase to that of the aggregates as a result of the averaging procedure described earlier.

4–4 Conclusions

The presented "network model" is by no means a representation of real physical materials nor a direct application of the continuum progressively fracturing solids theory presented in chapter II.

Still, the behaviour of this heterogeneous discrete model exhibits some modes of behaviour observed in real materials. The model will fail with stable progressive loss in stiffness under increasing deformations. It will exhibit both strain hardening and softening. It demonstrates the effects of heterogeneity in including size effects [3,126] and inducing localization of damage in a fairly small zone with the rest of the sample unloading.

This model behaves in a fashion similar to what is expected from the ideal progressively fracturing solid described by the continuum theory presented earlier. If localization is ignored, then the behaviour can always be attributed to the degradation of stiffness.

The discrete nature of the network model results in the finite jumps observed in the response to loading. If the number of nodes and members is increased infinitely and the size of the network is reduced to a point, then, in the limit, the network model will represent a point in a continuum described by the ideal progressively fracturing solids theory.

The behavioural aspects of the network model can thus be used to develop and refine the continuum model and increase its scope of applicability.

In summary, the network model is a progressively fracturing solid (though not an ideal continuum) and is path dependent, becomes more anisotropic with applied loading, loses the capacity to return to its initial state as a result of initial incompatibilities, depends in its behaviour on the initial state of damage, and is sensitive in its response under temperature loading to the degree of damage encountered.

The experiments performed on the network model suggest a number of ways in which the continuum theory of the ideal progressively fracturing solids should be extended. For the continuum model presented in chapter II to be more general the stress–strain relation in equation 2.3.1 should be expressed in terms of strain from the state of zero stress and the damage function used in the formulation of the constitutive law should include, in addition to strain, other

damage parameters that represent external variables the choice of which is dependent on the problem in question.

A regular network

(a)

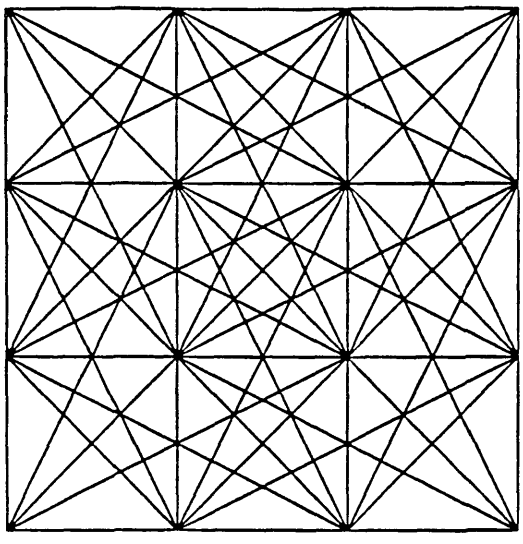

Random network (1)

Typical random networks

(b)

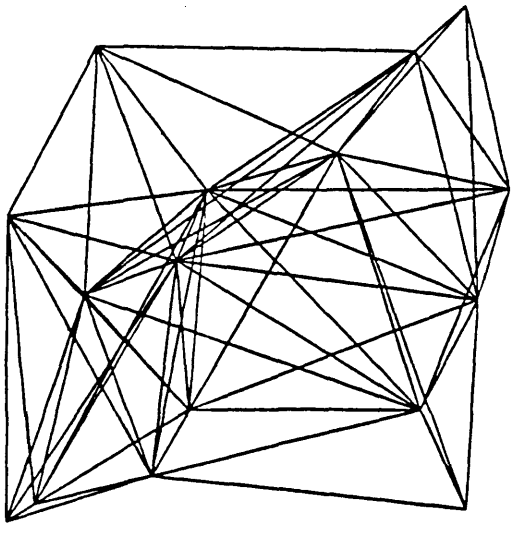

(2)

Fig. 4.1 Configuration of typical networks

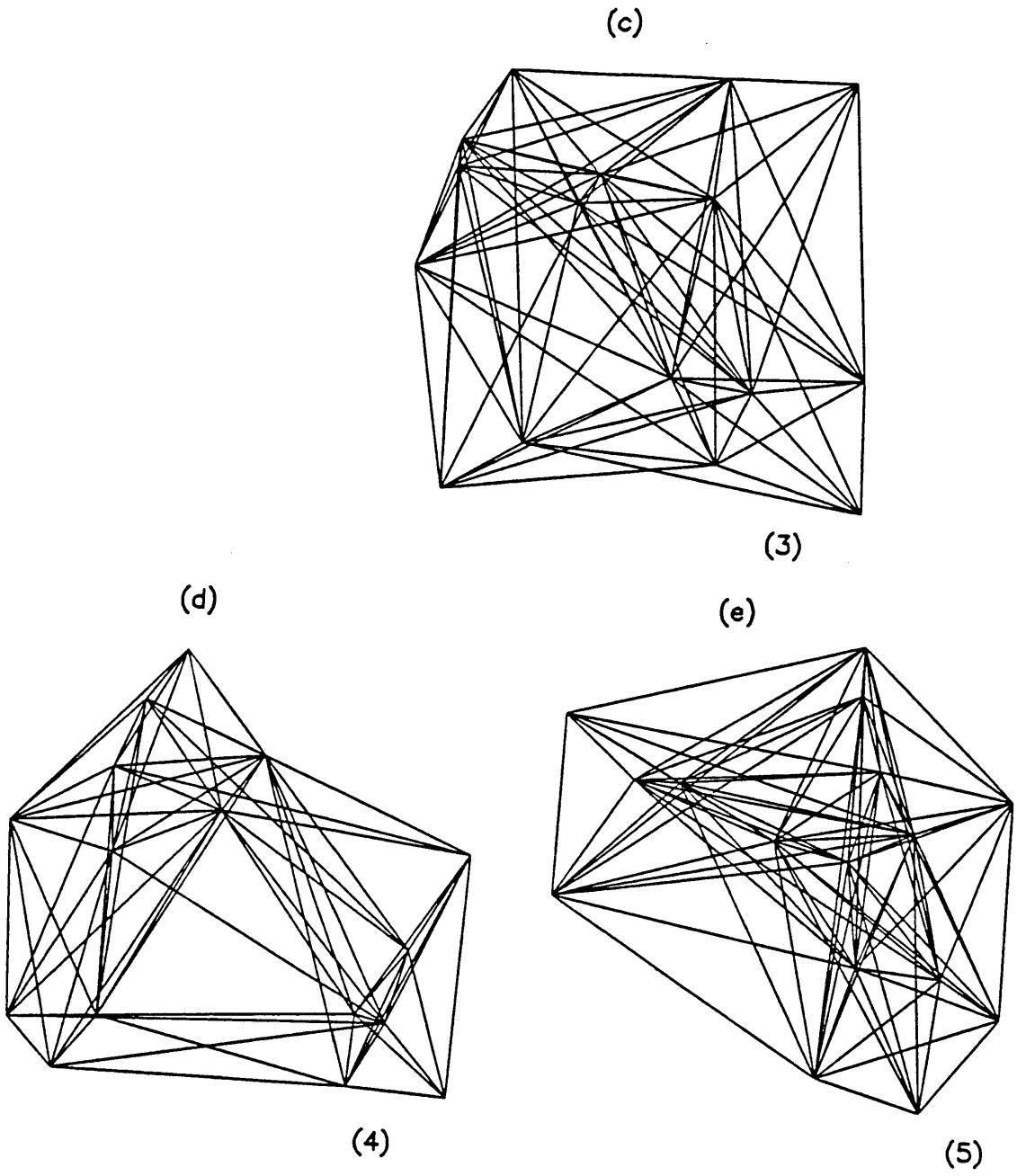

Fig. 4.1 (cont'd) Configuration of typical networks

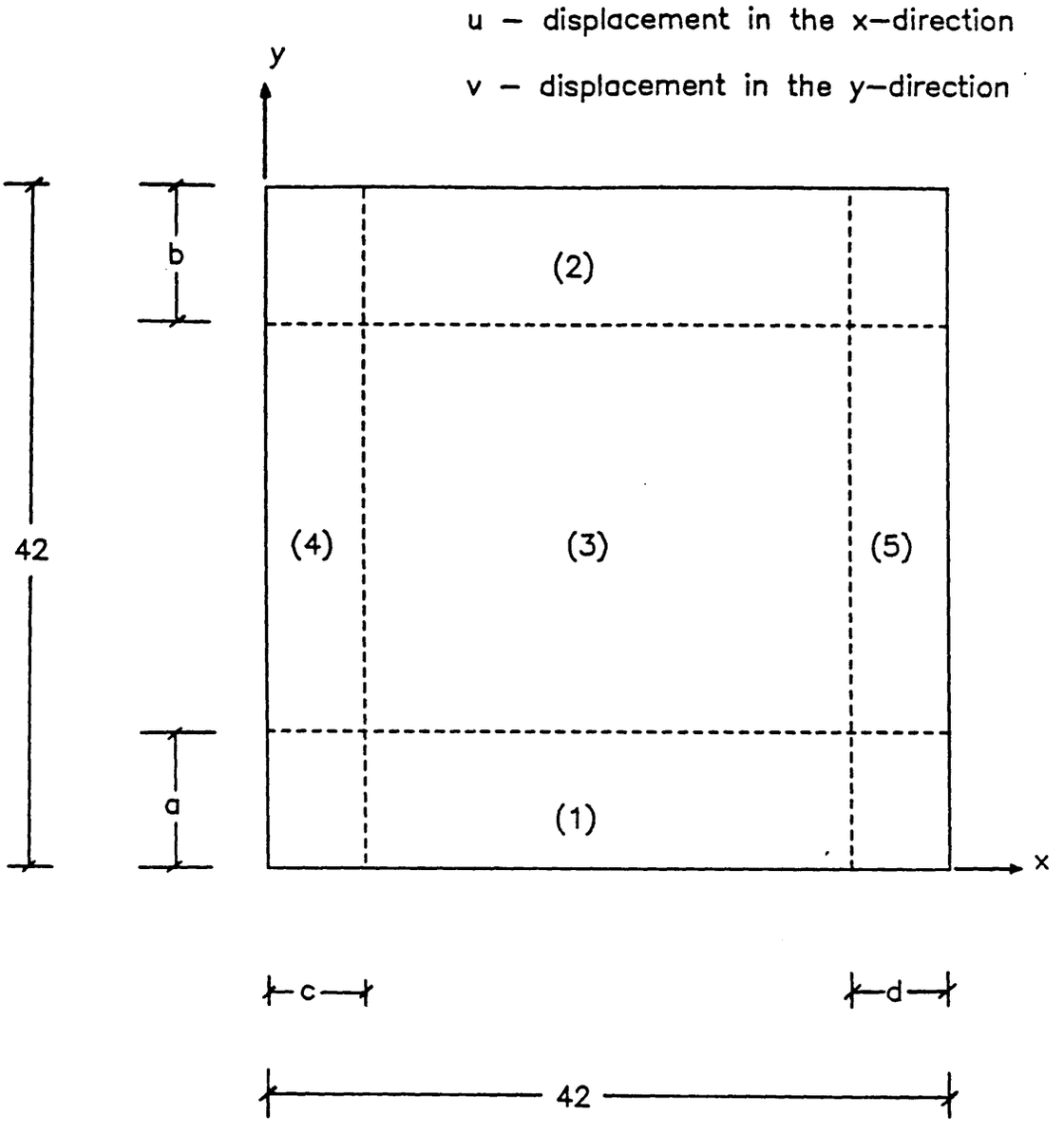

(1) v = 0 for all nodes and u=0 for one node

(2) v is prescribed for all nodes

Fig. 4.2 Boundary specifications for the random networks

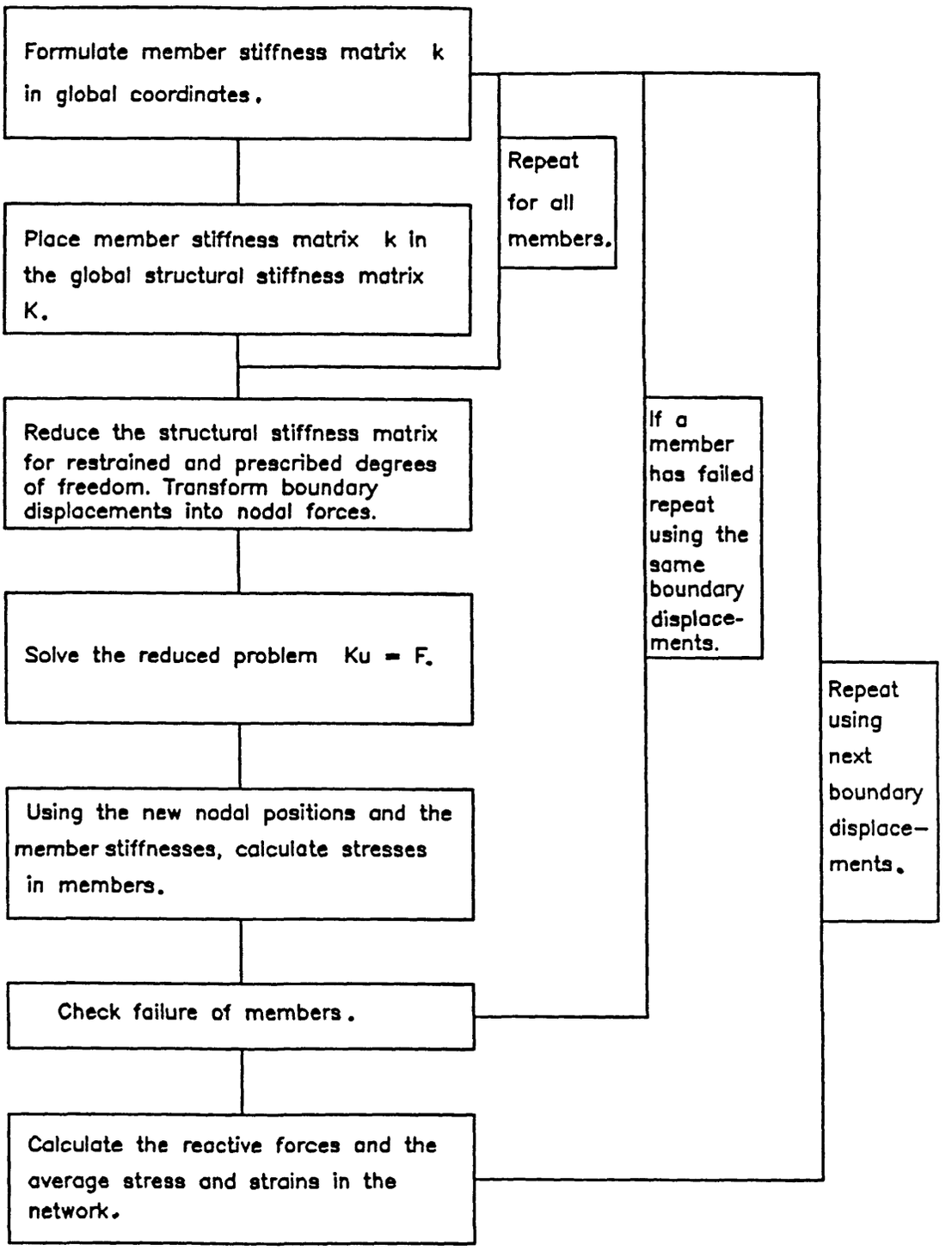

Fig. 4.3 Analysis of the network model under imposed deformations

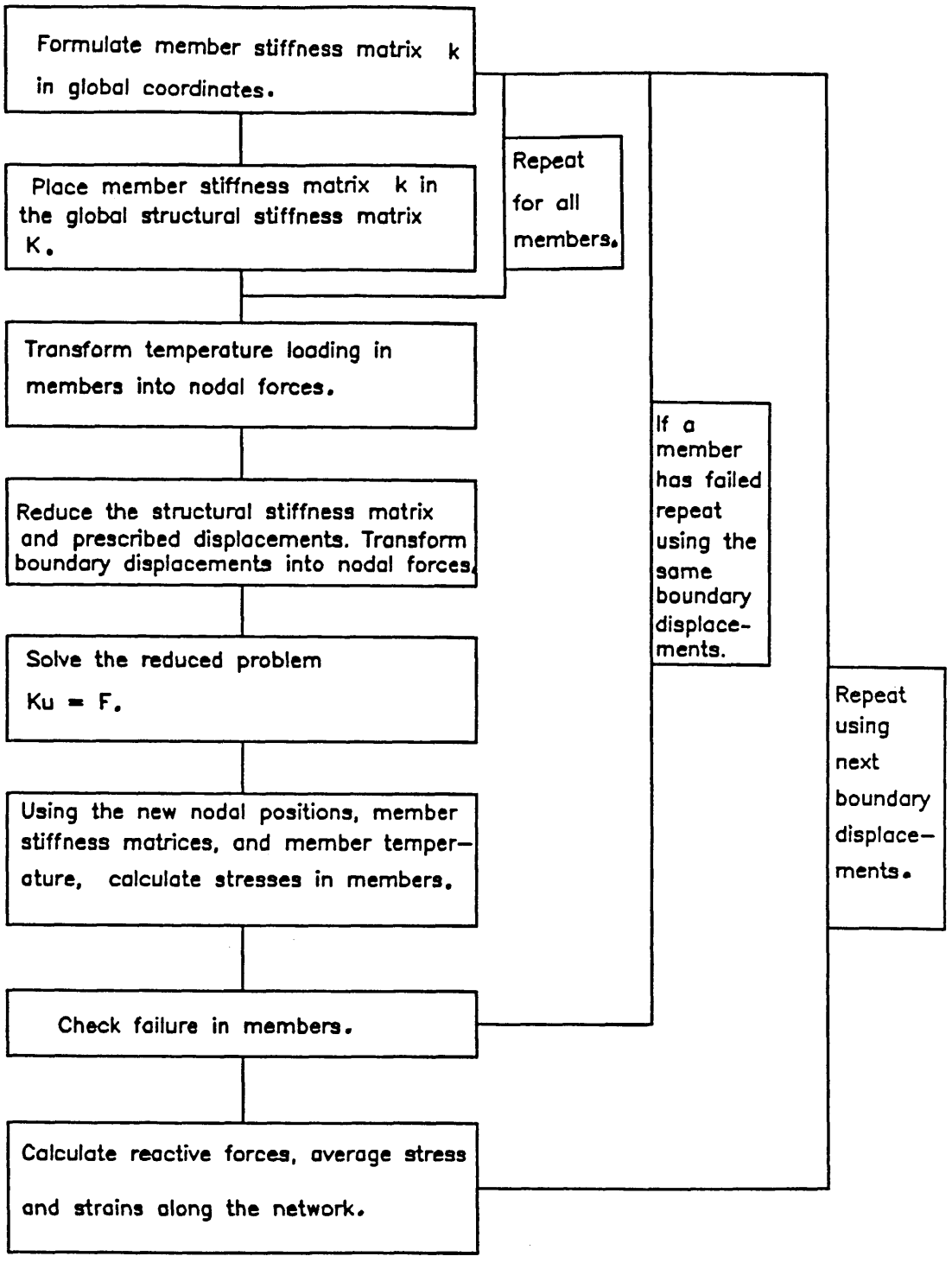

Fig. 4.4 Analysis of the network model under controlled deformations with a constantly applied temperature

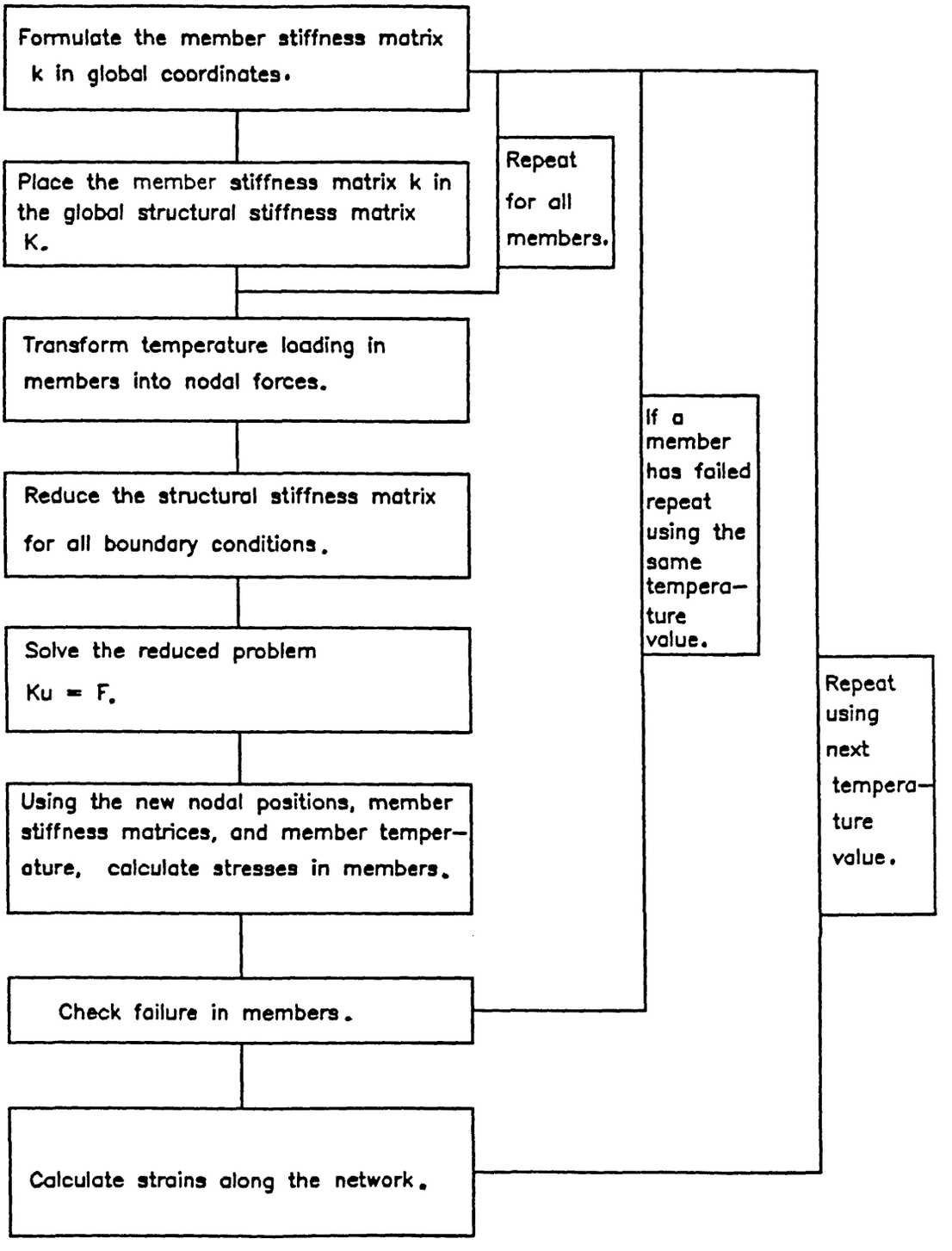

Fig. 4.5 Analysis of the network model under temperature loading

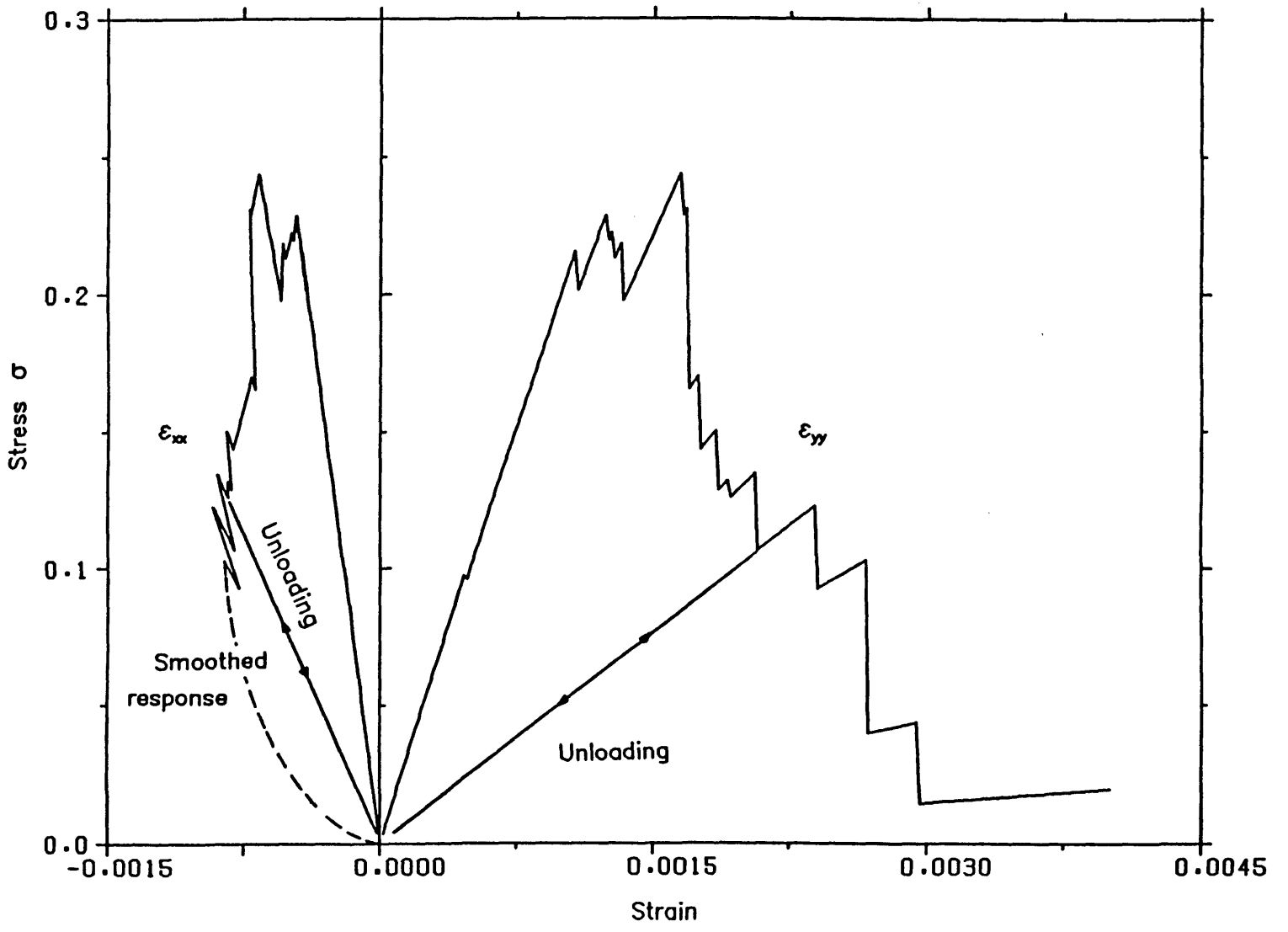

Fig. 4.6 Behaviour of the network model (3) in tension

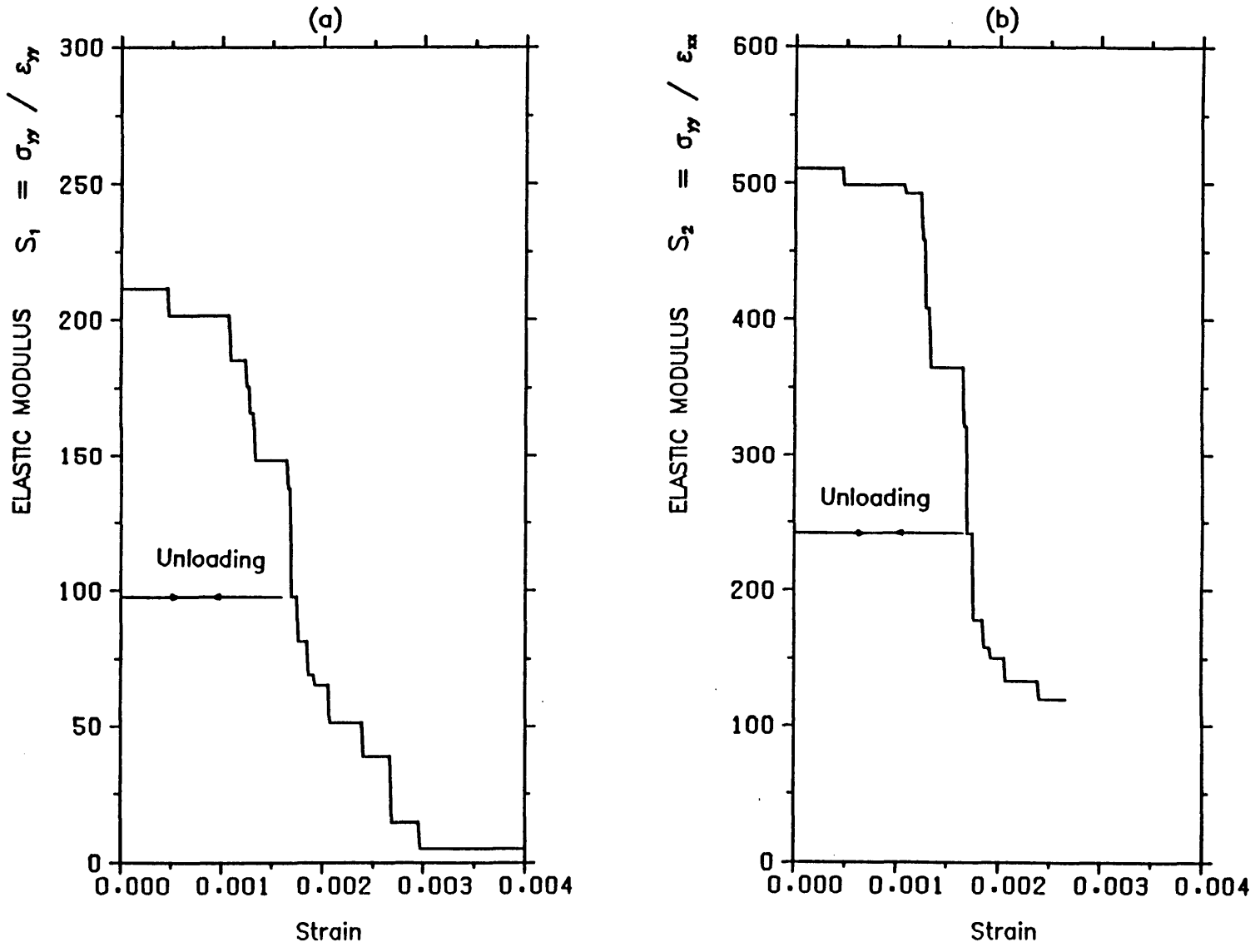

Fig. 4.7 Decrease of the elastic moduli during deformation for the network model (3)

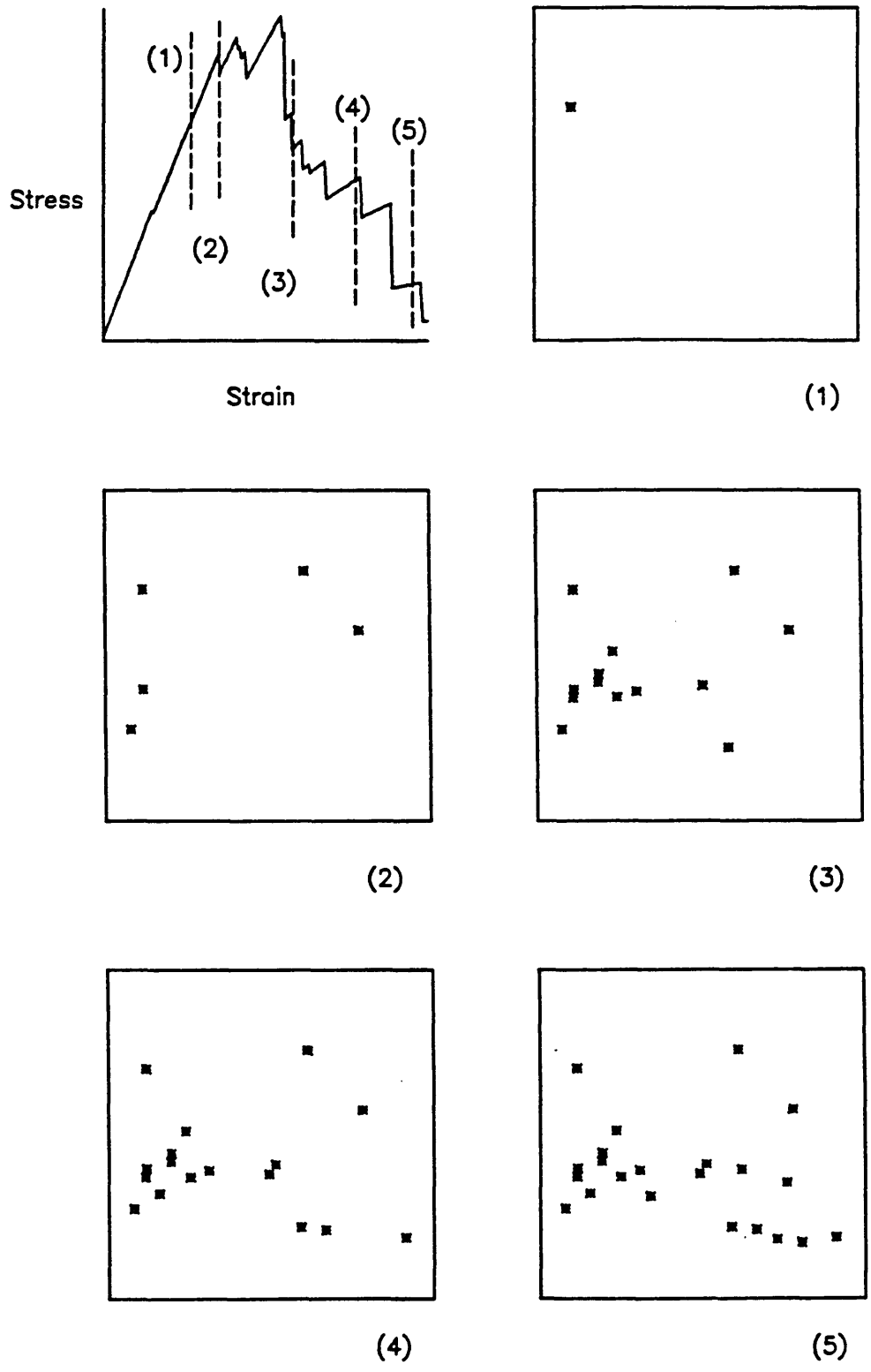

Fig. 4.8 Failure sequence for the network model upon deformation

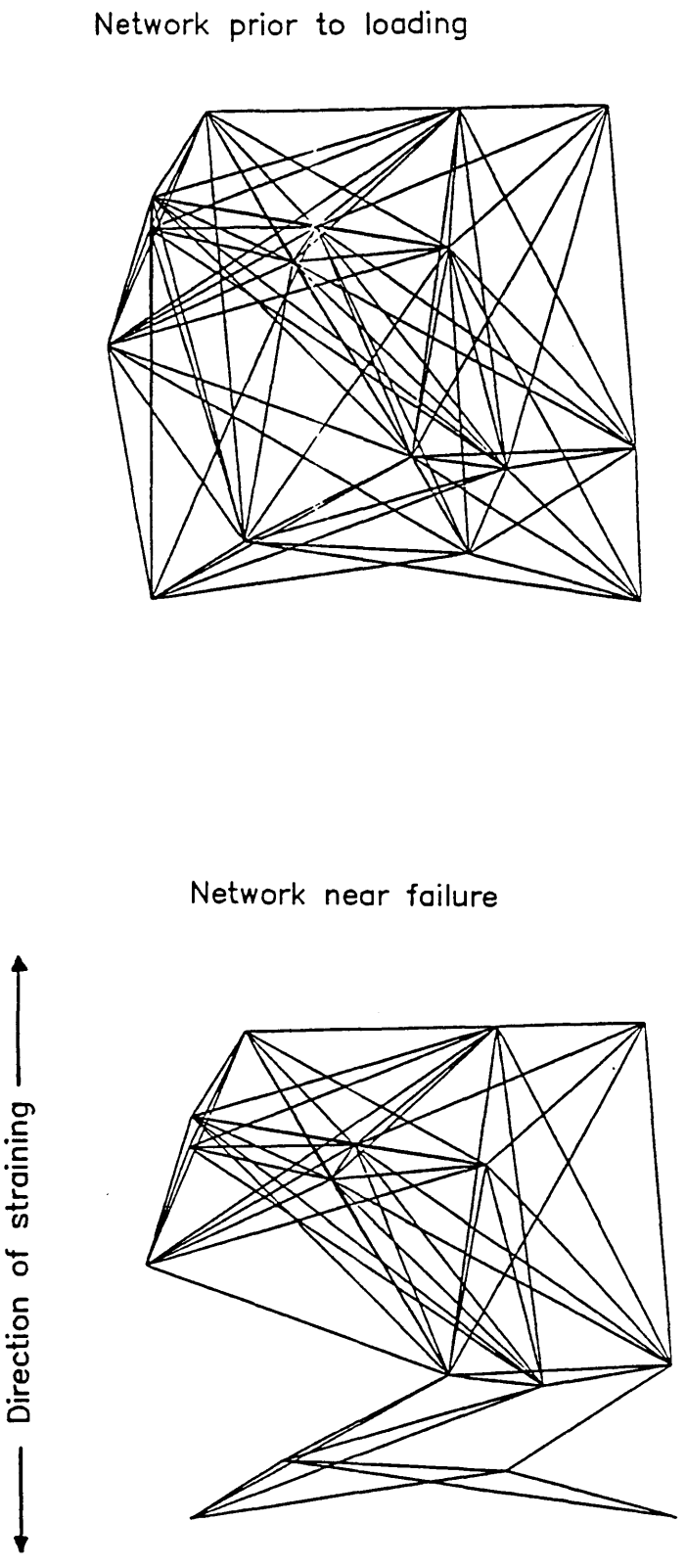

Fig. 4.9 Configuration of the network model (3) before and after deformation

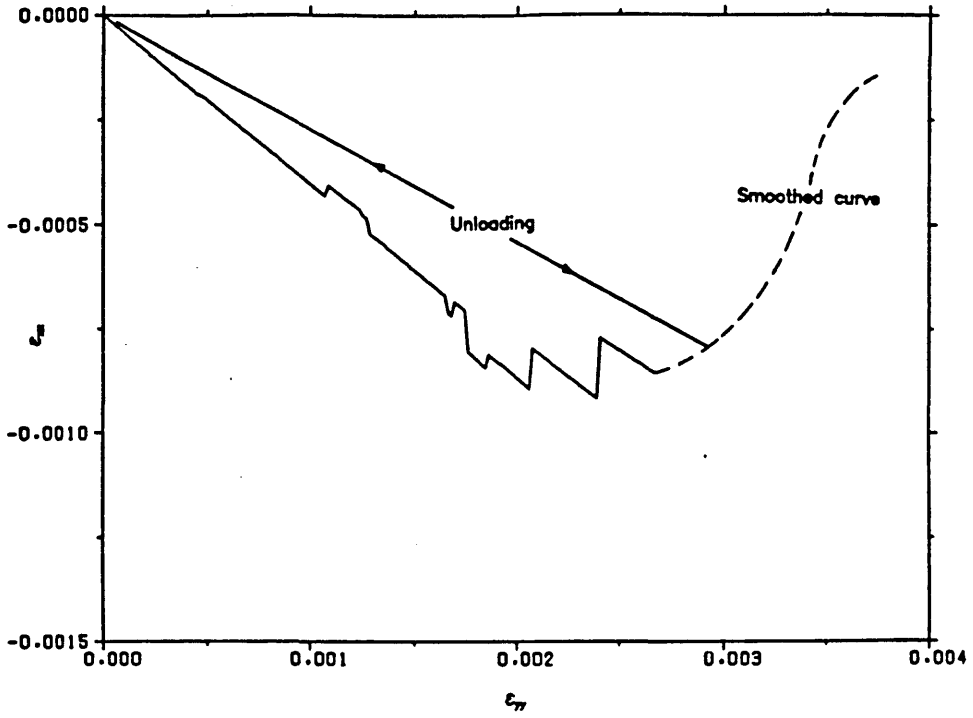

Fig. 4.10 Strain path followed by the network model (3) through deformation

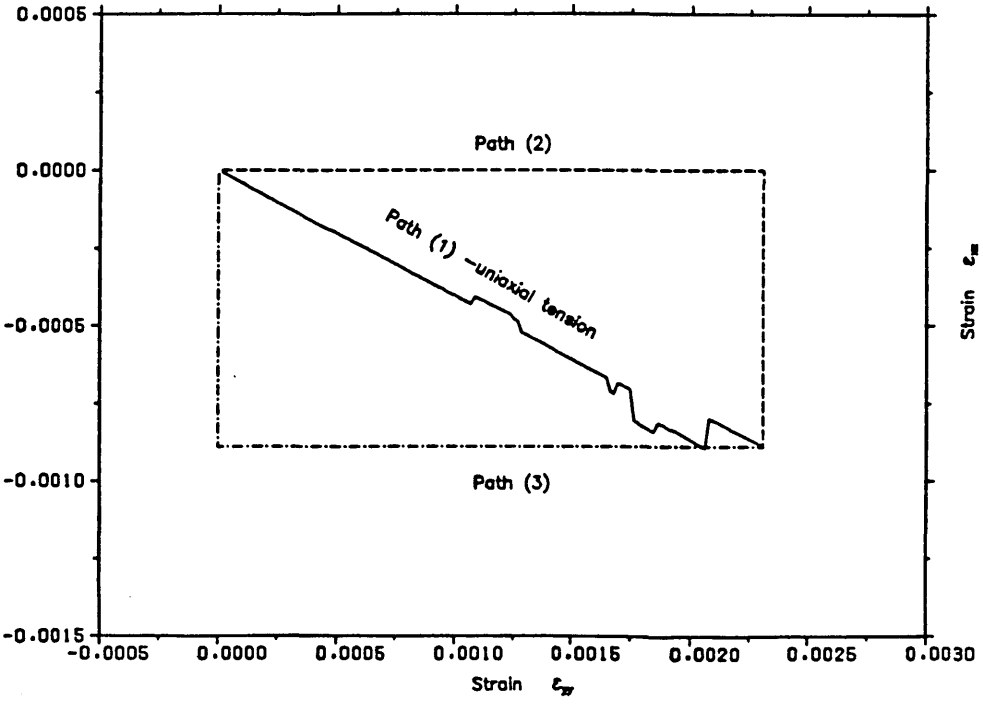

Fig. 4.11 Strain paths followed to illustrate path dependence of the response of the network model

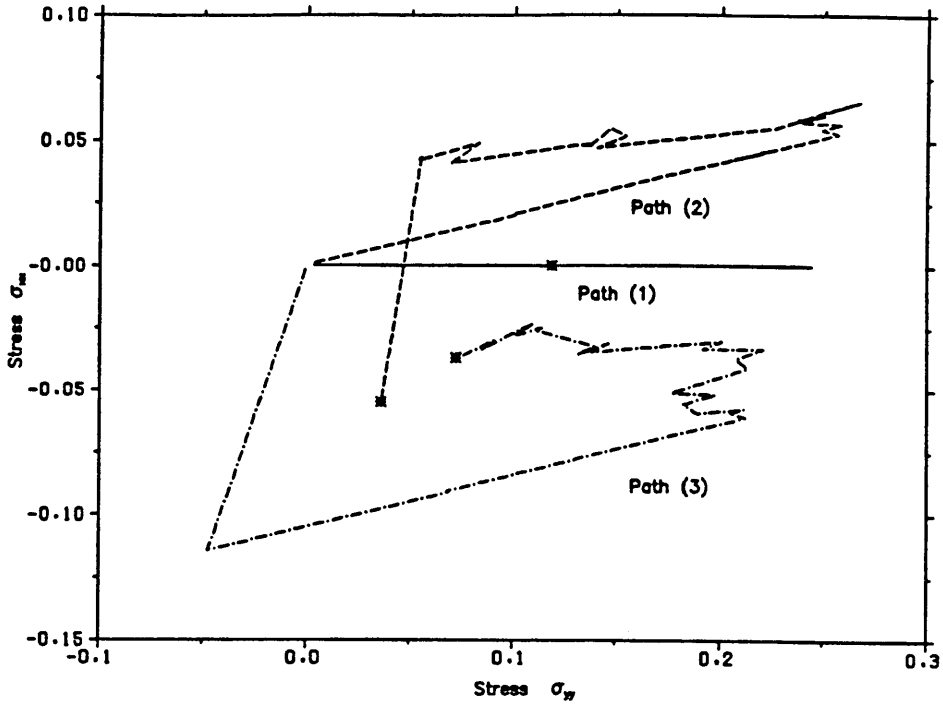

Fig. 4.12 Stress responses of the network model for different strain paths

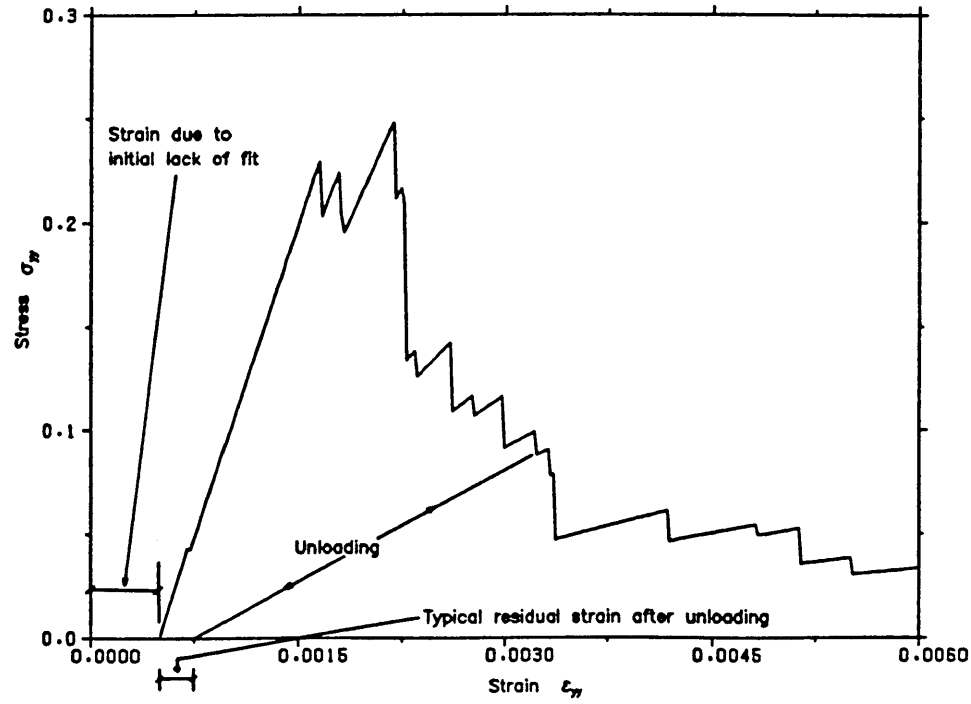

Fig. 4.13 Irrecoverable strains and loss of memory of the initial state caused by initial lack of fit

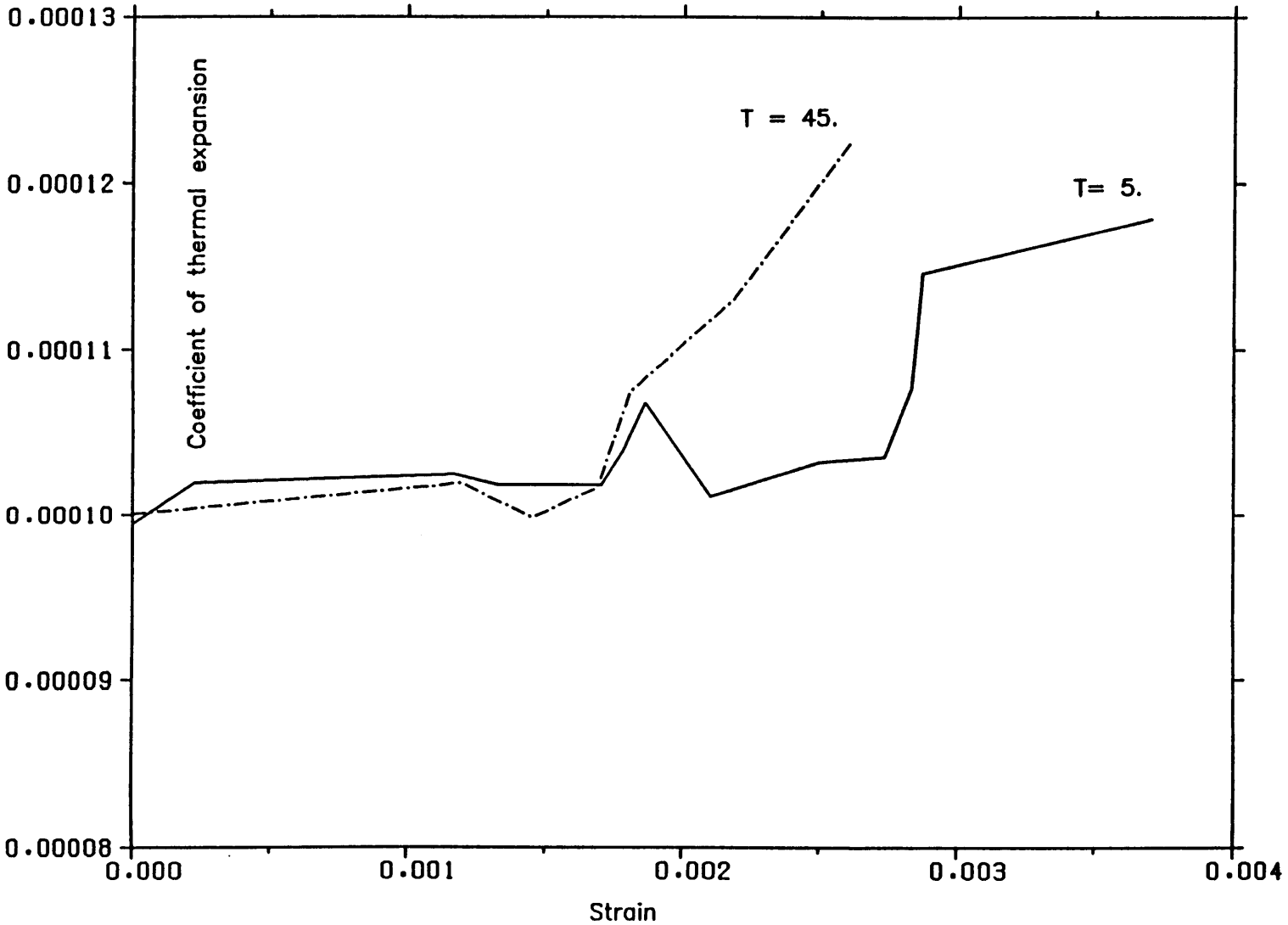

Fig. 4.14 Change of the models thermal coefficient upon loading

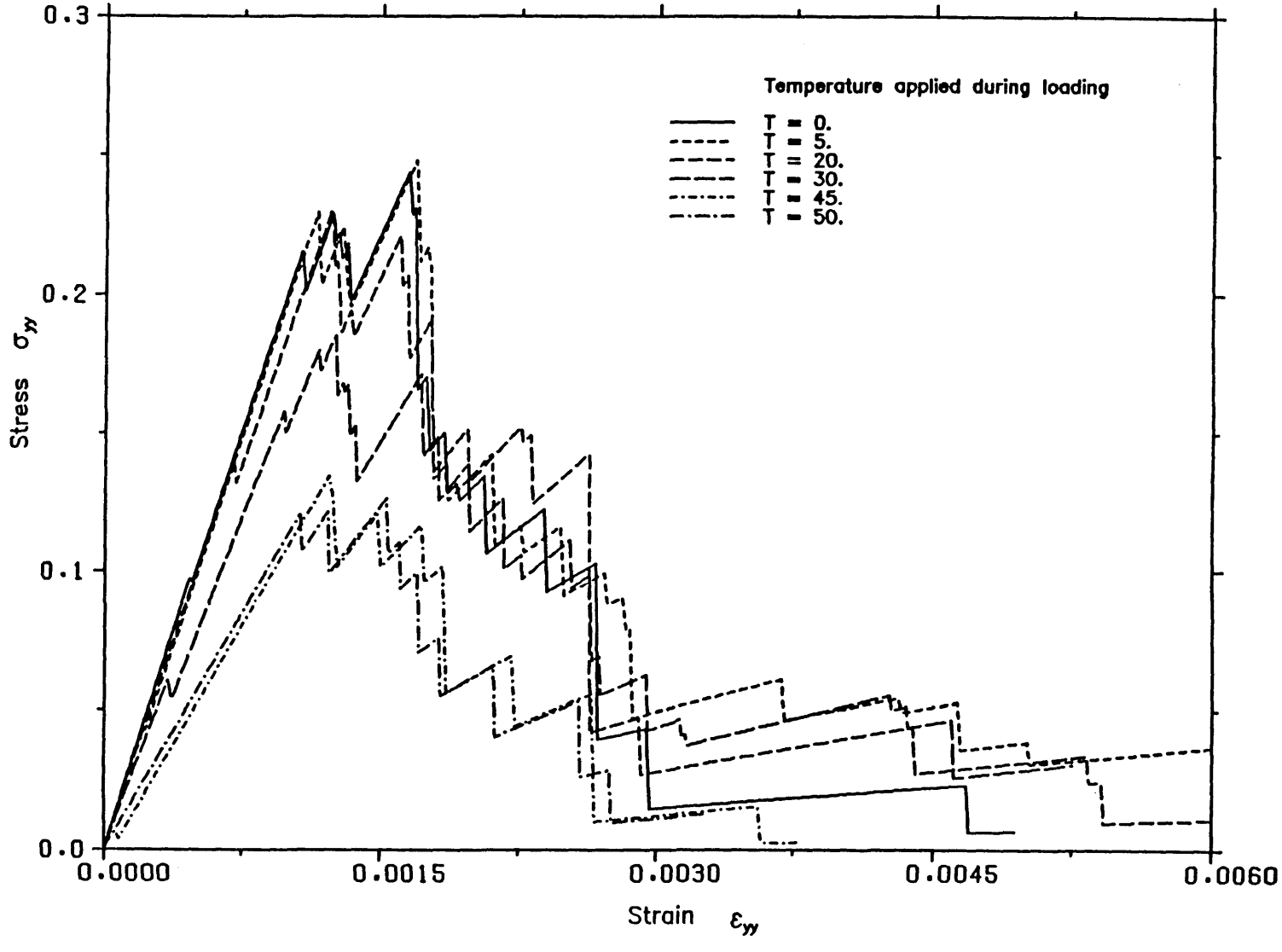

Fig. 4.15 Influence of the initial conditions on the behaviour of the network model

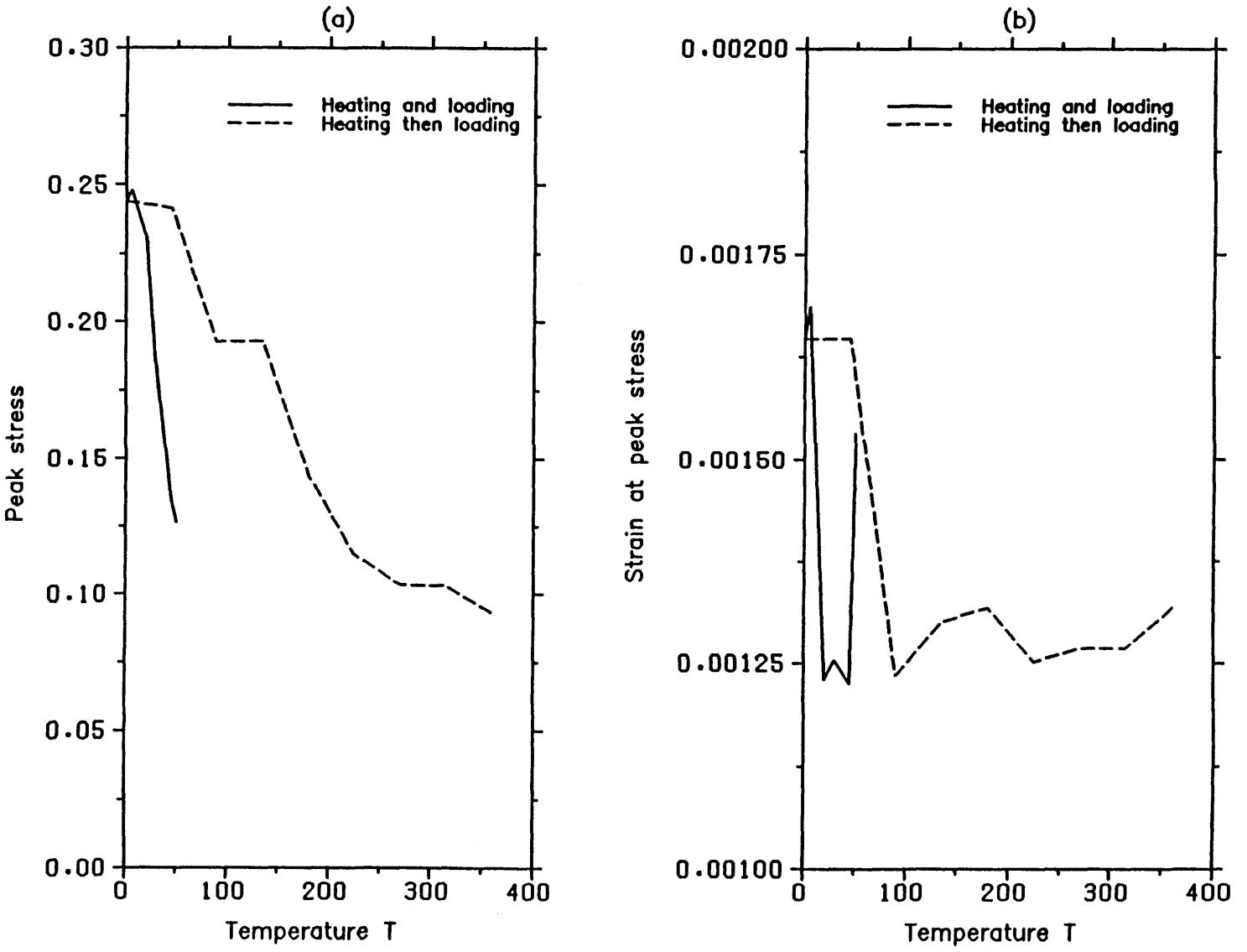

Fig. 4.16 Network strength and strain at peak stress with initial damage

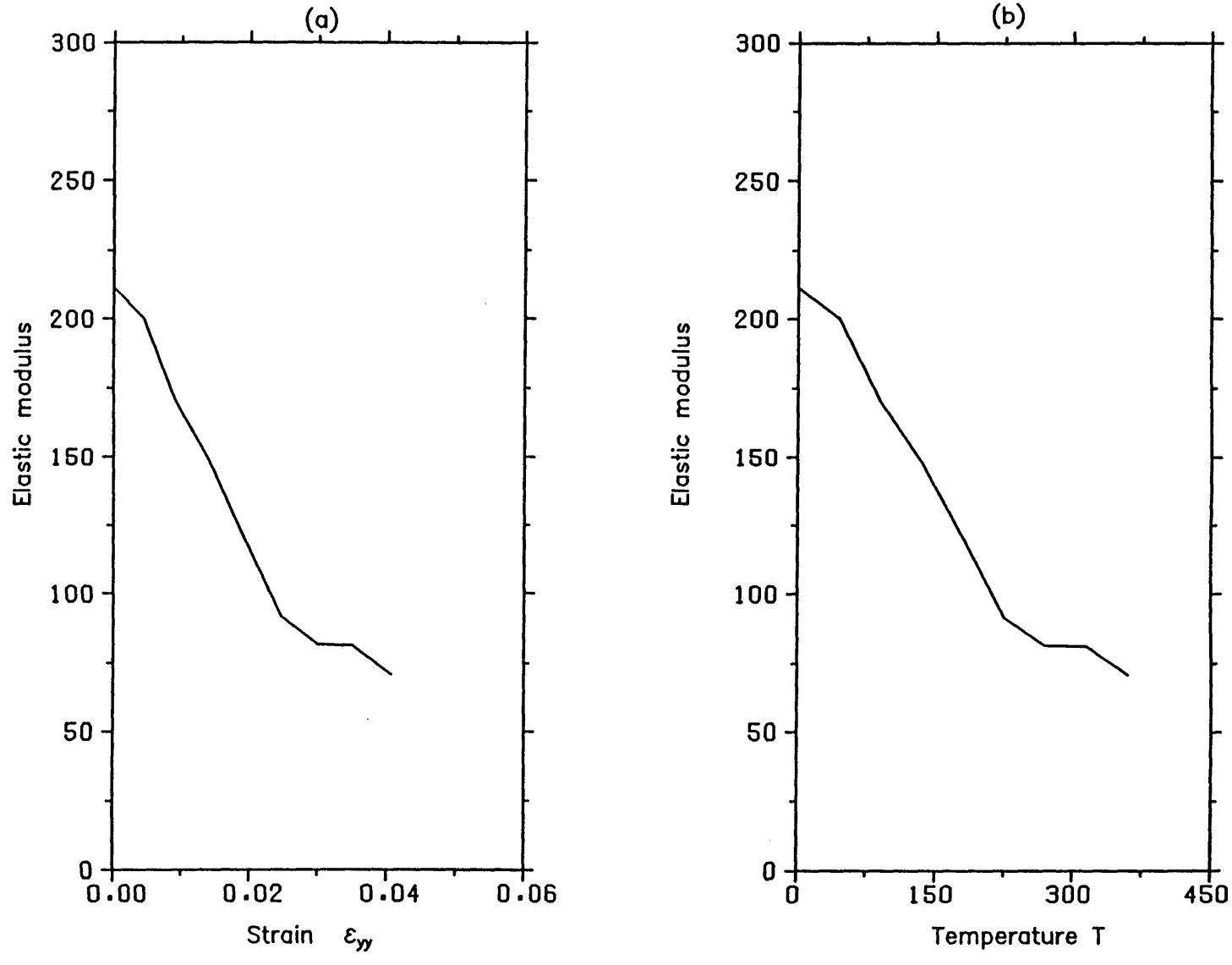

Fig. 4.17 Degradation of stiffness with deformation upon heating of the network model (3)

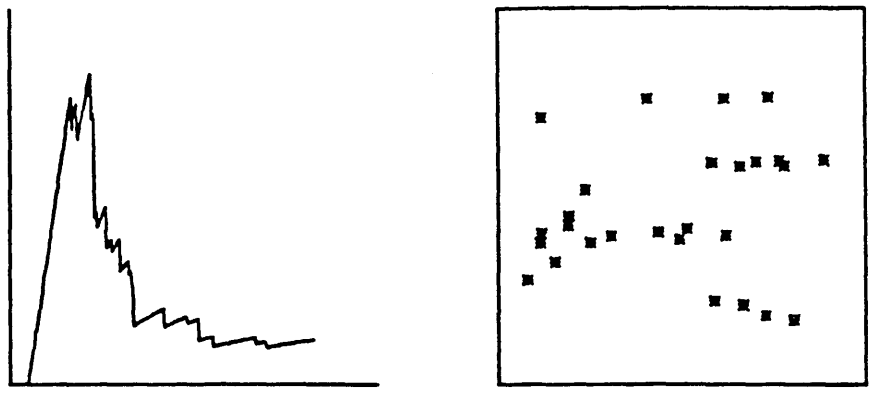

T = 5.

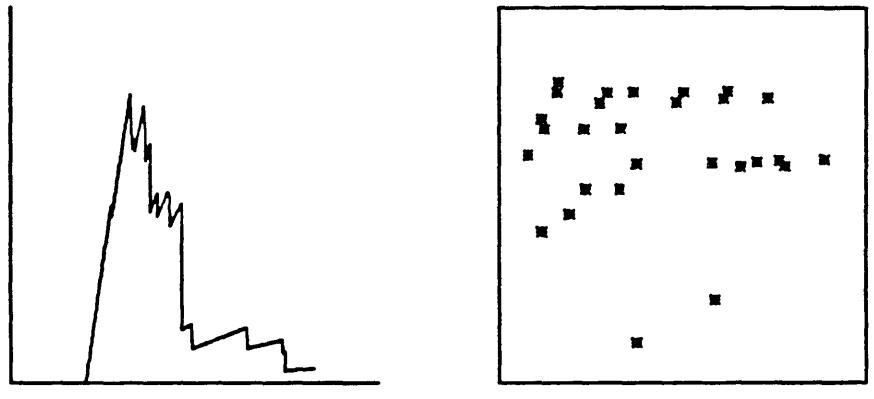

T = 20.

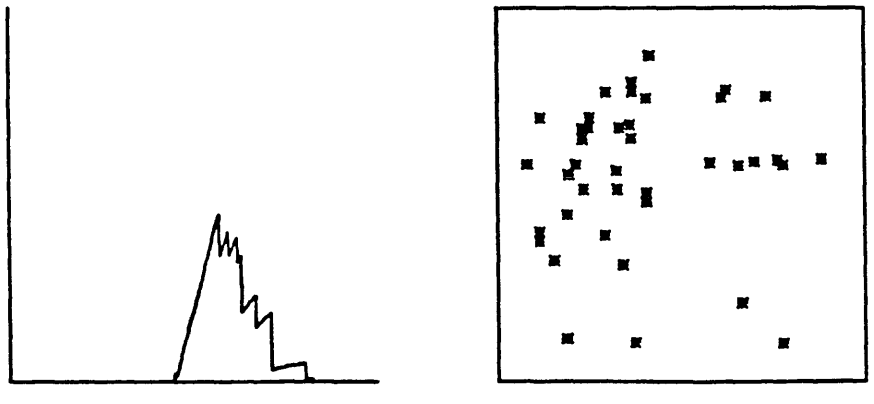

T = 45.

Fig. 4.18 Failure configuration of the network model with initial temperture

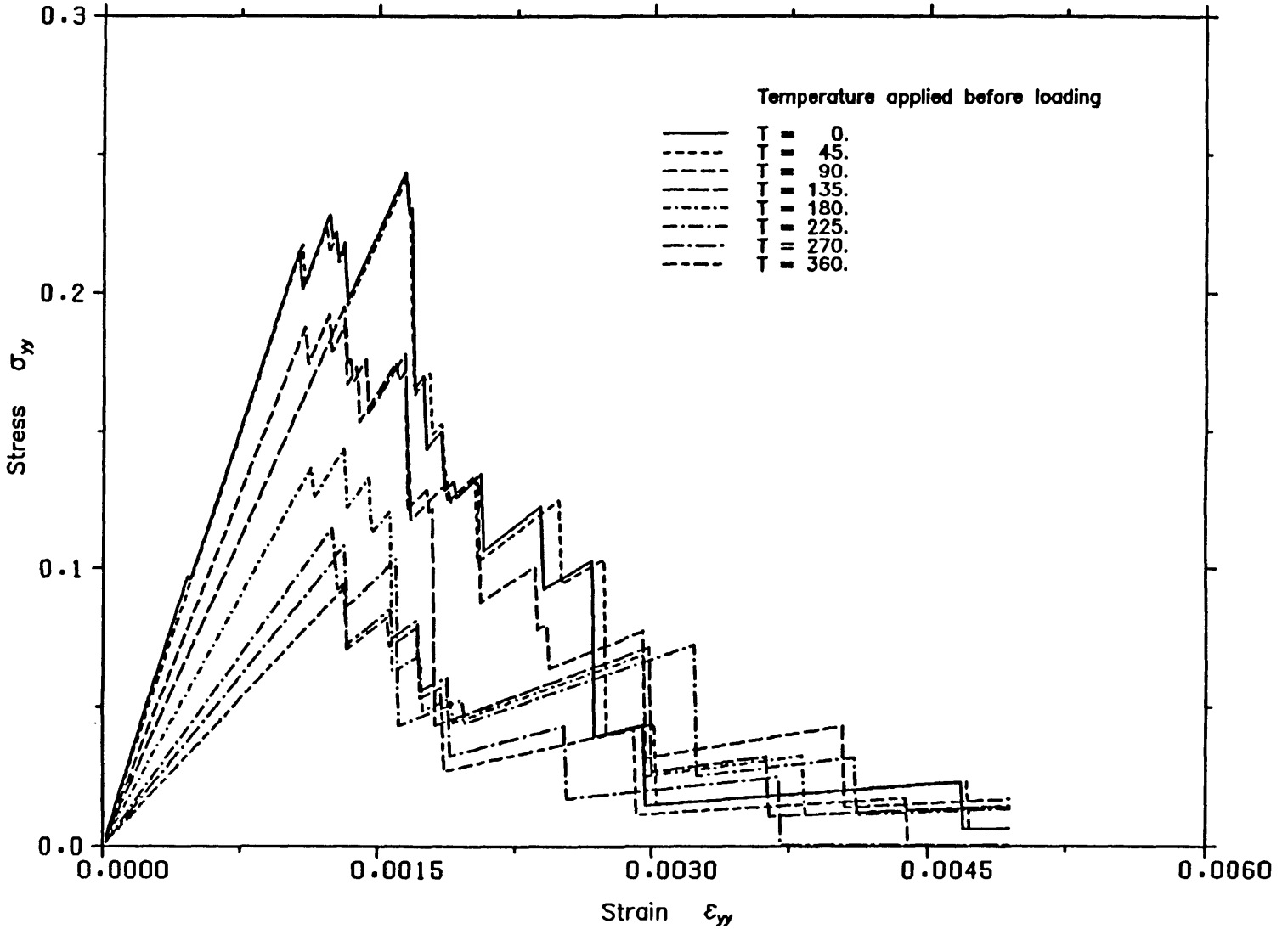

Fig. 4.19 Influence of the initial damage on the behaviour of the model

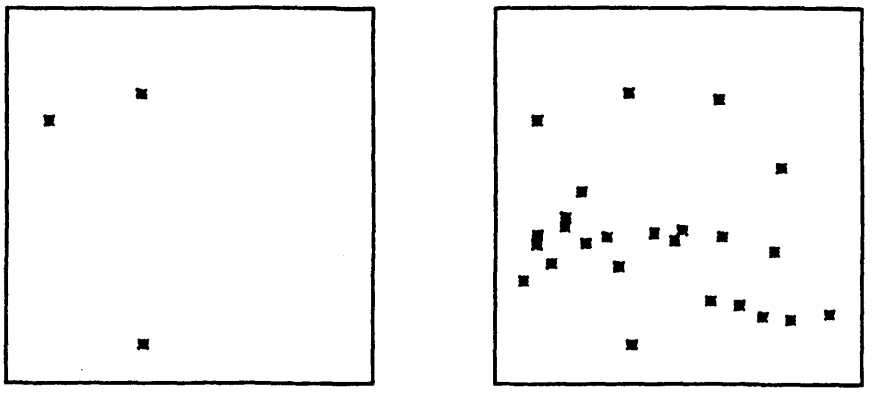

T = 45.

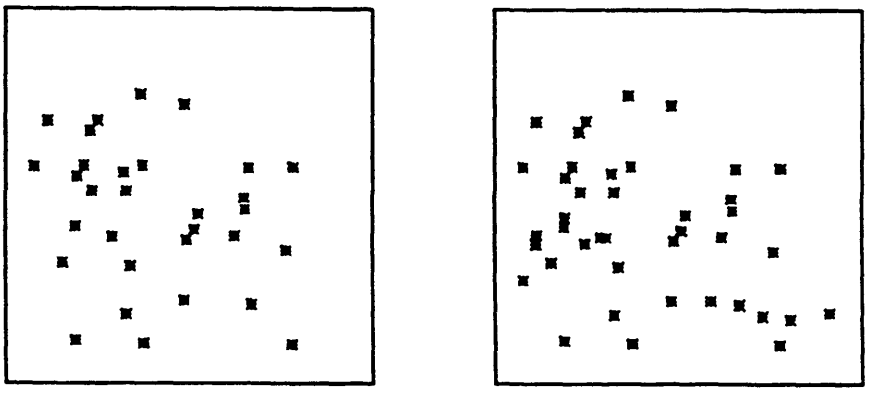

T = 180.

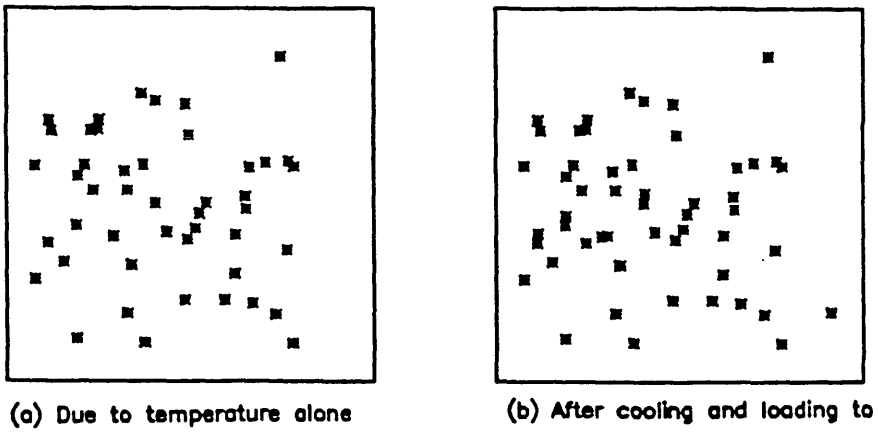

(a) Due to temperature alone (b) After cooling and loading to failure

T = 360.

Fig. 4.20 Failed members of the network model (3) due to heating–cooling prior to deformation

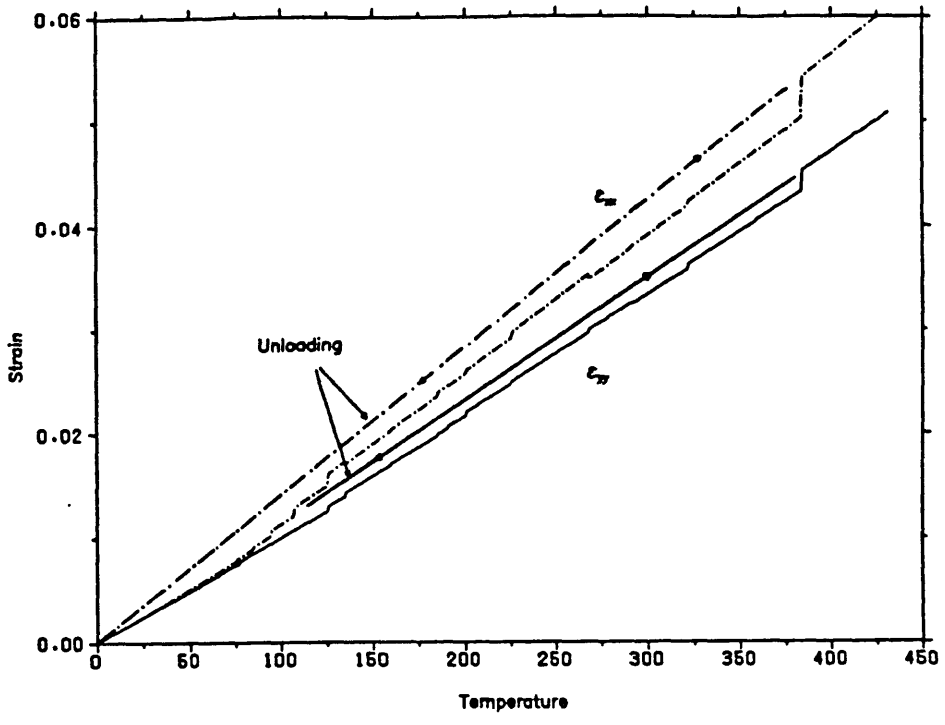

Fig. 4.21 Deformation of the network model (3) upon heating

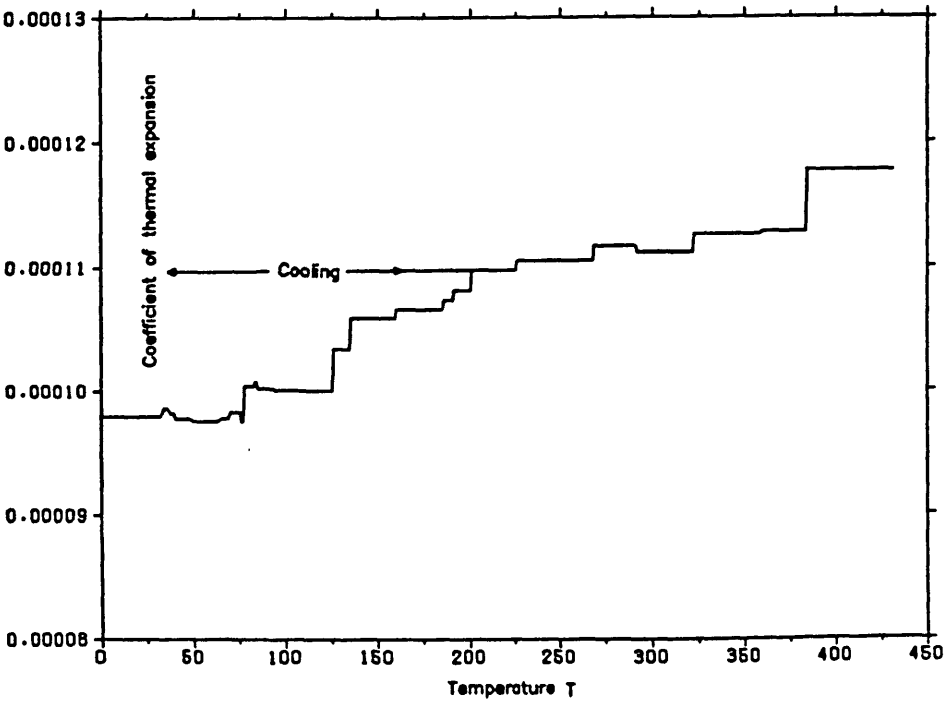

Fig. 4.22 Change of the network's thermal coefficient upon heating

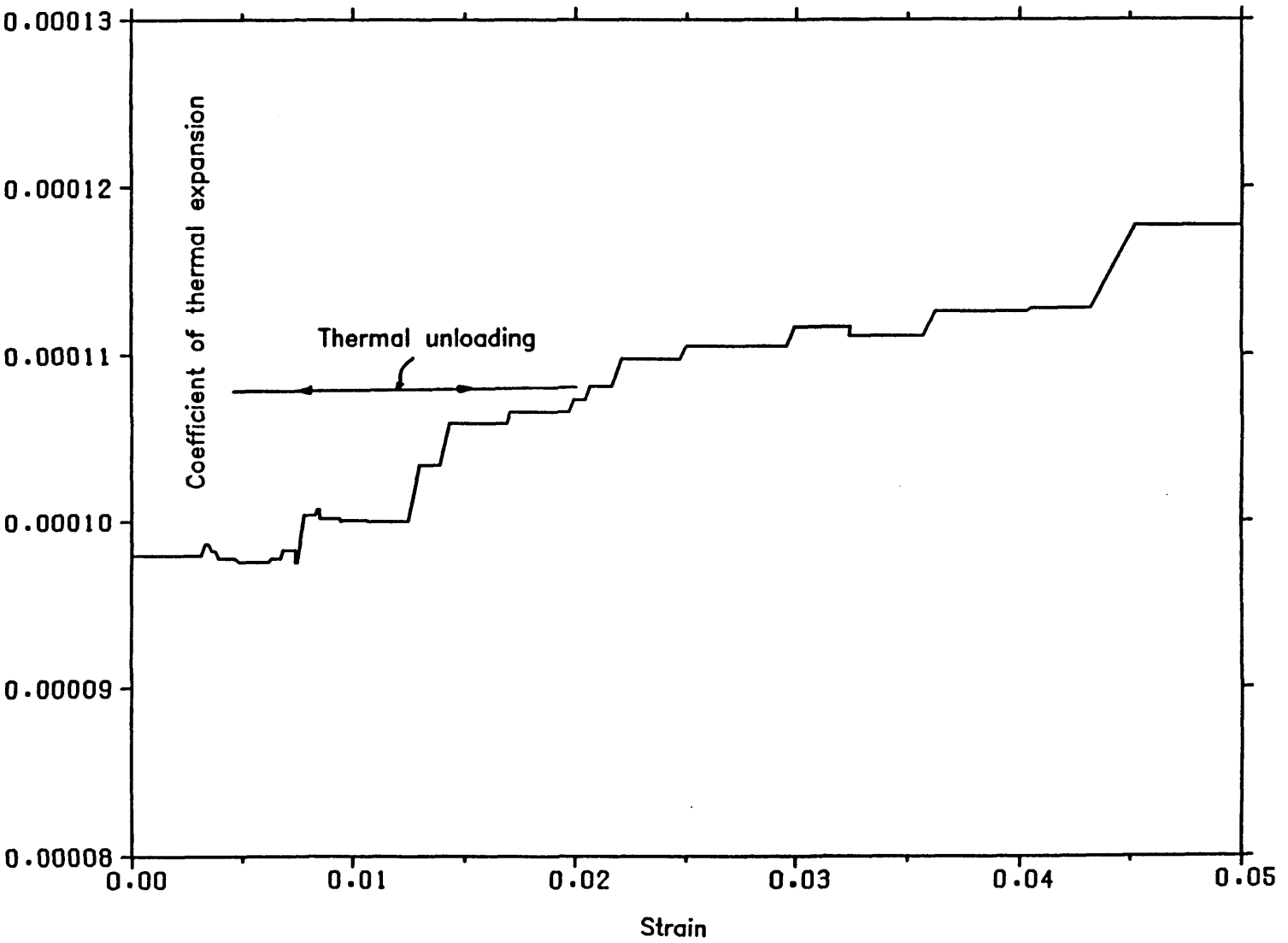

Fig. 4.23 Change of the network's thermal coefficient upon heating

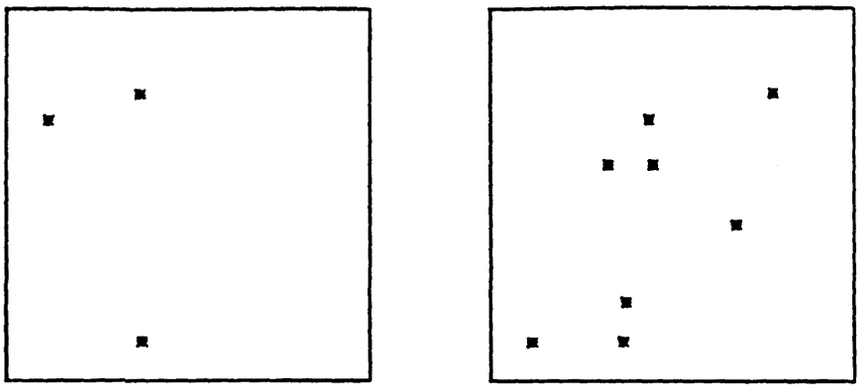

T = 45.

T = 90.

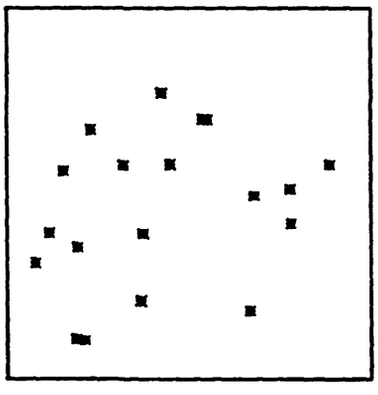

T = 135.

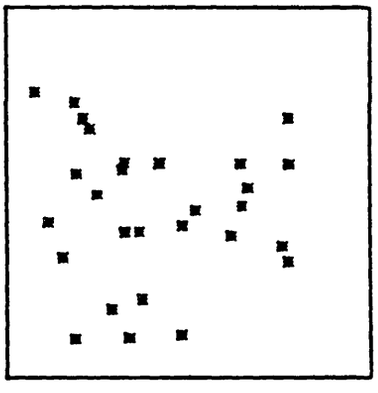

T = 180.

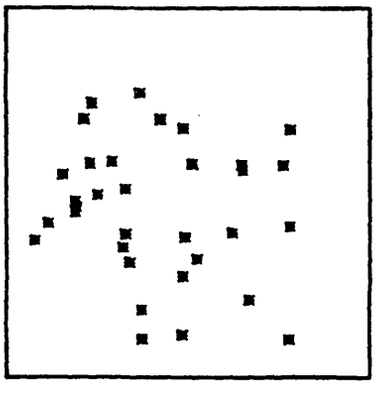

T = 225.

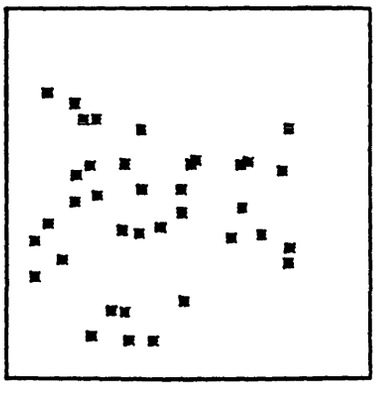

T = 315.

Fig. 4.24 Failed members of the network model(3) upon heating

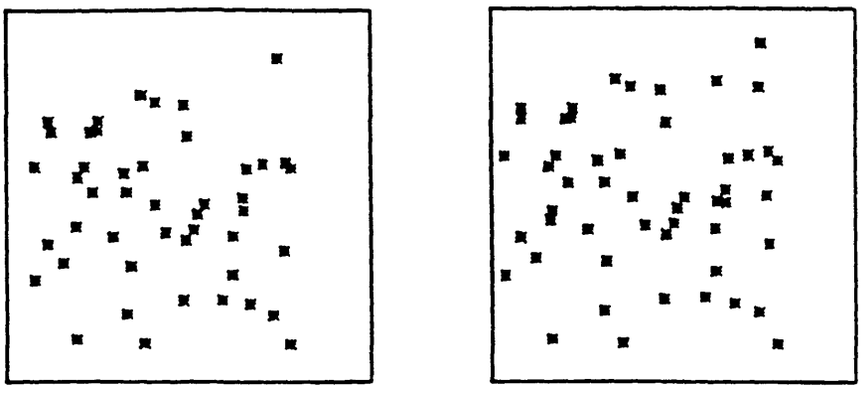

T = 360. T = 430.

Fig. 4.24 (cont'd) Failed members of the network model (3) upon heating

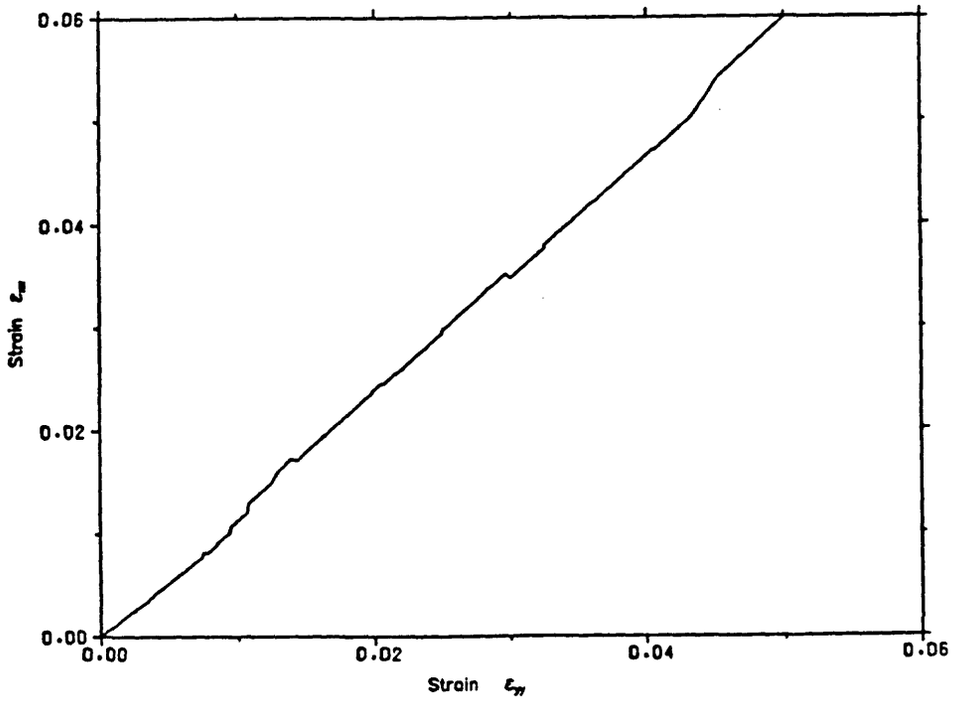

Fig. 4.25 Strain path of the network model (3) upon heating

Network before temperature loading

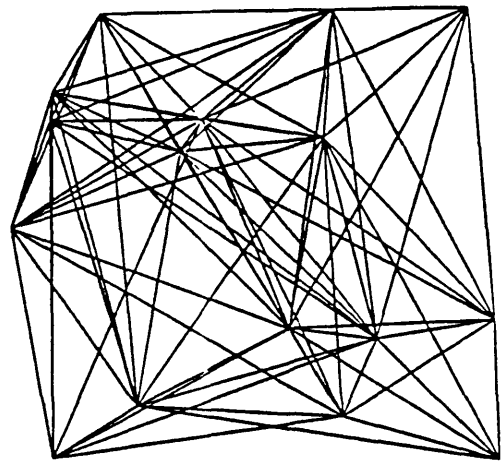

Failed network

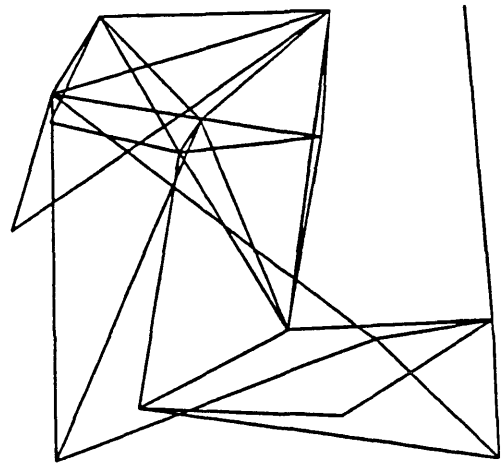

Fig. 4.26 Failed configuration of the network model(3) upon heating

CHAPTER V

A VISCOELASTIC/FRACTURING THEORY–EXTENSIONS TO THE THEORY OF THE PROGRESSIVELY FRACTURING SOLIDS

5–1 On the normality and convexity arguments of the time–independent progressively fracturing solid

In the classical theory of plasticity, a loading function F is normally defined. This function is intended to define conditions that distinguish between different modes of behaviour, namely elastic and plastic modes. This function F is usually defined in terms of the stress tensor σ_{ij} and some parameters defining plastic deformations. The form of the loading function is such that

$$F(\sigma_{ij},H_k) = 0 \qquad (5.1.1)$$

where σ_{ij} is the stress tensor and H_k is a stress hardening vector (of k parameters). Expression 5.1.1 defines a surface which, if defined in stress space, divides this space into points that can be reached without plastic deformations (those that lie within the surface and are such that $F \leq 0$) and points that are reached with consequential plastic deformations (points lying outside it). This surface is termed the "yield surface".

In the formulation of the time–independent progressively fracturing solids theory (section 2–3) a loading function F, assumed to be a function of the strain ϵ_{ij} and damage as defined by a damage vector H_k, was defined. This function defines conditions that describe elastic and progressively fracturing modes of behaviour. The loading function F is chosen such that the condition

$$F(\epsilon_{ij},H_k) = 0 \qquad (5.1.2)$$

defines a surface in strain space, termed the "fracture surface". At any stage in the process of deformation, this surface divides the strain space into a region of points, contained by the surface, that can be attained elastically ($F \leq 0$) and a region of points, outside the fracture surface, that can only be reached by further progressive fracture.

In this section some features related to the yield surface in stress space and the fracture surface in strain space are discussed. Essential to the formulations of the two theories are the arguments that the yield and fracture surfaces are convex in stress space and strain space respectively. The normality of

the plastic strain increment to the yield surface and the fracture stress decrement to the fracture surface is another important argument inherent in the formulations of the theories with consequential associated flow rules. These flow rules give expressions for the plastic strain increment and the fracture stress decrement.

It will be noted that the stress–strain law derived from 5.1.2, is in the form of a relation between the increments or rates of strain and the corresponding change or rate of stress. In chapter II, the condition that the fracture stress decrement (the inelastic component of the stress increment) is normal to the fracture surface was assumed as a result of the adoption that the material is linear in the small and that the definition of plastic deformation given by Il'ushin [30,31] is applicable. These assumptions and other arguments related to them are taken up in this section.

5–1–1 Drucker's postulate on stability and its consequences

Drucker [28,115] defined stable materials as a class of materials such that the work done by an external agency on the change of displacements it produces must be positive or zero during a complete cycle of loading and unloading. In other word

$$\int (\sigma - \overset{*}{\sigma})\, d\epsilon \geq 0 \qquad (5.1.3)$$

along any closed stress path, where σ and ϵ are the stress and strain state variables. $\overset{*}{\sigma}$ is the initial (and final) value of stress.

Consider a representative sample of an ideal elastoplastic material under stress $\overset{*}{\sigma}_{ij}$ corresponding to a point O in stress space (figure 5.1). Point O lies in the elastic region within the yield surface. Stress of the sample is changed to σ_{ij} such that at this stress state the material reaches yield (equation 5.1.1). This change can be represented by path OP in stress space (figure 5.1) such that P lies on the yield surface. Following yield, a small increment of stress $d\sigma_{ij}$, causing plastic deformations, is added after which unloading is followed to the original stress state $\overset{*}{\sigma}_{ij}$. Consider the work done during this complete closed cycle of stress represented by OPQS in stress space (figure 5.1). For the moment, it is assumed that the elastic moduli remain unchanged upon yield (and hence the loading and unloading moduli are identical) and that behaviour for loading paths within the yield surface is linear elastic. Hence, evaluating the integral 5.1.3

along the closed stress path OPQS, results in (figure 5.2)

$$(\sigma_{ij} - \overset{*}{\sigma}_{ij})\, d\epsilon^{P}_{ij} + \frac{1}{2}\, d\epsilon^{P}_{ij}\, d\sigma_{ij} \geq 0 \qquad (5.1.4)$$

where σ_{ij} is the stress tensor represented by point P and the total strain increment induced at point P by the stress increment $d\sigma_{ij}$ is given by

$$d\epsilon_{ij} = d\epsilon^{e}_{ij} + d\epsilon^{P}_{ij} \qquad (5.1.5)$$

$d\epsilon^{e}_{ij}$ is the elastic component of the strain increment and is dependent on $d\sigma_{ij}$. $d\epsilon^{P}_{ij}$ is the plastic component which is equal in this case to the permanent component of strain remaining after unloading. The description is limited to materials that are linear in the small in the sense that the direction of the plastic strain increment $d\epsilon^{P}_{ij}$ is independent on the applied stress increment $d\sigma_{ij}$.

The inequality 5.1.4 does not contain the elastic strain increment in its terms. This suggests that, upon a closed stress cycle in stress space, all the elastic work is recovered and the only work done is due to the plastic strain increment $d\epsilon^{P}_{ij}$.

Since the original stress $\overset{*}{\sigma}_{ij}$ is chosen arbitrary within the elastic region, it can be chosen such that σ_{ij} and $\overset{*}{\sigma}_{ij}$ are equal. This case is represented in stress space by the point O coinciding with point P (figures 5.1 and 5.2). Hence, inequality 5.1.4 becomes

$$\frac{1}{2}\, d\epsilon^{P}_{ij}\, d\sigma_{ij} \geq 0 \qquad (5.1.6)$$

Inequality 5.1.6 should hold for any choice of the stress increment $d\sigma_{ij}$ (which is directed outward to the yield surface at P). If $d\sigma_{ij}$ makes an angle β with the normal at P to the yield surface (figure 5.3), then for $d\sigma_{ij}$ to be arbitrary, the value of β should be such that

$$-\frac{\pi}{2} \leq \beta \leq \frac{\pi}{2} \qquad (5.1.7)$$

The geometric meaning of the inequality 5.1.6 is that the two increments $d\epsilon^{P}_{ij}$ and $d\sigma_{ij}$ should form an acute angle with each other (figure 5.3) whatever the choice of the increment $d\sigma_{ij}$ (which makes an angle β with the

normal and is directed outward to the yield surface). This means that

$$|d\epsilon^P_{ij}|\ |d\sigma_{ij}|\cos(\beta-\alpha) \geq 0 \qquad (5.1.8)$$

giving

$$-\frac{\pi}{2} \leq \beta-\alpha \leq \frac{\pi}{2} \qquad (5.1.9)$$

where α is the angle that $d\epsilon^P_{ij}$ makes with the outward normal at P to the yield surface. Expressions 5.1.9 with 5.1.7 imply that

$$\alpha = 0 \qquad (5.1.10)$$

This means that the plastic strain increment $d\epsilon^P_{ij}$ is directed along the outward normal PN to the yield surface ($F = 0$) at P (figure 5.1). Inherent in the conclusion of expression 5.1.10 from 5.1.9 and 5.1.7 is the assumption that the plastic strain increment is linear in the small and hence the angle α is fixed.

For a large value of $(\sigma_{ij} - \overset{*}{\sigma}_{ij})$ the second term in 5.1.4 can be neglected because it becomes small compared to the first term. Inequality 5.1.4 will reduce to

$$(\sigma_{ij} - \overset{*}{\sigma}_{ij})\, d\epsilon^P_{ij} \geq 0 \qquad (5.1.11)$$

Since the direction of $d\epsilon^P_{ij}$ is always along the normal to the yield surface, then inequality 5.1.11 suggests that $(\sigma_{ij} - \overset{*}{\sigma}_{ij})$ should always form an acute angle with the outward normal, at P, to the yield surface. For an arbitrary choice of $\overset{*}{\sigma}_{ij}$ (and hence point O), this can only be satisfied if all possible choices of O lie within the same side of the tangent at P to the yield surface containing the inward normal. The yield surface should thus be convex.

If due to plastic deformations the values of the unloading elastic moduli are different from those during loading, then the plastic strain increment, after a closed stress cycle, becomes no longer equal to the permanent strain increment (figure 5.4). The difference, $d\epsilon^S_{ij}$, is dependent on both $\overset{*}{\sigma}_{ij}$ (more specifically $(\sigma_{ij} - \overset{*}{\sigma}_{ij})$) and the values of the elastic moduli changes. Applying the integral 5.1.3 on the stress path, represented by OPQS in figure 5.4, results in

$$(\sigma_{ij} - \overset{*}{\sigma}_{ij})\, d\epsilon^P_{ij} + \frac{1}{2} d\epsilon^P_{ij}\, d\sigma_{ij} + \frac{1}{2} d\epsilon^S_{ij}\, (\sigma_{ij} + d\sigma_{ij} - \overset{*}{\sigma}_{ij}) \geq 0 \qquad (5.1.12)$$

For the case where σ_{ij} and $\overset{*}{\sigma}_{ij}$ are equal (point O lies on the yield surface), inequality 5.1.12 reduces to

$$\frac{1}{2} d\epsilon^{P}_{ij} \, d\sigma_{ij} + \frac{1}{2} d\epsilon^{S}_{ij} \, d\sigma_{ij} \geq 0 \qquad (5.1.13)$$

which means that the plastic strain increment $d\epsilon^{P}_{ij}$ need not be normal to the yield surface at point P.

For small changes in the elastic moduli upon unloading, the term $d\epsilon^{S}_{ij}$ becomes much smaller than $d\epsilon^{P}_{ij}$ (since it is a function of both the stress increment $d\sigma_{ij}$ and the changes in the elastic moduli, so actually it is a higher order quantity than $d\epsilon^{P}_{ij}$). In this case 5.1.13 reduces to 5.1.6 which results in the necessity of the normality of the plastic strain increment to the yield surface at P.

For large values of $(\sigma_{ij} - \overset{*}{\sigma}_{ij})$, higher order terms in 5.1.12 can be neglected and hence the inequality becomes

$$(\sigma_{ij} - \overset{*}{\sigma}_{ij}) \, d\epsilon^{P}_{ij} + \frac{1}{2} d\epsilon^{S}_{ij} \, (\sigma_{ij} - \overset{*}{\sigma}_{ij}) \geq 0 \qquad (5.1.14)$$

Convexity of the yield surface does not follow directly from 5.1.14, and concavity might be encountered. Palmer [39] noted that for small changes in the elastic moduli, slight concavity of the yield surface is possible depending on the sign of the quantity $d\epsilon^{S}_{ij} \, (\sigma_{ij} - \overset{*}{\sigma}_{ij})$ in the inequality 5.1.14.

Thus convexity of the yield surface does not hold for materials where the second term of 5.1.14 is positive. These materials absorb energy as a result of changing elastic moduli which is the case when these changes are positive. In other words, such solids stiffen upon plastic deformations. The degree of the concavity encountered is dependent on the amount of energy absorbed.

If the material is such that the elastic moduli reduce (or remain unchanged) upon plastic deformations, then energy is released during stiffness degradation and the second term in 5.1.14 becomes negative (or zero) and hence the first term should always be non–negative as in 5.1.11. The yield surface for such a material should be convex.

In summary, for materials whose elastic moduli remain unchanged upon plastic deformations, the plastic strain increment, if assumed to be linear in the small, is normal to the convex yield surface at the yield point. This is true

provided Drucker's definition of stability holds. For small changes in the elastic moduli, the plastic strain increment is still normal to the yield surface, but the convexity of the yield surface might be violated if energy is absorbed as a result of stiffening upon yield.

It should be noted that strain softening violates 5.1.3 for any stress cycle and hence is unstable in Drucker's sense.

5–1–2 Il'ushin's postulate of plastic deformations and its consequences

According to Il'ushin's definition of plasticity [30,31], the work done, upon the application and removal of loads to form a closed path in strain space, by an external agency should be positive or zero depending on whether or not the material has exhibited plastic deformations. Alternatively, Il'ushin's definition of plasticity can be analytically expressed by

$$\int -(\epsilon - \overset{*}{\epsilon})\, d\sigma \geq 0 \qquad (5.1.15)$$

upon any closed strain path. $\overset{*}{\epsilon}$ represnts the initial and final values of strain.

The use of strain space to describe the behaviour of such a solid is essential because the stability criterion is defined along a closed cycle of strain.

The yield surface ($F = 0$) in here is the set of points in strain space that can be reached from points within this surface ($F \leq 0$) along an elastic path and such that any point outside this surface can only be reached with induced plastic deformations.

Consider a representative sample of the ideal elastoplastic material under strain $\overset{*}{\epsilon}_{ij}$ corresponding to the point O in figure 5.5. Point O lies in the elastic region within the yield surface. Strain of the sample is changed to ϵ_{ij} such that at this strain state any additional applied strain will induce plastic deformations (equation 5.1.1). This change can be represented by path OP in strain space (figure 5.5) such that P lies on the yield surface. Following yield, a small increment of strain $d\epsilon_{ij}$, causing plastic deformations, is added after which unloading is followed to the original strain state $\overset{*}{\epsilon}_{ij}$. Consider the work done during this complete closed cycle of strain represented by OPQS in strain space (figure 5.5). For the moment, it is assumed that the elastic moduli remain unchanged upon yield (and hence the loading and unloading moduli are identical)

and that behaviour for loading paths within the yield surface is linear elastic. Assuming that the material follows Il'ushin's definition of plasticity, the evaluation of the integral 5.1.15 along the closed strain path OPQS (figure 5.6), results in

$$-(\epsilon_{ij} - \overset{*}{\epsilon}_{ij})\, d\sigma^{P}_{ij} - \frac{1}{2}\, d\sigma^{P}_{ij}\, d\epsilon_{ij} \geq 0 \qquad (5.1.16)$$

where ϵ_{ij} is the strain tensor represented by point P on the yield surface. The total stress increment induced at point P by the strain increment $d\epsilon_{ij}$ is given by

$$d\sigma_{ij} = d\sigma^{e}_{ij} + d\sigma^{P}_{ij} \qquad (5.1.17)$$

$d\sigma^{e}_{ij}$ is the elastic component of the stress increment. $d\sigma^{P}_{ij}$ is the plastic stress decrement assumed to be linear in the small in the sense that its direction is independent on the applied strain increment $d\epsilon_{ij}$.

For the case when the two strain states ϵ_{ij} and $\overset{*}{\epsilon}_{ij}$ are equal, point O will lie on the yield surface and will coincide with point P, so that 5.1.16 becomes

$$-\frac{1}{2}\, d\sigma^{P}_{ij}\, d\epsilon_{ij} \geq 0 \qquad (5.1.18)$$

which, in a fashion similar to the one following 5.1.6, implies the normality of the plastic stress decrement $d\sigma^{P}_{ij}$ to the yield surface at point P. The minus sign in 5.1.18 means that $d\sigma^{P}_{ij}$ actually lies along the inward rather than the outward normal.

For large values of $(\epsilon_{ij} - \overset{*}{\epsilon}_{ij})$, inequality 5.1.16 reduces, after neglecting higher order terms, to

$$-d\sigma^{P}_{ij}\, (\epsilon_{ij} - \overset{*}{\epsilon}_{ij}) \geq 0 \qquad (5.1.19)$$

requiring the convexity of the yield surface in strain space.

If upon plastic yield the material stiffness is changed, then the unloading elastic moduli will change (figure 5.7) and the permanent stress decrement upon a closed strain path becomes no longer equal to the plastic stress decrement $d\sigma^{P}_{ij}$. The difference, $d\sigma^{S}_{ij}$, is dependent on both the strain tensor $(\epsilon_{ij} - \overset{*}{\epsilon}_{ij})$ and the changes in the elastic moduli. Evaluating the integral 5.1.15 for the closed strain path OPQRS gives

$$- d\sigma^{P}_{ij} (\epsilon_{ij} - \overset{*}{\epsilon}_{ij}) - \frac{1}{2} d\sigma^{P}_{ij} d\epsilon_{ij}$$
$$+ \frac{1}{2} d\sigma^{S}_{ij} (\epsilon_{ij} + d\epsilon_{ij} - \overset{*}{\epsilon}_{ij}) \geq 0 \qquad (5.1.20)$$

For equal values of ϵ_{ij} and $\overset{*}{\epsilon}_{ij}$ 5.1.20 becomes

$$- \frac{1}{2} d\sigma^{P}_{ij} d\epsilon_{ij} + \frac{1}{2} d\sigma^{S}_{ij} d\epsilon_{ij} \geq 0 \qquad (5.1.21)$$

For small changes in the elastic moduli upon unloading, the term $d\sigma^{S}_{ij}$ becomes a higher order quantity than $d\sigma^{P}_{ij}$ (since it is a function of both $d\epsilon_{ij}$ and the changes in the elastic moduli). The second term in the above inequality can be neglected and 5.1.21 reduces to 5.1.18 which in turn requires that the plastic stress decrement, $d\sigma^{P}_{ij}$, be directed along the inward normal to the yield surface at point P.

For large values of $(\epsilon_{ij} - \overset{*}{\epsilon}_{ij})$, 5.1.20 reduces, after neglecting higher order terms, to

$$- d\sigma^{P}_{ij} (\epsilon_{ij} - \overset{*}{\epsilon}_{ij}) + \frac{1}{2} d\sigma^{S}_{ij} (\epsilon_{ij} - \overset{*}{\epsilon}_{ij}) \geq 0 \qquad (5.1.22)$$

Again, the convexity of the yield surface might be violated depending on the sign of the second term in 5.1.22. For small changes in the elastic moduli upon unloading, slight concavity is possible for positive values of the second term in the above inequality. This is the case when energy is absorbed upon yield as a result of increasing unloading elastic moduli. In this case the first term in 5.1.22 $(-d\sigma^{P}_{ij} (\epsilon_{ij} - \overset{*}{\epsilon}_{ij}))$ might take a negative value depending on the value of the second term.

For materials that release energy through plastic slip, resulting in the loss of stiffness, the second term of 5.1.22 has a negative value so that the term $(-d\sigma^{P}_{ij} (\epsilon_{ij} - \epsilon^{*}_{ij}))$ is always non–negative. This requires the convexity of the yield surface in strain space.

5–1–3 Some remarks on the arguments following stability criteria

It should be noted that Drucker's postulate that describes a class of stable materials (section 5–1–1) is more restrictive than the definition given by

Il'ushin (section 5–1–2), to describe plasticity, in the sense that it regards all forms of strain softening behaviour as unstable. If a solid is stable in Drucker's sense, then it does conform with the definition of plasticity according to Il'ushin but the reverse is not necessarily true. While Drucker's stability criterion, can only be applicable to hardening materials, the definition of plasticity according to Il'ushin applies to both hardening and softening modes of behaviour.

The yield surface can be defined as the set of stress states that divide the stress space into an elastic and a plastic region. Any point within the yield surface can be reached along an elastic path while those outside it can only be attained along paths accompanied by plastic deformations. If the yield surface is defined in strain space, then plastic stress decrements result whenever a strain path reaches this surface. No plastic stress decrements are induced along any elastic path.

If the material is such that yield is not associated with changes in the elastic moduli, then the plastic strain increment and the plastic stress decrement are normal to the yield surfaces in stress and strain space respectively. For such a material, the yield surface is convex.

When the unloading elastic moduli are changed upon plastic yield, then both the normality and convexity arguments might not follow from the stability criterion or the adopted definition of plasticity.

For small changes in the elastic moduli, the plastic strain increment (equation 5.1.5) and the plastic stress decrement (equation 5.1.17) are normal to the yield surfaces in stress and strain spaces respectively. The plastic strain increment will be directed along the outward normal to the yield surface in stress space at the yield point, while the plastic stress decrement will be directed along the inward normal at the yield point to the yield surface in strain space. Inherent in the arguments of normality and convexity is the assumption that the plastic strain increment (or alternatively the plastic stress decrement) is linear in the small and hence its direction is independent on the applied stress increment (or the applied strain increment).

Upon yield, the unloading stiffness moduli might change resulting in the absorption or release of energy. In general, if the elastic moduli increase as a result of internal reorientation of material particles, energy is absorbed. On the other hand, energy is dissipated if the elastic moduli decrease as a result of internal damage. When energy is dissipated, the yield surface (whether defined in

stress or strain space) retains its convexity. Concavity of the yield surface is possible if energy is absorbed as a result of material stiffening.

It should be noted that even when changes in the elastic moduli are not small, the plastic stress decrement is always directed along the inward normal to the yield surface in strain space (and the plastic strain increment is always directed along the outward normal to the yield surface in stress space) provided that energy is released upon plastic yield. In this case the second terms in 5.1.21 and 5.1.13 are negative and hence 5.1.18 and 5.1.6 always hold requiring normality.

5–1–4 Normality and convexity arguments for the progressively fracturing solids

The ideal progressively fracturing solid was described in chapter II. This solid fails by stable progressive decrease of its elastic stiffness moduli. At any stage of loading, the stress and strain tensors, σ_{ij} and ϵ_{ij}, are related by

$$\sigma_{ij} = S_{ijkm}\,\epsilon_{km} \qquad (5.1.23)$$

where S_{ijkm} is the tensor of the secant moduli. Upon unloading, the material goes back to the state of zero stress and zero strain.

A surface in strain space, termed the fracture surface, is defined to separate the strain states that can be reached along elastic paths from those states that can only be attained with accompanying damage involving loss of stiffness. This fracture surface is defined by

$$F(\epsilon_{ij}, H_k) = 0 \qquad (5.1.24)$$

where H_k is a damage vector of k parameters.

Starting from a strain state $\overset{*}{\epsilon}_{ij}$ within the elastic domain, such that the corresponding point O in strain space lies within the fracture surface, strain is added up to ϵ_{ij} such that the corresponding point P in strain space lies on the fracture surface. At P (corresponding to ϵ_{ij}) a strain increment $d\epsilon_{ij}$ is added so that the material strain state becomes $\epsilon_{ij}+d\epsilon_{ij}$ (figures 5.5 and 5.8). Denoting the stress corresponding to the strain ϵ_{ij} by σ_{ij}, then the stress corresponding to $\epsilon_{ij}+d\epsilon_{ij}$ can be denoted by $\sigma_{ij}+d\sigma_{ij}$ (represented by point Q in strain space). Hence the stress corresponding to point Q is

$$\sigma_{ij} + d\sigma_{ij} = (S_{ijkm} + dS_{ijkm})(\epsilon_{km} + d\epsilon_{km}) \tag{5.1.25}$$

with dS_{ijkm} as the change of the stiffness tensor due to the fracture inflicted by the change in strain $d\epsilon_{ij}$. The stress corresponding to the strain ϵ_{ij} is given by 5.1.23. Subtracting 5.1.23 from 5.1.25, results in the expression for the stress increment

$$d\sigma_{ij} = S_{ijkm} d\epsilon_{km} + dS_{ijkm} \epsilon_{km} + dS_{ijkm} d\epsilon_{km} \tag{5.1.26}$$

or

$$d\sigma_{ij} = d\sigma'_{ij} + d\sigma''_{ij} + d\sigma'''_{ij} \tag{5.1.27}$$

where

$$d\sigma'_{ij} = S_{ijkm} d\epsilon_{km} \tag{5.1.28}$$

and

$$d\sigma''_{ij} = dS_{ijkm} \epsilon_{km} \tag{5.1.29}$$

are termed the elastic stress increment and fracture stress decrement respectively. The last term

$$d\sigma'''_{ij} = dS_{ijkm} d\epsilon_{km} \tag{5.1.30}$$

is a higher order term compared to $d\sigma'_{ij}$ and $d\sigma''_{ij}$ and hence can be ignored in equation 5.1.27 so that

$$d\sigma_{ij} = d\sigma'_{ij} + d\sigma''_{ij} \tag{5.1.31}$$

which was essential in the formulation of the theory of progressively fracturing solids (chapter II).

Assuming that the material conforms with Il'ushin's definition of plasticity and applying inequality 5.1.15 to the strain path OPQRS gives (figure 5.8),

$$\begin{aligned} &-d\sigma''_{ij} (\epsilon_{ij} - \overset{*}{\epsilon}_{ij}) - \frac{1}{2} d\sigma''_{ij} d\epsilon_{ij} \\ &+ \frac{1}{2} d\sigma^{s}_{ij} (\epsilon_{ij} + d\epsilon_{ij} - \overset{*}{\epsilon}_{ij}) \\ &- d\sigma'''_{ij} (\epsilon_{ij} + \frac{1}{2} d\epsilon_{ij} - \overset{*}{\epsilon}_{ij}) \geq 0 \end{aligned} \tag{5.1.32}$$

where the third term of the above inequality measures the amount of energy dissipated as the result of stiffness degradation.

For the case when the material state is one of incipient fracture (ie. O and P are coincident), ϵ_{ij} and $\overset{*}{\epsilon}_{ij}$ will be equal and

$$d\sigma^{s}_{ij} = d\sigma'''_{ij} = dS_{ijkm} d\epsilon_{km} \tag{5.1.33}$$

In this case, the inequality 5.1.32 reduces to

$$-\frac{1}{2}\, d\sigma''_{ij}\, d\epsilon_{ij} \geq 0 \qquad (5.1.34)$$

which requires normality of the fracture stress decrement $d\sigma''_{ij}$ to the fracture surface at point P for any arbitrary choice of the strain increment $d\epsilon_{ij}$. It should be noted that for the progressively fracturing solid the normality criterion was reached without the restriction that the changes in the elastic moduli be small. In the case of small changes in the elastic moduli upon fracture, the tensor $d\sigma''_{ij}+d\sigma'''_{ij}$ will be very little affected by $d\sigma'''_{ij}$. Hence $d\sigma''_{ij}+d\sigma'''_{ij}$ will be collinear with $d\sigma''_{ij}$ and directed along the inward normal to the fracture surface. The same conclusion was reached in section 5–1–2 for the plastic stress decrement which in the sense of the present formulation is equal to $d\sigma''_{ij}+d\sigma'''_{ij}$.

For large values of $(\epsilon_{ij} - \overset{*}{\epsilon}_{ij})$, the stress decrement $d\sigma^s_{ij}$ is given by

$$d\sigma^s_{ij} = dS_{ijkm}\,(\epsilon_{km} - \overset{*}{\epsilon}_{km}) \qquad (5.1.35)$$

so that, after neglecting higher order terms. 5.1.32 reduces to

$$-d\sigma''_{ij}\,(\epsilon_{ij} - \overset{*}{\epsilon}_{ij}) + \frac{1}{2}\, d\sigma^s_{ij}\,(\epsilon_{ij} - \overset{*}{\epsilon}_{ij}) \geq 0 \qquad (5.1.36)$$

The second term in the above inequality is always negative as it is a measure of the amount of energy dissipated as the result of stiffness degradation. The first term is thus non–negative, as it should always be larger than a positive number. The directions of $(\epsilon_{ij} - \overset{*}{\epsilon}_{ij})$ and $-d\sigma''_{ij}$ (which is directed along the outward normal to the fracture surface as a result of 5.1.34) should always form an acute angle regardless of the choice of $\overset{*}{\epsilon}_{ij}$. This means that all points within the fracture surface should lie on the same side of the tangent to the fracture surface at P as the inward normal. Hence, the fracture surface must be convex.

In summary, for an ideal progressively fracturing solid, Il'ushin's stability criterion requires that upon fracture, the direction of the fracture stress decrement should lie along the inward normal to the convex fracture surface at the point of fracture. This is true provided the material is linear in the small in the sense that the direction of the fracture stress decrement is independent on the applied strain increment.

5–2 Extensions to the theory of progressively fracturing solids to include time and rate effects.

This section is concerned with the formulation of a theory for the description of the behaviour of the ideal progressively fracturing solid (chapter II), extended to include time and rate effects. The theory presented here is based on viscoelasticity and degradation.

5–2–1 The fracture surface – Loading criteria

As for the theories of plasticity and the time–independent progressively fracturing solid, a fracture surface is defined in order to distinguish between viscoelastic behaviour and degradation. With the spirit of the time–independent theory of the progressively fracturing solids, this surface is defined in strain space. To do this, a loading function is introduced of the form

$$F = F(\epsilon_{ij}, H_k, T_q) \qquad (5.2.1)$$

where ϵ_{ij} is the strain tensor, H_k is a damage vector of k parameters measuring the state of material damage or degradation, and the vector T_q is a measure of the time history of strain up to the current state. The loading function determines a surface in strain space, termed the "fracture surface", defined by

$$F = F(\epsilon_{ij}, H_k, T_q) = 0 \qquad (5.2.2)$$

In choosing this description, it should be noted that the vector H_k reflects the dependence of the shape and position of the fracture surface on the damage inflicted on the material by prior loading while the vector T_q reflects the dependence on the past time history of strain. It should also be noted that the formulation implies that coupling exists between the time–dependent effects and fracture due to degradation. At any time t, the state of the material can be described only by using all four of the state variables σ_{ij}, ϵ_{ij}, H_k, and T_q. The parameters H_k and T_q, thus, reflect the coupled effects of path and time history of strain respectively.

With the spirit of the terminology used by Naghdi and Murch [120], the set of all state variables necessary to define uniquely the response of the material at a certain time is termed as the "state" of the material. Thus, a point in strain space no longer defines a material state uniquely and the variables H_k and T_q corresponding to that state need to be mentioned.

The theory is to be formulated in such a way that it reduces to viscoelasticity or the theory for the time–independent progressively fracturing solid as special cases. In the limiting case of viscoelastic behaviour, the state of the material is determined by its strain ϵ_{ij}, which can be represented by a point in strain space, and the past time history of strain or T_q. On the other hand, for a time–independent progressively fracturing solid, the material state is defined by the strain path history H_k together with the strain ϵ_{ij}.

In order to arrange for these limiting cases to be available within the general theory, the parameters H_k and T_q are chosen such that

(a) $dH_k \neq 0$ and $dT_q = 0$	during time–independent progressive fracture
(b) $dH_k = 0$ and $dT_q = 0$	during linear elastic behaviour
(c) $dH_k = 0$ and $dT_q \neq 0$	during linear viscoelastic behaviour

and

(d) $dH_k \neq 0$ and $dT_q \neq 0$	during time–dependent progressive fracture

(5.2.3)

Conditions (a) and (b) combined will result in the reduction of the present theory to the already established time–independent progressively fracturing solids theory (chapter II).

The fracture surface in strain space defined by 5.2.2 separates those states that can be accessible without a change in the damage of the material from those states that are only accessible through fracture. The sign of the loading function is chosen such that F is negative for all strain states within the surface. These states can be reached via strain paths that are linear elastic or viscoelastic. With $F = 0$ the material is in a viscoelastic/fracturing state. Starting from such a state, subsequent behaviour may lead to a neighboring viscoelastic state (unloading) or may involve degradation of material properties (loading).

The different loading criteria can be understood if the changes in the loading function F accompanying the changes $d\epsilon_{ij}$, dH_k, and dT_q, starting form a viscoelastic/fracturing state ($F = 0$), are examined.

The differential form of 5.2.1 is

$$dF = \frac{\partial F}{\partial \epsilon_{ij}} d\epsilon_{ij} + \frac{\partial F}{\partial H_k} dH_k + \frac{\partial F}{\partial T_q} dT_q \qquad (5.2.4)$$

For a change of state, starting from a viscoelastic/fracturing state (F = 0) to a viscoelastic state (F < 0), dF should be negative. In this case, no degradation of material properties occurs so that $dH_k = 0$. Thus, for linear behaviour

$$F = 0 \text{ and } \frac{\partial F}{\partial \epsilon_{ij}} d\epsilon_{ij} + \frac{\partial F}{\partial T_q} dT_q \leq 0$$

(unloading) (5.2.5)

For the special case of condition 5.2.5 when a change leads to a neighbouring point on the fracture surface such that

$$F = dF = 0 \qquad (5.2.6)$$

with no degradation occurring, then dH_k is again zero. This requires

$$F = 0 \text{ and } \frac{\partial F}{\partial \epsilon_{ij}} d\epsilon_{ij} + \frac{\partial F}{\partial T_q} dT_q = 0$$

(neutral loading) (5.2.7)

It is important to note that the "neutral loading" (F = dF = 0) is not a tangential loading in strain space, since it is defined by 5.2.7 and not by

$$\frac{\partial F}{\partial \epsilon_{ij}} d\epsilon_{ij} = 0 \qquad (5.2.8)$$

as was the case for the ideal time–independent progressively fracturing solid. The behaviour during neutral loading is also linear viscoelastic so it is not a distinct condition of loading and hence is included in 5.2.5

To complete the above description of loading criteria, it is noted from 5.2.5 and 5.2.7 that for

$$F = 0 \text{ and } \frac{\partial F}{\partial \epsilon_{ij}} d\epsilon_{ij} + \frac{\partial F}{\partial T_q} dT_q > 0$$

(loading) (5.2.9)

the behaviour leads to another viscoelastic/fracturing state with dH_k different from zero. This behaviour is accompanied by material degradation.

In summary, the loading conditions, that provide criteria for distinguishing different modes of behaviour (figure 5.10), are

(a) viscoelastic behaviour $F < 0$

(b) linear viscoelastic unloading

$$F = 0 \text{ and } \frac{\partial F}{\partial \epsilon_{ij}} d\epsilon_{ij} + \frac{\partial F}{\partial T_q} dT_q \leq 0$$

(c) loading

$$F = 0 \text{ and } \frac{\partial F}{\partial \epsilon_{ij}} d\epsilon_{ij} + \frac{\partial F}{\partial T_q} dT_q > 0 \qquad (5.2.10)$$

5–2–2 Some remarks on the fracture surface

The use of the term T_q provides the dependence of the material behaviour on time. As a result, a strain increment may lead to loading at some rate of application while it may cause viscoelastic unloading at another applied strain rate.

It is the presence of T_q that results in the neutral loading being a non–tangential loading in strain space as was the case for the former time–independent progressively fracturing solids theory (and the classical theory of plasticity). While neutral loading is defined by 5.2.7, tangential loading is described by 5.2.8. The expressions 5.2.7 and 5.2.8 are not identical in general due to the presence of T_q.

When the behaviour of the material is in the viscoelastic range ($dH_k = 0$ with no degradation occurring), time–dependence, reflected by T_q, results in the dependence of the occurrence of degradation on the strain time history even when no degradation is actually progressing. As a result of this, the position and shape of the fracture surface may change with time in strain space eventhough no degradation is occurring ($dH_k = 0$). That is, if the material is in the viscoelastic domain ($F < 0$) such that

$$\frac{\partial F}{\partial T_q} \neq 0 \qquad (5.2.11)$$

then the fracture surface may change in strain space depending on the strain time history even if no progressive fracture takes place. This is different from the former time–independent progressively fracturing solids theory where the fracture surface could vary only when the behaviour is accompanied by progressive fracture.

In view of 5.2.11, a fixed initial fracture surface, similar to that in the

time–independent formulation in chapter II (or the initial yield surface in the classical theory of plasticity) no longer can be defined. The behaviour of the surface defined by 5.2.2 resembles a surface that changes continuously even during viscoelastic behaviour and unloading.

Clearly, as a possible simplification, F and T_q could be chosen such that when the behaviour is viscoelastic ($F < 0$)

$$\frac{\partial F}{\partial T_q} = 0 \qquad (5.2.12)$$

so that the fracture surface can change only when fracture occurs.

The expression 5.2.11 is more general as it allows a time–dependent description of material behaviour under no additional loading. It includes in the description the dependence of fracture initiation on the time history of strain rather than on the additional application of deformations only.

Prager [128] has suggested a similar formulation for temperature dependent plasticity where the vector T_q was used to describe temperature rather than time dependence. Again coupling was considered but between stress and thermal effects.

5–2–3 Convexity of the fracture surface – The argument of normality

(a) Basic definitions

Naghdi and Murch [120] have investigated the requirements for convexity and normality for a linear viscoelastic/plastic material. The description and arguments were developed in stress space and the material exhibited coupling between stress path history and stress time history of the form suggested in section 3–4–3 for a strain space based description. The arguments that follow are similar to those in their theory with the additional consideration of the effects of the changes in the elastic stiffness moduli due to fracture.

In their theory, the concept of a "rapid path" in stress space was introduced. Such a path is traversed in stress space in an infinitesimally small interval of time. "The instantaneous yield surface" was also defined as the yield surface, corresponding to a given state in stress space, that can be reached from that state by any rapid path.

Consider a state of a representative sample of an ideal progressively fracturing material in the viscoelastic domain defined by $\epsilon_{ij}^{(a)}$, $H_k^{(a)}$, and $T_q^{(a)}$. This material state can be represented by a point in strain space defined by the components of the tensor $\epsilon_{ij}^{(a)}$ and allocated the values of the vectors $H_k^{(a)}$ and $T_q^{(a)}$. Starting from that material state, strain is added up to a viscoelastic/fracturing state in a finite period of time Δt. This change in strain can be represented by a strain path in strain space but this path is associated with the time interval Δt and the corresponding changes in the vector T_q. It should be noted that the same strain path can lead to the same final state of strain for different values of Δt. In particular, for infinitesimally small Δt ($\Delta t \rightarrow 0$), the path will be called a rapid strain path. For this particular path, time effects are simply absent because deformation occurs in practically no time, and the strain states reached will have similar properties to those encountered in the time–independent progressively fracturing solids theory. For a rapid strain path

$$dT_q = 0 \qquad (5.2.13)$$

so that T_q remains unchanged in both the viscoelastic and viscoelastic/fracturing domains. Observing 5.2.3 (a) and (b) explains why the behaviour of the fracture surface reached by a rapid path is expected to be similar to that obtained for the time–independent progressively fracturing solid. It should be noted that the behaviour does not reduce to that of an ideal time–independent progressively fracturing solid but is somehow scaled from the limiting case of the time–independent behaviour with T_q as a scaling factor (dT_q has the value of zero but not T_q).

The fracture surface, corresponding to a certain state of the representative sample, that can be reached from that state by any rapid strain path, is termed as the "instantaneous fracture surface" corresponding to that state. Such a fracture surface is uniquely determined for a given state in strain space because a rapid strain path is followed and hence T_q remains unchanged ($dT_q = 0$). This is similar to the uniqueness encountered in the time–independent progressively fracturing solids theory. If a point A in strain space, defined by $\epsilon_{ij}^{(a)}$, and allocated the values $T_q^{(a)}$, and $H_k^{(a)}$ at time t_a ($t_a \geq 0$), is such that

$$F(\epsilon_{ij}^{(a)}, H_k^{(a)}, T_q^{(a)}) < 0 \qquad (5.2.14)$$

then the state of the material represented by A (and the allocated values of H_k and T_q) is within the viscoelastic domain and corresponding to it is a surface in

strain space defined by

$$F_a = F(\epsilon_{ij}, H_k^{(a)}, T_q^{(a)}) = 0 \qquad (5.2.15)$$

This surface is termed "the instantaneous fracture surface" corresponding to the material state represented by A in strain space and defined by $\epsilon_{ij}^{(a)}$, $H_k^{(a)}$, and $T_q^{(a)}$. This surface is dependent on the loading path and time history leading to that material state. It is noted (expressions 5.2.14 and 5.2.15) that T_q remains unchanged from the material state represented by A to the instantaneous fracture surface so that

$$dT_q = 0 \qquad (5.2.16)$$

along any path from A to this surface. Thus a rapid strain path is followed by definition.

(b) Stability, work, and energy considerations

In the formulation of the time–independent progressively fracturing solids theory, Il'ushin's postulate of plastic deformation was used as a criterion from which normality of the fracture stress decrement to the fracture surface and the convexity of such a surface followed. In the present formulation the same criterion is assumed with the time domain taken into account.

If a body undergoes an arbitrary process, which can be represented by a strain path AB in strain space, after which the sense of loading is changed so that the body returns back to the original strain, the body is then said to have performed a closed strain cycle. Considering every intermediate state to be in equilibrium, then the path is considered to have satisfied Il'ushin's definition of plasticity if the work done along it is non–negative. This requires that

$$W = \int \sigma_{ij}\, d\epsilon_{ij} \geq 0 \qquad (5.2.17)$$

along any closed cycle of strain. Since the work done by a constant stress $\overset{*}{\sigma}_{ij}$ along a closed strain cycle is always zero then 5.2.17 can be replaced by

$$W = \int (\sigma_{ij} - \overset{*}{\sigma}_{ij})\, d\epsilon_{ij} \geq 0 \qquad (5.2.18)$$

In considering time–dependent behaviour, the time within which the closed strain cycle is traversed affects the work integral so that 5.2.17 and 5.2.18 should be replaced by

$$W = \int_0^T \sigma_{ij}\, \dot{\epsilon}_{ij}\, dt \geq 0 \qquad (5.2.19)$$

and

$$W = \int_0^T (\sigma_{ij} - \overset{*}{\sigma}_{ij})\, \dot{\epsilon}_{ij}\, dt \geq 0 \qquad (5.2.20)$$

where W is evaluated along a closed strain cycle during the finite interval of time $0 \leq t \leq T$. The dots in 5.2.19 and 5.2.20 stand for derivatives with respect to time.

The above consideration of work along a certain closed strain path restricts the description presented in here to a class of materials that conform with Il'ushin's definition of plasticity. It is worth mentioning that this consideration is less restrictive than that that would have followed if Drucker's stability criterion was adopted.

As in [115,120], it is sometimes convenient to define the work integrals in terms of two alternative strain paths $\epsilon_{ij}^{(1)}$ and $\epsilon_{ij}^{(2)}$ to which two distinct stress fields $\sigma_{ij}^{(1)}$ and $\sigma_{ij}^{(2)}$ correspond. The two paths are considered to be identical at time $t = 0$ after which they diverge. For Il'ushin's definition of plasticity to be satisfied, the following inequality should always hold

$$\int_0^T (\sigma_{ij}^{(2)} - \sigma_{ij}^{(1)})\, (\dot{\epsilon}_{ij}^{(2)} - \dot{\epsilon}_{ij}^{(1)})\, dt \geq 0 \qquad (5.2.21)$$

along any two closed strain cycles $\epsilon_{ij}^{(1)}$ and $\epsilon_{ij}^{(2)}$. In [115,120] the above inequality was introduced as a stability criterion, derived from Drucker's definition of a class of stable materials, along closed stress paths so that if Il'ushin's postulate of stable deformations is assumed, the use of 5.2.21 defined along closed strain paths is justified.

Since the present theory is defined in strain space, it is more convenient to express the work integral 5.2.20 as

$$W = -\int_0^T (\epsilon_{ij} - \overset{*}{\epsilon}_{ij})\, \dot{\sigma}_{ij}\, dt \geq 0 \qquad (5.2.22)$$

where $\overset{*}{\epsilon}_{ij}$ is the initial strain state. In the case of two strain paths $\epsilon_{ij}^{(1)}$ and

$\epsilon_{ij}^{(2)}$ and the corresponding stress paths $\sigma_{ij}^{(1)}$ and $\sigma_{ij}^{(2)}$, the work integral becomes

$$-\int_0^T (\epsilon_{ij}^{(2)} - \epsilon_{ij}^{(1)})\,(\dot{\sigma}_{ij}^{(2)} - \dot{\sigma}_{ij}^{(1)})\,dt \geq 0 \qquad (5.2.23)$$

The superior dots denote derivatives with respect to time.

In the integral 5.2.23 the two state variables $\epsilon_{ij}^{(1)}$ and $\epsilon_{ij}^{(2)}$, and their corresponding stress tensors $\sigma_{ij}^{(1)}$ and $\sigma_{ij}^{(2)}$, correspond to two different loading paths in strain space. Both paths start, at time t=0, at the same material state represented by point A in strain space. At time $t=0^+$ they diverge into two strain paths and they return back again, at time t=T, to two distinct material states represented by points A_1 and A_2 such that all three states (the initial and the two final states) have the same strain tensor $\overset{*}{\epsilon}_{ij}$ (other state variables being possibly different). Hence the three points A, A_1, and A_2 coincide in strain space.

Consider (figure 5.10) the two strain paths $\epsilon_{ij}^{(1)}$ and $\epsilon_{ij}^{(2)}$ such that path (2) (defined by $\epsilon_{ij}^{(2)}$) is identified with a stationary state of strain. This means that $\epsilon_{ij}^{(2)}$ remains at a constant value of $\overset{*}{\epsilon}_{ij}$. To this stationary strain path corresponds a stress path $\overset{*}{\sigma}_{ij}$ which is not stationary due to viscoelatic effects. Path (2) is chosen so that the material is always in the viscoelastic range along the time interval $0 \leq t \leq T$ and hence no degradation is associated with $\dot{\sigma}^*_{ij}$.

Path (1) is such that the material follows a closed strain cycle in strain space during the same defined finite interval of time $0 \leq t \leq T$. At time t=0 the material state with strain $\overset{*}{\epsilon}_{ij}$, is represented by point A in strain space. For the time interval $0 \leq t \leq t_1$ strain is added such that at time t_1 the material state reaches the fracture surface. This strain change is represented by the path ABC (figure 5.10) in strain space such that point C is on the current fracture surface. This fracture surface is a function of the state variables at point C. In other words, it is dependent on the state variables represented by point A and the changes encountered along path ABC. The fracture surface (F = 0) is thus the surface reached by the specific loading path and history ABC.

For a small time interval $t_1 < t \leq t_2$ strain is applied to cause fracture. This change is represented by path CD and is accompanied by a fracture stress decrement $d\sigma''_{ij}$. After t_2, viscoelastic unloading is followed and is represented by path DEA. The strain of the material returns back to $\overset{*}{\epsilon}_{ij}$. Unloading occurs for the time interval $t_2 < t \leq T$.

Applying the integral 5.2.23 to the above two strain paths over the finite interval of time T, gives

$$-\int_0^T (\epsilon_{ij} - \overset{*}{\epsilon}_{ij})(\dot{\sigma}_{ij} - \dot{\sigma}^*_{ij})dt \geq 0 \qquad (5.2.24)$$

It should be noted that the superscript (1) is no more used and (2) is replaced by *. Hence the tensor ϵ_{ij} in the integral 5.2.24 represents the strain along the strain path (1) described above and σ_{ij} denotes the corresponding stress along the same path. At time t=0 the strain ϵ_{ij} assumes the value of $\overset{*}{\epsilon}_{ij}$.

On the other hand, path (2) is described by the constant strain $\overset{*}{\epsilon}_{ij}$ at all times and the corresponding stress $\overset{*}{\sigma}_{ij}$ which changes during the time interval $0 \leq t \leq T$ due to viscoelastic effects.

The increment of stress at any time is expressed as the sum of two components so that

$$\dot{\sigma}_{ij} = \dot{\sigma}'_{ij} + \dot{\sigma}''_{ij}$$

and

$$\dot{\sigma}^*_{ij} = \dot{\sigma}^{*'}_{ij} + \dot{\sigma}^{*''}_{ij} \qquad (5.2.25)$$

where $\dot{\sigma}'_{ij}$ is the viscoelastic stress increment and $d\dot{\sigma}''_{ij}$ is the fracture stress decrement along the first path. Similar definitions apply to the components of the stress rate, $\dot{\sigma}^*_{ij}$, along the second path. Substituting 5.2.25 in 5.2.24 gives

$$-\int_0^T (\epsilon_{ij} - \overset{*}{\epsilon}_{ij}) \left[(\dot{\sigma}'_{ij} - \dot{\sigma}^{*'}_{ij}) + (\dot{\sigma}''_{ij} - \dot{\sigma}^{*''}_{ij})\right] dt \geq 0 \qquad (5.2.26)$$

It is important to note that $\dot{\sigma}^{*''}_{ij}$ is always zero, since path (2) is always in the viscoelastic domain. Also $\dot{\sigma}''_{ij}$ is always zero along path (1) except in the interval $t_1 < t \leq t_2$ (with $\Delta t = t_2 - t_1$) since, by definition, a fracture stress decrement occurs only upon loading outside the fracture surface. During the time intervals $0 \leq t < t_1$ and $t_2 \leq t < T$ the material, along path (1), deforms in a viscoelastic fashion represented by paths AC and DA in strain space (figure 5.10). Thus the integral 5.2.26 can be rewritten as

$$\int_0^T -(\epsilon_{ij} - \overset{*}{\epsilon}_{ij})(\dot{\sigma}'_{ij} - \dot{\sigma}^{*'}_{ij})dt - \int_{t_1}^{t_2} (\epsilon_{ij} - \overset{*}{\epsilon}_{ij})\,\dot{\sigma}''_{ij}dt \geq 0 \tag{5.2.27}$$

Writing the first integral of 5.2.27 as

$$\int_0^T (\epsilon_{ij} - \overset{*}{\epsilon}_{ij})\,[-(\dot{\sigma}'_{ij} - \dot{\sigma}^{*'}_{ij})]\,dt = \overset{T}{\underset{t=0}{\Pi}} \tag{5.2.28}$$

the inequality 5.2.27 becomes

$$\overset{T}{\underset{t=0}{\Pi}} + \int_{t_1}^{t_2} (\epsilon_{ij} - \overset{*}{\epsilon}_{ij})\,(-\dot{\sigma}''_{ij})\,dt \geq 0 \tag{5.2.29}$$

$\overset{T}{\underset{t=0}{\Pi}}$ is a measure of the viscoelastic work done during the time interval $0 \leq t \leq T$. For a sufficiently small interval of time Δt ($\Delta t = t_2 - t_1$), and thus for a small increment of the fracture stress $d\sigma''_{ij}$, the second term of 5.2.29 can be replaced by its Taylor series expansion about $t = t_1$, so that

$$\int_{t_1}^{t_2} (\epsilon_{ij} - \overset{*}{\epsilon}_{ij})\,(-\dot{\sigma}''_{ij})\,dt = \left[(\epsilon_{ij} - \overset{*}{\epsilon}_{ij})\,\frac{-d\sigma''_{ij}}{\Delta t}\,\Delta t + \frac{1}{2}(\Delta t)^2 \frac{d\epsilon_{ij}}{\Delta t}\,\frac{-d\sigma''_{ij}}{\Delta t}\right]_{t=t_1} + \text{higher order terms} \tag{5.2.30}$$

Neglecting higher order terms in 5.2.30 and denoting time rates by superior dots result in

$$\int_{t_1}^{t_2} (\epsilon_{ij} - \overset{*}{\epsilon}_{ij})\,(-\dot{\sigma}''_{ij})\,dt$$

$$= \Delta t \left[(\epsilon_{ij} - \overset{*}{\epsilon}_{ij})\,(-\dot{\sigma}''_{ij}) + \frac{1}{2}\,d\epsilon_{ij}\,(-\dot{\sigma}''_{ij})\right]_{t=t_1} \tag{5.2.31}$$

with $\Delta t = t_2 - t_1$. Substituting 5.2.31 in 5.2.29 gives

$$\prod_{t=0}^{T} + \Delta t \left[(\epsilon_{ij} - \overset{*}{\epsilon}_{ij})\,(-\dot{\sigma}''_{ij}) + \frac{1}{2}\,d\epsilon_{ij}\,(-\dot{\sigma}''_{ij})\right]_{t=t_1} \geq 0 \tag{5.2.32}$$

It should be mentioned that the energy considerations presented above will lead to the arguments of convexity and normality as will be seen in the following section. These considerations are based on Il'ushin's definition of plasticity and hence all description is limited to a class of materials that conform with such a definition.

(c) Convexity of the instantaneous fracture surface and normality of the instantaneous fracture stress decrement

In this section the convexity of the instantaneous fracture surface reached by a rapid path and the normality of the fracture stress decrement to this surface are considered.

Consider a representative sample of the material, at time t_a, characterized by $\overset{*}{\epsilon}_{ij}$, $H_k^{(a)}$, and $T_q^{(a)}$ such that the material state is within the viscoelastic domain. This material state is represented by point A in strain space, defined by $\overset{*}{\epsilon}_{ij}$ and allocated the values of $H_k^{(a)}$ and $T_q^{(a)}$. Starting from this state two strain paths are assumed to be followed by the material:

(i) In the first path (figure 5.10). strain is increased until fracture occurs at time t_1 ($t_1 \geq t_a$). The material state at time t_1 is characterized by $\epsilon_{ij}^{(c)}$, $H_k^{(c)}$, and is represented by point C in strain space. It is important to note that dH_k is zero along path AC since fracture is only initiated at C. Thus $H_k^{(a)}$ and $H_k^{(c)}$ are equal, so that the equation

$$F_c = F(\epsilon_{ij}, T_q^{(c)}, H_k^{(a)}) = 0 \qquad (5.2.33)$$

represents a set of possible fracture surfaces each corresponding to a different time history reflected by different values of T_q which is dependent on the time history of loading along strain path AC. A spectrum of fracture surfaces corresponding to the various states at fracture can thus be defined by 5.2.33 for a given value of the damage vector $H_k^{(a)}$ (figure 5.11). The point C representing the state at fracture in strain space is not necessary the same for all strain paths because the fracture state is dependent on the time history along the strain path. In particular, for a rapid path $T_q^{(a)}$ and $T_q^{(c)}$ become equal and 5.2.33 will reduce to 5.2.15 and all fracture surfaces described by 5.2.33 will converge to the instantaneous fracture surface corresponding to the material state at time t_a (which is represented by point A in strain space).

A fracture stress decrement $\dot{\sigma}''_{ij}$ is induced due to an additional strain increment $d\epsilon_{ij}$, applied at the time of fracture t_1, which causes loading. After fracture, viscoelastic unloading is followed back to the original strain $\overset{*}{\epsilon}_{ij}$ at time T (figure 5.10).

(ii) In the second path, strain is kept constant at the value of $\overset{*}{\epsilon}_{ij}$ during the time interval $t_a \leq t \leq T$. Corresponding to this strain path is the stress path $\overset{*}{\sigma}_{ij}$ (which is not constant due to viscoelastic effects).

These two paths being similar to those that has led to inequality 5.2.32, the following should hold

$$\frac{1}{\Delta t} \prod_{t=t_a}^{T} + \left[(\epsilon_{ij} - \overset{*}{\epsilon}_{ij})(-\dot{\sigma}''_{ij}) + \frac{1}{2} d\epsilon_{ij}(-\dot{\sigma}''_{ij}) \right]_{t=t_1} \geq 0 \qquad (5.2.34)$$

where in the second term ϵ_{ij} and $\dot{\sigma}''_{ij}$ are the strain and the fracture stress decrement along the first path evaluated at t_1 (i.e. at the fracture point C) and Δt is given by

$$\Delta t = t_2 - t_1 \qquad (5.2.35)$$

The first term in 5.2.34, $\prod_{t=t_a}^{T}$, has to be evaluated along the two intervals $t_a \leq t \leq t_2$ and $t_2 \leq t \leq T$ keeping in mind the possible changes in the elastic moduli

upon unloading. Thus

$$\prod_{t=t_a}^{T} = \int_{t_a}^{t_2} (\epsilon_{ij} - \overset{*}{\epsilon}_{ij}) [-(\dot{\sigma}'_{ij} - \dot{\sigma}^{*\prime}_{ij})] \, dt + \int_{t_2}^{T} (\epsilon_{ij} - \overset{*}{\epsilon}_{ij}) [-(\dot{\sigma}'_{ij} - \dot{\sigma}^{*\prime}_{ij})] \, dt \tag{5.2.36}$$

where ϵ_{ij} represents the strain along the first path and $\dot{\sigma}'_{ij}$ is the corresponding viscoelastic stress increment. The term $\overset{*}{\epsilon}_{ij}$ represents the constant strain along the second path with $\dot{\sigma}^{*\prime}_{ij}$ as the corresponding viscoelastic stress component (which is not constant due to viscoelastic effects).

The expression 5.2.36 applies for any strain cycle (path ACDA in figure 5.10). In particular, for a rapid path traversed in an infinitely small time, $T \rightarrow t_a$, $\Delta t_1 \rightarrow 0$, and $\Delta t_2 \rightarrow 0$ (where $\Delta t_1 = t_1 - t_a$ and $\Delta t_2 = T - t_2$). The change in the strain time history vector dT_q vanishes along this path so that the fracture surface at the material state represented by point C coincides with the instantaneous fracture surface corresponding to the initial material state represented by point A in strain space. This instantaneous surface is given by 5.2.15. It should be noted that

$$\int_{t_a}^{T} (\epsilon_{ij} - \overset{*}{\epsilon}_{ij}) \, \dot{\sigma}^{*\prime}_{ij} \, dt = 0 \tag{5.2.37}$$

for a very small interval of time $(T - t_a)$, since in this case $\dot{\sigma}^{*\prime}_{ij}$ is constant along this small interval of time (with vanishing viscoelastic effects). Using 5.2.37 and expressing 5.2.36 as a Taylor series expansion evaluated at t_2 will give

$$\begin{aligned} \prod_{t=t_a}^{T} &= -\frac{1}{2} \left[\epsilon_{ij} - \overset{*}{\epsilon}_{ij} \right]_{t_2} \Delta_1 \sigma'_{ij} - \frac{1}{2} \left[\epsilon_{ij} - \overset{*}{\epsilon}_{ij} \right]_{t_2} \Delta_2 \sigma'_{ij} \\ &= -\frac{1}{2} \left[\epsilon_{ij} - \overset{*}{\epsilon}_{ij} \right]_{t_2} (\Delta_1 \sigma'_{ij} + \Delta_2 \sigma'_{ij}) \\ &= \frac{1}{2} \left[\epsilon_{ij} + d\epsilon_{ij} - \overset{*}{\epsilon}_{ij} \right]_{t_1} d\sigma^s_{ij} \end{aligned} \tag{5.2.38}$$

where $\Delta_1 \sigma'_{ij}$ is the difference in the viscoelastic stress between time t_2 and t_a, $\Delta_2 \sigma'_{ij}$ is the difference in the viscoelastic stress between time T and t_2, and $d\sigma^s_{ij}$ is given by

$$d\sigma^s_{ij} = -(\Delta_2 \sigma'_{ij} + \Delta_1 \sigma'_{ij}) \tag{5.2.39}$$

The term ϵ_{ij} (in the last term of 5.2.38) is the strain along the first path evaluated at the time of fracture t_1 and $d\epsilon_{ij}$ is the strain increment along the same path applied also at the time of fracture.

Although $\Delta_1\sigma'_{ij}$ and $\Delta_2\sigma'_{ij}$ are the changes in the viscoelastic stress during the intervals $t_a \leq t \leq t_2$ and $t_2 \leq t \leq T$, they reduce in this case to the changes in stress due to the elastic deformation because dT_q is zero along the whole strain path rendering the viscous effects zero. The stress increment $d\sigma^s_{ij}$ is nothing but the change in the state of the stress at the same strain value $\overset{*}{\epsilon}_{ij}$ due to the difference in the elastic moduli between loading and unloading. The quantity $\Pi_{t=t_a}^{T}$ becomes the work done due to the changes in these moduli. It measures the energy absorbed or dissipated as a result of the changes in the material stiffness. Substituting 5.2.38 in 5.2.34 gives

$$(\epsilon_{ij} - \overset{*}{\epsilon}_{ij})(-\dot{\sigma}''_{ij}) + \frac{1}{2} d\epsilon_{ij} (-\dot{\sigma}''_{ij}) + \frac{1}{2} \frac{d\sigma^s_{ij}}{\Delta t} (\epsilon_{ij} + d\epsilon_{ij} - \overset{*}{\epsilon}_{ij}) \geq 0 \qquad (5.2.40)$$

Multiplying all terms by the time increment returns the above expression into an incremental form

$$(\epsilon_{ij} - \overset{*}{\epsilon}_{ij})(-d\sigma''_{ij}) + \frac{1}{2} d\epsilon_{ij} (-d\sigma''_{ij}) + \frac{1}{2} d\sigma^s_{ij} (\epsilon_{ij} + d\epsilon_{ij} - \overset{*}{\epsilon}_{ij}) \geq 0 \qquad (5.2.41)$$

In the above two inequalities, 5.2.40 and 5.2.41, the terms ϵ_{ij} and $d\epsilon_{ij}$ are the strain and the strain increment along the first path at the time of fracture. It should be noted that 5.2.41 followed as a result of neglecting the change in the stress increment $d\sigma_{ij}$ due to changes in the elastic moduli during the small interval of time $(t_2 - t_1)$ during which a small increment of strain was applied. If this change is not ignored then 5.2.25 will become

$$\dot{\sigma}_{ij} = \dot{\sigma}'_{ij} + \dot{\sigma}''_{ij} + \dot{\sigma}'''_{ij} \qquad (5.2.42)$$

where $\dot{\sigma}'''_{ij}$ is the stress increment due to changes in the elastic moduli in the short interval of time $t_2 - t_1$. A derivation similar to that that has lead to 5.2.41 gives (by replacing $\dot{\sigma}''_{ij}$ by $\dot{\sigma}''_{ij} + \dot{\sigma}'''_{ij}$)

$$(\epsilon_{ij} - \overset{*}{\epsilon}_{ij})(-d\sigma''_{ij}) + \frac{1}{2} d\epsilon_{ij} (-d\sigma''_{ij})$$
$$+ \frac{1}{2} d\sigma^{s}_{ij} (\epsilon_{ij} + d\epsilon_{ij} - \overset{*}{\epsilon}_{ij})$$
$$-d\sigma'''_{ij} (\epsilon_{ij} + \frac{1}{2} d\epsilon_{ij} - \overset{*}{\epsilon}_{ij}) \geq 0 \qquad (5.2.43)$$

Inequality 5.2.43 was reached for the material when time dependence was not included (inequality 5.1.32). This is expected because a rapid path was followed for the formulation of 5.2.43.

For an initial material state on the fracture surface ($\epsilon_{ij} = \overset{*}{\epsilon}_{ij}$), inequality 5.2.43 reduces to (noting that in this case $d\sigma'''_{ij}$ and $d\sigma^{s}_{ij}$ become equal)

$$-\frac{1}{2} d\sigma''_{ij} d\epsilon_{ij} \geq 0 \qquad (5.2.44)$$

requiring the normality of the fracture stress decrement following a rapid path to the instantaneous fracture surface at the point of fracture.

For large values of $(\epsilon_{ij} - \overset{*}{\epsilon}_{ij})$ expression 5.2.43 will reduce, after neglecting higher order terms and noting that $d\sigma'''_{ij}$ becomes negligible compared to $d\sigma^{s}_{ij}$, to

$$(\epsilon_{ij} - \overset{*}{\epsilon}_{ij})(-d\sigma''_{ij}) + \frac{1}{2} d\sigma^{s}_{ij} (\epsilon_{ij} - \overset{*}{\epsilon}_{ij}) \geq 0 \qquad (5.2.45)$$

Three different cases emerge depending on the sign of the last term of 5.2.45:

(i) $d\sigma^{s}_{ij} (\epsilon_{ij} - \overset{*}{\epsilon}_{ij}) > 0$: This occurs for solids that absorb energy upon fracture due to increases in their elastic moduli, probably as a result of internal reorientation or dislocation of material constituents. This component of energy is different from that dissipated due to fracture. For such a solid, convexity of the instantaneous fracture surface might be violated. The degree of concavity depends on the amount of energy acquired and hence on the degree of increase in the elastic moduli.

(ii) $d\sigma^{s}_{ij} (\epsilon_{ij} - \overset{*}{\epsilon}_{ij}) = 0$ or more specifically $d\sigma^{s}_{ij} = 0$: This is the case of a solid that unloads with no changes in its elastic moduli. This is an ideal viscoelastic/plastic solid which was considered by Naghdi and Murch [120]. For such a solid, the elastic moduli are unaffected by viscoplastic deformations with no degradation occurring. The solid described in the present formulation differs

from that described in [120] in that strain softening is considered a stable mode of behaviour as a result of adopting Il'ushin's definition of plasticity rather than Drucker's postulate of stability. For this case, the instantaneous fracture surface must be convex.

(iii) $d\sigma^{s}_{ij}\,(\epsilon_{ij} - \overset{*}{\epsilon}_{ij}) < 0$: This is the case when energy is dissipated as a result of the degradation of the elastic moduli during loading. As in case (ii), the instantaneous fracture surface must be convex.

The present formulation, being an extension of the time–independent progressively fracturing solids theory, depends on the assumption of material degradation as a result of stable fracture and hence case (iii) is applicable. Thus, any instantaneous fracture surface is convex as a result of material stability, and the fracture stress decrement following a rapid strain path is always directed along the inward normal to this fracture surface at the point of fracture.

(d) Convexity of any fracture surface

Convexity of any fracture surface, whose definition is given by 5.2.33, follows directly by realizing that the approach given in section (c) is valid for any arbitrary choice of the initial material state represented by point A (figure 5.10 and 5.11) including a viscoelastic/fracturing one. In other words, if point A is chosen to be on the current fracture surface, then any material state that satisfies equation 5.2.15 has the same instantaneous fracture surface as that state (represented by point A). Hence, all points Q in strain space that fall within the domain defined by the instantaneous fracture surface (expression 5.2.15) corresponding to state A, which is on the current fracture surface, will have F_a (5.2.15) as their instantaneous fracture surface. This instantaneous fracture surface coincides with the current fracture surface at the material state represented by point A. It is thus enough to define any of these points to get the instantaneous fracture surface corresponding to the current fracture point A. In particular, this applies to the points on the boundary of this region that is the points on the instantaneous fracture surface. If fracture is initiated by a non–rapid path, then the fracture surface at the fracture point coincides with the instantaneous fracture surface corresponding to the last point on the path. The fracture surface acts as the instantaneous fracture surface for all points defined by

$$F_a = F(\epsilon_{ij}, H_k^{(a)}, T_q^{(a)}) = 0 \qquad (5.2.46)$$

where A is the point in strain space representing the state of the material at

fracture. All points in strain space within and on the surface defined by F_a have F_a as their instantaneous fracture surface. Hence F_a is convex because in section (c) it was concluded that any instantaneous fracture surface is convex (for the progressively fracturing solid presented in here).

Thus, for the material represented by the present formulation, convexity of the fracture surface holds for all such surfaces independently of the time or path history.

5–2–4 Material specifications – The constitutive law

So far no restriction on the behaviour of the material has been suggested other than that it should be linear viscoelastic and progressively fracturing in a stable degrading fashion upon fracture as a result of the reduction of its elastic moduli with damage. For the time–independent formulation of the theory (chapter II), a particular type of material was considered in which unloading was linear elastic with the additional condition that if the sense of applied deformations is reversed the material returns to the compatible state of zero stress and zero strain. This suggested a constitutive law between stress σ_{ij} and strain ϵ_{ij} of the form

$$\sigma_{ij} = S_{ijkm}\,\epsilon_{km} \qquad (5.2.47)$$

where the tensor of secant moduli, S_{ijkm}, is dependent on the current fracture state of the material and hence changes upon loading. Expression 5.2.47 can be represented in an incremental form as

$$d\sigma_{ij} = d\sigma'_{ij} + d\sigma''_{ij} + d\sigma'''_{ij} \qquad (5.2.48)$$

where $d\sigma'_{ij} = S_{ijkm}\,d\epsilon_{km}$ is the elastic stress increment and $d\sigma''_{ij} = dS_{ijkm}\,\epsilon_{km}$ is the fracture stress decrement. The last term in 5.2.48, $d\sigma'''_{ij} = dS_{ijkm}\,d\epsilon_{km}$, is a higher order term and hence can be neglected reducing 5.2.48 into

$$d\sigma_{ij} = d\sigma'_{ij} + d\sigma''_{ij} \qquad (5.2.49)$$

For the present formulation, when time effects are taken into consideration, an expression similar to 5.2.49 is sought in which time effects are included. The stress increment $d\sigma_{ij}(t)$ at a certain time t is expressed as

$$d\sigma_{ij}(t) = L_{ijkm}(t-\tau,H_k)\,d\epsilon_{km}(\tau) + dL_{ijkm}(t-\tau,H_k)\,\epsilon_{km}(\tau) \qquad (5.2.50)$$

where L_{ijkm} is termed the relaxation modulus tensor, a function of time and damage. $d\sigma_{ij}(t)$ is the change of stress at time t due to a change in strain $d\epsilon_{ij}(\tau)$ and/or in the relaxation modulus tensor dL_{ijkm} occurring at time τ ($t \geq \tau$). The state of the material at time τ is described by the vector H_k and ϵ_{ij} (both evaluated at time τ).

The implications of the incremental equation 5.2.50 and the restrictions imposed on the material behaviour are not immediately obvious. However, the significance of this equation upon the behaviour of the proposed material can be provided by examining the behaviour of the time–independent ideal material described by the progressively fracturing solids theory.

Consider the time–independent progressively fracturing solid with ϵ_{ij}, σ_{ij}, and S_{ijkm} as its initial state variables. This material state is represented by point A in figure 5.12. The stress at point A is given by equation 5.2.47. The changes of these state variables resulting from a change in strain, $d\epsilon_{ij}$, which causes fracture can be visualized by examining equations 5.2.47 and 5.2.48. The form of these equations suggest that it is permissible to imagine the final state of the material, represented by point B in figure 5.12, to be obtained from the initial state by unloading the material and then reloading it to a strain $(\epsilon_{ij}+d\epsilon_{ij})$ using the revised stiffness tensor $(S_{ijkm}+dS_{ijkm})$. Thus 5.2.47 can be used to evaluate the initial stress at point A and

$$\sigma_{ij} + d\sigma_{ij} = (S_{ijkm} + dS_{ijkm})(\epsilon_{km} + d\epsilon_{km}) \tag{5.2.51}$$

would evaluate the stress of the material represented by point B in figure 5.12. Subtracting equation 5.2.47 from 5.2.51 results in the expression of $d\sigma_{ij}$ given by 5.2.48. The formulation given above for the case of the time–independent solid is an essential feature which distinguishes this solid from others that might degrade in a different fashion.

Keeping the above argument in mind, let the strain $\epsilon_{ij}(\tau)$ and the damage vector $H_k(\tau)$ be the variables defining the state of a representative sample of the time–dependent material. The corresponding relaxation modulus is denoted by $L_{ijkm}(t-\tau, H_k)$. This state is represented by a point A in strain space. The stress $\sigma_{ij}(t)$, corresponding to this state, is determined for all values of time

t ($t \geq \tau$) by the entire history of strain and the structural breakdown prior to time τ. A change in the strain at time τ to $\epsilon_{ij}(\tau+d\tau)$ in a small interval of time $d\tau$ will result in corresponding changes in the damage vector and the relaxation moduli. These changes cause an additional amount of stress $d\sigma_{ij}(t)$ at time t to the subsequent history of stress. An expression of $d\sigma_{ij}(t)$ in terms of these changes is sought.

This can be achieved by visualizing the effects of degradation to be identical to unloading followed by reloading with the modified moduli within the short interval of time $d\tau$. This results in

$$\sigma_{ij}(t) + d\sigma_{ij}(t) = \sigma_{ij}(t) - L_{ijkm}(t-\tau, H_k(\tau))\, \epsilon_{km}(\tau) + L_{ijkm}(t-(\tau+d\tau), H_k(\tau+d\tau))\, \epsilon_{km}(\tau+d\tau) \qquad (5.2.52)$$

so that

$$d\sigma_{ij}(t) = -L_{ijkm}(t-\tau, H_k(\tau))\, \epsilon_{km}(\tau) + L_{ijkm}(t-(\tau+d\tau), H_k(\tau+d\tau))\, \epsilon_{km}(\tau+d\tau) \qquad (5.2.53)$$

For a small interval of time $d\tau$

$$H_k(\tau+d\tau) = H_k(\tau) + dH_k \qquad (5.2.54)$$

so that 5.2.53 becomes

$$d\sigma_{ij}(t) = -L_{ijkm}(t-\tau, H_k(\tau))\, \epsilon_{km}(\tau) + L_{ijkm}(t-(\tau+d\tau), H_k(\tau)+dH_k))\, \epsilon_{km}(\tau+d\tau) \qquad (5.2.55)$$

For a small value of $d\tau$ and, thus, dH_k the following simplifications are possible

$$\epsilon_{ij}(\tau+d\tau) = \epsilon_{ij} + \frac{\partial \epsilon_{ij}}{\partial \tau} d\tau \qquad (5.2.56)$$

and

$$L_{ijkm}(t-\tau-d\tau, H_k(\tau)+dH_k) = L_{ijkm}(t-\tau, H_k) + \frac{\partial L_{ijkm}}{\partial H_k}(t-\tau, H_k(\tau))\, dH_k - \frac{\partial L_{ijkm}}{\partial \tau}(t-\tau, H_k(\tau))\, d\tau \qquad (5.2.57)$$

Substituting 5.2.56 and 5.2.57 in 5.2.55 gives

$$d\sigma_{ij}(t) = L_{ijkm}(t-\tau,H_k(\tau)) \frac{\partial \epsilon_{km}}{\partial \tau} d\tau +$$
$$\left[\frac{\partial L_{ijkm}}{\partial H_k}(t-\tau,H_k(\tau))\, dH_k - \frac{\partial L_{ijkm}}{\partial \tau}(t-\tau,H_k(\tau))\, d\tau \right]$$
$$\times \left[\epsilon_{km} + \frac{\partial \epsilon_{km}}{\partial \tau} d\tau \right] \qquad (5.2.58)$$

It should be noted that for a small value of $d\tau$ the following approximations can also be used

$$\frac{\partial \epsilon_{ij}}{\partial \tau} d\tau = d\epsilon_{ij} \qquad (5.2.59)$$

and

$$\frac{\partial L_{ijkm}}{\partial H_k}(t-\tau,H_k(\tau))\, dH_k - \frac{\partial L_{ijkm}}{\partial \tau}(t-\tau,H_k(\tau))\, d\tau$$
$$= dL_{ijkm}(t-\tau,H_k) \qquad (5.2.60)$$

so that, after neglecting higher order terms, 5.2.58 becomes

$$d\sigma_{ij}(t) = L_{ijkm}(t-\tau,H_k)\, d\epsilon_{km}(\tau)$$
$$+ dL_{ijkm}(t-\tau,H_k)\, \epsilon_{km}(\tau) \qquad (5.2.61)$$

where H_k is evaluated at time τ.

The above expression is identical to 5.2.50. This illustrates the similarity with the time–independent behaviour of the fracturing solid and may provide the basis of an experimental investigation an real materials. It is significant to note that the extension of the time–independent theory to include time effects through the constitutive law 5.2.61 provides considerable generality and reduces to linear elasticity ($t-\tau=0$ and $dH_k=0$), linear viscoelasticity ($dH_k=0$), and time–independent progressive fracture ($t-\tau=0$) as limiting cases.

Thus the stress increment at time t, due to an applied strain increment $d\epsilon_{ij}(\tau)$ at time τ, can be defined as

$$d\sigma_{ij}(t) = d\sigma'_{ij}(t) + d\sigma''_{ij}(t) \qquad (5.2.62)$$

where

$$d\sigma'_{ij}(t) = L_{ijkm}(t-\tau,H_k(\tau))\, d\epsilon_{km}(\tau) \qquad (5.2.63)$$

is the viscoelastic stress increment and

$$d\sigma''_{ij}(t) = dL_{ijkm}(t-\tau,H_k(\tau))\, \epsilon_{km}(\tau) \qquad (5.2.64)$$

is the time–dependent fracture stress decrement.

Equations 5.2.63 and 5.2.64 form the bases for the constitutive relations. At a certain time, if the components of the relaxation modulus L_{ijkm} are known, the viscoelastic stress component can be calculated using 5.2.63. For the computation of the fracture stress decrement, expression 5.2.64, together with an appropriate flow rule, should be used. Alternatively, an evolution law, which gives the values of L_{ijkm} and the changes of this tensor with time and fracture, can be used. This law can be formulated by deriving the variation of dL_{ijkm} from the flow rule.

The flow rule gives an expression for the time–dependent fracture stress decrement which, in here, is dependent on both the past time and path history of strain. This flow rule satisfies the loading conditions (5.2.10), the normality of the fracture stress decrement to the instantaneous fracture surface, and the consistency of the fracture surface (that is the value of F is zero for all viscoelastic/fracturing states). Thus

$$F = dF = 0 \qquad (5.2.65)$$

for a change from one viscoelastic/fracturing state to another.

The loading criteria (5.2.10) suggest that, if degradation occurs to cause a fracture stress decrement $d\sigma''_{ij}(\tau)$ at time τ, it possible to write, with no loss of generality,

$$d\sigma''_{ij}(\tau) = g_{ij}\left[\frac{\partial F}{\partial \epsilon_{km}} d\epsilon_{km} + \frac{\partial F}{\partial T_q} dT_q\right]_{t=\tau} \qquad (5.2.66)$$

where g_{ij} is a tensor dependent on time among other state variables. Since $d\sigma''_{ij}(\tau)$ is taken to be normal to the instantaneous fracture surface at the time of fracture, then

$$d\sigma''_{ij}(\tau) = -K\left[\frac{\partial F}{\partial \epsilon_{km}} d\epsilon_{km} + \frac{\partial F}{\partial T_q} dT_q\right] \frac{\partial F}{\partial \epsilon_{ij}} \quad \text{at } t=\tau \qquad (5.2.67)$$

where K is a scalar to be determined.

It should be noted that the above expression gives values of the instantaneous response to degradation and not the actual response because normality was found to be satisfied at the time of fracture τ. Hence $d\sigma''_{ij}(\tau)$ rather than $d\sigma''_{ij}(t)$ is given by 5.2.67. Also, the expression for K will be found by satisfying the consistency condition (dF=0) at the time of fracture τ. Clearly this results from the use of a viscoelastic/fracturing model (rather than an

elastic/viscofracturing formulation). In the present formulation, one way of avoiding the difficulty of calculating $d\sigma''_{ij}(t)$ is to choose the loading function in such a way that the actual response to degradation, $d\sigma''_{ij}(t)$, is fully prescribed by the instantaneous response described by $d\sigma''_{ij}(\tau)$. This will be illustrated in section 5–3.

As in the formulation of the time–independent theory, the damage vector is taken to be dependent on the fracture stress decrement so that

$$H_k = H_k(\sigma''_{ij}) \tag{5.2.68}$$

This limits the application to a particular class of materials where the expression 5.2.68 is satisfied. It is noted that

$$\frac{\partial F}{\partial H_k}\, dH_k = -\left[\frac{\partial F}{\partial \epsilon_{km}}\, d\epsilon_{km} + \frac{\partial F}{\partial T_q}\, dT_q\right] \text{ at } t=\tau \tag{5.2.69}$$

as a result of dF being zero during progressive fracture. Using the flow rule (5.2.67) with 5.2.69 gives

$$d\sigma''_{ij}(\tau) = \left[-K \frac{\partial F}{\partial \epsilon_{ij}} \left(-\frac{\partial F}{\partial H_k}\, dH_k\right)\right] \text{ at } t=\tau \tag{5.2.70}$$

Using the incremental form of 5.2.68

$$\frac{\partial F}{\partial H_k}\, dH_k = \frac{\partial F}{\partial H_k} \frac{\partial H_k}{\partial \sigma''_{ij}}\, d\sigma''_{ij} \tag{5.2.71}$$

results, together with 5.2.70, in

$$K = \frac{1}{\dfrac{\partial F}{\partial H_k} \dfrac{\partial F}{\partial \epsilon_{ij}} \dfrac{\partial H_k}{\partial \sigma''_{ij}}} \text{ at } t=\tau \tag{5.2.72}$$

The flow rule 5.2.67 becomes

$$d\sigma''_{ij}(\tau) = -\frac{\dfrac{\partial F}{\partial \epsilon_{ij}} \left[\dfrac{\partial F}{\partial \epsilon_{km}}\, d\epsilon_{km} + \dfrac{\partial F}{\partial T_q}\, dT_q\right]}{\dfrac{\partial F}{\partial H_k} \dfrac{\partial H_k}{\partial \sigma''_{rs}} \dfrac{\partial F}{\partial \epsilon_{rs}}} \text{ at } t=\tau \tag{5.2.73}$$

5–2–5 Summary and conclusions

The time–dependent progressively fracturing solids theory presented in here, describes a material that degrades by the loss of its stiffness as a result of

time–dependent fracture. The material may be unstable in the sense defined by Drucker but conforms to the class of materials described by Il'ushin's postulate of plasticity. Il'ushin's definition of plasticity is less restrictive than the stability criterion proposed by Drucker as it allows the description of strain softening as a stable mode of behaviour.

The arguments leading to the formulation of this time–dependent theory are similar to those presented by Naghdi and Murch [120] which describes the behaviour of a continuum viscoelastic/plastic solid. Their theory reduces to the classical linear viscoelasticity theory and the classical theory of plasticity as limiting cases. It should be pointed out that the theory presented here differs from that given in [120] in that it includes strain softening as a possible mode of behaviour and allows the elastic moduli to change upon fracture. It has the advantage, over that in [120], that it describes all time effects by a single vector T_q without excluding coupling between these effects and those due to degradation.

The present theory is characterized by the following aspects:

– The theory is formulated in strain space rather that stress space. This allows the behaviour of the material under controlled deformations to be described resulting in possible strain hardening and softening.

– Behaviour is described by means of a fracture surface in strain space that separates viscoelastic states from viscoelastic/fracturing ones. For this progressively fracturing solid, this fracture surface is always convex. This surface is not fixed in strain space even when the material is in the viscoelastic domain, resulting in the existence of a spectrum of possible fracture surfaces each corresponding to a specific time strain history.

– An instantaneous fracture surface in strain space corresponds to each material state. This surface is reached by following a rapid path, a strain path in an infinitesimally small interval of time after which fracture occurs.

– Time–dependence is described by a single vector T_q which measures the dependence of subsequent behaviour, at a certain time, on the previous strain time history.

– At any time, the stress increment caused by a strain increment is

composed of a viscoelastic and a time–dependent fracturing component. The direction of the instantaneous fracture stress decrement is along the inward normal to the instantaneous fracture surface at the point of fracture. The evaluation of this stress decrement is achieved by means of a flow rule (5.2.73) which follows from the normality argument and the consistency of the fracture surface at the time of fracture. An evolution law is needed to relate the instantaneous response to the actual behaviour. The viscoelastic stress is related to the strain tensor by an incremental constitutive law involving a relaxation modulus.

– The theory will reduce to the linear elastic, linear viscoplastic, and time–independent progressively fracturing solid theories as limiting cases. However, as has been pointed out, the theory is not complete in that only the instantaneous fracture response is given rather than the history of stress changes following instantaneous degradation. A proposal giving one way to define a complete model is presented in the following section.

5–3 The revised model – A complete model consistent with the viscoelastic fracturing theory

The formulation presented in the preceding sections has led to the expressions giving the instantaneous response of the time dependent progressively fracturing solid as a result of applied deformations or strains. In other words, the instantaneous rather than the actual response to fracture can be calculated following the formulation presented so far. The difficulty of determining the stress history at any time arises because the normality and consistency conditions were found to be satisfied at the time of fracture and not at any time. The flow rule (5.2.73) gives an expression of $d\sigma''_{ij}(\tau)$ at the time τ of fracture rather than of $d\sigma''_{ij}(t)$ at any time t ($t \geq \tau$).

The approach adopted here to deal with this difficulty is to assume that the response of the material at any time t is fully described by the instantaneous response at all times τ ($\tau \leq t$). It is thus assumed that the total stress increment $d\sigma_{ij}(t)$ at a time t due to a stress increment $d\sigma_{ij}(\tau)$ at time τ, resulting instantaneously from a strain increment $d\epsilon_{ij}(\tau)$, is given by

$$d\sigma_{ij}(t) = d\sigma_{ij}(\tau)\, \varphi(t-\tau) \tag{5.3.1}$$

where φ is a monotonically decreasing function with boundary values

$$\varphi(0) = 1 \tag{5.3.2}$$

$$\varphi(\infty) \geq 0 \tag{5.3.3}$$

The flow rule

$$d\sigma''_{ij}(\tau) = -\frac{\dfrac{\partial F}{\partial \epsilon_{ij}}\left[\dfrac{\partial F}{\partial \epsilon_{km}}\, d\epsilon_{km} + \dfrac{\partial F}{\partial T_q}\, dT_q\right]}{\dfrac{\partial F}{\partial H_k}\, \dfrac{\partial H_k}{\partial \sigma''_{rs}}\, \dfrac{\partial F}{\partial \epsilon_{rs}}} \quad \text{at } t=\tau \tag{5.3.4}$$

gives the instantaneous value of the fracture stress decrement at the time of fracture. Applying the constitutive law (5.2.62, 5.2.63, and 5.2.64) gives

$$d\sigma_{ij}(t) = L_{ijkm}(t-\tau, H_k)\, d\epsilon_{km}(\tau) + dL_{ijkm}(t-\tau, H_k)\, \epsilon_{km}(\tau) \tag{5.3.5}$$

which when applied at the time of fracture results in

$$d\sigma_{ij}(\tau) = L_{ijkm}(0, H_k)\, d\epsilon_{km}(\tau) + dL_{ijkm}(0, H_k)\, \epsilon_{km}(\tau) \tag{5.3.6}$$

where H_k is the damage vector evaluated at time τ. Since the instantaneous response is dependent only on the values of the current damage vector $H_k(\tau)$, strain $\epsilon(\tau)$, and the applied strain increment $d\epsilon(\tau)$, then the relaxation tensor L_{ijkm} can be replaced by an instantaneous tensor $S_{ijkm}(H_k)$ which represents the instantaneous relaxation moduli. Thus 5.3.6 becomes

$$d\sigma_{ij}(\tau) = S_{ijkm}(H_k)\, d\epsilon_{km}(\tau) + dS_{ijkm}(H_k)\, \epsilon_{km}(\tau) \tag{5.3.7}$$

This expression gives the instantaneous response of the model material to applied strains. It is similar to the expression obtained for the response of the time–independent progressively fracturing solid (expression 2.3.2).

Adopting similar notations for the stress increments as those of the time–independent case, the instantaneous elastic stress increment and the instantaneous fracture stress decrement at time τ can be defined as

$$d\sigma'_{ij}(\tau) = S_{ijkm}(H_k)\, d\epsilon_{km}(\tau) \tag{5.3.8}$$

and

$$d\sigma''_{ij}(\tau) = dS_{ijkm}(H_k)\, \epsilon_{km}(\tau) \tag{5.3.9}$$

respectively, with H_k evaluated at τ.

The actual response at time t can be calculated by applying 5.3.1 so that

$$d\sigma_{ij}(t) = \left[d\sigma'_{ij}(\tau) + d\sigma''_{ij}(\tau) \right] \varphi(t-\tau) \tag{5.3.10}$$

Integrating the above incremental equation gives

$$\sigma_{ij}(t) = \int_0^t \left[\frac{d\sigma'_{ij}}{d\tau} + \frac{d\sigma''_{ij}}{d\tau} \right]_{t=\tau} \varphi(t-\tau)\, d\tau \tag{5.3.11}$$

The integral 5.3.11 resembles a damage evolution law which gives the total stress at time t as a weighted cumulative sum of past time instantaneous stress increments resulting from elastic and fracturing responses.

It might seem that the above simplifications has merely introduced a linear viscoelastic term and that any coupling between time–dependence and fracture has been lost. This is not necessarily so because the inclusion of the term T_q in the definition of the loading function correlates damage to time in a manner independent of H_k. In other words, the instantaneous response is not

time–independent due to the presence of the vector T_q.

The instantaneous change in the relaxation moduli, represented by $dS_{ijkm}(H_k)$ can be found in a similar fashion to that adopted for the time–independent case presented in chapter II. The flow rule given by 5.2.67 can be written, by multiplying the numerator and the denominator by $\frac{\partial F}{\partial \epsilon_{ij}}\epsilon_{ij}$, as

$$d\sigma''_{ij}(\tau) = -K \frac{\frac{\partial F}{\partial \epsilon_{ij}} \left[\frac{\partial F}{\partial \epsilon_{rs}} d\epsilon_{rs} + \frac{\partial F}{\partial T_q} dT_q \right] \frac{\partial F}{\partial \epsilon_{km}} \epsilon_{km}}{\frac{\partial F}{\partial \epsilon_{pq}} \epsilon_{pq}} \tag{5.3.12}$$

so that from 5.3.9

$$dS_{ijkm}(H_k) = -K \frac{\frac{\partial F}{\partial \epsilon_{ij}} \left[\frac{\partial F}{\partial \epsilon_{rs}} d\epsilon_{rs} + \frac{\partial F}{\partial T_q} dT_q \right] \frac{\partial F}{\partial \epsilon_{km}}}{\frac{\partial F}{\partial \epsilon_{pq}} \epsilon_{pq}} + R_{ijkm} \tag{5.3.13}$$

requiring that the tensor R_{ijkm} is symmetric and satisfies

$$R_{ijkm}\epsilon_{km} = 0 \text{ at } t=\tau \tag{5.3.14}$$

In order to evaluate the tensor R_{ijkm}, further restrictions on the material behaviour are needed. One possibility is to assume that R_{ijkm} is always zero which clearly satisfies 5.3.14 and is symmetric. Another possibility, similar to that used for the time–independent solid (chapter II), is to assume that the solid is both path and time independent in the small so that the changes in the instantaneous relaxation moduli are not dependent on the path or time followed by a small increment of strain $d\epsilon_{ij}$. This requires that the terms $\frac{\partial F}{\partial H_k} dH_k$ and $\left[\frac{\partial F}{\partial \epsilon_{km}} d\epsilon_{km} + \frac{\partial F}{\partial T_q} dT_q\right]$ are constant for small strain increments and

$$\frac{\partial \dot{S}_{ijkm}}{\partial \epsilon_{rs}} d\epsilon_{rs} = 0 \tag{5.3.15}$$

for all states on the instantaneous fracture surface. In a manner similar to that presented in [4], the above restrictions will result in the following expression for the tensor R_{ijkm}

$$R_{ijkm} = -\left[K \frac{\partial^2 F}{\partial \epsilon_{ij} \partial \epsilon_{km}} + \frac{\partial F}{\partial \epsilon_{ij}} \frac{\partial K}{\partial \epsilon_{km}}\right] \dot{f} \qquad (5.3.16)$$

with

$$\dot{f} = \left[\frac{\partial F}{\partial \epsilon_{km}} d\epsilon_{km} + \frac{\partial F}{\partial T_q} dT_q\right] \qquad (5.3.17)$$

This completes the description of the time–dependent progressively fracturing solid.

5–4 Some remarks on the model parameters and laws

Although the theory presented here is not intended to describe real physical materials directly, the different functions used to formulate it should be such that the overall performance resembles modes of behaviour noted in real materials. If this theory is used in conjunction with other continuum theories describing ideal materials, then the overall response would be more realistic. This suggests that the parameters used in the present theory be, in a way, deduced from the physical behaviour of real materials.

The most critical parameter in the present theory is the vector T_q which measures time dependence. This parameter is obviously dependent on the type of analysis required. Time dependence of material response is noted in many engineering applications. These include loading or deformation of material under different rates, creep and relaxation,etc (chapter III). Clearly, an understanding of the mechanisms governing the behaviour of materials under such circumstances will help in suggesting forms of the vector T_q. Experiments would help in proving the validity of such forms. Also, they might suggest forms of T_q that are purely empirical and hence dependent on the application required.

An expression of T_q which applies to all time–dependent engineering applications is difficult, if not impossible, to formulate. For example, rate sensitive tests on materials suggest that T_q be a function of instantaneous strain rate $\dot{\epsilon}_{ij}$, or the stress rate $\dot{\sigma}_{ij}$. In other applications it might be more practical to assume that T_q takes the form of a cumulative integral along time of a function $\Psi(\dot{\epsilon},\epsilon,..)$. Clearly these forms of T_q depend on the particular application (creep, relaxation, high rate loading) and must be based on experimental results performed in a way where the form of T_q can be deduced or fitted.

For the application of the revised model given in section 5–3, several assumptions and simplifications should be taken depending on the particular problem in hand. These assumptions about the forms of the functions to be used should include:

a) The damage evolution law (5.3.10–5.3.11) as described by the relaxation function φ.

b) The loading function, F, and its dependence on time through the

vector T_q.

Hence, analysis is performed using the expressions giving the instantaneous response. These expressions are derived from the equation of the instantaneous fracture surface by means of the flow rule and the degradation of the instantaneous relaxation moduli. The actual response can then be calculated by means of the damage evolution law.

It is interesting to note that the damage evolution law has resulted from the assumption that the instantaneous response of the material will relax with time into the actual response. This is similar to the concept adopted in damage mechanics theories where the actual stress is thought to be related to a fictitious stress quantity by a damage law.

The similarity between the present approach and the damage mechanics approach can be seen if the evolution law (5.3.11)

$$\sigma_{ij}(t) = \int_0^t \frac{d\sigma_{ij}(\tau)}{d\tau} \varphi(t-\tau)\, d\tau \qquad (5.4.1)$$

is expressed in terms of a pseudo quantity $\pi_{ij}(t)$. This quantity can be thought of as the current instantaneous value of stress. At any time the actual stress can hence be given, in view of 5.4.1, by

$$\sigma_{ij}(t) = \pi_{ij}(t)\,(1-D) \qquad (5.4.2)$$

where

$$\pi_{ij}(t) = \int_0^t \frac{d\sigma_{ij}(\tau)}{d\tau}\, d\tau \qquad (5.4.3)$$

and D is a time measure of damage related to the past load and time history of deformations. It should be noted that, in 5.4.1 and 5.4.3, the integrated stress increments at time τ are deduced from the instantaneous response and can be calculated as described in section 5–3.

Thus, for a time–dependent progressively fracturing solid, damage can be thought to be a result of two mechanisms. First, the solid is fractured as a result of load application in a fashion dependent on past time and path history of applied strains. This form of damage is described by the continuum theory in terms of incremental equations evaluated instantaneously at the time of fracture. Secondly, time dependent damage, described by 5.4.1 is inflicted on the material

during and after the application of loads.

From the damage mechanics point of view, this time–dependent fracture can be thought to occur as a result of time enhanced effective stress bearing area reduction, or increasing internal cracks. In previous damage mechanics continuum theories, where material fracture was assumed to be a result of growing of well dispersed cracks or a homogeneous reduction of the effective stress bearing area, expressions similar to 5.4.2 and 5.4.3 were used (chapter II).

It was assumed, in the present formulation, that the relaxation function φ is a scalar independent of damage and is a function of time only. More generally, this function can be assumed to be dependent on the state of material damage as well as orientation so that it can be resembled by a tensor of the form $\varphi_{ijkm}(t,H_k)$. The form of this parameter can be assumed to follow from a rheological idealization for computational convenience. Alternatively, an experimental procedure on real materials, whose behaviour is to be simulated, can be adopted to find an expression of φ. If the ideal material described by the present theory is loaded to a specified strain ϵ_{ij}^0 instantaneously, then for all subsequent times t the stress is given by

$$\sigma_{ij}(t) = \sigma_{ij}^0 \varphi(t) \qquad (5.4.4)$$

where σ_{ij}^0 is the stress level reached by the material upon the application of ϵ_{ij}^0 at time t=0. Tests or real materials under constant strains applied instantaneously will result in justified forms of φ. The assumption of the independence of the form of φ on the degree of damage and orientation can be tested by repeating such tests up to various levels of strains and at different directions.

Further simplifications on the "revised model" (section 5–3) can be done. Any dependence on time can be neglected in the instantaneous response to degradation. The vector T_q is neglected in the analysis of the instantaneous response and time dependence is merely catered for by (5.3.11). At any time, the instantaneous response is dependent only on the strain path history and thus can be performed following a similar procedure to that followed in the time–independent analysis of the progressively fracturing solid. The actual response can then be deduced from the instantaneous one by superimposing a relaxation function over a the time–independent instantaneous behaviour.

A concept similar to the above was used by Browning, Gurtin, and

Williams in [125]. This model was described in section 3–4–3.

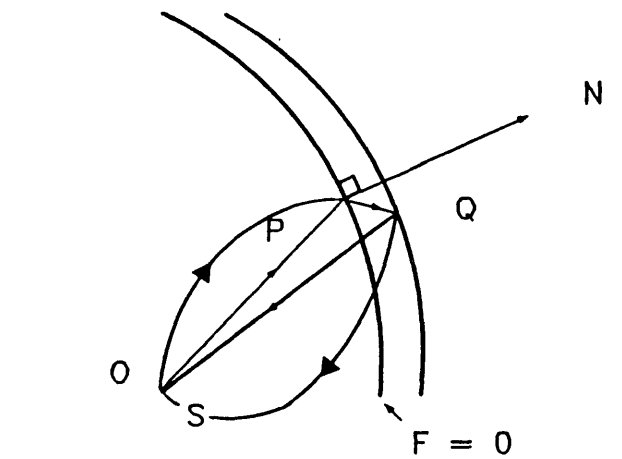

Fig. 5.1 Yield surface F=0 and stress path OPQS

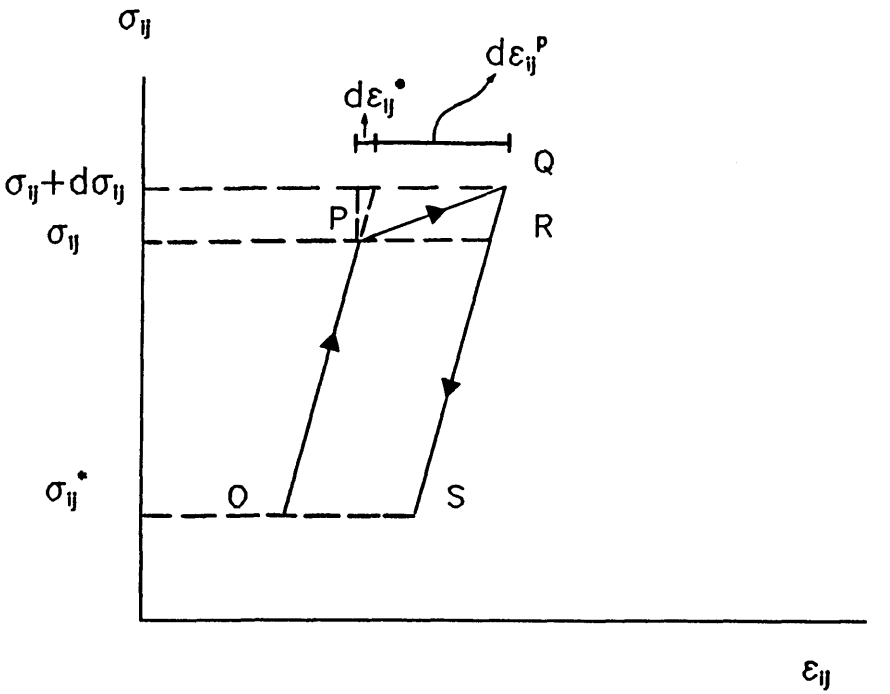

Fig. 5.2 Loading stress path OPQRS in stress–strain space

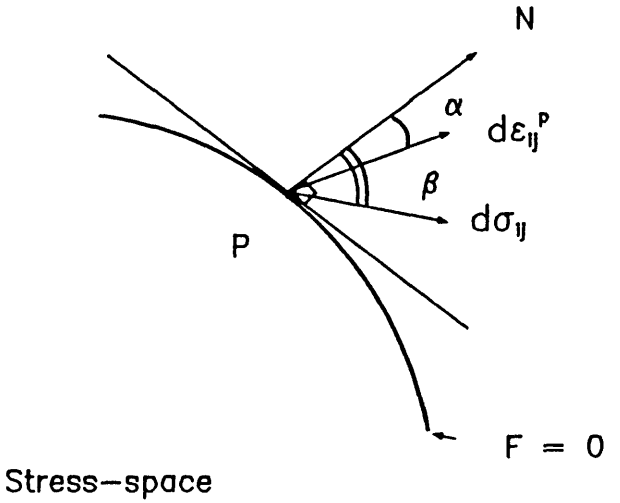

Fig. 5.3 Yield surface F=0 ,tangent hyperplane to F and the normal at yield

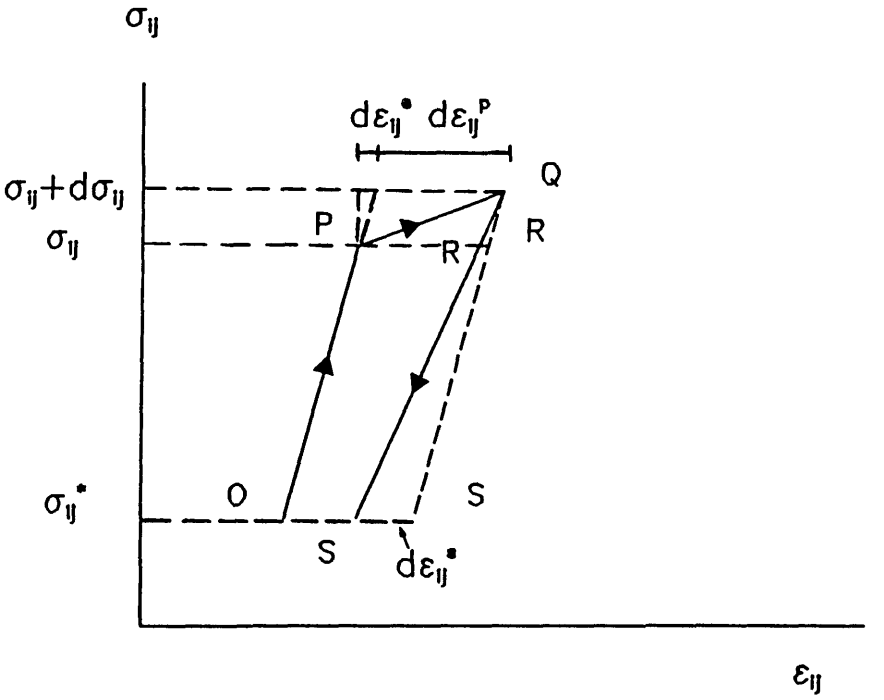

Fig. 5.4 Loading stress path OPQRS in stress–strain space

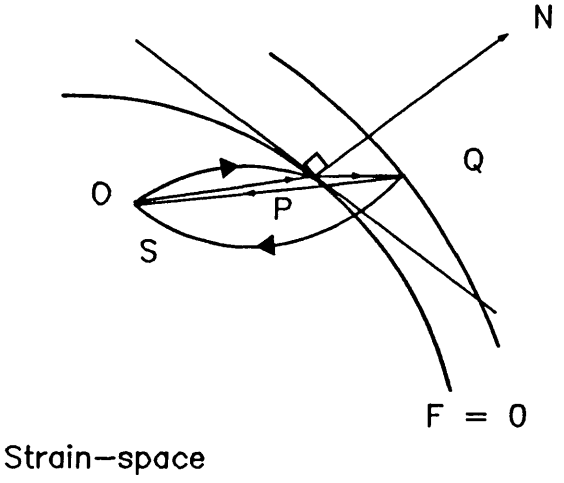

Strain–space

Fig. 5.5 Yield surface F=0 ,tangent hyperplane to F , the normal at yield, and strain path OPQS

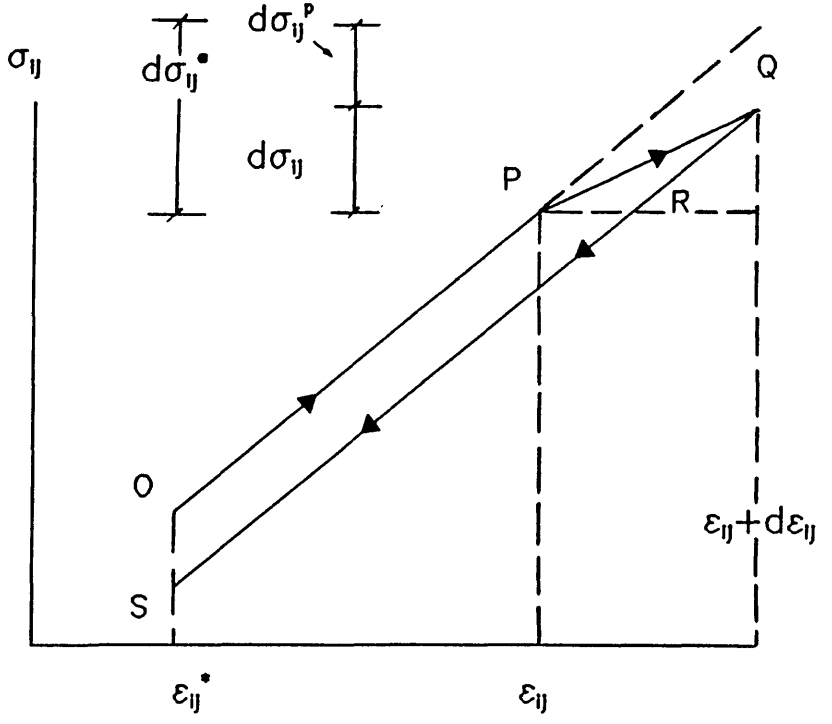

Fig. 5.6 Loading strain path OPQRS in stress–strain space

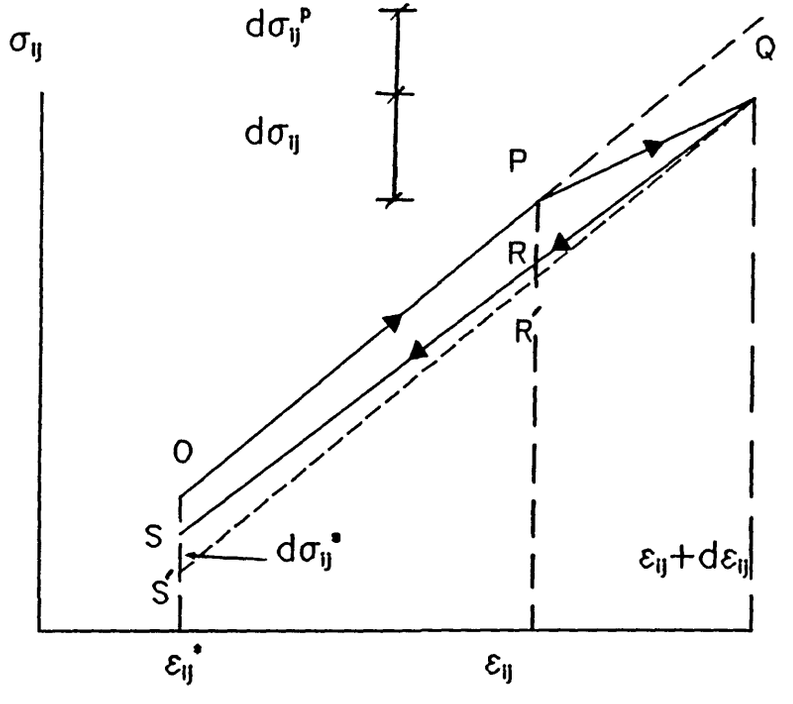

Fig. 5.7 Loading strain path OPQRS in stress–strain space

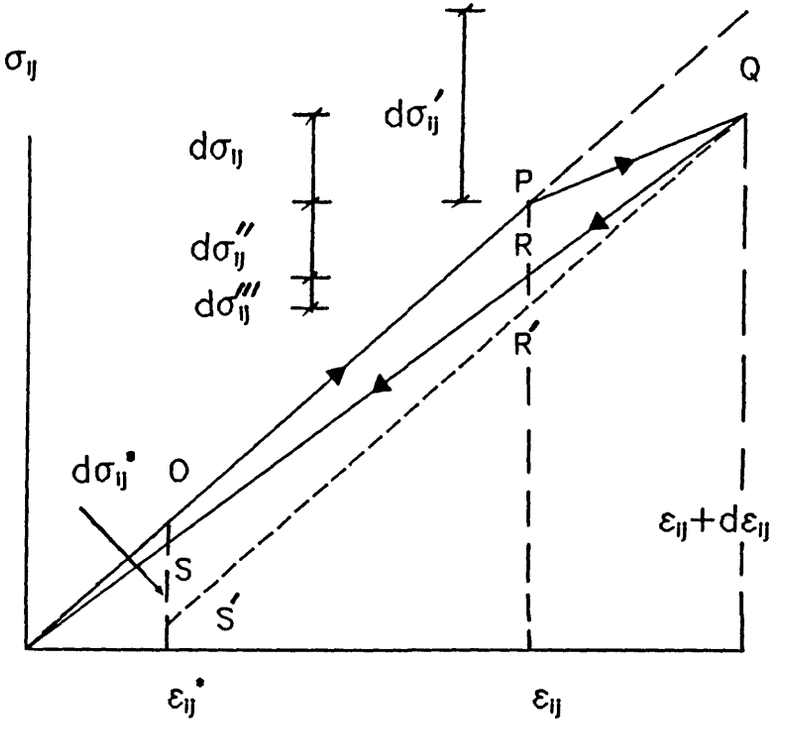

Fig. 5.8 Loading strain path OPQRS in stress–strain space for an ideal progressively fracturing solid

$$dF' = \frac{\partial F}{\partial \varepsilon} d\varepsilon + \frac{\partial F}{\partial T_q} dT_q$$

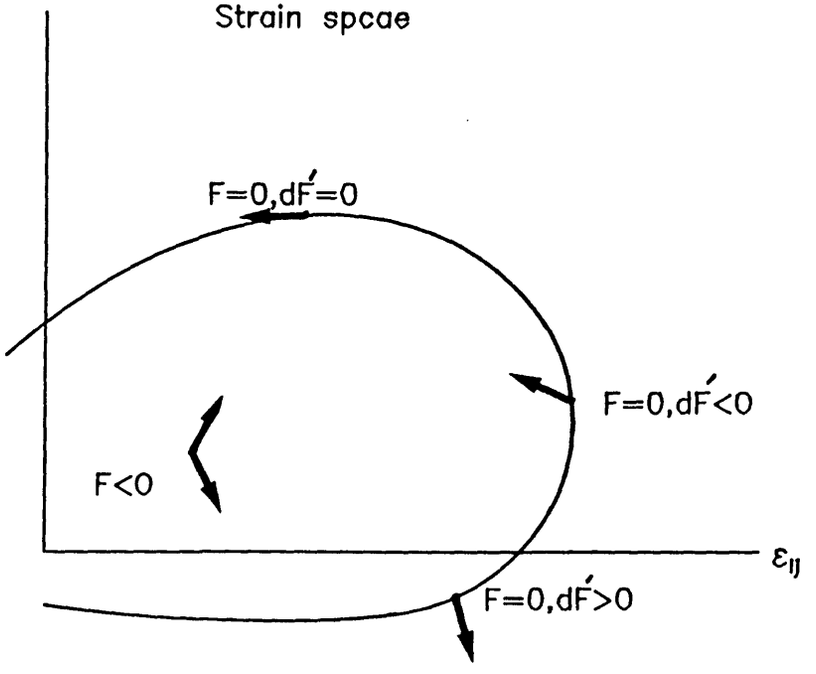

Fig. 5.9 Loading criteria related to the fracture surface in strain space

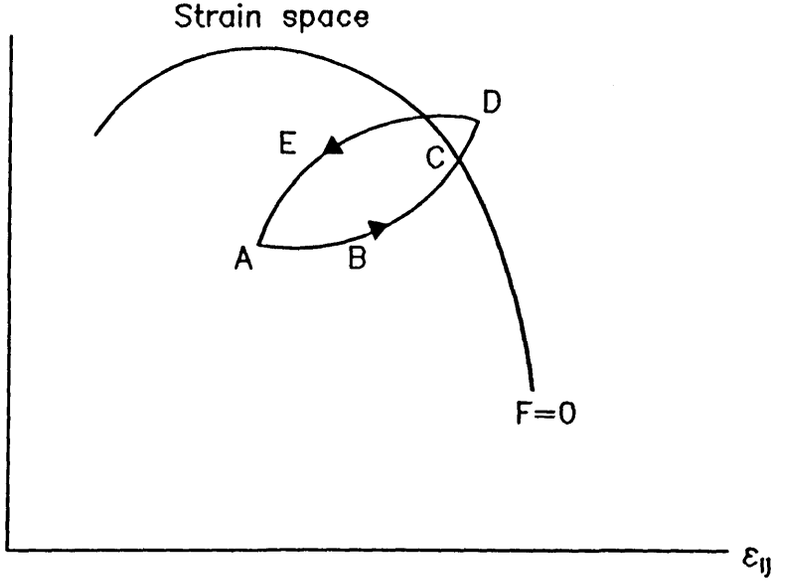

Fig. 5.10 Loading strain path ABCDEA in strain space

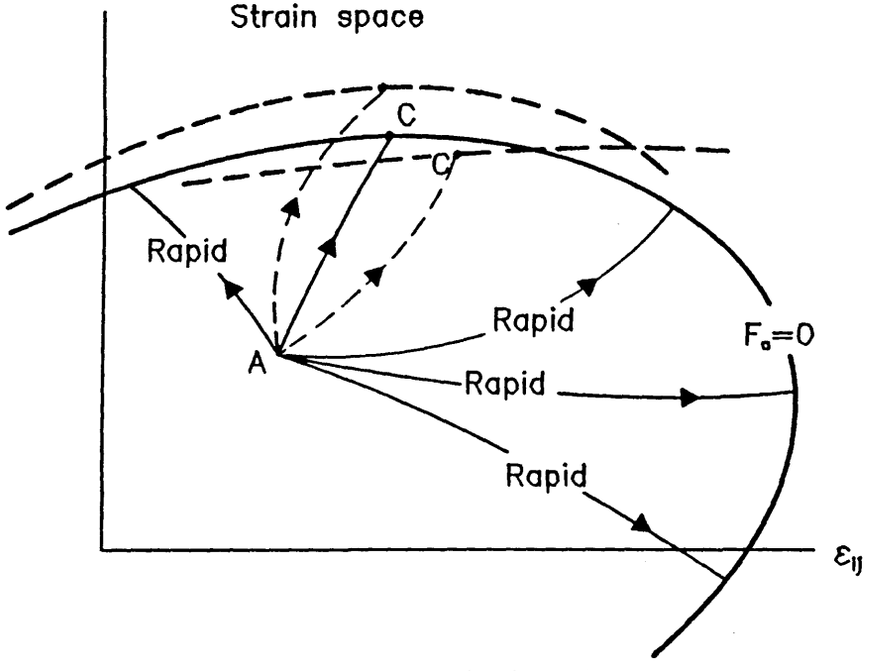

Fig. 5.11 Spectrum of the fracture surfaces and the instantaneous fracture surface in strain space

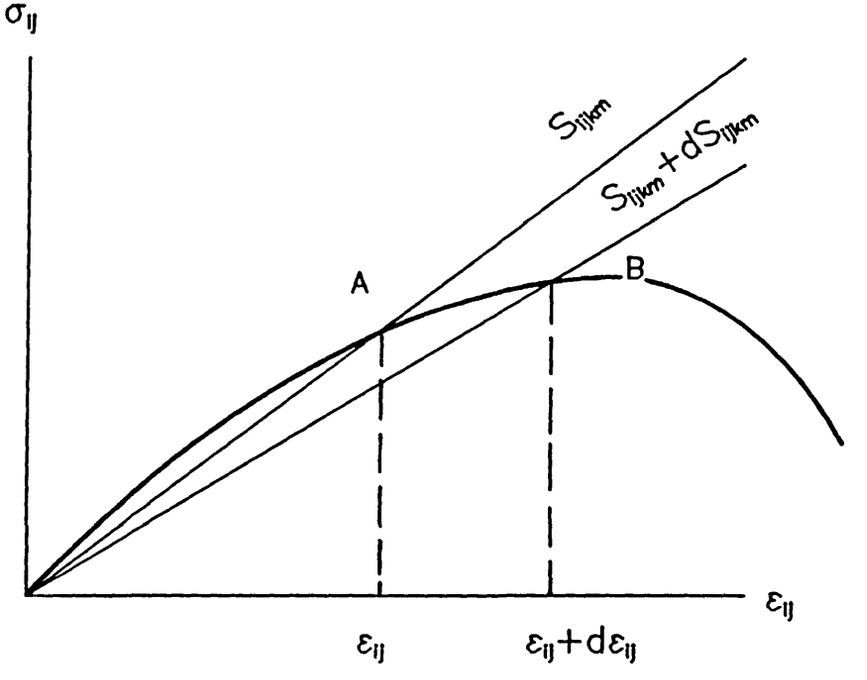

Fig. 5.12 Stress –strain behaviour of an ideal progressively fracturing solid

CHAPTER VI

BEHAVIOUR OF THE TIME–DEPENDENT PROGRESSIVELY FRACTURING SOLID – ANALYSIS OF IDEAL MODEL MATERIALS

6–1 Introduction

The behaviour of some time–dependent progressively fracturing model materials is investigated. The response of such materials to applied deformations, as well as to conditions of constant strain or stress, is studied. This chapter summarizes the theoretical background to such tests and presents the computational techniques used in the analysis.

The general theory of a time–dependent progressively fracturing solid was formulated in chapter V. The behaviour of such a solid can be investigated by looking at the response of ideal model materials that exhibit time–dependent progressive fracture even if these model materials do not completely conform with the continuum description. On the other hand, such a behaviour can be studied by investigating solids that are described by the continuum theory or a particular form of the theory.

Keeping the above arguments in mind, two model materials are investigated :

(i) a time–dependent discrete "network model" of the form studied in chapter IV. The work described extends the study explored in chapter IV to include time–dependent behaviour. The general aspects of behaviour of a stable time–dependent progressively fracturing solid can be well understood by studying the performance of the network model with time effects taken into consideration.

(ii) a time–dependent "fibre bundle model" (section 2–4). The adoption of this model material corresponds to the use of independent linear loading functions to implement the general theory for progressively fracturing solids as has been done for the time–independent behaviour by Rida [51]. The same model, extended to incorporate time effects, is used here to demonstrate the applicability of the continuum theory formulated in chapter V.

6–2 The "network model"

A random planar network, the elements of which are linear elastic/brittle, was used in chapter IV to illustrate a stable progressively fracturing mode of behaviour. Non–linearity in the overall response of the network was due solely to breakage of its members. Loading was performed by applying controlled deformations to all nodes within a well defined edge zone (figure 4.2). At any stage of loading, a member was considered to have failed if the stress within it exceeds a preset limiting value. Because behaviour of each component is linear elastic up to failure, this stress limit failure criterion can be equally well expressed in terms of strain or work done per unit volume with no change in the network's response.

Time effects are introduced in the force displacement (or stress–strain) relationship and the failure criterion of the individual bar elements. Except for the inclusion of these effects, the networks used are identical to those generated in chapter IV.

6–2–1 Geometry

Geometrically, the networks analysed in this and the following chapter are produced in exactly the same manner described in section 4–1–1. A square matrix (42.0 × 42.0 units of length), containing N randomly dispersed joints, is used. The nodes are connected by simple planar pin–jointed bars the lengths of which are limited to a specified length L_c in a random fashion. Some typical networks are shown in figure 4.1. These are perfectly reproducible because of the use of random numbers generator computer routines whose output sequences can be controlled and reproduced.

6–2–2 Loading and boundary specifications

Boundary zones, where prescribed or suppressed nodal displacements are imposed, are defined (figure 4.2). The definition of these zones allows the use of equations 4.1.10 and 4.1.11 for the calculation of the average longitudinal and transverse strains along the network. The average stress in a sample of the model material is determined in the same way described in section 4–1–3.

In all tests, displacements of all nodes in zone (1) (figure 4.2) are prevented in the vertical direction and one node, at least, is prevented from

lateral motion. Prescribed displacements are applied to all nodes in zone (2).

Tests simulating strain controlled uniaxial tensile conditions, at different applied strain rates, were performed. Conditions of constant overall strain or stress were also applied to the model material. These conditions are of the same type as those in relaxation and creep tests applied to real physical materials.

6–2–3 Stress–strain relationship

A set of time and rate dependent stress–strain relationships is used to replace the linear elastic/brittle law implemented in chapter IV. The behaviour of individual elements is expressed as a set of incremental and integral equations relating the stress at any time t to the strain along the interval of time $0 \leq \tau \leq t$.

In the spirit of the continuum theory developed in chapter V, the existence of an instantaneous stress $\overset{*}{\sigma}_i$, within the i^{th} member, directly related to the element strain ϵ_i, is postulated. The change in this instantaneous stress during an increment of time $d\tau$ is assumed to be a function of the strain increment, $d\epsilon_i(\tau)$, and its rate of application. The actual stress, σ_i, is assumed to be related to the instantaneous stress, $\overset{*}{\sigma}_i$, through a damage evolution law of the form 5.3.11.

The behaviour of the i^{th} member of the network is hence determined by

(i) an instantaneous constitutive law relating strain, ϵ_i, to the instantaneous response of the member, $\overset{*}{\sigma}_i$, and

(ii) a damage evolution law giving the true stress, σ_i, in terms of the instantaneous stress, $\overset{*}{\sigma}_i$. This relationship has the form of a relaxation function with σ_i reducing with time from an initial value $\overset{*}{\sigma}_i$.

Considering first the instantaneous constitutive law, if strain within the element, at a certain time τ, changes by $d\epsilon_i(\tau)$ during the time interval $d\tau$, then the instantaneous response of the element can be determined by

$$d\overset{*}{\sigma}_i(\tau) = f(d\epsilon_i(\tau).d\tau) \qquad (6.2.1)$$

In a more general formulation the function in 6.2.1 might also depend on other quantities such as the extent of damage induced by time–independent or instantaneous behaviour. For example the description could reduce to that for the time–independent fracturing solid or that for ideal plasticity. Here, however, the material is taken to be rate–dependent linear elastic so that the instantaneous response is affected only by the increment of strain and its duration.

In the damage evolution law, the true stress σ_i is determined by the amount of time delayed damage that has occurred during a given lapse of time. Accordingly, the true stress is a function of the instantaneous stress and time only. The actual stress increment $d\sigma_i(t)$ at any time $t \geq \tau$ becomes a fraction of $d\overset{*}{\sigma}_i(\tau)$.

This relaxation of the instantaneous stress with time is assumed to be of the form

$$d\sigma_i(t) = \varphi(t-\tau)\, d\overset{*}{\sigma}_i(\tau) \qquad (6.2.2)$$

where φ is a relaxation function decreasing with time, such that

$$\varphi(0) = 1.0$$

and (6.2.3)

$$\varphi(\infty) \geq 0$$

The stress within a member at a time t, being a result of all strain increments, $d\epsilon_i(\tau)$, and the corresponding instantaneous stress increments, $d\overset{*}{\sigma}_i(\tau)$, applied at all times $\tau \leq t$, is thus given by

$$\sigma_i(t) = \int_0^t \varphi(t-\tau)\, d\overset{*}{\sigma}_i(\tau) \qquad (6.2.4)$$

The two relationships (6.2.1) and (6.2.4), together with an appropriate failure criterion, are enough to describe the behaviour of the i^{th} member.

It should be noted that the instantaneous law resembles the response that the material would follow at high strain rates and the evolution law links this response to the actual time lapse.

6–2–4 Forms of the instantaneous constitutive laws

The instantaneous response of each member is assumed to be dependent

on the change in strain within the member and the time rate of such change. The form of the instantaneous law (6.2.1) is assumed to be

$$d\overset{*}{\sigma}_i(\tau) = S_i(\tau)\, d\epsilon_i(\tau) \qquad (6.2.5)$$

where $S_i(\tau)$, the instantaneous stiffness of the i^{th} member, is dependent on the strain rate at time τ. The rate–dependent modulus, $S_i(\tau)$, is taken to have the form

$$S_i(\tau) = \begin{cases} E_i \left[\dfrac{\dot{\epsilon}_i(\tau)}{\dot{\epsilon}_{i0}} \right]^{\frac{1}{x_i}} & \text{for intact members} \\ 0 & \text{for failed members} \end{cases} \qquad (6.2.6)$$

where x_i is a material property, $\dot{\epsilon}_{i0}$ is a reference strain rate, termed the "static" strain rate, $\dot{\epsilon}_i(\tau)$ is the current value of the strain rate within the element, and E_i is the value of $S_i(\tau)$ at the reference strain rate, termed the "static" stiffness modulus. It is assumed that 6.2.6 is applicable only for strain rates higher than the static value. The instantaneous modulus, $S_i(\tau)$, is assumed to have the value of E_i for all strain rates $\dot{\epsilon}_i$ less than the static rate.

The power law (6.2.6) has been chosen for computational convenience and is not an empirical expression for the increase in the instantaneous stiffness modulus of a real physical material. Still, it resembles some aspects of the response of true materials at high levels of strain rates. Power laws have been used (chapter III) to express the dependence of material stiffness on the strain rates. Figure 6.1 depicts the variation of $S_i(\tau)$ with applied strain rate as dictated by equation 6.2.6. As seen from figure 6.1, the instantaneous stiffness increases with increasing strain rate above the static value. This phenomenon was observed in the behaviour of real materials as was concluded in chapter III where an increase in the stiffness of a class of engineering materials with applied strain rates was reported.

6–2–5 Forms of the total constitutive laws

The total constitutive law, governing the behaviour of the i^{ih} member

is obtained by combining the instantaneous stress–strain law (6.2.5) with the damage evolution law (6.2.4). This gives

$$\sigma_i(t) = \int_0^t \varphi(t-\tau)\, S_i(\tau)\, d\epsilon_i(\tau) \qquad (6.2.7)$$

where the function $\varphi(t)$ remains to be prescribed as a material property.

Analysis of the network model is performed by invoking equilibrium of forces at nodes at all times. This requires that the above integral constitutive law be expressed in terms of force and displacement within the member rather than stress and strain, so that

$$F_i(t) = \frac{A_i}{L_i} \int_0^t \varphi(t-\tau)\, S_i(\tau)\, \frac{d\Delta L_i(\tau)}{d\tau}\, d\tau \qquad (6.2.8)$$

where A_i is the area of the i^{th} member and L_i is its length. The force $F_i(t)$ and the elongation $\Delta L_i(\tau)$ are related to the stress and strain by

$$F_i(t) = A_i \sigma_i(t) \qquad (6.2.9)$$

and

$$\Delta L_i(t) = L_i \epsilon_i(\tau) \qquad (6.2.10)$$

It should be noted that changes in the strain rate with time can occur within a member even when the rate of application of nodal displacements in the edge zone of the model material is kept constant. This results from breakage of members and the consequent stress redistribution among the remaining intact members. Of course, if the rate of application of the prescribed displacements is altered, the strain rate within individual members is expected to change. In general, integrals 6.2.7 and 6.2.8 have to be evaluated for changing values of $S_i(\tau)$, depending on the value of the strain rate at time τ.

The network model is analysed following a direct stiffness approach modified to incorporate time effects. This requires the expression of members constitutive laws in matrix form and the assembly of a global stiffness matrix modified to account for applied deformations and boundary conditions. This formulation is discussed in the following section.

6–2–6 Matrix formulation

Consider (figure 6.2) the i^{th} member of the network. Let θ_i be the angle this member makes with the x–axis in the reference coordinate system (figure 4.2).

At any time t, the force within the member can be decomposed into its components along the member's local coordinate system so that

$$\begin{bmatrix} F'_{i1} \\ F'_{i2} \\ F'_{i3} \\ F'_{i4} \end{bmatrix}_{(t)} = \begin{bmatrix} -1 \\ 0 \\ 1 \\ 0 \end{bmatrix} F_i(t) \qquad (6.2.11)$$

where F'_{ij} (j=1,4) represents the components of the force $F_i(t)$, as depicted in figure 6.2(a), in the member's local coordinate system (figure 6.2(b)). The change in the member's elongation can also be expressed in terms of its components in the member's local coordinate system. This is expressed in matrix form, at any time t, as

$$d\Delta L_i(t) = [-1 \quad 0 \quad 1 \quad 0] \begin{bmatrix} du'_{i1} \\ du'_{i2} \\ du'_{i3} \\ du'_{i4} \end{bmatrix}_{(t)} \qquad (6.2.12)$$

where du'_{ij} (j=1,4) represents the components of the change in the elongation in the element's local coordinate system (figure 6.2(b)). Transformation of the force and the change in elongation of the member from local coordinates (6.2(b)) to the global coordinate system (figure 6.2(c)) can be achieved by

$$\begin{bmatrix} F_{i1} \\ F_{i2} \\ F_{i3} \\ F_{i4} \end{bmatrix}_{(t)} = \begin{bmatrix} \lambda_i & -w_i & 0 & 0 \\ w_i & \lambda_i & 0 & 0 \\ 0 & 0 & \lambda_i & -w_i \\ 0 & 0 & w_i & \lambda_i \end{bmatrix} \begin{bmatrix} F'_{i1} \\ F'_{i2} \\ F'_{i3} \\ F'_{i4} \end{bmatrix}_{(t)} \qquad (6.2.13)$$

and

$$\begin{bmatrix} du'_{i1} \\ du'_{i2} \\ du'_{i3} \\ du'_{i4} \end{bmatrix}(t) = \begin{bmatrix} \lambda_i & w_i & 0 & 0 \\ -w_i & \lambda_i & 0 & 0 \\ 0 & 0 & \lambda_i & w_i \\ 0 & 0 & -w_i & \lambda_i \end{bmatrix} \begin{bmatrix} du_{i1} \\ du_{i2} \\ du_{i3} \\ du_{i4} \end{bmatrix}(t) \qquad (6.2.14)$$

where λ_i and w_i are the cosine and the sine of the angle θ_i, and $F_{ij}(j=1,4)$ and $du_{ij}(j=1,4)$ represent the components of the force and the change in the elongation of the i^{th} member in the global coordinate system (figure 6.2(c)).

Noting that $F_i(t)$ is given by the total constitutive law in 6.2.8, and that the matrix expressions 6.2.11–6.2.14 can be used together to relate the components of the force, $F_i(t)$, and the change in the elongation, $d\Delta L_i$, in the global coordinate system, will give

$$\begin{bmatrix} F_{i1} \\ F_{i2} \\ F_{i3} \\ F_{i4} \end{bmatrix}(t) = \frac{A_i}{L_i} \begin{bmatrix} \lambda_i^2 & \lambda_i w_i & -\lambda_i^2 & -\lambda_i w_i \\ \lambda_i w_i & w_i^2 & -\lambda_i w_i & -w_i^2 \\ -\lambda_i^2 & -\lambda_i w_i & \lambda_i^2 & \lambda_i w_i \\ -\lambda_i w_i & -w_i^2 & \lambda_i w_i & w_i^2 \end{bmatrix}$$

$$\times \begin{bmatrix} \int_0^t \varphi(t-\tau)\, S_i(\tau)\, du_{i1}(\tau) \\ \int_0^t \varphi(t-\tau)\, S_i(\tau)\, du_{i2}(\tau) \\ \int_0^t \varphi(t-\tau)\, S_i(\tau)\, du_{i3}(\tau) \\ \int_0^t \varphi(t-\tau)\, S_i(\tau)\, du_{i4}(\tau) \end{bmatrix} \qquad (6.2.15)$$

The matrix form of the stress–strain law given in (6.2.15) is enough to describe the response of any intact member. It should be noted that for a failed member the force and the stress are assumed to vanish, so that all components represented by F_{ij} (j=1,4) reduce to zero. This can be achieved by setting $S_i(\tau)$ to zero not only at time t, but for all times $0 \leq \tau \leq t$.

So far the constitutive laws provide a description of the members prior

to their breakage. No failure criterion, governing this breakage, has been mentioned. Before the members fail, their behaviour is fully described by the constitutive laws given. When a member is considered to have failed, it is ignored in all subsequent steps of analysis. In the next section, an energy failure criterion is discussed.

6–2–7 Failure of the network members

In the time–independent analysis of the "network model" (chapter IV), an energy limiting criterion could be made interchangeable with a stress or strain limit. When time effects are taken into account, this interchangeability no longer applies and hence the failure criterion for the members should be specified more "precisely".

An energy failure criterion has been used [129a] for a number of different applications in describing the time–dependent behaviour of polymers. In these applications, fracture was assumed to be initiated or to propagate if some energy parameters reach limiting values. These limiting values are normally taken to be dependent on the rate of load application. It was suggested [129b] that an energy failure criterion would be most appropriate when dealing with time–dependent fracture.

For the network model, at any stage of loading, the work done per unit volume by the deformation of the i^{th} member is given by

$$W_i(t) = \int_0^t \sigma_i(\tau) d\epsilon_i(\tau) \qquad (6.2.16)$$

This amount of energy is released in the system when the member fails.

An energy limit criterion is adopted for the network model. Members are assumed to have limits on the amounts of energy that they can dissipate when they fail under tensile and compressive loading. Hence, a member is considered to be intact as long as $W_i(t)$ (equation 6.2.16) does not exceed a limiting value W_{if} in tension and $\beta_i W_{if}$ in compression, where β_i is a scalar defining the ratio of compressive to tensile energy limits.

The limiting values of W_i, in the present formulation, are assumed to be constant for a given member and independent of the rate of deformation.

The use of this energy limit failure criterion requires integration along time and hence does not seem as straight forward as that adopted in the time–independent case. Nevertheless, it is computationally possible. If the network model is to be physically built, the assumed failure criterion can be achieved by monitoring the work done by each member and "cutting" the member if this quantity reaches its limits.

6–2–8 Member properties

In order to complete the description of the network model, the properties of all members need to be specified and stored in the computer memory. These properties include

(i) the length L_i and the direction cosines λ_i and w_i. These are computed from the coordinates of the nodes between which the member extends.

(ii) the area A_i, the reference "static" stiffness modulus E_i, and the critical energy limit in tension W_{if}. These are chosen from sets of random numbers following normal distributions with specified means and standard deviations. These sets are truncated so that only positive values are assigned.

(iii) the ratio β_i of the compressive limiting dissipative energy to the tensile value, the power parameter x_i, and the reference static strain rate $\dot{\epsilon}_{i0}$ (expression 6.2.6). These are taken to be the same for all members.

(iv) and the relaxation function $\varphi(t)$. This function is assumed to be of the form

$$\varphi(t) = g_1 \mathrm{EXP}(-g_2 t) + g_3 \qquad (6.2.17)$$

which satisfies the conditions in 6.2.3 for positive values of g_1,g_2, and g_3 such that

$$g_1 + g_3 = 1.0 \qquad (6.2.18)$$

The parameters g_1,g_2, and g_3 are taken to be the same for all members.

Analysis of the network model can be performed provided the material properties, the constitutive laws, and the failure criteria are defined and stored in the computer memory.

6–2–9 Analysis of the network model

(a) Incremental equations

Analysis of the network model is performed in an incremental manner along time. Each term of the right hand side column matrix in (6.2.15) can be approximated by the form

$$\int_0^t \varphi(t-\tau)\, S_i(\tau)\, du_{ij}(\tau) = \sum_0^{t-\Delta t} \varphi(t-\tau)\, S_i(\tau)\, \Delta u_{ij}(\tau) + S_i(t)\, \Delta u_{ij}(t) \qquad (6.2.19)$$

where $\Delta u_{ij}(t)$ represents the changes in the displacements at the nodes between which the i^{th} member extends (j=1,4). It is expressed as a forward difference so that

$$\Delta u_{ij}(t) = u_{ij}(t+\Delta t) - u_{ij}(t) \qquad (6.2.20)$$

The strain rate within a member, at time t, is approximated by the forward difference expression

$$\dot{\epsilon}_i(t) = \frac{\Delta L_i(t+\Delta t) - \Delta L_i(t)}{L_i\, \Delta t} \qquad (6.2.21)$$

where $\Delta L_i(t)$ is the elongation of the i^{th} element at time t, and Δt is the time increment.

In order to express the strain rate (6.2.21) in matrix form, the matrix equations 6.2.12 and 6.2.14 are substituted in 6.2.21 to give

$$\dot{\epsilon}_i(t) = [-\lambda_i \; w_i \; \lambda_i \; -w_i] \begin{bmatrix} \Delta u_{i1} \\ \Delta u_{i2} \\ \Delta u_{i3} \\ \Delta u_{i4} \end{bmatrix}_{(t)} \frac{1}{L_i\, \Delta t} \qquad (6.2.22)$$

For the analysis of the model to be computationally possible, the overall equilibrium equation (6.2.15) should be approximated by an incremental or discrete form. This is achieved by substituting the approximate expression 6.2.19 in 6.2.15 to give

$$\underset{\sim}{f} - \underset{\sim}{b} = \underset{\sim}{k}\,\underset{\sim}{\Delta u} \tag{6.2.23}$$

where

$$\underset{\sim}{f} = \begin{bmatrix} F_{i1} \\ F_{i2} \\ F_{i3} \\ F_{i4} \end{bmatrix}(t) \tag{6.2.24}$$

is the nodal force vector,

$$\underset{\sim}{b} = \frac{A_i}{L_i} x \begin{bmatrix} \lambda_i^2 & \lambda_i w_i & -\lambda_i^2 & -\lambda_i w_i \\ \lambda_i w_i & w_i^2 & -\lambda_i w_i & -w_i^2 \\ -\lambda_i^2 & -\lambda_i w_i & \lambda_i^2 & \lambda_i w_i \\ -\lambda_i w_i & -w_i^2 & \lambda_i w_i & w_i^2 \end{bmatrix} \times \begin{bmatrix} \sum_0^{t-\Delta t} \varphi(t-\tau) S_i(\tau) \Delta u_{i1}(\tau) \\ \sum_0^{t-\Delta t} \varphi(t-\tau) S_i(\tau) \Delta u_{i2}(\tau) \\ \sum_0^{t-\Delta t} \varphi(t-\tau) S_i(\tau) \Delta u_{i3}(\tau) \\ \sum_0^{t-\Delta t} \varphi(t-\tau) S_i(\tau) \Delta u_{i4}(\tau) \end{bmatrix} \tag{6.2.25}$$

is the past time equivalent nodal force vector,

$$\underset{\sim}{k} = \frac{A_i}{L_i} S_i(t) \begin{bmatrix} \lambda_i^2 & \lambda_i w_i & -\lambda_i^2 & -\lambda_i w_i \\ \lambda_i w_i & w_i^2 & -\lambda_i w_i & -w_i^2 \\ -\lambda_i^2 & -\lambda_i w_i & \lambda_i^2 & \lambda_i w_i \\ -\lambda_i w_i & -w_i^2 & \lambda_i w_i & w_i^2 \end{bmatrix} \tag{6.2.26}$$

is the current instantaneous member stiffness matrix, and

$$\underset{\sim}{\Delta u} = \begin{bmatrix} \Delta u_{i1} \\ \Delta u_{i2} \\ \Delta u_{i3} \\ \Delta u_{i4} \end{bmatrix}(t) \tag{6.2.27}$$

is the change in nodal displacements vector.

To complete this discretization procedure, the energy $W_i(t)$ (6.2.16), that can be dissipated by the breakage of the i^{th} member at time t, is approximated by

$$W_i(t) = \sum_0^t \sigma_i(\tau)\, d\epsilon_i(\tau) \qquad (6.2.28)$$

with the stress $\sigma_i(t)$ given by

$$\sigma_i(t) = \sum_0^t \varphi(t-\tau)\, S_i(\tau)\, \dot{\epsilon}_i(\tau)\, \Delta t \qquad (6.2.29)$$

(b) Scope of analysis

The analysis is designed to reproduce the types of loading encountered in physical testing using a displacement controlled actuator for loading in at least one direction. Because of this, the analysis has been restricted to the following situations:

(i) uniaxial tensile displacement controlled tests with both loading and reactive edges friction free,

(ii) uniaxial tensile displacement controlled tests, with both loading and reactive edges friction free, followed by relaxation, and

(iii) uniaxial tensile displacement controlled tests, with both loading and reactive edges friction free, followed by creep.

In both situations (i) and (ii), displacements for all nodes in zone (2) (figure 4.2) are prescribed at all times so that analysis for both cases can be performed using the same computer routines. For the third case (iii), forces rather than displacements are prescribed in the creep phase. This requires some modifications to the analysis procedure.

The computer programs were written so that it would be possible to deal with situations where rate effects are ignored in the instantaneous response of the individual members. For this case, the instantaneous stress increment, $d\overset{*}{\sigma}_i(\tau)$, induced by a strain increment $d\epsilon_i(\tau)$, is assumed to be a function of the value of $d\epsilon_i(\tau)$ only with no dependence on the time rate of this strain increment. The time–dependent behaviour of each member is determined solely by the damage evolution law (expression 6.2.4). The instantaneous value of the stiffness of the i^{th} member, $S_i(\tau)$, is taken to be of a constant value equal to the reference static modulus, E_i, at all times. Damage, within each member in this case, is only

a result of stress relaxation with time.

(c) Computation

If nodal displacements are prescribed for all nodes in the edge zone (2) (figure 4.2) at all times, then the analysis of the behaviour of the network is performed in an incremental manner. A direct stiffness method, modified to incorporate time effects is used. Appendix B describes the steps of analysis followed in this case.

If stress along the network is to be kept constant after a specified time t_c then, for all times less than t_c, analysis follows the same procedure in Appendix B. For all times greater than t_c, analysis still proceeds as before except that no reduction of the structural stiffness matrix for prescribed displacements is performed and no transformation of such displacements into nodal forces is done. In each step of analysis, all nodal forces are assumed to retain their values as in the previous time step. This ensures that the overall average stress along the network remains constant. This state of constant overall stress is accompanied by nodal displacements as well as changes in stresses within the individual members. Members breakage under these conditions is, hence, possible.

Some care should be taken when choosing the time increment Δt. A large value of Δt will result in large errors. These errors result from the failure of more than one member during the same increment of time and from the use of discrete sums over time to approximate various integral relations. On the other hand, a very small increment of time will result in large computer time usage with not much improvement in accuracy. It also results in some calculations involving indefinitely small numbers that can not be performed accurately by the computer.

For each test run, some trial tests on the model were run to choose an appropriate time increment Δt. This increment is chosen so that no more than one member fails at the same time and such that a further reduction in its value will not alter the response numerically (by more than 0.1%). It was found convenient, and computer time saving, to increase the time increment (by orders of magnitude) during creep or relaxation phases, if the loading rates prior to these phases are relatively high compared to those during constant strain or stress conditions. If, at any stage of loading, the response of the network was

found to be highly brittle (with more than one member breaking), reduction of Δt (by half) was imposed. This is possible unless failure is unstable in the sense that members breakage occurs rapidly within a short time. In this case, failure of a member leaves the network in an unstable state that can only be stabilized by further members failing.

Results of tests performed on the network model will be presented in the next chapter together with those performed on another material model termed the fibre bundle model. The description of the bundle model and the procedure followed in its analysis are presented in the following section.

6–3 The "fibre bundle" model

As an alternative to the discrete formulation presented in the previous section to describe time–dependent progressive fracture, a continuum model is presented in here. This model is built up in a similar fashion to that followed in the formulation of the general time–dependent progressively fracturing solids theory of chapter V.

Consider an ideal time–dependent progressively fracturing solid having its fracture surface in strain space of the form

$$F = \lambda_{ij}\,\epsilon_{ij} - h(D,T) = 0 \qquad (6.3.1)$$

where the tensor λ_{ij} represents symmetric multipliers and h, a positive function describing damage in the material, is a function of the energy dissipated, D, and time. T is a parameter describing time and rate effects.

The fracture surface (expression 6.3.1) is a hyperplane in strain space and the function h provides a limit on the strain which is associated with fracture. A similar device has been developed in plasticity by Sander [130] where the material description involved the use of several independent linear loading functions each defining a hyperplane. The yield surface that is observed in tests on real materials would correspond to the boundary of the internal region formed by the intersection of these independent yield surfaces.

This continuum description, provided by equation 6.3.1, can be closely linked to a two dimensional physical model consisting of fibres held in parallel so that, at any time, strain is identical for all fibres. If the fibres within a bundle are aligned at an angle θ (figure 6.4) to the coordinate axis '1', where $0 \leq \theta \leq \pi$, then the multipliers, λ_{ij}, would be calculated from the directional cosines of the angle θ using the equations in 2.4.3. In these terms, an individual fibre within a bundle is assumed to break in tension when its axial strain reaches a limiting value f_t, assumed to be rate dependent. The limiting strains of all fibres are assumed to be continuously distributed between zero and infinity.

The parameter h in equation 6.3.1 is hence the current value of f_t required to break the next fibre in the bundle, where all fibres with limiting strains between zero and f_t have already been broken. Since the limiting strains of the individual fibres are assumed to be dependent on the time history of strain, then h serves a measure of the past path and time history of deformations.

The linear loading function idealization is equivalent to a fibre bundle so that the use of a number of independent linear loading functions correspond to a model comprising a number of differently aligned fibre bundles responding to an applied strain field.

A full investigations of this model, with time and rate effects completely ignored, was presented by Rida in [51].

6–3–1 Continuum formulation

In chapter V a continuum theory, for the description of the behaviour of an ideal time–dependent progressively fracturing solid, was developed. The present fibre bundle model is derived in a similar fashion. In fact, it is a particular case of this theory. Most of the assumptions adopted in the formulation of the general theory are assumed to hold in the present formulation.

In this section the theoretical background necessary for the continuum formulation of the model involving linear loading functions is presented and all the necessary derivations are performed for the complete description of the material behaviour.

At any time t, the stress increment $d\sigma_{ij}(t)$, within a fibre bundle, is assumed to be composed of two components so that

$$d\sigma_{ij}(t) = d\sigma'_{ij}(t) + d\sigma''_{ij}(t) \qquad (6.3.2)$$

where $d\sigma'_{ij}(t)$ is the viscoelastic stress increment and $d\sigma''_{ij}(t)$ is the fracture stress decrement.

The expressions of the different instantaneous stress increments in 6.3.2 in terms of the instantaneous relaxation moduli and their changes are given, at the time of fracture τ, by expressions similar to those in 5.3.7. Hence

$$d\overset{*}{\sigma}_{ij}(\tau) = S_{ijkm}(\tau)\, d\epsilon_{km}(\tau) + dS_{ijkm}(\tau)\, \epsilon_{km}(\tau) \qquad (6.3.3)$$

so that, with 6.3.2,

$$d\overset{*'}{\sigma}_{ij}(\tau) = S_{ijkm}(\tau)\, d\epsilon_{km}(\tau) \qquad (6.3.4)$$

and

$$d\overset{*''}{\sigma}_{ij}(\tau) = dS_{ijkm}(\tau)\, \epsilon_{km}(\tau) \qquad (6.3.5)$$

where the superscript * refers to the instantaneous responses at the time of

fracture τ. $S_{ijkm}(\tau)$ is termed the instantaneous secant stiffness modulus.

It is assumed that, to any state of the model material, represented by a point in strain space, there corresponds an instantaneous fracture surface defined by 6.3.1. This surface is determined by the damage parameter h (and hence D and T) evaluated at that point (section 5–2).

As for the general theory, the direction of the instantaneous fracture stress decrement, $d\overset{*''}{\sigma}_{ij}(\tau)$ at the time of fracture τ, is along the inward normal to the instantaneous fracture surface at the current point of fracture. Progressive fracture is assumed to occur when

$$\left[\frac{\partial F}{\partial h}\,dh\right] < 0 \qquad (6.3.6)$$

Inequality 6.3.6 and the normality criterion suggest a flow rule of the form

$$d\overset{*''}{\sigma}_{ij}(\tau) = -K\,\frac{\partial F}{\partial \epsilon_{ij}}\left[-\frac{\partial F}{\partial h}dh\right] \quad \text{at } t=\tau \qquad (6.3.7)$$

where K is a scalar to be determined. In view of the expression of the fracture surface (6.3.1) the above flow rule becomes

$$d\overset{*''}{\sigma}_{ij}(\tau) = -K\,\lambda_{ij}\,dh \quad \text{at } t=\tau \qquad (6.3.8)$$

It should be noted that during progressive fracture

$$F(\tau) = \lambda_{ij}\,\epsilon_{ij}(\tau) - h(\tau) = 0 \qquad (6.3.9)$$

and

$$dF(\tau) = \lambda_{ij}\,d\epsilon_{ij}(\tau) - dh(\tau) = 0 \qquad (6.3.10)$$

In view of the incremental form of the stress in 6.3.3, the value of the increment of dissipated energy, released instantaneously at the time of fracture τ, can be assumed to be given by [51]

$$dD(\tau) = -\frac{1}{2}\,d\overset{*''}{\sigma}_{ij}(\tau)\,\epsilon_{ij}(\tau) \qquad (6.3.11)$$

Multiplying both sides of the flow rule (6.3.8) by ϵ_{ij} gives

$$d\overset{*''}{\sigma}_{ij}(\tau)\,\epsilon_{ij}(\tau) = -K\,\lambda_{ij}\,\epsilon_{ij}\,dh \quad \text{at } t=\tau \qquad (6.3.12)$$

Substituting equation 6.3.11 in 6.3.12 gives

$$K = \frac{2dD}{\lambda_{ij}\,\epsilon_{ij}\,dh} \quad \text{at } t=\tau \qquad (6.3.13)$$

Noting that $\lambda_{ij}\epsilon_{ij} = h$ at $t=\tau$ (equation 6.3.9), the flow rule becomes

$$d\sigma^{*''}_{ij}(\tau) = -\frac{2\lambda_{ij}}{h}\,dD \quad \text{at } t=\tau \tag{6.3.14}$$

or

$$d\sigma^{*''}_{ij}(\tau) = \frac{-2\lambda_{ij}\,dD\,\lambda_{km}\,\epsilon_{km}}{h^2} \quad \text{at } t=\tau \tag{6.3.15}$$

so that from (6.3.5)

$$dS_{ijkm}(\tau) = \left[\frac{-2}{h^2}\lambda_{ij}\lambda_{km}\,dD\right]_{t=\tau} + R_{ijkm}(\tau) \tag{6.3.16}$$

where $R_{ijkm}(\tau)$ is a symmetric tensor such that $R_{ijkm}(\tau)\epsilon_{km}(\tau)=0$. Taking all components of $R_{ijkm}(\tau)$ to be zero [51] gives

$$dS_{ijkm}(\tau) = \frac{-2}{h^2}\lambda_{ij}\lambda_{km}\,dD \text{ at } t=\tau \tag{6.3.17}$$

The above expression completes the continuum description of the instantaneous response of the model material. Still, in order for the formulation to be implemented, the forms of the various functions (T, D, h) should be known or assumed based on past experience of experimental results of some physical materials. Also, for computational convenience, the material description should be expressed in terms of incremental rather than continuum relations. These two aspects are tackled in the next section.

6–3–2 Expressions for the various functions

The instantaneous response of a fibre bundle is assumed to be dependent on the current strain rate. A simple power form of T, involving only strain rates, is assumed,

$$T(\tau) = \left[\frac{\dot{\epsilon}_0}{\dot{\epsilon}_r(\tau)}\right]^{\frac{1}{x}} \quad \text{for } \dot{\epsilon}_r \geq \dot{\epsilon}_0 \tag{6.3.18}$$

where x is a power parameter , $\dot{\epsilon}_0$ is the reference "static" equivalent strain rate, and $\dot{\epsilon}_r(\tau)$ is the absolute value of the current strain rate along the direction of the bundle.

If within a small increment of time $d\tau$, the strain changes by $d\epsilon_{ij}(\tau)$ then the strain rate can be approximated by

$$\dot{\epsilon}_r(\tau) = \left| \frac{\lambda_{ij} \, d\epsilon_{ij}(\tau)}{d\tau} \right| \qquad (6.3.19)$$

In the time–independent analysis of this material model [51] the energy dissipation function, D, was assumed to be related to the damage parameter h by

$$D = D_{max} \left[\frac{h}{h+\beta_f} \right]^3 \qquad (6.3.20)$$

where D_{max} is the maximum energy that can be dissipated upon complete failure, and β_f is a parameter controlling brittleness of the response.

It is assumed , for the present formulation, that at any level of damage, the energy dissipated upon fracture is higher for higher values of strain rate, and that the total energy that can be extracted from the fibre bundle has an upper bound of a value D_{max}. This allows the extension of 6.3.20 into

$$D = D_{max} \left[\frac{h}{h + T\beta_f} \right]^3 \qquad (6.3.21)$$

with the strain rate parameter T given by 6.3.18.

Figure 6.3 depicts the variation of D with h for various values of T. It is noted that for the same value of the damage parameter h, the energy dissipated at the time of fracture τ is higher for lower values of T (associated with higher strain rates).

From 6.3.21

$$dD(\tau) = \frac{\partial D}{\partial h} dh + \frac{\partial D}{\partial T} dT = \frac{3 \, D_{max} \, \beta_f}{h^2} \left[\frac{h}{h+T\beta_f} \right]^4 (T \, dh - h \, dT) \text{ at } t=\tau \qquad (6.3.22)$$

In view of equation 6.3.17, the change in the instantaneous relaxation modulus $dS_{ijkm}(\tau)$ can be given as

$$dS_{ijkm}(\tau) = \left[\frac{-2C}{h^2} \lambda_{ij} \lambda_{km} dD \right]_{t=\tau} \qquad (6.3.23)$$

where $dD(\tau)$ is given by (6.3.22) and

(i) C=0 for $F(\tau) \leq 0$ and $\lambda_{ij} d\epsilon_{ij}(\tau) \leq 0$ (elastic unloading)

$F(\tau) < 0$ and $\lambda_{ij} d\epsilon_{ij}(\tau) > 0$ (elastic loading)

(iii) C=1 for $F(\tau) = 0$ and $\lambda_{ij} d\epsilon_{ij}(\tau) > 0$ (progressive fracture)

(6.3.24)

Noting that during progressive fracture equations 6.3.9 and 6.3.10 apply, the allocation of the changes in the damage parameter, dh, and the loading function, dF, at the time of fracture can be performed as

$$dh(\tau) = 0$$
$$dF(\tau) = \lambda_{ij} d\epsilon_{ij}(\tau) \qquad \text{for } C = 0 \qquad (6.3.25)$$

and

$$dh(\tau) = \lambda_{ij} d\epsilon_{ij}(\tau)$$
$$dF(\tau) = 0 \qquad \text{for } C = 1 \qquad (6.3.26)$$

As a result of the incremental form of the above equations, overshooting the instantaneous fracture surface might occur and has to be catered for in computation. The expressions in 6.3.25 should thus be modified if $\lambda_{ij} d\epsilon_{ij}(\tau) > |F|$, since this condition results in overshooting the instantaneous fracture surface. In this case, 6.3.25 is replaced by

$$dF(\tau) = |F(\tau)|$$
$$dh(\tau) = \lambda_{ij} d\epsilon_{ij}(\tau) - |F(\tau)| \qquad (6.3.27)$$

At the time of fracture τ, the strain rate $\dot{\epsilon}_r(\tau)$ is approximated by 6.3.19 and the change in the strain rate parameter T, at time τ, is approximated by the backward difference expression

$$dT(\tau) = T(\tau) - T(\tau - d\tau) \qquad (6.3.28).$$

6–3–3 Calculation of the initial instantaneous stiffness

In the previous section, incremental equations were formulated to describe the instantaneous response of the model material at any time. The initial response of the material (at time zero) still needs to be described so that, at any time, the material response be described by the cumulative instantaneous responses from time zero.

In the time–independent version of the present theory (progressively fracturing solids theory using linear loading functions [51]), the initial stiffness can be calculated unambiguously from the dissipation function D(h) on the assumption that the stiffness is reduced to zero when all fibres are broken and $D = D_{max}$. The initial stiffness S_{ijkm} is hence calculated using

$$S_{ijkm}(0) + \int_0^\infty \frac{dS_{ijkm}}{dh}\, dh = 0 \qquad (6.3.29)$$

where h is a function of damage and is independent of time. A similar argument in the present formulation gives

$$S_{ijkm}(0) + \int_0^{\infty} \frac{dS_{ijkm}(t)}{dt} dt = 0 \qquad (6.3.30)$$

if the instantaneous stiffness is to reduce to zero at $t = \infty$ when the bundle is completely damaged. The above expression, with equation 6.3.17, gives

$$S_{ijkm}(0) = \int_0^{\infty} \left[\frac{2}{h^2} \lambda_{ij} \lambda_{km} dD\right]_T \qquad (6.3.31)$$

The above expression illustrates the difficulty encountered here in the calculation of the initial instantaneous stiffness. The integration has to be performed along time since the function to be integrated is dependent on time. This means that the initial instantaneous stiffness is no more a material property but is a function of the history of loading the material is expected to follow. This is a direct result of the assumption that the damage function h is dependent on both the damage parameter D and the strain rate parameter T.

One way of overcoming this difficulty is to choose the damage function in such a way that $\frac{dD}{h^2}$ is independent on time. This allows the integration (6.3.31) to be performed independently of T. This additional assumption on the material behaviour allows the calculation of the initial instantaneous stiffness to be performed directly from the damage function h as in the case of the time–independent behaviour.

In the present formulation an alternative assumption is adopted. The initial instantaneous material stiffness is assumed to be dependent on the initial loading conditions applied on the material regardless of any loading to follow. In other words, the initial instantaneous stiffness $S_{ijkm}(0)$ is calculated by assuming that the fibre bundle is strained from $t = 0$ to $t = \infty$ at the same strain rate $\dot{\epsilon}_r(0)$, where $\dot{\epsilon}_r(0)$ is the strain rate at time $t = 0$. Corresponding to $\dot{\epsilon}_r(0)$ is the parameter T(0) (expression 6.3.18). Using the incremental equation 6.3.22 and noting that, in this case, dT=0 all over the integral 6.3.31 will give

$$S_{ijkm}(0) = \lambda_{ij} \lambda_{km} \frac{2D_{max}}{\left[\beta_f T(0)\right]^2} \qquad (6.3.32)$$

The initial instantaneous stiffness being calculated, the stiffness at all

other times can be calculated as will be seen in the next section.

6–3–4 Changes in the instantaneous stiffness moduli

At any time τ, the change in the instantaneous stiffness modulus S_{ijkm} is given by expression 6.3.23

$$dS_{ijkm}(\tau) = \left[-\frac{2C}{h^2} \lambda_{ij} \lambda_{km} \, dD \right]_{t=\tau} \tag{6.3.33}$$

with C given by expression 6.3.24. The above expression can be evaluated if the change in the energy dissipated upon fracture, $dD(\tau)$, is known. From the incremental equation 6.3.22

$$dD = \frac{\partial D}{\partial h} dh + \frac{\partial D}{\partial T} dT \tag{6.3.34}$$

where

$$\frac{\partial D}{\partial h} = \frac{3D_{max} \beta_f}{h^2} T \left[\frac{h}{h + T\beta_f} \right]^4 \tag{6.3.35}$$

and

$$\frac{\partial D}{\partial T} = -\frac{3D_{max} \beta_f}{h} \left[\frac{h}{h + T\beta_f} \right]^4 \tag{6.3.36}$$

The expressions in 6.3.34 to 6.3.36 can be used to calculate the change in the incremental energy dissipated upon fracture. This increment of energy being calculated will be used in expression 6.3.33 to evaluate dS_{ijkm}, at the time of fracture τ.

It was found that in some applications an alternative formulation of the stiffness moduli proves more convenient from the computational point of view. This formulation is achieved by noting that expressions 6.3.14, 6.3.3, 6.3.5, and 6.3.24 give

$$d\overset{*}{\sigma}_{ij}(\tau) = S_{ijkm}(\tau) \, d\epsilon_{km}(\tau) - \left[\frac{2C}{h} \lambda_{ij} \, dD \right]_{t=\tau} \tag{6.3.37}$$

and that $dh = \lambda_{ij} d\epsilon_{ij}$ at $t=\tau$. Substituting 6.3.34 in 6.4.37 gives

$$d\overset{*}{\sigma}_{ij}(\tau) = M_{ijkm}(\tau) \, d\epsilon_{km}(\tau) - \left[\frac{2C\lambda_{ij}}{h^2} \lambda_{km} \epsilon_{km} \frac{\partial D}{\partial T} dT \right]_{t=\tau} \tag{6.3.38}$$

where

$$M_{ijkm}(\tau) = S_{ijkm}(\tau) - \left[\frac{2C}{h} \lambda_{ij} \lambda_{km} \frac{\partial D}{\partial h} \right]_{t=\tau} \tag{6.3.39}$$

is termed the instantaneous tangent stiffness modulus at the time of fracture.

6–3–5 Scalar representation

A scalar representation was adopted in which stresses and strains are represented in terms of their scalar equivalent projected along the direction of the fibre bundle. These scalar definitions allow the representation of the tangential and secant stiffness moduli and their incremental changes in terms of scalar quantities. This is a convenience for numerical applications, particularly in assuring convergence of the incremental solution (Appendix C–Appendix F).

The strain along the direction of the fibre bundle is a scalar $\overline{\epsilon}(\tau)$ given by

$$\overline{\epsilon}(\tau) = \lambda_{ij}\epsilon_{ij}(\tau) \qquad (6.3.40)$$

The instantaneous scalar stress $\overset{*}{\overline{\sigma}}(\tau)$ along the same direction is calculated by

$$\overset{*}{\overline{\sigma}}_{ij} = \lambda_{ij}\overset{*}{\sigma}_{ij}(\tau) \qquad (6.3.41)$$

with

$$\overset{*}{\sigma}_{ij}(\tau) = \int_0^{\tau} d\overset{*}{\sigma}_{ij}(s) \qquad (6.3.42)$$

where $d\overset{*}{\sigma}_{ij}(s)$ is the instantaneous increment of stress at time t=s, $0 \leq s \leq \tau$, resulting from an increment of strain $d\epsilon_{ij}(s)$.

Following the same representation of Rida [51], the initial instantaneous secant modulus (equation 6.3.32) is thus given by

$$S_{ijkm}(0) = \lambda_{ij}\lambda_{km}\overline{S}(0) \qquad (6.3.43)$$

where the scalar $\overline{S}(0)$ is given by

$$\overline{S}(0) = \frac{2D_{max}}{\left[\beta_f T(0)\right]^2} \qquad (6.3.44)$$

At any time τ, the instantaneous secant modulus $S_{ijkm}(\tau)$ can be calculated by the approximate discrete sum

$$S_{ijkm}(\tau) = S_{ijkm}(0) + \sum_{s=0}^{\tau-d\tau} dS_{ijkm}(s) \qquad (6.3.45)$$

where dS_{ijkm} is given by (6.3.33) and $d\tau$ is the time increment over which discretization is performed. In scalar form the above expression becomes

$$S_{ijkm}(\tau) = \lambda_{ij}\lambda_{km}\overline{S}(\tau) \tag{6.3.46}$$

with

$$\overline{S}(\tau) = \overline{S}(0) + \sum_{s=0}^{\tau-d\tau}\left[-\frac{2C}{h^2}dD\right]_{at\ s} \tag{6.3.47}$$

The scalar representation of the stress, strain, and stiffness moduli allows the stress–strain instantaneous law to be expressed as

$$\overset{*}{\overline{\sigma}}(\tau) = \overline{S}(\tau)\,\overline{\epsilon}(\tau) \tag{6.3.48}$$

For the next time increment the following scalar representation applies

$$\overset{*}{\overline{\sigma}}(\tau+d\tau) = \overline{S}(\tau+d\tau)\,\overline{\epsilon}(\tau+d\tau) \tag{6.3.49}$$

so that, for a small increment of time

$$\overset{*}{\overline{\sigma}}(\tau) + d\overset{*}{\overline{\sigma}}(\tau) = \left[\overline{S}(\tau) + d\overline{S}(\tau)\right]\left[\overline{\epsilon}(\tau) + d\overline{\epsilon}(\tau)\right] \tag{6.3.50}$$

with

$$d\overline{S}(\tau) = \frac{-2C}{h^2}dD \quad \text{at } t=\tau \tag{6.3.51}$$

The instantaneous tangential stiffness modulus can also be expressed in scalar form as

$$M_{ijkm}(\tau) = \lambda_{ij}\lambda_{km}\overline{M}(\tau) \tag{6.3.52}$$

with

$$\overline{M}(\tau) = \overline{S}(\tau) - \left[\frac{2C}{h}\frac{\partial D}{\partial h}\right]_{t=\tau} \tag{6.3.53}$$

so that from 6.6.38

$$\overset{*}{d\overline{\sigma}}(\tau) = \overline{M}(\tau)\,d\overline{\epsilon}(\tau) - \left[\frac{2C}{h^2}\overline{\epsilon}(\tau)\frac{\partial D}{\partial T}dT\right]_{t=\tau} \tag{6.3.54}$$

6–3–6 Calculation of the actual stress

So far, the continuum and incremental formulations have been able to represent the instantaneous response of the fibre bundle. Further assumptions, relating the actual response to the instantaneous one, are hence needed.

As in the continuum model (section 5–3), the actual stress at any time is assumed to be fully described by all previous instantaneous stress increments.

The stress increment $d\sigma_{ij}(t)$ at a time t, due to a strain increment $d\epsilon_{ij}(\tau)$ occurring at time τ, is assumed to be related to the instantaneous stress increment $d\overset{*}{\sigma}_{ij}(\tau)$ at time τ by a damage evolution law (5.3.1) so that

$$\sigma_{ij}(t) = \int_0^t \varphi(t-\tau)\, d\overset{*}{\sigma}_{ij}(\tau) \qquad (6.3.55)$$

or approximately

$$\sigma_{ij}(t) = \sum_0^t \varphi(t-\tau) \frac{d\overset{*}{\sigma}_{ij}(\tau)}{d\tau} d\tau \qquad (6.3.56)$$

The relaxation function $\varphi(t)$ is taken to be of the form

$$\varphi(t) = g_1 EXP(-g_2 t) + g_3 \qquad (6.3.57)$$

where g_1, g_2, and g_3 are positive constants such that $g_1+g_3=1.0$. This function is monotonically decreasing with time and is such that $\varphi(0)=1.0$ and that $\varphi(t)$ approaches a value of g_3 asymptotically with time.

This completes the description of the behaviour of a fibre bundle or equivalently a solid whose behaviour is governed by a single linear loading function. The following section provides the additional assumptions and expressions involved when a system of two or more such bundles are assembled together.

6–3–7 Analysis of some systems assembled from several fibre bundles – Numerical techniques

Two different systems of fibre bundles were tested under various loading conditions. Results of these tests are presented in chapter VII together with those of the network model.

In this section, the steps followed in the analysis of these two systems of fibre bundles are presented.

The first system comprises fibre bundles held in a homogeneous strain field (figure 6.4). The fibre bundles are oriented at different angles with the reference coordinate system. The homogeneity of the strain field in all direction ensures that, at any time, the components of strain for all bundles, in the reference coordinate system, are the same. In other words $\epsilon_{ij}(t)$ is the same for all fibre bundles in the reference coordinate system. This system was studied in

[51] with all time and rate effects ignored.

Analysis of this system was followed incrementally along time. The system was studied under conditions of zero shear strains at all times ($\epsilon_{12}=\epsilon_{21}=0$). Two sets of tests were performed. In the first one, both longitudinal and transverse strain components (ϵ_{11} and ϵ_{22}) were prescribed at all times. In the second case, only ϵ_{11} was prescribed with the stress component in the transverse direction σ_{22} being zero at all times.

The second system comprised two fibre bundles in series (figure 6.5). In this case, analysis can always be performed along the direction of the assembly and is hence one dimensional. Analysis is followed incrementally along time for the case of continuously prescribed total deformation $u_2(t)$ (figure 6.5), and the case where $u_2(t)$ is prescribed up to a specified time t_c after which $u_2(t)$, for $t>t_c$, is allowed to vary so that the stress along the assembly remains constant.

(a) A system of fibre bundles in a homogeneous strain field – Strain always prescribed

As mentioned earlier, this system of fibre bundles is an idealization of the continuum description of fracture provided by the use of several independent linear loading functions of the form 6.3.1.

For such a system, the total instantaneous stiffness modulus of the assembly can be calculated by summing individual terms each representing a fibre bundle (or a linear loading function). In other words,

$$S^T_{ijkm}(\tau) = \sum_{n=1}^{N} S^n_{ijkm}(\tau) = \sum_{n=1}^{N} \lambda^n_{ij}\lambda^n_{km}\overline{S}^n(\tau) \qquad (6.3.58)$$

$$dS^T_{ijkm}(\tau) = \sum_{n=1}^{N} dS^n_{ijkm}(\tau) = \sum_{n=1}^{N} \lambda^n_{ij}\lambda^n_{km}d\overline{S}^n(\tau) \qquad (6.3.59)$$

and

$$M^T_{ijkm}(\tau) = \sum_{n=1}^{N} M^n_{ijkm}(\tau) = \sum_{n=1}^{N} \lambda^n_{ij}\lambda^n_{km}\overline{M}^n(\tau) \qquad (6.3.60)$$

where the superscript n stands for terms related to the n^{th} bundle and T for total

terms.

These expressions of total terms as well as the expressions described earlier for the behaviour of individual fibre bundles are enough to describe the response of this system of fibre bundles.

The analysis procedure, followed to describe the behaviour of such a system of fibre bundles under fully prescribed applied strains, is described in Appendix C. This procedure can be used to study the response under monotonically increasing strains at a constant strain rate, and partially restrained conditions where strain in one or more directions is kept constant at all times.

(b) A system of fibre bundles in a homogeneous strain field – Not all strains prescribed

In this case, strain in one or more directions (in the reference coordinate system (figure 6.4)) is not prescribed but left to vary such that stress along these directions is prescribed. In particular, the stress along the direction where strain is not prescribed is kept zero at all times. For this case

$$\sigma(t) = \sum_{0}^{t} \varphi(t-\tau)\, d\overset{*}{\sigma}(\tau) = 0 \text{ for all times } t \qquad (6.3.61)$$

along the directions where strain is not prescribed.

For a given form of $\varphi(t)$, equation 6.3.61 can only be satisfied at all times t if, for all fibre bundles,

$$d\overset{*}{\sigma}(\tau) = 0 \text{ for all times } \tau \qquad (6.3.62)$$

For example, if ϵ_{22} is not prescribed and is such that $\sigma_{22}(t)=0$ always , then $d\overset{*}{\sigma}_{22}(\tau)=0$ at all times, for all fibre bundles.

Because of the dependence of the new instantaneous stiffness modulus of the assembly on the strain increment $d\epsilon_{ij}$, the evaluation of this stiffness can not be performed directly (since not all components of $d\epsilon_{ij}(\tau)$ are prescribed). An iterative technique was, thus, adopted. The analysis procedure followed, in this case, is presented in Appendix D.

It should be noted that if $\sigma(t)$ was held constant at a value other than

zero, no direct conclusion can be drawn regarding the values of the instantaneous stress increments in the different fibre bundles. The instantaneous stress can vary with time for the various bundles with the overall stress of the assembly unchanged. This imposes a difficulty in the analysis of this system under conditions simulating creep tests. These tests can only be performed if iterative techniques are adopted where the instantaneous stress increments are assumed and the response of the system is calculated and then checked if it is in accordance with the assumed instantaneous stress increments.

The behaviour of an ideal progressively fracturing solid under conditions of constant applied stress can be understood if, instead of a parallel arrangement of individual fibre bundles, a system of bundles held in series under the same stress is tested. The analysis procedure followed for such a system is presented in the following section.

(c) A system of two fibre bundles in series – Total deformation always prescribed

For such a system (figure 6.5) the force across the two bundles is the same at all times. Assuming that the total area is the same for the two fibre bundles, then the stress is the same for both bundles at all times.

At any time, the strain $\epsilon_1(t)$ and $\epsilon_2(t)$ for the two bundles are given by

$$\epsilon_1(t) = \frac{u_1(t)}{L_1} \qquad (6.3.63)$$

and

$$\epsilon_2(t) = \frac{u_2(t) - u_1(t)}{L_2} \qquad (6.3.64)$$

where u_1 and u_2 are the nodal displacements (figure 6.5) and L_1 and L_2 are the lengths of the two fibre bundles. The two equations 6.3.63 and 6.3.64 give

$$L_1 \epsilon_1(t) + L_2 \epsilon_2(t) = u_2(t) \qquad (6.3.65)$$

It should be noted that $u_2(t)$ is the total displacement applied to the system. In incremental form, equation 6.3.65 becomes

$$L_1 d\epsilon_1(t) + L_2 d\epsilon_2(t) = du_2(t) \qquad (6.3.66)$$

The above expression has followed directly from compatibility conditions and should be satisfied at all times regardless of the type of loading.

Denoting the instantaneous stress increments in the two bundles at any

time τ by $d\overset{*}{\sigma}_1(\tau)$ and $d\overset{*}{\sigma}_2(\tau)$ respectively, then the stress $\sigma(t)$ along the assembly at any time is given by

$$\sigma(t) = \sum_{\tau=0}^{t} \varphi(t-\tau)\, d\overset{*}{\sigma}_1(\tau) = \sum_{\tau=0}^{t-dt} \varphi(t-\tau)\, d\overset{*}{\sigma}_1(\tau) + d\overset{*}{\sigma}_1(t) \tag{6.3.67}$$

or

$$\sigma(t) = \sum_{\tau=0}^{t-dt} \varphi(t-\tau)\, d\overset{*}{\sigma}_2(\tau) + d\overset{*}{\sigma}_2(t) \tag{6.3.68}$$

The above two equations give

$$d\overset{*}{\sigma}_1(t) - d\overset{*}{\sigma}_2(t) = \sum_{\tau=0}^{t-dt} \varphi(t-\tau)\, (d\overset{*}{\sigma}_2(\tau) - d\overset{*}{\sigma}_1(\tau)) = \int_0^{t-dt} \tag{6.3.69}$$

The above incremental expressions together with the individual incremental description of the behaviour of the two fibre bundles are implemented in the overall analysis of the system. The analysis procedure is given in Appendix E.

This procedure was used to analyse the behaviour of such a system under linearly increasing $u_2(t)$ with time or constant values of $u_2(t)$ (at all times $t > t_r$) following a linearly increasing $u_2(t)$ with time (up to t_r).

(d) A system of two fibre bundles in series – Total displacement prescribed up to time t_c

Up to a specified time t_c, the system is loaded under prescribed displacements, $u_2(t)$, so that the analysis procedure follows that described in section (c). For all times $t \geq t_c$, stress is kept at a constant value of $\sigma(t_c)$ which was attained at time t_c.

The instantaneous stress increments $d\overset{*}{\sigma}_1(t)$ and $d\overset{*}{\sigma}_2(t)$, in expressions 6.3.67 and 6.3.68, at time $t \geq t_c$ can be calculated by

$$d\overset{*}{\sigma}_1(t) = \sum_{\tau=0}^{t-\Delta t} \varphi(t-\tau)\, d\overset{*}{\sigma}_1(\tau) + \sigma(t_c) \tag{6.3.70}$$

and

$$d\overset{*}{\sigma}_2(t) = -\sum_{\tau=0}^{t-\Delta t} \varphi(t-\tau)\, d\overset{*}{\sigma}_2(\tau) + \sigma(t_c) \tag{6.3.71}$$

Appendix F gives the procedure followed for the analysis of the behaviour of this system of fibre bundles when stress is held constant across the two bundles at all times $t \geq t_c$.

(e) Some remarks on the present formulation of the fibre bundle model

The continuum formulation of the fibre bundle model, presented in this chapter, does not follow exactly the general continuum description given in chapter V. This is because the parameter T_q, used in chapter V, is not used explicitly in the equation of the fracture surface (6.3.1). The continuum description presented in chapter V suggested the form of the loading function to be

$$F = F(\epsilon_{ij}, h, T) \tag{6.3.72}$$

where damage is described by the parameter h and time dependence is described by the parameter T. In the present model the description of the material behaviour is based on a loading function of the form

$$F = F(\epsilon_{ij}, h) \tag{6.3.73}$$

with

$$h = h(D, T) \tag{6.3.74}$$

This results in the use of

$$\frac{\partial F}{\partial \epsilon_{ij}}\, d\epsilon_{ij} > 0 \tag{6.3.75}$$

to describe progressive fracture (with F=0) rather than

$$\frac{\partial F}{\partial \epsilon_{ij}}\, d\epsilon_{ij} + \frac{\partial F}{\partial T_q}\, dT_q > 0 \tag{6.3.76}$$

adopted in chapter V.

Despite this simplification, the formulation incorporates time effects in two ways:

(i) The energy dissipated at any time is assumed to be a function of the damage parameter h and its time rate.

(ii) The response of the model is assumed to be a result of the relaxation with time of the instantaneous response.

Condition (ii) ensures that the response of the model material is always dependent on the past time history of deformation. The dependence of the instantaneous response on the strain rate and its changes follows from (i). It should be noted that the dependence of the instantaneous response on time follows only during progressive fracture due to (6.3.75). During elastic instantaneous behaviour, the instantaneous response becomes insensitive to changes in strain rate and will only be dependent on the value of the strain rate prior to viscoelastic behaviour. Time effects will still be catered for by the actual response of the material because of the damage evolution law following from (ii) above.

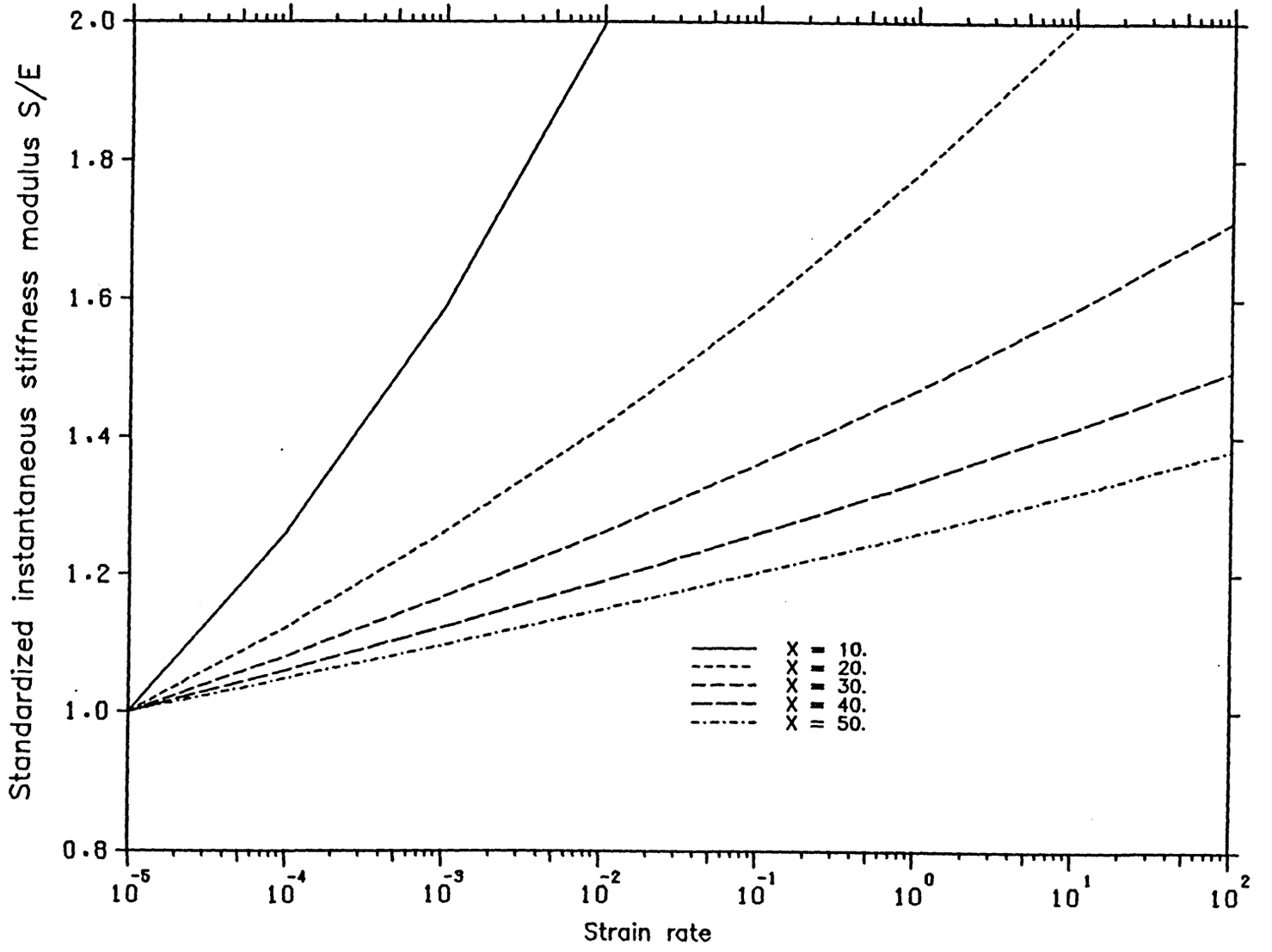

Fig. 6.1 Influence of the strain rate on the instantaneous stiffness modulus (equation 6.2.6).

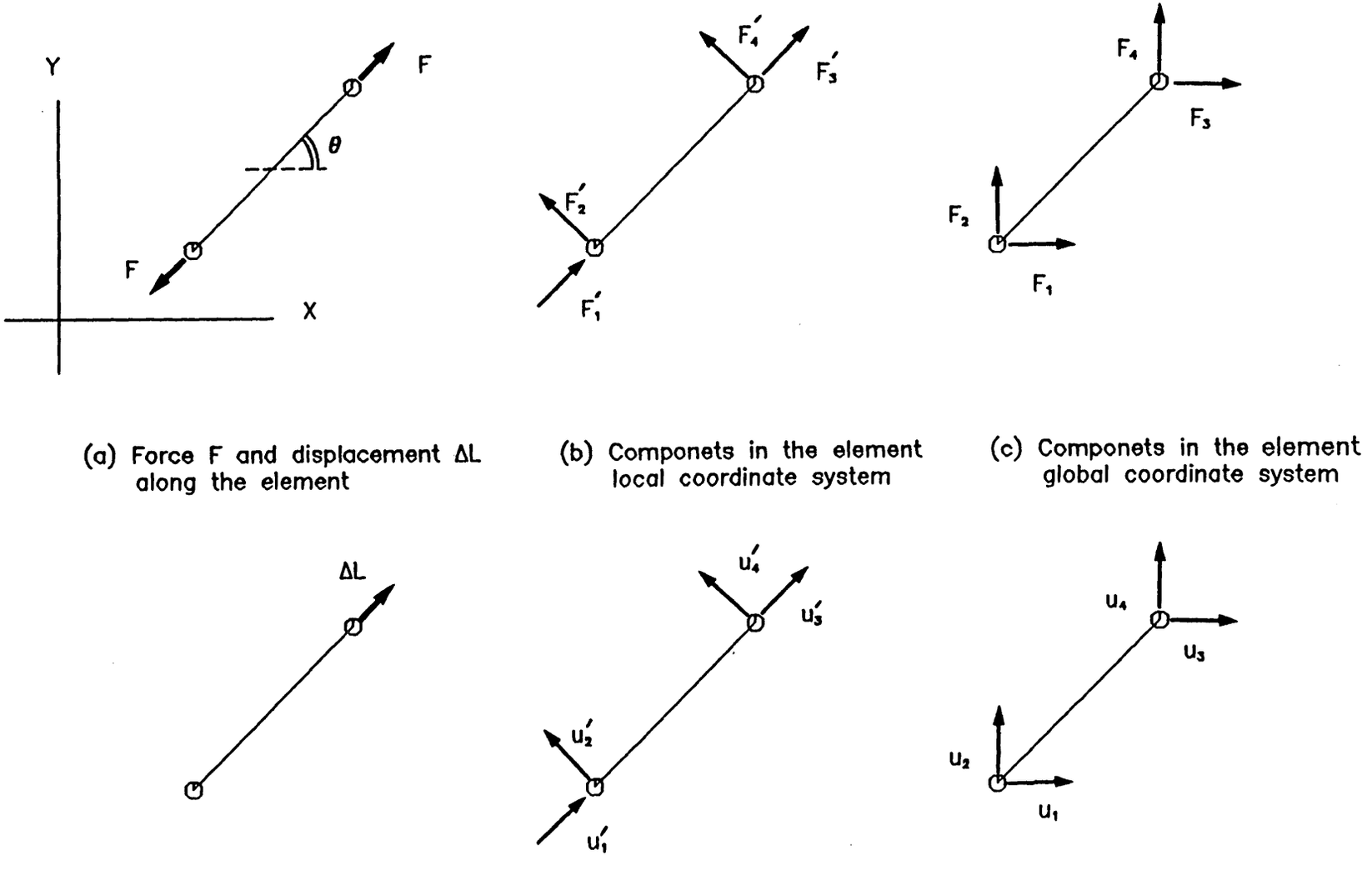

(a) Force F and displacement ΔL along the element

(b) Componets in the element local coordinate system

(c) Componets in the element global coordinate system

Fig. 6.2 Componenets of the force and displacement within a typical bar element in the network model

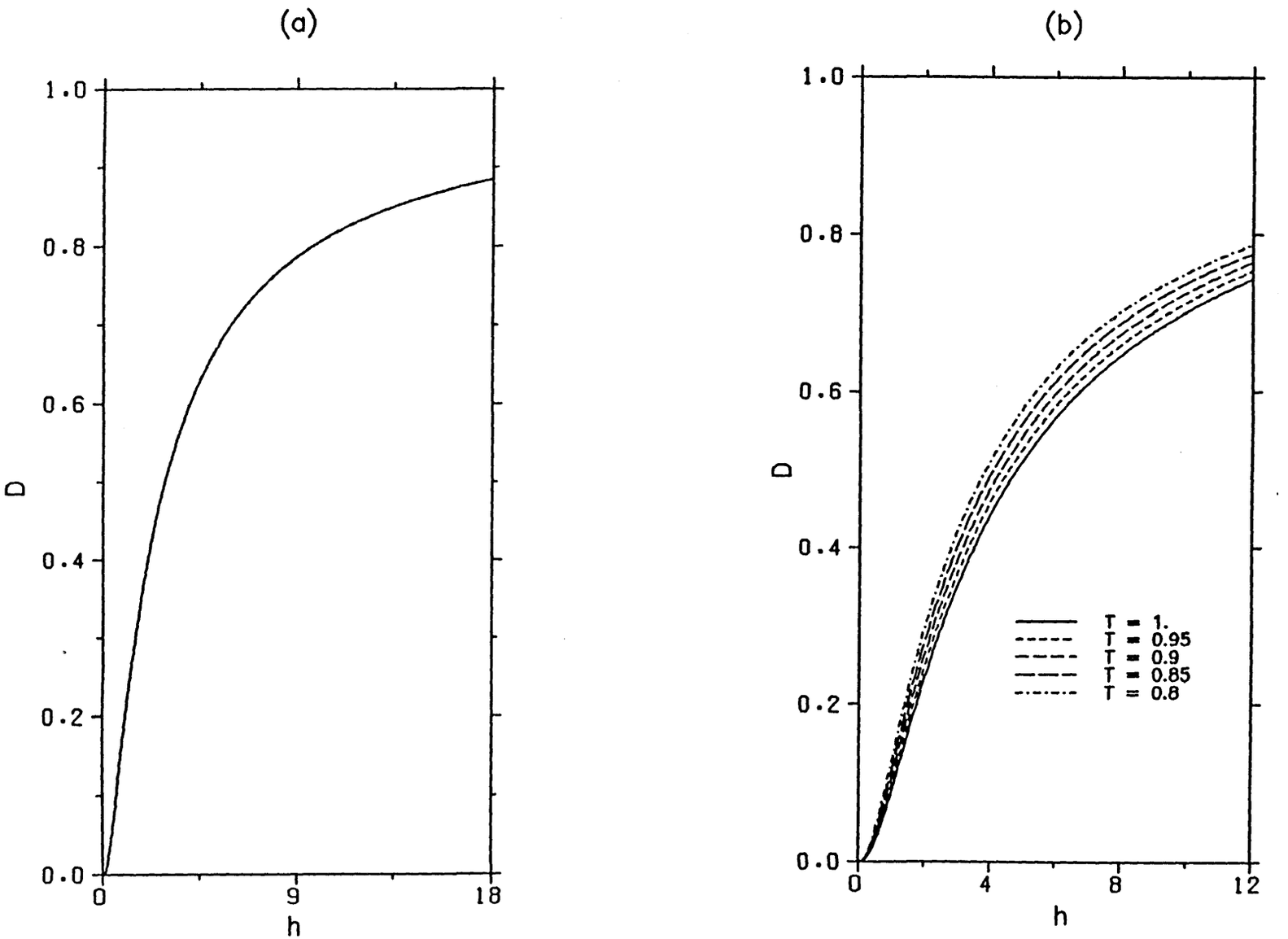

Fig. 6.3 Form of the dissipation function D

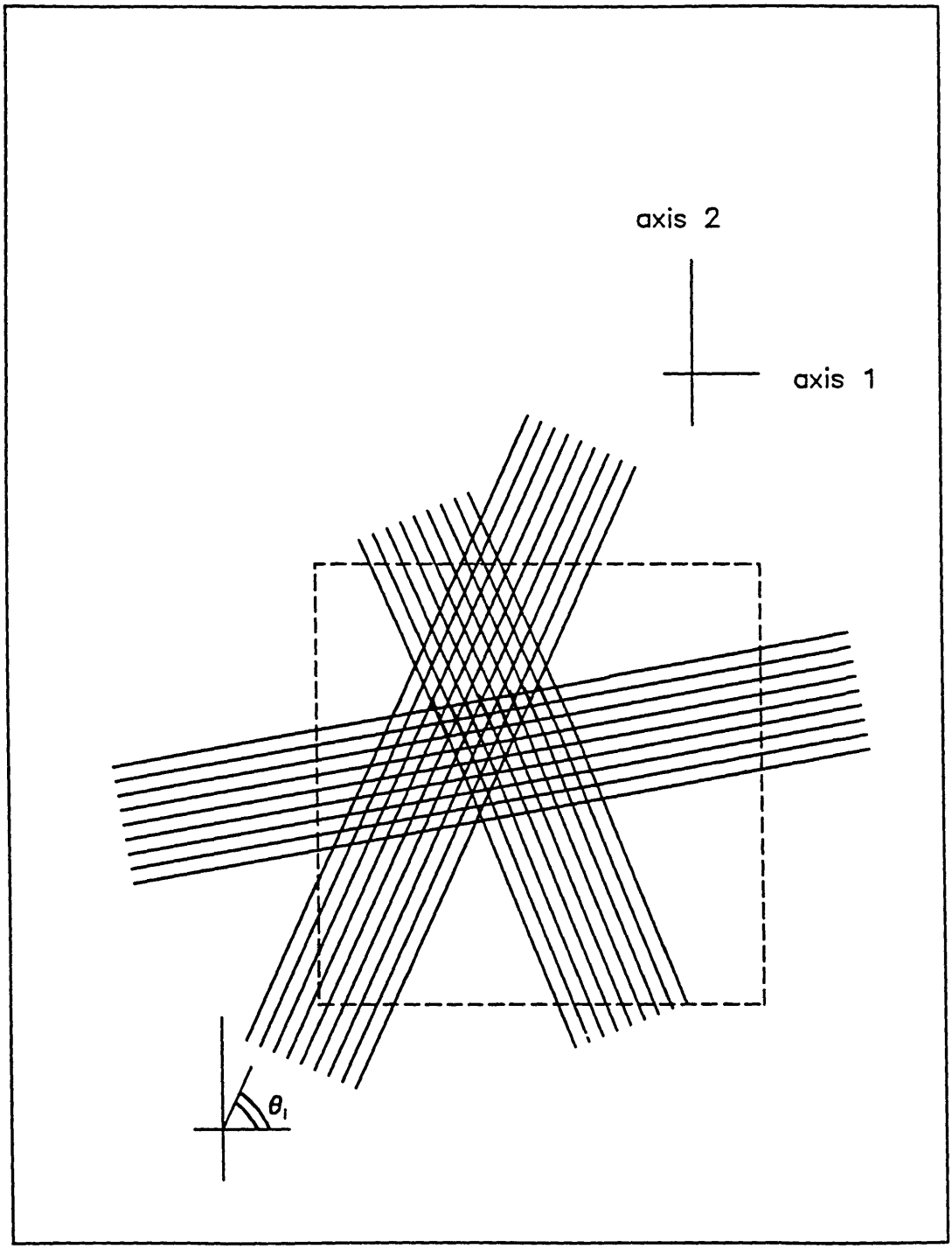

Fig. 6.4 A system of N fibre bundles in a homogeneous strain field (N = 3)

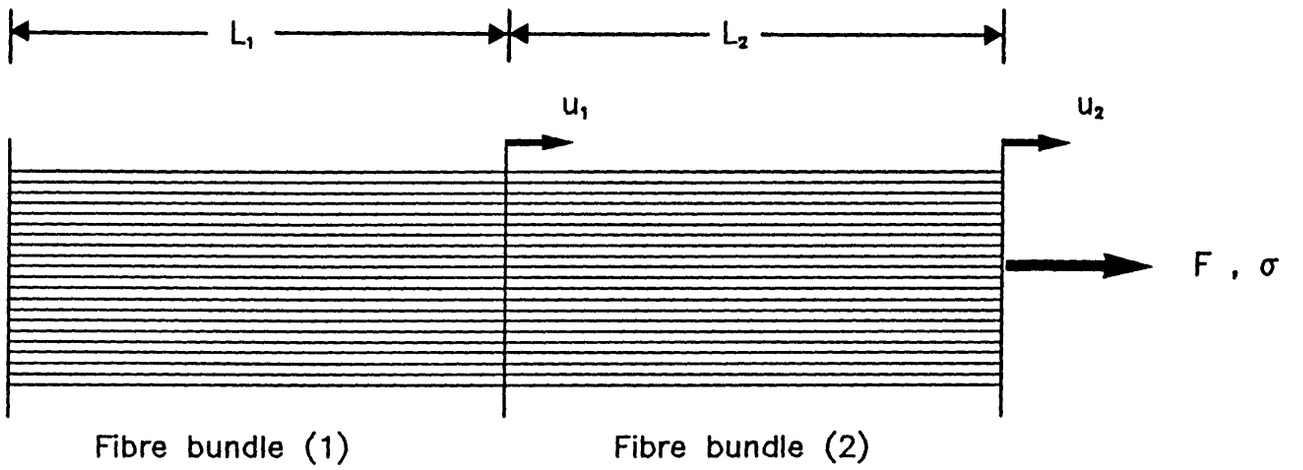

Fig. 6.5 A system of 2 fibre bundles in series

CHAPTER VII

THE RESPONSE OF SOME TIME–DEPENDENT PROGRESSIVELY FRACTURING MODEL MATERIALS

7–1 Introduction

In this chapter results from numerical testing, performed on the "network model" and the "fibre bundle model", are presented.

The network model was tested under conditions of uniaxial tension obtained by applying prescribed end displacements. Conditions simulating creep and relaxation tests, were also performed.

Following this, and as a way of exploring the behaviour of a material whose response is described by several independent linear loading functions, a system of fibre bundles with different orientations, held in a homogeneous strain field, was tested under conditions simulating uniaxial tensile, uniaxial extension, and biaxial extension tests. These tests were performed at different applied strain rates.

It was mentioned earlier that the assumption of a homogeneous strain field and the use of discrete bundles lead to a difficulty in specifying force boundary conditions. The simplification involving the use of a homogeneous strain field is the same as that resulting from layering displacement controlled finite elements where elements are imagined as working in parallel with the same displacement boundary conditions. At the other extreme, elements could be combined in series or overlaid in such a way to experience the same stress. In order to explore the behaviour of such an idealization, two fibre bundles, held in series, were tested under monotonically increasing applied deformations (at different applied strain rates). This system was also tested under conditions simulating creep and relaxation tests. In what follows, the results of these tests are presented.

7–2 Behaviour of the network model

7–2–1 Specifications of the network

The network model (figure 4.1) was tested under applied deformations. At any time t, the displacement v applied to all nodes in zone (2) along the y–direction (figure 4.2) is given by

$$v = \dot{v}\, t \qquad (7.2.1)$$

where $\dot{v}$ is the rate of application of displacements. The rate of the average strain applied to the sample follows from expression 4.1.10

$$\dot{\epsilon}_{yy} = \frac{\dot{v}}{Y^0_2 - Y^0_1} \qquad (7.2.2)$$

where Y^0_1 and Y^0_2 are the initial averages of the ordinates of all nodes in zones (1) and (2) respectively (figure 4.2).

The member properties assigned to the network are given in table 7.1. The network comprised 83 members connecting 16 nodes (figure 4.1(c)). The limitation on the number of nodes was set in order to keep the size of computation within reasonable bounds for the time history analysis. The choice of relatively large values of the standard deviations of the distributions is to ensure heterogeneity in member properties.

Table 7.1–Network model parameters

Statistical variables chosen from normal distributions truncated so that only positive values are assigned.

		Mean	S.D.
A_i	Area	10.0	2.0
E_i	Static stiffness modulus	60.0	12.0
W_{if}	Critical energy limit	83.33E–06	16.67E–06

Compressive to tensile ratio of dissipative energy, β_i,		100.0
Power parameter (ref. equation 6.2.6), x_i,		30.0
Reference static strain rate, $\dot{\epsilon}_{i0}$,		$0.01/L_i$
Relaxation parameters (ref. expression 6.2.17)		
	g_1	0.4
	g_2	0.005
	g_3	0.6

The choice of a reference static strain rate dependent on the length L_i of the individual members is only for computational convenience. Since equilibrium and compatibility conditions are to be invoked using forces and displacements (rather than stresses and strains), it is more convenient to assume a static displacement rate rather than a static strain rate. The static displacement rate was assigned the value 0.01 for all members, and hence the expression $0.01/L_i$ for the member's static strain rate. The dependence of the reference static strain rate on the member length imposes some bias on the network in the sense that, under the same strain rate, long members become stiffer than short ones (all other factors ignored).

Because of the relatively small number of nodes, a significant area of the sample had to be assigned boundary displacements in order to ensure ample connectivity between the core of the sample and the boundary zones. In physical terms, with a rather loose structure, there would be difficulties in testing if not enough connecting points are gripped by the loading system.

For the particular network tested (figure 4.1(c)), the lengths **a** and **b** of the boundary zones (1) and (2) (figure 4.2) were taken as 4.6 and 4.0 respectively. This reduces the length of the sample tested from a theoretical maximum of 42.0 units to a region between grips of 33.4 units long. The boundary zones (4) and (5) are defined only to measure the lateral strain ϵ_{xx}. No displacements are imposed on nodes in these zones and hence their sizes do not reduce the width of the sample. The widths **c** and **d** of these zones were taken as 5.0 and 5.5 respectively.

7–2–2 Deformation controlled tensile tests

(a) Results from tensile testing at different rates of applied deformations

At all strain rates, the response of the network model is characterized by two modes of behaviour. Hardening is observed up to the peak stress after which strain softening occurs (figure 7.1). It is noted that the peak stress increases with strain rate and that the strain corresponding to the peak stress is reduced. Corresponding to these changes is a reduction in the material stiffness from fast to slow rates of loading.

Figure 7.2 shows in detail the peak stress corresponding to different

loading rates. Above a strain rate of around 10^{-03}, the material can be considered to be rate dependent and unaffected by the choice of $\dot{\epsilon}_{i0}$. Below this value, rate effects are not so apparent and the time dependence arises mainly from the choice of the relaxation function.

Below a certain value of the applied strain rate (10^{-06} in these tests), no changes in the response of the network model were detected. This is expected because of the forms of the instantaneous stress strain law (6.2.5 and 6.2.6) and the damage evolution law (6.2.7 and 6.2.17) adopted. At a very slow rate, the instantaneous stiffness modulus within each member becomes equal to its reference static value and the form of $\varphi(t)$ (expression 6.2.17) suggests that at a very slow rate $\varphi(t)$ will assume a constant value of g_3 (0.6 in this case). Hence, below a certain value of the applied strain rate the behaviour of the network model becomes time and rate independent.

The time–dependence of the response of the network model is a result of an interaction between the rate sensitive instantaneous constitutive law and the time delayed damage which is catered for by the damage evolution law. The contribution of each of these factors to the model's response is dependent on the rate of applied deformations.

At high levels of strain rate, the rate sensitivity of the instantaneous response outweighs the delayed damage effects. Strain is applied in such a small interval of time so that $\varphi(t)$ is approximately 1.0 for all times up to complete failure.

At low values of the applied deformation rate, the contribution of the delayed damage outweighs that due to instantaneous strain rate sensitivity. At such rates, the strain rate within individual members becomes close to the static strain rate $\dot{\epsilon}_{io}$ and hence the instantaneous stiffness modulus S_i becomes close to to the reference static value E_i (expression 6.2.6).

This change in the mode of behaviour from one range of applied average strain rate to another is also apparent in the results for the network stiffness given in figure 7.3.

There is no unique definition for the stiffness of the network. The stiffness of a sample of real materials is usually defined as the initial tangent

modulus or the secant (or tangent) modulus at some predefined strain level. Figure 7.3 shows the variation of the initial tangent stiffness and other stiffness moduli, at preset strain levels, with applied strain rate. All moduli are observed to be higher for higher values of strain rate. The variations of the stiffness moduli conform with the suggestion that above a certain strain rate (10^{-3} in here) response in mainly controlled by the instantaneous strain rate sensitivity and that below another value of strain rate (10^{-6}) it is controlled by a time delayed damage. Between these two limits the response is a transition between the two modes detected at high and low rates respectively.

The reduction of the values of the strain at peak stress with increasing applied strain rate (figure 7.4) is a result of the assumption that the total energy released when a member breaks is constant and rate independent. A member will break at a smaller value of strain if the strain rate is increased. This simplification does not necessarily result in the overall energy dissipated by the network up to peak stress, or to complete failure, being the same for all strain rates. In fact, figure 7.1 suggests that the energy dissipated by the network model up to peak stress is greater for higher strain rates. For the energy dissipated up to complete failure the same conclusion is, in most cases, true.

This is so because the mode of failure of the network is more localized at high strain rates as will be seen in the next section when the distribution of broken members at different strain rates is looked upon. More energy is needed to break the network at high strain rates than at low ones eventhough the individual members dissipate the same energy at all applied strain rates.

Because of the inconsistency in published results regarding the variation of strain at peak stress with applied strain rates, for real physical materials (section 3–2), no attempt was made to refine the assumption that the total dissipative energy within each member is rate and time insensitive.

The results obtained by testing the network model are by no means a quantitative simulation of real material behaviour. The range of strain rates used and the forms of the variation of the network's response with applied strain rates are a direct result of the numerical values allocated to the network parameters and the forms of the instantaneous stress strain law and the damage evolution law. Still, many aspects of the model's response are comparable qualitatively to physical materials. Tests on concrete show that the strength, as measured by the peak stress, increases with an increase in applied strain rate in tension and compression and so does the stiffness (to a lesser extent). The change of the peak

stress of concrete with applied strain rate (sections 3–2), shows that the variation is dependent on the value of the strain rate. In other words, at high levels of strain rate the form of the peak stress–strain rate curve is different from that obtained at low strain rate levels.

In summary, the nonlinearity observed in the response of the network model is a result of two factors:

(i) strain rate sensitivity and time delayed damage within individual members, and

(ii) breakage of members.

The second factor was the sole cause of nonlinearity in the response of the time independent network model (chapter IV).

It should be noted that the above two factors are interrelated. Equilibrium of actual, rather than the instantaneous, forces at each node results in members breakage being time dependent.

(b) Tensile tests – Modes of failure

The network is considered to have failed completely if it has reached a state where an addition of a small increment of strain would result in the separation of the network into two or more parts.

Before the peak stress is attained, the distribution of failed members was more or less uniform (or random) through the network. Near and after the peak stress, failed members tend to cluster in localized zones. This localization was observed at all strain rates as shown by the distribution of the centroids of failed members (figure 7.5). The distribution of failed elements is not the same for all strain rates and although is always localized at failure, the failure of the network tends to be more localized at higher strain rates. The increase in the brittleness of the response at higher strain rates, as seen by the slopes of the stress strain curves in the post peak response in figure 7.1, is supported by this increase in the intensity of localized failure.

Zeilinski [109] observed this increase in localization of cracks in concrete under impact loading and based his semi–empirical formulation on these observations.

It was noted earlier that although the energy dissipated upon the

failure of an individual bar element is taken as a constant, the total energy dissipated by the network as a whole increases with increasing strain rate. This is a consequence of increased localized failure at high strain rates.

At low strain rates, ample time exists for "weak" elements to fail across the network until a tear forms forcing all deformations to occur across it. At high strain rates, deformation occurs in such a short time that fracture is forced to propagate across a tear at early stages of loading and hence passes through "strong" and "weak" elements. Hence, the contribution of failed elements to the total energy dissipated is higher for higher applied strain rates.

Failure of the network model at all strain rates is localized in the sense that at failure, a "tear" of broken members forms across the network. The direction of this tear is normal to the direction of applied deformations and its size is controlled by members dimensions. The rest of the network is fairly intact even at failure. These suggestions are confirmed in figure 7.6 which shows the configuration of the network (figure 4.1(c)) before and after straining at a strain rate of 1.65E+00.

7–2–3 Relaxation tests

Relaxation tests were undertaken in order to determine the response of the network model under conditions of sustained overall strain in the y–direction (figure 4.2). Prior to holding the boundary displacements at constant values, the network is loaded by applying boundary displacements at a specified rate until a preset value of the average strain, ϵ_{yy}, is attained.

A stress relaxation curve for a typical network (4.1(c)), strained up to a value of 0.001 units of strain, ϵ_{yy}, at an average strain rate of (1.65E–03) is shown in figure 7.7. Provided the network did not fail completely prior to the relaxation phase, the residual stress attained exists, is definite, and is different from zero. Figure 7.7 is hence typical for all networks that survive the short term loading. At any level of strain, relaxation tests were stable in the sense that the network's overall stress will decrease at a decreasing rate with time towards a residual value.

At all levels of strains following any value of strain rate, stress relaxation was found to be dependent only on the "time delayed damage". No member breakage was recorded in any computer run during the relaxation

phases.

Figure 7.8 shows the stress strain curves obtained while loading at two values of the average strain rate and the corresponding relaxation loci. The relaxation locus corresponding to a stress strain curve is the set of residual equilibrium stress points obtained after complete relaxation of stress starting from all stress points on that stress strain curve. Relaxation loci are complete in the sense that they are obtainable for all levels of strains (including those in the post peak phase of behaviour).

Figure 7.9 compares relaxation loci corresponding to two different strain rates applied prior to the relaxation phase. As seen from the figure, the final state of stress is a function of strain level, strain rate prior to relaxation, and consequently the degree of damage as determined by the intensity and distribution of broken members. The value of the equilibrium state of stress is also dependent on the form of the relaxation function $\varphi(t)$ and the values assigned to its parameters g_1, g_2, and g_3.

Relaxation tests are difficult to perform on real materials especially those starting from a post peak state of stress. The network model provides a qualitative description of the response of a progressively fracturing material under such tests. It is thus feasible to expect that physical materials, whose response to loading is accompanied by progressive fracture, would response to relaxation conditions in a manner similar to that of the network model.

7–2–4 Creep tests – Modes of behaviour

The behaviour of the network model under conditions simulating creep tests, shows resemblance to the behaviour obtained in concrete and concrete like materials. After loading the network, by applying boundary displacements at a specified average strain rate, the stress is kept constant at a specified value.

As would be expected, creep was observed to be dependent on the level of stress applied. At low levels of sustained stress, strain increases at a decreasing rate. Strain approaches asymptotically a value termed the "creep strain".

At high levels of stress, creep seems to be initially similar to that obtained at low levels of stress but strain then increases rapidly with time until complete failure of the network. For the creep tests undertaken, at or near the

peak stress, creep failure occurs in a very short interval of time and at some instances is instantaneous.

If stress is kept constant, at any point in the post peak portion of the stress strain curve, then the network will fail in a very short interval of time and is almost instantaneous. For some of the creep tests performed, near the peak stress and at post peak stress states, a short range unstable behaviour under constant stress conditions was observed. This behaviour is due to the discrete nature of the network model and is illustrated in figure 7.10.

Figure 7.11 shows the different modes of creep behaviour in the context of the corresponding short term stress strain curve and its relaxation locus. It is noted that the relaxation locus corresponding to a specified strain rate serves as a datum for distinguishing these different modes of creep behaviour. The peak stress of the relaxation locus serves as an approximate upper limit for stable creep, that that will not end in complete failure. The set of equilibrium creep strains is almost identical to that portion of the relaxation locus prior to the peak residual stress.

The behaviour of the network under creep conditions as shown in figure 7.11 is qualitatively similar to that obtained for concrete (up to peak stress) in tension and compression (figures 3.18, 3.19, and 3.20(b)).

It was noted earlier that the jumps observed in the response of the network model are due to its discrete nature. Figure 7.12 depicts the expected behaviour of a smoothed network, that that contains a large number of members in a small volume. Such a network can be idealized as a continuum. This smoothed behaviour is very similar to that observed in real materials (figures 3.18, 3.19, and 3.20(b)) up to the peak stress. It would also compare well to the expected behaviour of an ideal time–dependent progressively fracturing solid.

The creep behaviour of the network model and that of the smoothed network model compare qualitatively well with that of physical materials up to peak stress. No creep tests were performed on real physical materials in the post peak portion of the behaviour. The response of the network model to conditions of constant stress in the post peak portion of the stress–strain curve gives an insight on the behaviour expected from real materials whose response to loading exhibits progressive fracture.

Figures 7.13 shows the variation of strain with time at various levels of

stress. The creep curves compare qualitatively well with those obtained for real physical materials (figures 3.21, 3.22, and 3.25). At low levels of stress, strain increases at a decreasing rate up to a limiting level. As has been mentioned earlier, the coarse structure of the model introduces discontinuities due to individual member breakage so that occasional, sharp vertical jumps are observed in the creep curves. At low stress levels, the sample remains stable even with the occurrence of some member failure. This is because the extent of breakdown is not sufficient for the consequential redistribution of member forces to cause further progressive unstable breakdown in the sample.

At high levels of stress, creep will start in a fashion similar to that at low stress levels. This mode of behaviour will be followed by member breakage accompanied by vertical jumps in the creep curve. Eventually, complete failure occurs when a "tear" of broken members forms rapidly across the network.

Figure 7.14 shows a typical creep curve of the network model at 0.7 of the peak stress (following a strain rate of 1.65E+00). The distribution of the broken members before and after the creep phase is also shown in figure 7.14 and the configuration of the network before and after the test is shown in figure 7.15.

It should be noted that although creep is accompanied by progressive failure, complete failure of the network occurs in a relatively short interval of time and is unstable. Hence, for high levels of stress, creep results in failure and is characterized by by two phases:

(i) an initially gradual increase in strain (at a decreasing rate) accompanied by progressive fracture resulting from breakage of members. This is manifested by vertical jumps in the creep curve corresponding to breakdown of individual members. Subsequent to this

(ii) a rapid increase in strain occurs in a very short interval of time leading to complete failure. This failure is progressive but cannot be contained and so builds up rapidly into failure of the overall network. These two modes of behaviour are illustrated in figure 7.14.

The time to complete failure is essentially determined by the duration of the first phase , since the second phase occurs instantaneously. This time was found to be shorter for higher levels of applied stress. Figure 7.16 shows the increase of the time to failure with decreasing applied stress in creep tests. It is shown that this time increases indefinitely when the stress is decreased asymptotically to the limiting value below which the network will creep in a stable fashion without complete failure. Similar results were obtained for concrete

(figure 3.20(a)).

7–2–5 Remarks on the stability of the network model

The behaviour of the network model under conditions simulating uniaxial tensile, creep and relaxation tests gives an insight on the stability of the network model in the post peak portion of the stress strain curve.

The post peak behaviour is stable in strain space in the sense that starting from an equilibrium point on the stress strain curve, the response is always in equilibrium if strain is controlled (either kept constant or increased). On the other hand, it is unstable in stress space because any increase in stress (starting from an equilibrium point in the softening region) will cause complete instantaneous failure. Moreover, if stress is kept constant, complete failure will occur instantaneously. This reflects the difficulties faced in real material testing involving strain softening. If the behaviour of the network model is to explain the instability observed in some physical testing, then one should assume that unless testing conditions are perfectly strain controlled, brittle failure might result as a consequence of instability in stress space.

7–2–6 Role of the relaxation function $\varphi(t)$

It was noted earlier in this section that the sensitivity of the response of the network model to the rate of application of imposed deformations is not solely a result of the strain rate sensitivity of the instantaneous response of the individual bar elements. The delayed damage effects, manifested by the damage evolution law (expression 6.2.7), do result in strain rate sensitivity of the overall response especially at low levels of applied strain rates.

This can be manifested by testing the network model with individual elements being strain rate insensitive in their instantaneous response. Tests on this "revised network model" not only illustrate the role of the relaxation function $\varphi(t)$ but also present an alternative simpler model that could be deployed if time effects are to be studied independently of rate effects. This can be achieved by modifying the computer program used so that the instantaneous stiffness modulus S_i is always equal to the reference static value E_i (expression 6.2.6).

The network tested is identical to that used in the previous tests except

for the ignoring of strain rate sensitivity of the instantaneous response. At any level of loading, the instantaneous response of the network is solely determined by the distribution of broken members.

Figure 7.17 shows the response of the network model at different applied strain rates. The response at all strain rates above a certain limit (1.65E–04) and below another limit (1.65E–07) becomes strain rate insensitive and identical to the response at these upper or lower limits respectively.

The presence of the damage evolution law will result in an overall rate sensitive response (figure 7.17) similar to that observed when the instantaneous response of individual members was taken to be rate sensitive. In contrast to the results presented in section 7–2–2, strain rate sensitivity is only observed along a limited range of strain rates.

Breakage of members is still rate sensitive as seen in the distribution of the centroids of broken members (figure 7.18).

The behaviour of the "revised" model is thus similar to that observed in the general case (section 7–2–1 to 7–2–5) except that strain rate sensitivity is only observed within a range of rates of applied deformations. Outside this range, the behaviour of the network becomes strain rate insensitive.

It might be more realistic to assume that the final equilibrium states of stress after relaxation tests are only dependent on the damage inflicted on the network prior to relaxation phase, and hence independent on the strain rate followed prior to relaxation (except in how this strain rate actually influences member breakage prior to relaxation phase). In other words, the relaxation locus is to be dependent only on the intensity of broken members and their distribution along the network.

In real material's testing, strain is normally applied "instantaneously" up to a certain value and kept constant thereafter. This instantaneous strain rate is usually taken to be the nominal "static" strain rate. It is thus justified to test the network model under conditions of rate independent instantaneous response.

Figure 7.19 shows the relaxation loci of a typical network model (4.1(c)) corresponding to two different strain rates (1.65E –04 and 1.65E–05). The two loci are almost identical except near failure. This confirms that the equilibrium stress state is only dependent on the form of $\varphi(\tau)$ and the state of the

network (in terms of broken members prior to relaxation tests). The state of the network, as measured by the intensity and distribution of broken members, is in turn a function of the strain applied prior to relaxation phase, and the time history of strain (the strain rate in this case). It should be noted that at any strain rate above 10^{-5}, both the stress strain curve and the relaxation locus corresponding to it become insensitive to strain rate. Thus the instantaneous or static strain rate can be assigned any value above 10^{-5} without altering the resulting relaxation locus. Figure 7.20 shows the stress strain curve at a strain rate of 1.65E–04 and its corresponding relaxation locus. The behaviour is similar to that obtained when the strain rate was not ignored in the instantaneous response of the individual members (figure 7.8).

Again, it is interesting to note that creep behaviour obtained in these tests (figures 7.21–7.24) is qualitatively similar to that observed if the instantaneous response of the individual elements was assumed to be rate sensitive. If time delayed damage, as defined by the damage evolution law, is taken as the only source of time dependence, then an "instantaneous" strain rate can be defined (1.0E–05) and hence can be used as a reference "static" strain rate suitable for creep analysis.

The different modes of creep behaviour shown in figure 7.21 are similar to those in figure 7.11. The forms of the creep curves at different stress levels (figure 7.22) are similar to those obtained in figure 7.13. The network model failed in a manner similar to that when strain rate sensitivity was not ignored in the instantaneous response, (figures 7.23 and 7.24 compared to 7.14 and 7.15).

These observations justify the use of a simplified analysis when creep is investigated. The same was found true in relaxation tests. Unless the effects of the strain rate, applied prior to creep and relaxation tests, are to be investigated, the behaviour of the network model under conditions of constant strain or stress can be fully understood by performing these tests with strain rate sensitivity of the instantaneous response completely ignored.

7–3 Behaviour of a system of fibre bundles held in a homogeneous strain field under conditions simulating strain controlled testing

In this section a system of fibre bundles, assembled in a homogeneous strain field, is studied, under conditions of applied strains at different rates. The theoretical formulation was derived in sections 6–3.

As has been noted in chapter VI, the use of fibre bundles, with a continuous distribution of properties within each bundle, should produce the same results as would be attained using several independent linear loading functions for the continuum theory of chapter V. More practically relevant to the type of computer experiments being undertaken, it can be expected that the adoption of this continuum description will eliminate the jumps in the material response observed with the network model and associated with induced member breakage.

A mesh of 16 fibre bundles having the same parametric properties, but each oriented at a certain angle θ_i, was tested. For each fibre bundle, the instantaneous dissipated energy is expressed by 6.3.21 with β_f and D_{max} assigned the values 0.001 and 0.75 respectively. The strain rate parameter T is of the form 6.3.18 with x and $\dot{\epsilon}_0$ assigned the values of 10.0 and 10^{-05} respectively. The orientations of the bundles were chosen from a set of random numbers between zero and π. Table 7.2 gives the values of the angles θ_i assigned for the 16 bundles.

Table 7.2–Orientation of the various bundles

Bundle	Angle with axis "1" θ_i
1	0.1608015920 π
2	0.0243762666 π
3	0.2335974714 π
4	0.1692959141 π
5	0.0202885629 π
6	0.3628989579 π
7	0.8194429017 π
8	0.2558658581 π
9	0.7680836334 π
10	0.9843878061 π
11	0.9579935822 π
12	0.8030606378 π
13	0.9908664627 π
14	0.0912841771 π
15	0.2906100824 π
16	0.1704511243 π

Thus in this model, heterogeneity is not introduced but there is a departure from isotropy due to the nonuniformity of the orientations of the fibre bundles which affects the directional properties. Figure 7.25 shows the orientation of the fibre bundles used in the following tests.

The damage evolution law was taken to be of the form 6.3.55 and 6.3.57 with g_1, g_2, g_3 taken as 0.4, 0.005, and 0.6 respectively.

The response of the model to conditions simulating uniaxial extension tests (ϵ_{11} prescribed and $\epsilon_{22}=0$), uniaxial tension tests ($\sigma_{22}=0$, ϵ_{11} prescribed), and biaxial extension tests ($\epsilon_{11} = \epsilon_{22}$ prescribed), is explored. In all tests shear deformation is suppressed ($\epsilon_{12} = \epsilon_{21} = 0$).

7–3–1 Uniaxial extension tests

Figure 7.26 shows the stress strain curves for the system at different applied strain rates for conditions simulating uniaxial extension tests. Rida [51] adopted a fibre bundle system where the different bundles are uniformly oriented between 0 and π. For such a system an initially isotropic behaviour was observed provided that an ample number of bundles was used. The random orientation of the bundles in the present tests results in lack of symmetry or anisotropy. This has resulted in the presence of shear stress, σ_{12}, under conditions of uniaxial extension tests (figure 7.26(c)). The magnitude of the different components of the stress σ_{22}, σ_{11}, and σ_{12} is influenced by the orientation of the bundles and if the response is to simulate an idealized behaviour (such as that under isotropic plane strain conditions) the bundles should be oriented in such a way to result in that behaviour. The solid lines in figure 7.26 (as well as those in figures 7.27–7.30) represent the response of the bundle assembly if time and rate sensitivity are ignored, all other parameters kept the same. This response has no significance in the present discussion and is merely depicted as a reference test.

It is important to keep in mind that isotropy is not only affected by the orientation of the bundles but is also dependent on strain rate sensitivity in the sense that the components of the stiffness of the individual bundles are different for different values of strain rate.

The stress strain curves in figure 7.26 for the model material show that:
(i) an increase in the applied strain rate results in an increase in the

peak stress experienced by the material,

(ii) the initial tangent moduli increase with increasing applied strain rates,

(iii) the secant moduli, measured at the strain corresponding to peak stress, increase with increasing strain rates,

(iv) an increase in the applied strain rate results in a decrease in the strain at peak stress,

(v) and an increase in the slope of the post peak stress strain curve, indicating a more brittle response, results from increasing the applied strain rate.

7–3–2 Uniaxial tensile and biaxial extension tests

The response of the model under uniaxial tensile tests (figure 7.27) shows similar strain rate sensitivity to that obtained under the uniaxial extension tests. A reduction in the strength of the model material, as a result of the removal of the lateral constraint and the resistance associated with it, is noted.

These tests show some aspects of real materials behaviour other than strain rate sensitivity. At any strain rate, the material model exhibits a higher initial value of the tangent modulus, a higher secant modulus (at peak stress), a higher peak stress value, and a lower strain at peak stress when tested under equibiaxial extension conditions (figure 7.28(a)) than under uniaxial extension conditions (figure 7.26(a)). The behaviour is also more brittle.

This enhancement in the response, as a result of the increase in the lateral confinement, is more apparent if the stress strain curves of the uniaxial extension tests (figure 7.26(a)) and the equibiaxial tests (figure 7.28(a)) are compared to those obtained in the uniaxial tensile tests (figure 7.27). Conditions of uniaxial extension tests, and more adversely those of biaxial extension tests, serve as confinements (tensile) to the model material sample and hence the enhancement in the strength and stiffness.

7–3–3 Remarks on the model's strain rate sensitivity

The response of the material model to different applied strain rates suggests that the behaviour is influenced by different factors depending on the value of the applied strain rate.

At "high" strain rates, the response is mainly influenced by the rate sensitivity of the instantaneous response with little effects from the time delayed

damage manifested by the damage evolution law and the relaxation function $\varphi(t)$ (expressions 6.3.55 and 6.3.57). This can be confirmed by comparing the actual response of the model material in figures 7.26, 7.27, and 7.28 to the instantaneous response (figures 7.29–7.31). The instantaneous response results by ignoring the relaxation of stress or the time delayed damage and can be obtained by running the tests on the model material with the function $\varphi(t)$ allocated the value of unity at all times. Comparison of the actual response of the model material with the instantaneous response (figures 7.26–7.28 and 7.29–7.31) shows that at high levels of strain rates little, if any, differences between the actual and the instantaneous responses can be detected. This confirms that, at high strain rate levels, the contribution of the instantaneous strain rate sensitivity to the actual response overweighs the contribution of the time delayed damage.

On the other hand, at low strain rates, the actual response of the model material becomes less affected by the instantaneous strain rate sensitivity and more influenced by the damage evolution law that reflects a time delayed damage. The difference between the actual response (figures 7.26–7.28) and the instantaneous response (figures 7.29–7.31)becomes significant at low strain rates. In this case, the only time dependence in the response of the model material is that due to the time delayed damage expressed as a damage evolution law.

It can hence be concluded that the rate dependent response of this model material is a result of two factors. The contribution of each of these two factors is dependent of the value of the strain rate. At high strain rates, the actual response does not differ much from the instantaneous response and hence any dependence on strain rate can be fully described by the instantaneous stress strain relationship. At low strain rates, strain rate dependence in the actual response of the model material is a result of the damage evolution law describing time delayed damage. At intermediate strain rates, the response is an interaction between these two factors.

The numerical values of strain rates, that determine the ranges within which strain rate is considered as "low", "intermediate", or "high", are dependent on:

(i) the form of the instantaneous stress strain law and the value allocated for the assumed reference strain rate below which the instantaneous response is taken as rate insensitive, and

(ii) the form of the relaxation function $\varphi(t)$ and the values allocated to the parameters defining it.

The results obtained in these tests illustrate the concepts of the "instantaneous fracture surface" and the "instantaneous response". At very high strain rates, strains are applied in a very short time so that

$$\varphi(t) = \varphi(0) = 1.0 \qquad (7.3.1)$$

for all the duration of the test. Hence, the actual response and the instantaneous response become identical. The changes in the response of the model material with increasing applied strain rate become solely due to changes in the "instantaneous response" or, in other words, changes in the "instantaneous fracture surface" in strain space.

At low strain rates, the value of which are less than the reference static strain rate, the instantaneous response becomes strain rate insensitive and hence the instantaneous fracture surface becomes fixed in strain space. The actual response becomes dependent on the applied strain rate as a result of the function $\varphi(t)$. In the limiting case when the strain rate is very low, the function $\varphi(t)$ assumes the value

$$\varphi(t) = \varphi(\infty) = g_3 \qquad (7.3.2)$$

for all times. The response corresponding to such case is termed the "infinitely slow response".

All the tests undertaken are intended to study the time–dependent behaviour of ideally progressively fracturing solids with no intention to study the complex interaction between progressive fracture and the model's isotropy, symmetry, or state of stress (uniaxial or multiaxial). It was observed that under uniaxial tensile conditions, when the transverse stress is held zero, computer runs required many iterations before convergence was attained. As mentioned in chapter VI, if the stress components were to be held constant at values other that zero, to simulate creep tests, an iterative technique should also be adopted. Since creep and relaxation tests on real materials are normally intended to study the effects of time history of load in the simplest form possible, it is justified to test these conditions on a one dimensional model comprising two fibre bundles in series. Results of these tests are given in the next section. If the effects of the load time history are to be studied in conjunction with those due to material isotropy and stress state, then the present model of fibre bundles in a homogeneous strain field would be more appropriate.

The results of the strain controlled tests performed on this model material are in good qualitative agreement with those performed on the network model (section 7–2) under varying applied rates of deformation. The present

model, being a particular case of the continuum formulation of chapter V, has a smooth response with no jumps in its stress strain curves. Its behaviour illustrates the capability of the general continuum theory to describe some modes of behaviour noted in real physical testing regarding sensitivity to applied strain rates.

7–4 The response of a system of two fibre bundles held in series

The assembly of two fibre bundles held in series is shown in figure 6.5. The behaviour of the assembly is studied under monotonically increasing total displacement (u_2 in figure 6.5) at different rates. Tests, thus, simulate displacement controlled uniaxial extension conditions and are one dimensional. Table 7.3 gives the values of the parameters allocated for the two fibre bundles.

Table 7.3–Parameters allocated to the bundles

Fibre bundle	D_{max}	β_f	L	$\dot{\epsilon}_0$	x
1	2.5	0.001	10.	1.0E–05	30.
2	3.0	0.003	15.	1.0E–05	30.

where D_{max}, β_f, $\dot{\epsilon}_0$, and x are the parameters in equations 6.3.21 and 6.3.18 and L is the length of the bundle.

In all tests the damage evolution law is of the form 6.3.55 with $\varphi(t)$ given by 6.3.57. The parameters g_1, g_2, and g_3 in 6.3.57 are allocated the values 0.4, 0.005, and 0.6 respectively.

7–4–1 Extension tests

The response of the model material to strain controlled testing is shown in figure 7.32. The strain rate for each test is calculated by dividing the rate of applied deformations by the overall length of the assembly.

The results show similar strain rate sensitivity to that observed for the network model and for the fibre bundle model of section 7–3. An increase in the applied strain rate will result in an increase in the peak stress (figure 7.33), an increase in the initial tangent stiffness (figure 7.34), an increase in the strain softening slope indicating a more brittle behaviour, and an increase or decrease in the strain at peak stress (figure 7.35) depending on the value of the strain rate. A displacement controlled test was performed on the model material with the parameter x (equation 6.3.18) taken as 10,000.0 and $\varphi(t)$ as 1.0 at all times. Values of the stiffness, peak stress, and strain at peak stress of this test were used to normalize figures 7.33–7.35. The response under this test is insignificant in the present context. It resembles the behaviour of the model material if all time and rate dependent effects were ignored, all other parameters being the same. Another test, with the parameter x taken as 10,000.0 and $\varphi(t)$ as g_3 (0.6 in here),

was also performed. The results of these two tests are plotted in figure 7.32 (the solid lines) and are merely shown for comparison with the rate–dependent results.

As in the cases of the network model and the system of fibre bundles in a homogeneous strain field, the dependence of the response on strain rate is due to:

(i) the strain rate dependence of the instantaneous response. This comes into effect at all strain rates greater than the assumed reference strain rate ($\dot{\varepsilon}_0$ in 6.3.18). It is thus justified to expect that the contribution of this factor to the actual response of the material model becomes more dominant at high levels of strain rate.

(ii) the time delayed damage manifested by the damage evolution law. The forms of the damage evolution law and the relaxation function $\varphi(t)$ (6.3.57) suggest that, at high strain rates, deformation occurs so quickly that $\varphi(t)$ assumes the value of 1.0 at all times. Hence the contribution of this delayed damage to rate sensitivity is limited to a range of low strain rate levels in which $\varphi(t)$ varies with time.

In summary, the model material exhibits time and rate sensitivity as a result of an instantaneous strain rate dependence and a delayed damage action. While the two mechanisms are theoretically effective at all strain rates, the effects of delayed damage will diminish at high strain rates and those due to instantaneous strain rate sensitivity will vanish at low strain rates. The ranges of strain rates within which these factors become effective are a function of the values allocated to the parameters defining the damage evolution law and the instantaneous stress strain law.

It is interesting to note the time histories of strain of the individual fibre bundles (figure 7.36). While one of the fibre bundles is strained monotonically at a constant strain rate (fibre bundle (2) in this case), the other bundle unloads at a decreasing strain rate when a certain strain is attained. This strain corresponds to the peak stress within the other fibre bundle as seen in figure 7.37 that depicts the stress strain behaviour of the individual bundles. It should be mentioned that this localized behaviour (in the sense that only one of the two bundles exhibit strain softening while the other one unloads viscoelastically) is a function of the parameters that describe the bundle. The parameters are directly related to strength, stiffness, damage capacity and load bearing capability.

7–4–2 Relaxation tests

If, following a certain strain rate, the overall strain across a system of two fibre bundles held in series is kept constant, then the resultant stress will decrease with time at a decreasing rate, and will approach asymptotically a residual value. To any point on a stress strain curve, corresponding to an applied strain rate, there would correspond an equilibrium stress value that the assembly would relax to if strain is held constant. Figure 7.38 shows the stress strain curve of the model material, with parameters allocated the same values as those in section 7–4–1, at a strain rate of 4.0E–04 together with the corresponding locus of residual points that are reached following relaxation tests. Relaxation is followed at any level of strain even in the post peak portion of the stress–strain curve.

The results obtained in the relaxation tests are similar to those of the network model if the response is smoothed (figure 7.12). The peak stress on the stress strain curve and that on the relaxation locus correspond to the same value of strain. This result was also observed for the network model. This is expected because of the use of the same relaxation function $\varphi(t)$ regardless of the level of stress prior to the relaxation phase.

Figure 7.39 shows the relaxation loci corresponding to two different applied strain rates. The final state of stress following a relaxation test is dependent on the value of stress prior to relaxation which in turn is dependent on the strain rate applied to reach that stress. The final state of damage of the model material at a given strain is hence dependent on the past time history from the start of straining. Similar dependence was noted for the network model following relaxation tests.

7–4–3 Creep tests – Modes of behaviour

If stress is kept constant at any level, the model material will creep to complete failure or to an equilibrium state of strain depending on the level of stress. Figure 7.40 depicts this behaviour for stress values attained at a strain rate of 4.0E–04. At all stress levels below the peak stress in the corresponding locus of relaxation points, strain will increase with time, if stress is kept constant, and will approach that value of strain, corresponding to this stress, on the corresponding locus of relaxation points.

For all stress values above the peak stress in the corresponding locus of

relaxation points but below the peak stress of the actual stress strain curve, strain will increase with time at a constant stress but will eventually result in complete unstable failure of the model material. At all stress levels in the strain softening portion of the stress strain curve, complete failure will be initiated instantaneously if stress is kept constant.

Results of both relaxation and creep tests compare well with those of the idealized/smoothed network model (figure 7.12). Apart from the verticality of the failure envelop, the results are also in good agreement with those reported for real materials (chapter III). The verticality of the failure envelop is a direct result of the use of a relaxation function which is independent on the level of sustained load. If the failure envelop was to be non vertical (for both the present model and the idealized/smoothed network model), the form of the function $\varphi(t)$ should be such that it caters for the level of load applied prior to creep or relaxation phases.

The correspondence in behaviour between the present model and that of the idealized network model suggests that if the size of the network is reduced to a point, its behaviour will resemble that of a point in a continuum progressively fracturing solid.

7–4–4 Creep tests – Creep curves and time to failure

Figure 7.41 shows typical relaxation and creep curves. At any stage of loading, if the overall strain along the network is held constant, stress will decrease with time at a decreasing rate and will approach asymptotically a residual value. If stress is held constant, strain will increase with time. If the level of stress is low, strain will increase with time at a decreasing rate and will approach asymptotically the value of strain on the locus of relaxation points corresponding to the given constant stress. At high levels of the applied stress (above the peak stress in the corresponding locus of relaxation points but below the actual peak stress (figure 7.40)), strain will initially increase with time at a decreasing rate but will then increase with an increasing rate up to complete failure. At failure, strain increases rapidly in an unstable fashion resulting in instantaneous failure. At any state in the post peak stress strain curve, failure is always instantaneous.

The time needed for complete failure as a function of applied stress in creep tests is shown in figure 7.42. As seen from the figure, the time to complete failure increases from vanishingly small durations at high levels of stress to

infinitely large durations at low levels of stress. Similar variations were observed for the network model (figure 7.16) and for physical materials (figure 3.20(a)).

7–4–5 General remarks on creep and relaxation tests

Results from the creep and relaxation tests show an interdependence between the two modes of behaviour. The locus of relaxation points, corresponding to a given strain rate, serves as a reference curve, in conjunction with the actual stress strain curve, to distinguish between the different modes of creep behaviour (figures 7.38 and 7.40).

It should be noted that for this model material, the peak stress on the stress strain curve and that on the corresponding locus of relaxation points correspond to the same value of strain. The value of the creep strain, corresponding to any creep test at a stress level between these two peaks, corresponds also to the value of strain at peak stress on the stress strain curve.

The resulting residual points following relaxation tests and the resulting equilibrium and failure points following creep tests are primarily a result of the time delayed damage but are also dependent on the rate of application of strain prior to these tests. This is confirmed by the variation of the loci of equilibrium relaxation points with the strain rate applied prior to relaxation phases (figure 7.39).

It is interesting to look at the stability of the post peak response of the model material. This can be investigated by observing the response obtained when stress or strain are kept constant. The model material is stable in the post peak mode of behaviour under strain controlled conditions but is unstable under stress controlled conditions. At any level of loading, if strain is kept constant, stress will relax in a stable fashion down to an equilibrium state. On the other hand, if stress is kept constant or increased starting from an equilibrium state in the post peak portion of the behaviour, the model material will fail instantaneously in an unstable manner. The same observations were made regarding the post peak behaviour of the network model.

The results of creep and relaxation tests, as well as those of the uniaxial extension tests, show resemblance to the response obtained in real physical testing (chapter III). The present simple model illustrate how the general continuum theory can be deployed in a simple fashion to describe some aspects of material behaviour associated with progressive fracture and time–dependence.

7–4–6 The role of $\varphi(t)$ – Tests on a "revised" model

It was mentioned earlier that the effects on strain rate sensitivity of the damage evolution law, in the actual response of the model material, are only manifested at low strain rates. This can be confirmed by testing the material model with strain rate sensitivity of the instantaneous response completely ignored. This is achieved by assuming that the strain rate parameter T in 6.3.21 is always 1.0 regardless of the strain rate. This "revised" model is easy to analyse and gives an insight on the role of the relaxation function $\varphi(t)$.

Figure 7.43 shows the results from such tests. It was found that any strain rate above 4.0E–04 results in little if any changes in the stress response if compared to that obtained at a strain rate of 4.0E–04. The same is true for all tests at strain rates lower than 4.0E–09 if compared to results attained at a strain rate of 4.0E–09. This suggests the existence of an infinitely fast and an infinitely slow response that are fixed and are properties of the model material.

At high strain rates the relaxation modulus φ become insignificant and will always assume the value of 1.0. The model's response becomes instantaneous and time–independent. On the other hand, at slow strain rates the relaxation modulus will always assume the value of $\varphi(\infty)$ (0.6 in here). The response is termed the infinitely slow response and again is time–independent. Numerically, there exists two values of the strain rate that act as thresholds defining the range of applicable strain rates (upper and lower). Outside these limits, the response is either infinitely fast (instantaneous) or infinitely slow and is time and rate insensitive. At any intermediate strain rate, the function φ becomes effective and the response becomes time and rate sensitive (figure 7.43).

The behaviour of the individual fibre bundles following an infinitely fast, an infinitely slow and an intermediate strain rate is shown in (figure 7.44). While, in all tests, one of the bundles follows a complete stress strain curve of hardening and softening (fibre bundle (2)), the other bundle unloads when the stress across the assembly reaches its maximum values. In all tests, the fibre bundle that unloads (1) will assume a value of zero strain at zero stress. The suggestion that the responses following an infinitely fast and an infinitely slow strain rates are not time dependent is confirmed by the linearity of the unloading moduli of the fibre bundle (1) in σ–ϵ space indicating the non–presence of viscoelastic effects ($\varphi(t)$ being constant).

It is interesting to note that although the response of the model

material is rate sensitive within a range of strain rates, damage is dependent on the strain and its path history only. Figure 7.45 shows the variation of the effective instantaneous secant moduli of the individual fibre bundles with applied strain. The variation is identical for all strain rates, and hence the conclusion that damage is dependent on time only in the form of delayed effects (evolution law) with the instantaneous stiffness, while path dependent, being time independent.

In real material testing, creep and relaxation tests normally follow loading at a reference "static" rate, assumed to be "instantaneous". It is thus more practical to perform these tests on the material model presented in here by neglecting all strain rate effects in the instantaneous response of the fibre bundles. Such tests have proved the existence of an infinitely fast and an infinitely slow response (figure 7.43) characteristics of the assembly.

Figure 7.46 shows that, if strain rate sensitivity is ignored in the instantaneous response, the locus of equilibrium relaxation points, corresponding to a stress strain curve obtained by applying the strain instantaneously (in here at a rate greater than 10^{-4}) exists and is identical to the stress strain curve obtained if strain is applied at an infinitely small rate (in here at a rate less than 10^{-9}).

The infinitely slow response of the model material, being identical to the locus of relaxation points, will serve as a reference to distinguish between different modes of creep behaviour (figure 7.47).

Results from creep and relaxation tests on this simplified material model (figures 7.46, 7.47, and 7.48) are qualitatively identical to those obtained in the general case when strain rate sensitivity was included in the instantaneous response of the individual fibre bundles (figures 7.38, 7.40, and 7.41). This justifies the use of this simplified version of the assembly when the behaviour under creep and relaxation tests is to be modelled. The only difference between the general model (sections 7–4–1 to 7–4–5) and the simplified tests is that when strain rate sensitivity is ignored in the instantaneous response, the response to an infinitely slow strain controlled test will be identical to the locus of relaxation points at any strain rate and not only the ones causing an infinitely fast response.

Figure 7.49 shows that if relaxation tests follow loading at an intermediate strain rate, then the response at an infinitely slow applied strain rate will still coincide with the locus of the corresponding stress relaxation points.

The response of this simplified model at different strain rates (figure 7.43) shows that at any strain rate, the stress strain curve would never intersect that obtained at an infinitely high test but might cross that at an infinitely slow rate (the strain rate sensitivity in the instantaneous response being ignored). One unusual phenomena is observed in these tests. When the stress, prior to a relaxation test, is lower than the corresponding stress at the same strain on the stress strain curve following an infinitely slow strain rate, then the stress would increase with time at a decreasing rate up to the corresponding level on the infinitely slow response (figure 7.49).

Figure 7.50 shows that, in relaxation tests, the stress might increase or decrease depending on whether the initial value of stress is higher or lower than that on the stress strain curve following an infinitely slow rate at the same value of strain. In both cases behaviour is stable and would not result in failure.

This increase in stress has not been reported to exist in real materials. Nevertheless, relaxation tests are not only sparse but are also normally performed following strain rates that are considered infinitely fast or instantaneous (nominal static rates). If the results obtained here are to be used to simulate real material behaviour then the possibility of stress, following an applied strain at a slow rates, being undervalued due to viscous effects should not be overruled. If due to these effects stress, at a given strain, is below stable equilibrium value, then if strain is kept constant stress should increase with time up to that value.

Creep tests (figures 7.51, 7.52) on the model material (with rate effects ignored in the instantaneous response) following a strain rate below that causing an infinitely fast response, will result in similar modes of behaviour to those obtained in the general case (figures 7.40 and 7.41) and when following an infinitely fast strain rate for the revised model (figures 7.47 and 7.48).

Unlike the previous tests, at stress levels in the post peak portion of the stress strain curve, where the strain is less than the corresponding strain on the stress strain curve following an infinitely slow loading, creep tests would not result in an instantaneous failure but strain will increase with time at a decreasing rate in a stable fashion, until it approaches the corresponding value obtained in an infinitely slow test (figures 7.51 and 7.52).

In summary, the general behaviour of this simplified material model gives good qualitative resemblance to creep and relaxation tests performed on real materials. Results similar to those obtained for the general model (sections

7–4–1 to 7–4–5) can be obtained if tests follow an infinitely fast loading.

Similar conclusions to those of the general model (sections 7–4–1 to 7–4–5) are drawn if stability of the post peak behaviour is studied following an infinitely fast (static) loading. If the strain rate applied does not result in an infinitely fast response, then the possibility of stable creep starting from an equilibrium state in the post peak states arises. Stability under constant strains is still attained eventhough relaxation tests might result in an increase rather than a decrease in stress at constant strains.

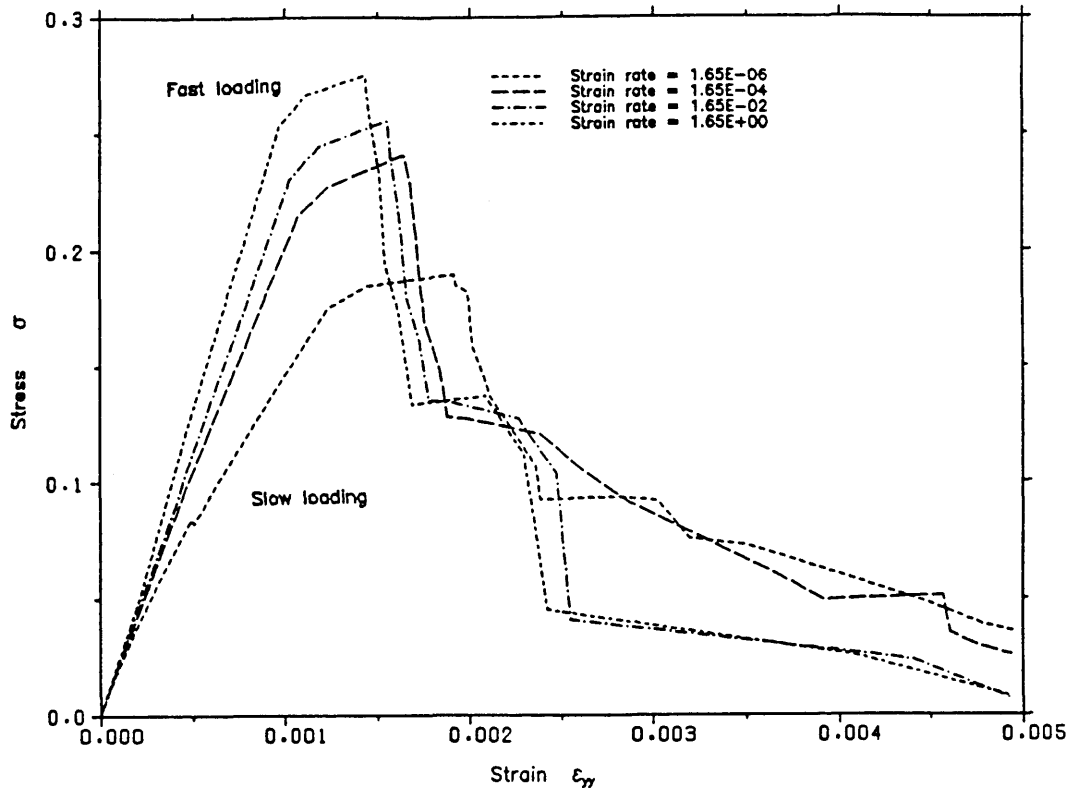

Fig. 7.1 Stress strain curves for the network model at different strain rates

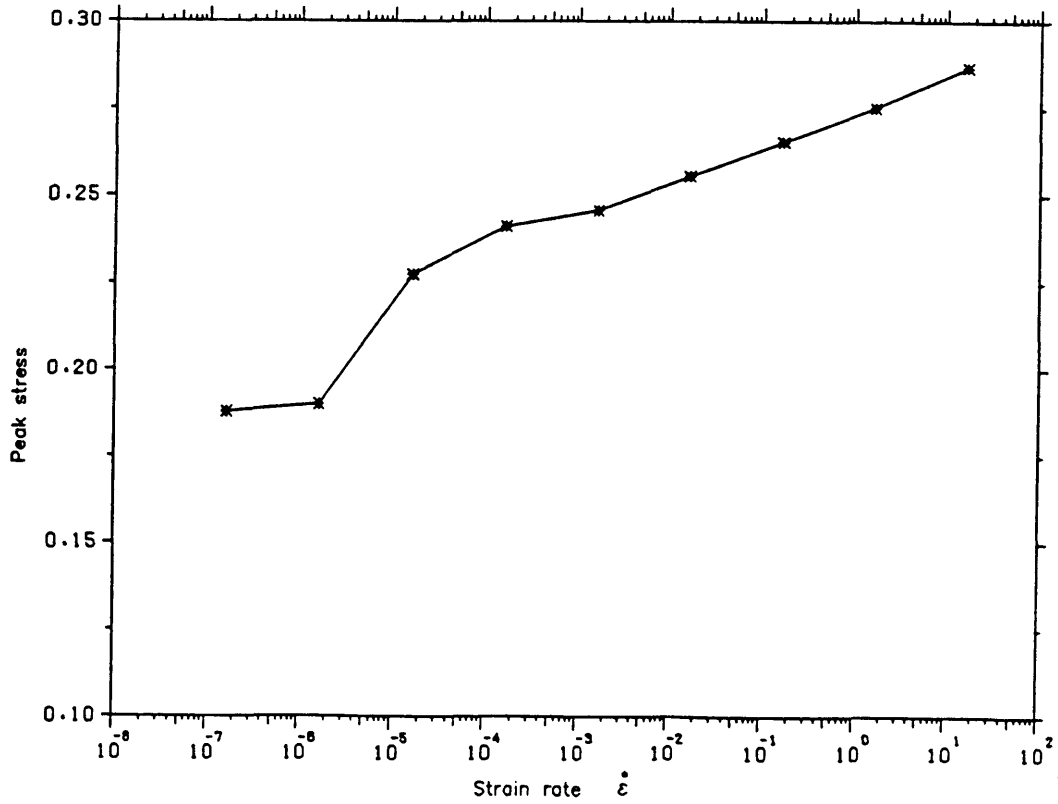

Fig. 7.2 Change of peak stress with strain rate for the network model

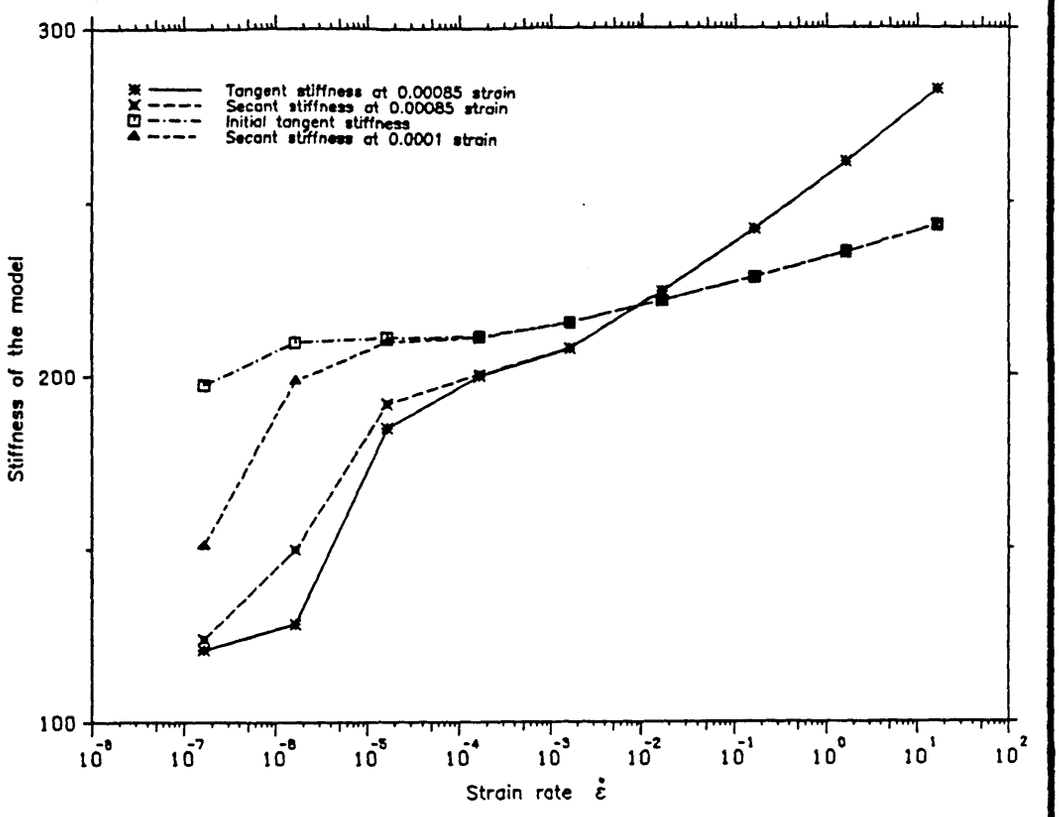

Fig. 7.3 Change of the stiffness with strain rate for the network model

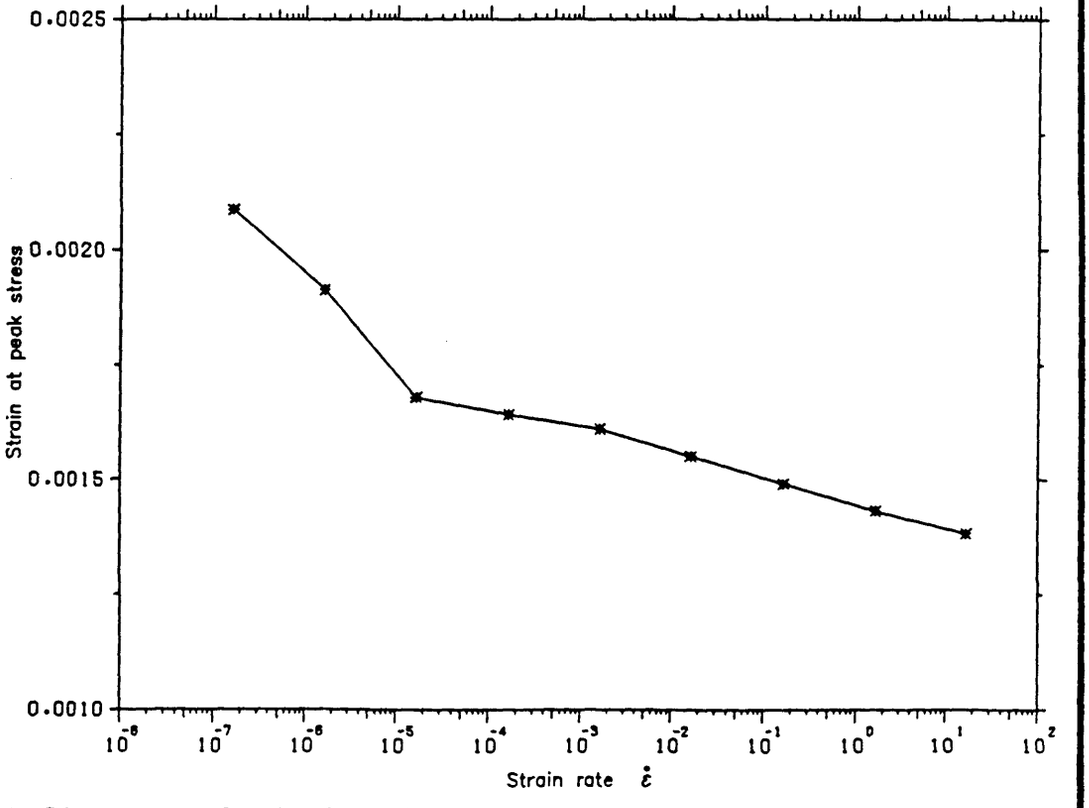

Fig. 7.4 Change of strain at peak stress with strain rate for the network model

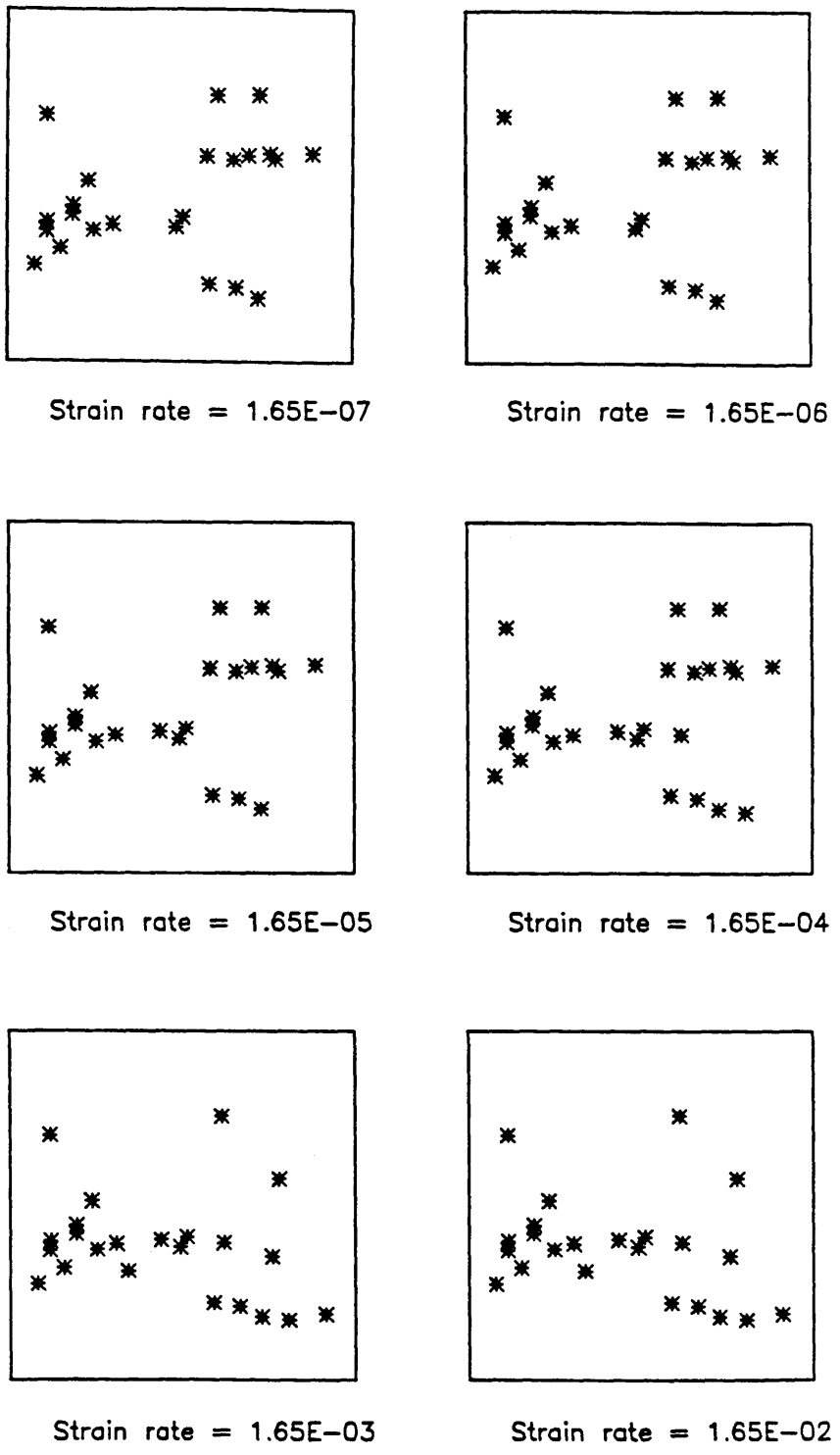

Fig. 7.5 Distribution of failed members for a typical network near complete failure

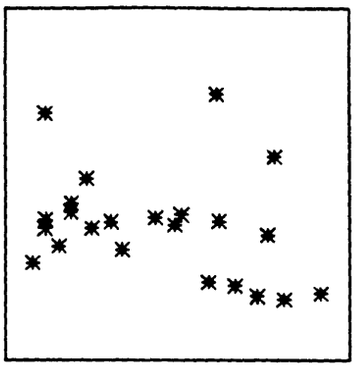

Strain rate = 1.65E−01

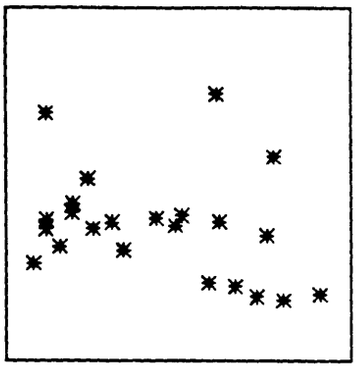

Strain rate = 1.65E+00

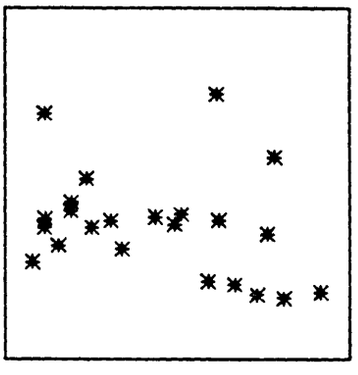

Strain rate = 1.65E+01

Fig. 7.5 (cont'd) Distribution of failed members for a typical network near complete failure

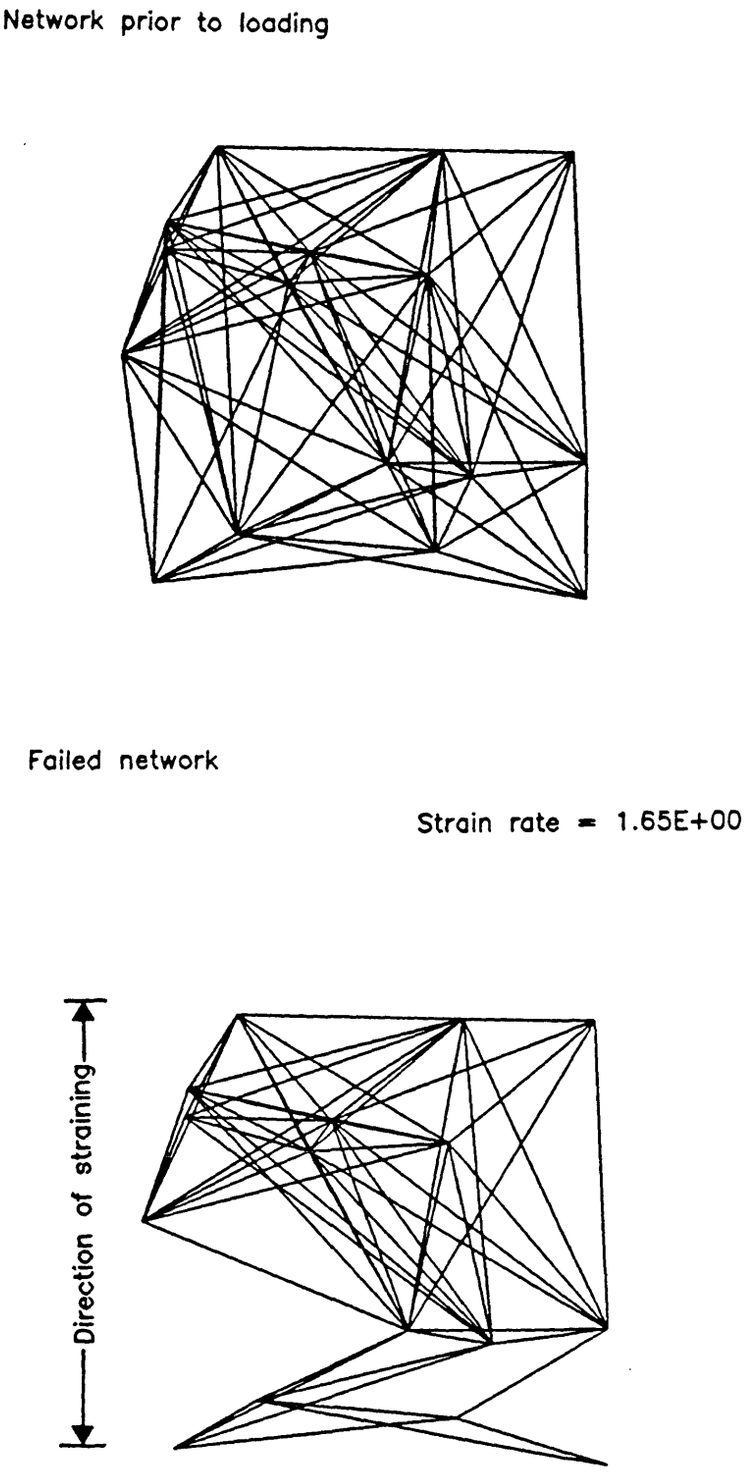

Fig. 7.6 Configuration of a typical network prior and after loading

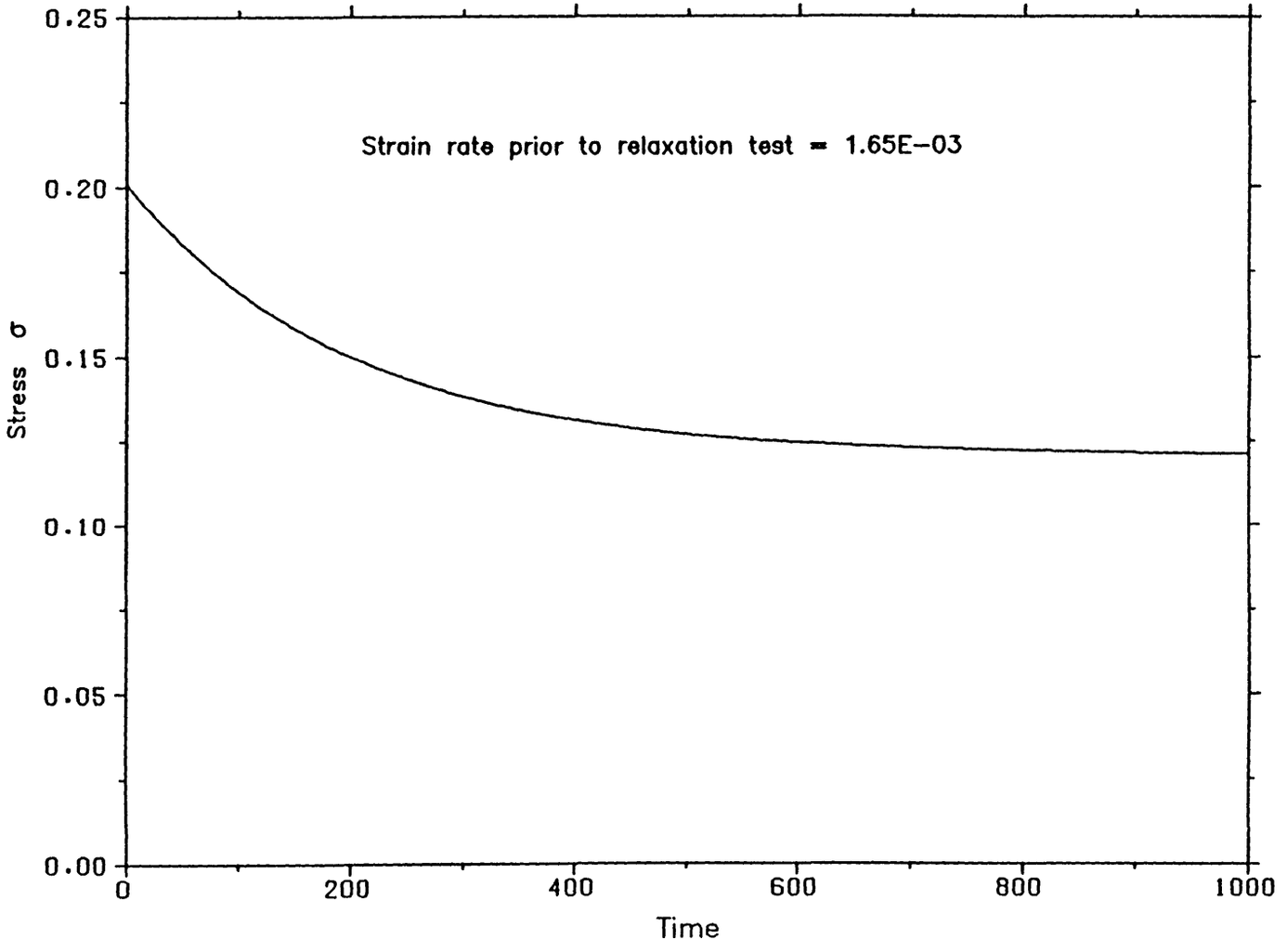

Fig. 7.7 Behaviour of a typical network model upon a relaxation test

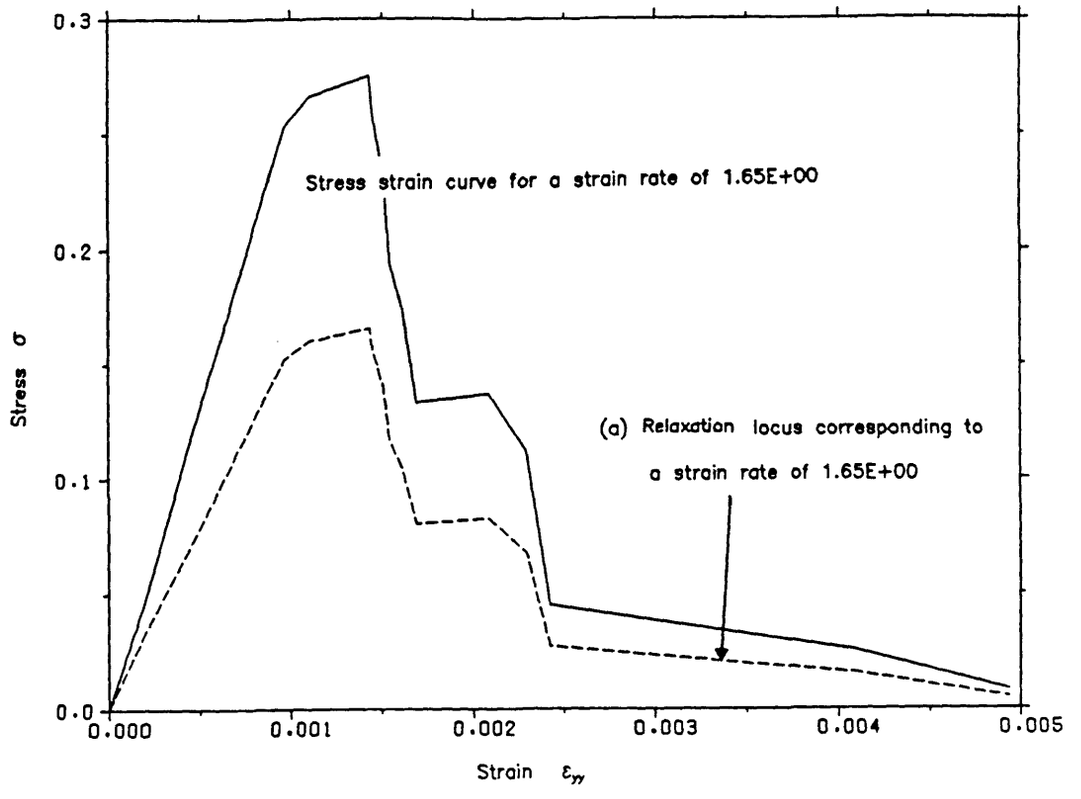

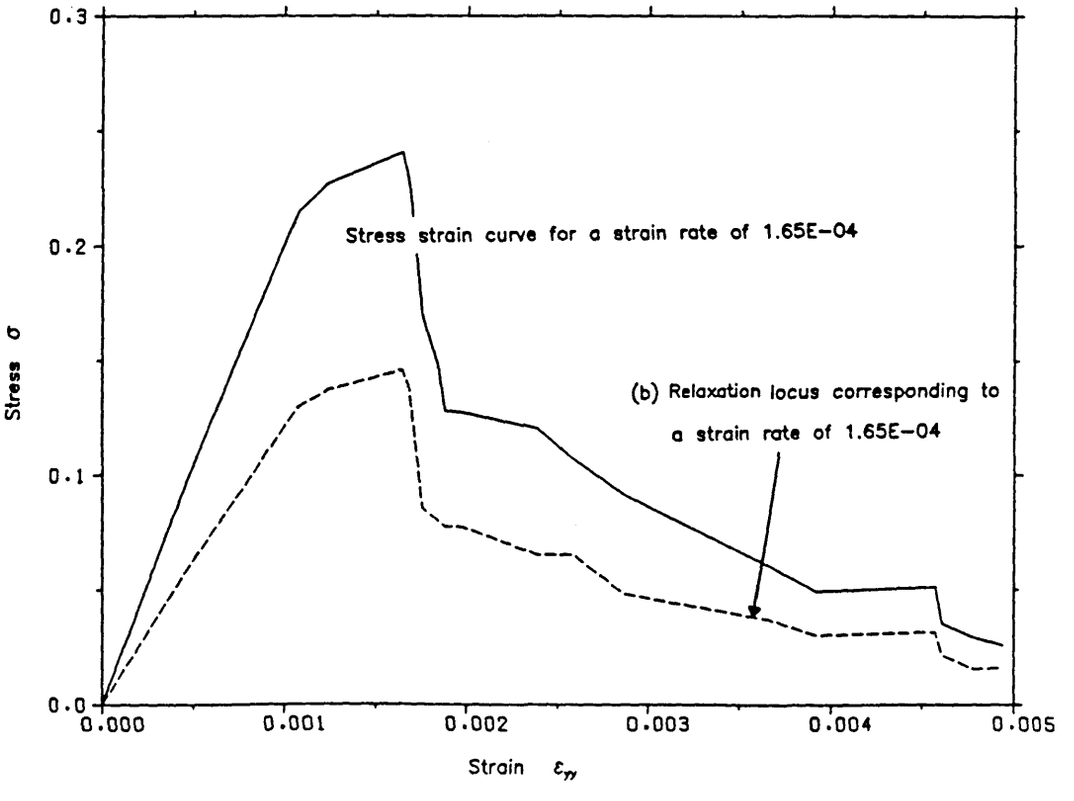

Fig. 7.8

Stress strain curves of the network model following different strain rates and the corresponding relaxation loci

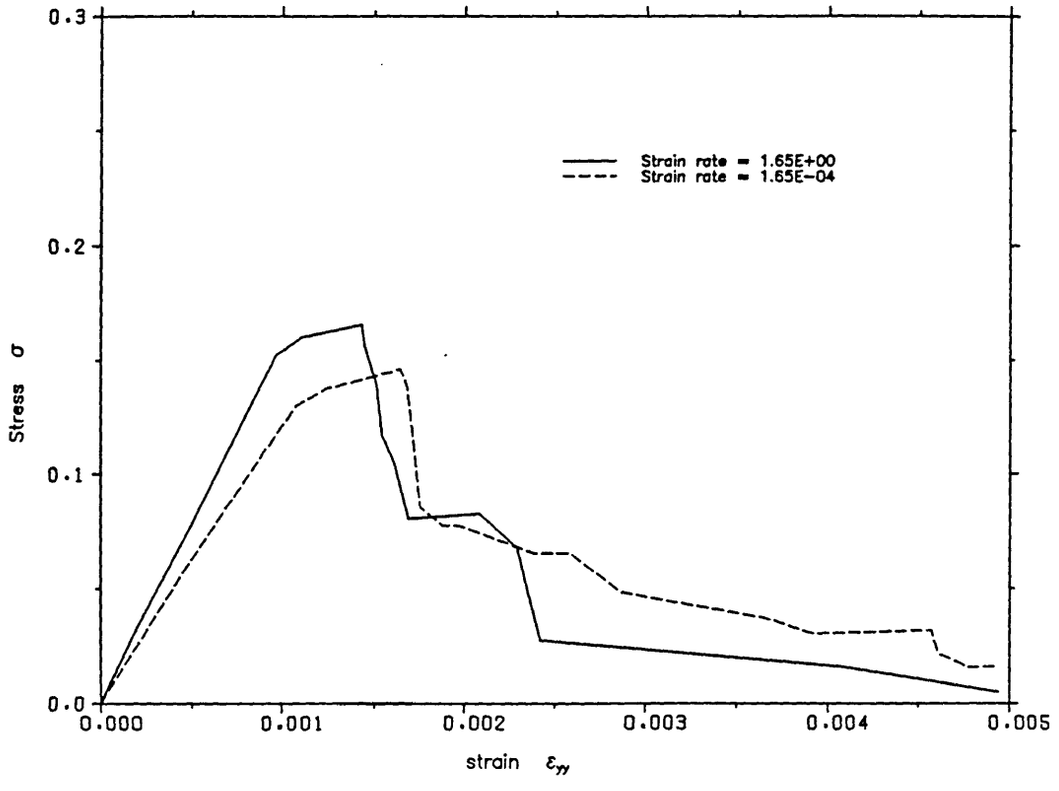

Fig. 7.9 Relaxation loci of the network following two different strain rates

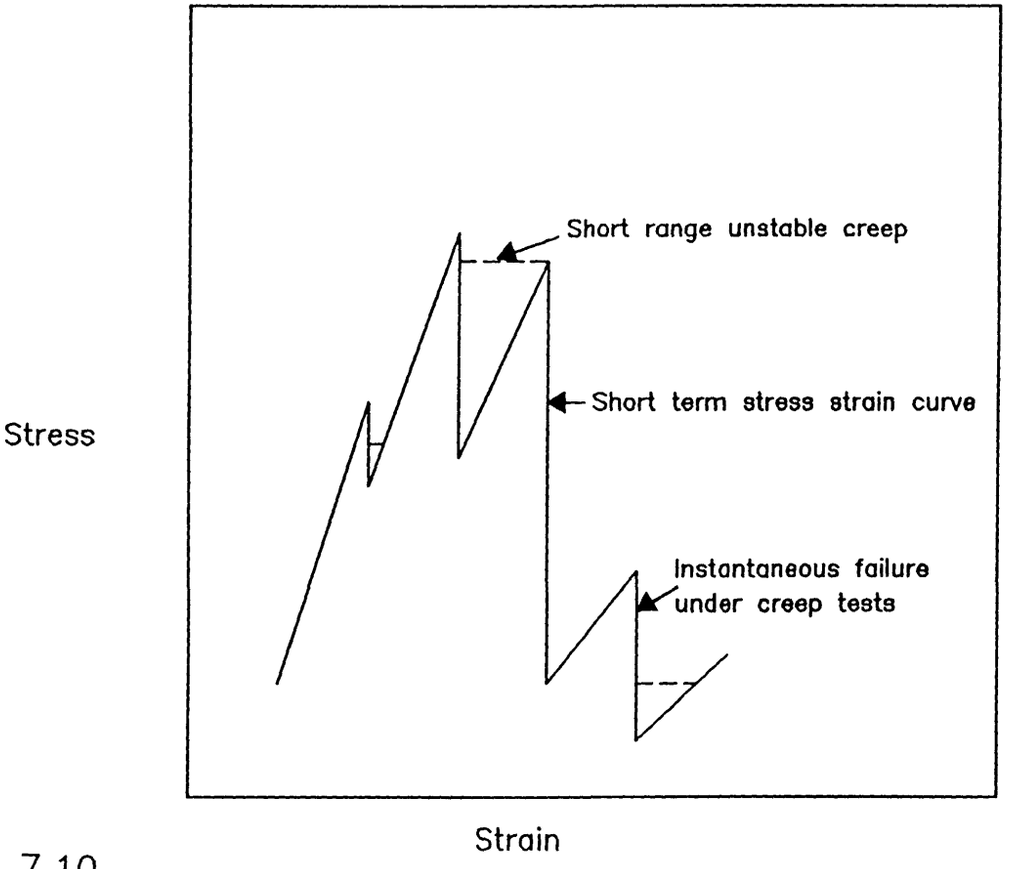

Fig. 7.10
Short range unstable creep behaviour due to the discrete nature of the network model

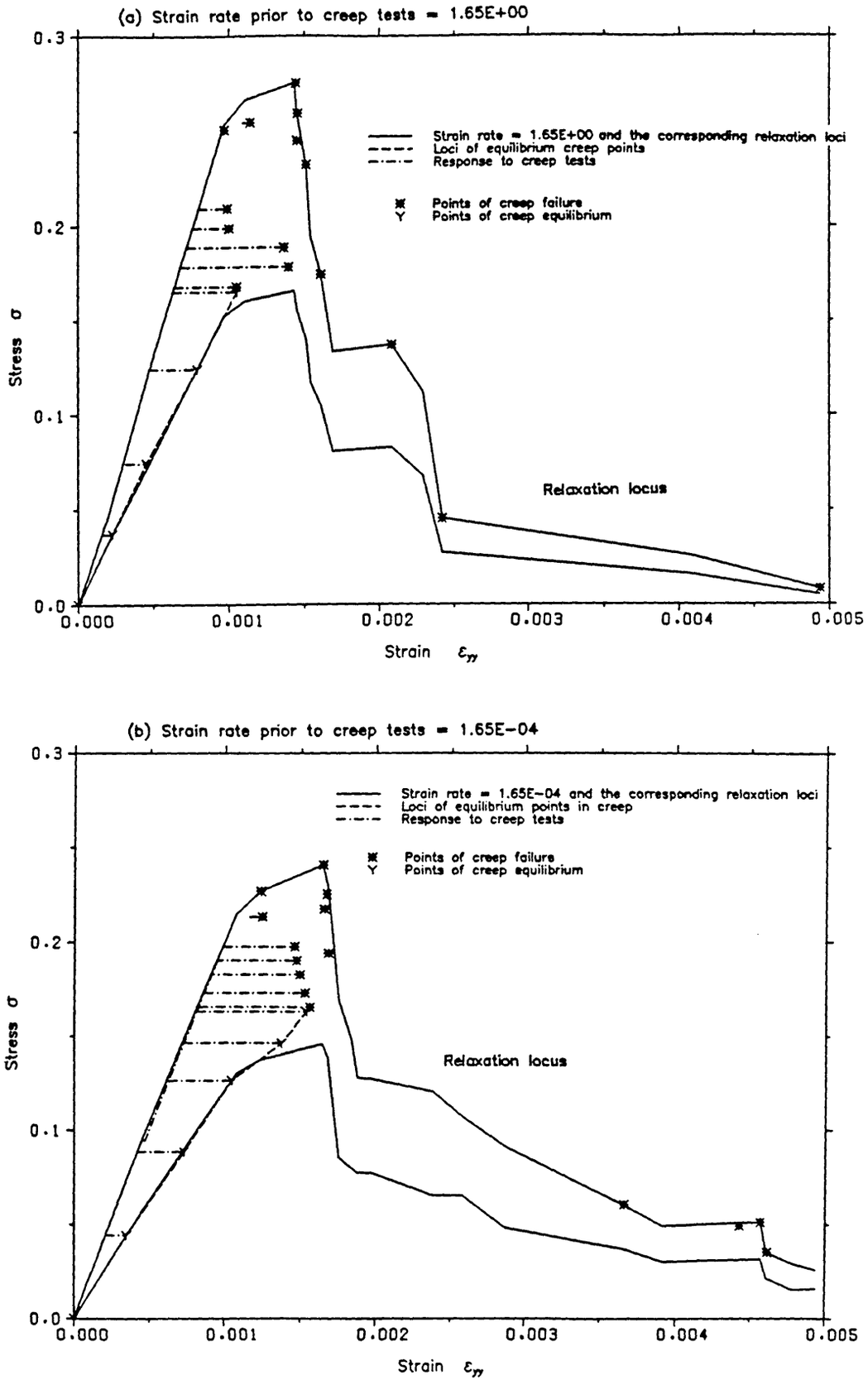

Fig. 7.11 Behaviour of the network model following creep tests

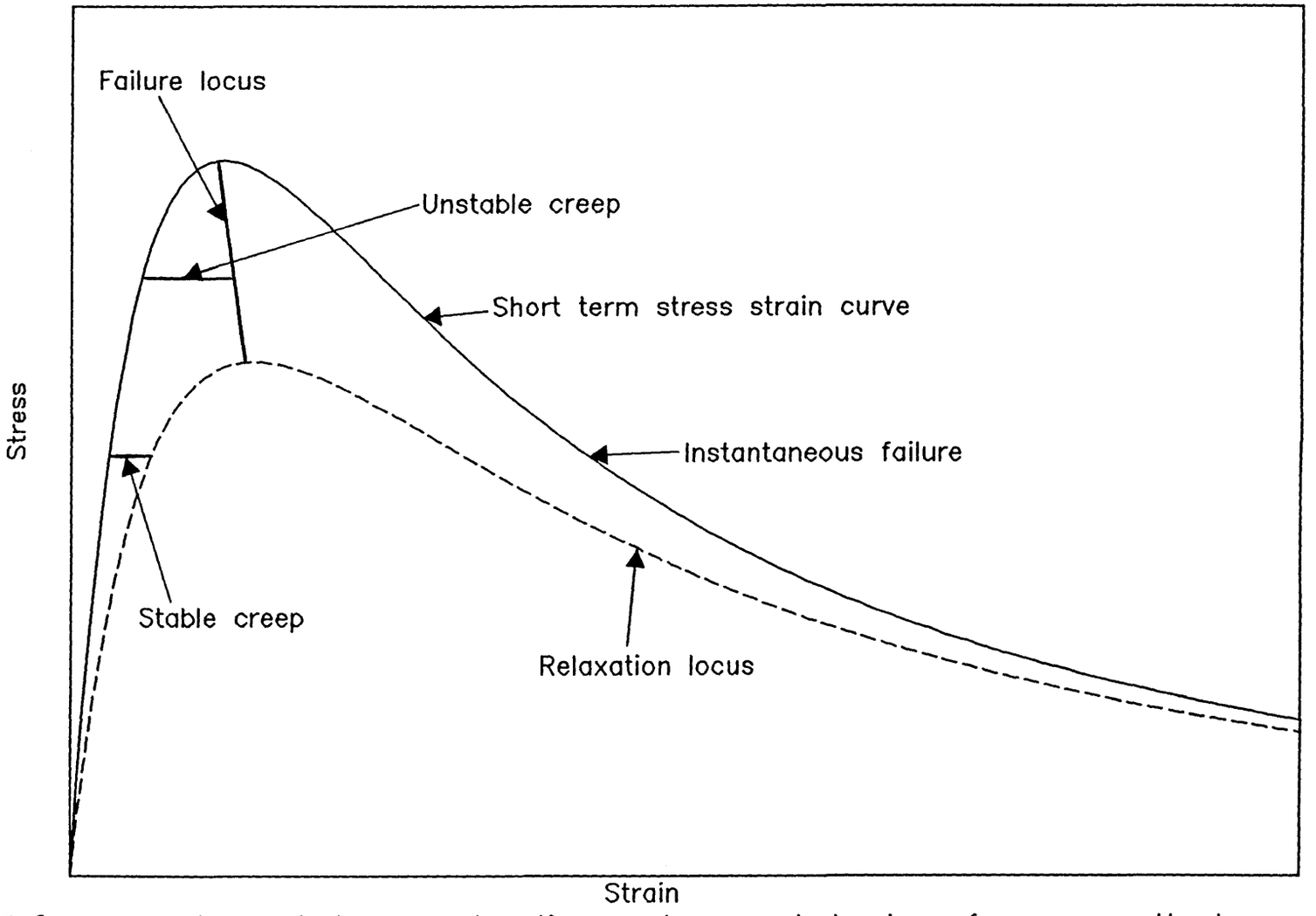

Fig. 7.12 Correspondence between relaxation and creep behaviour for a smoothed network model

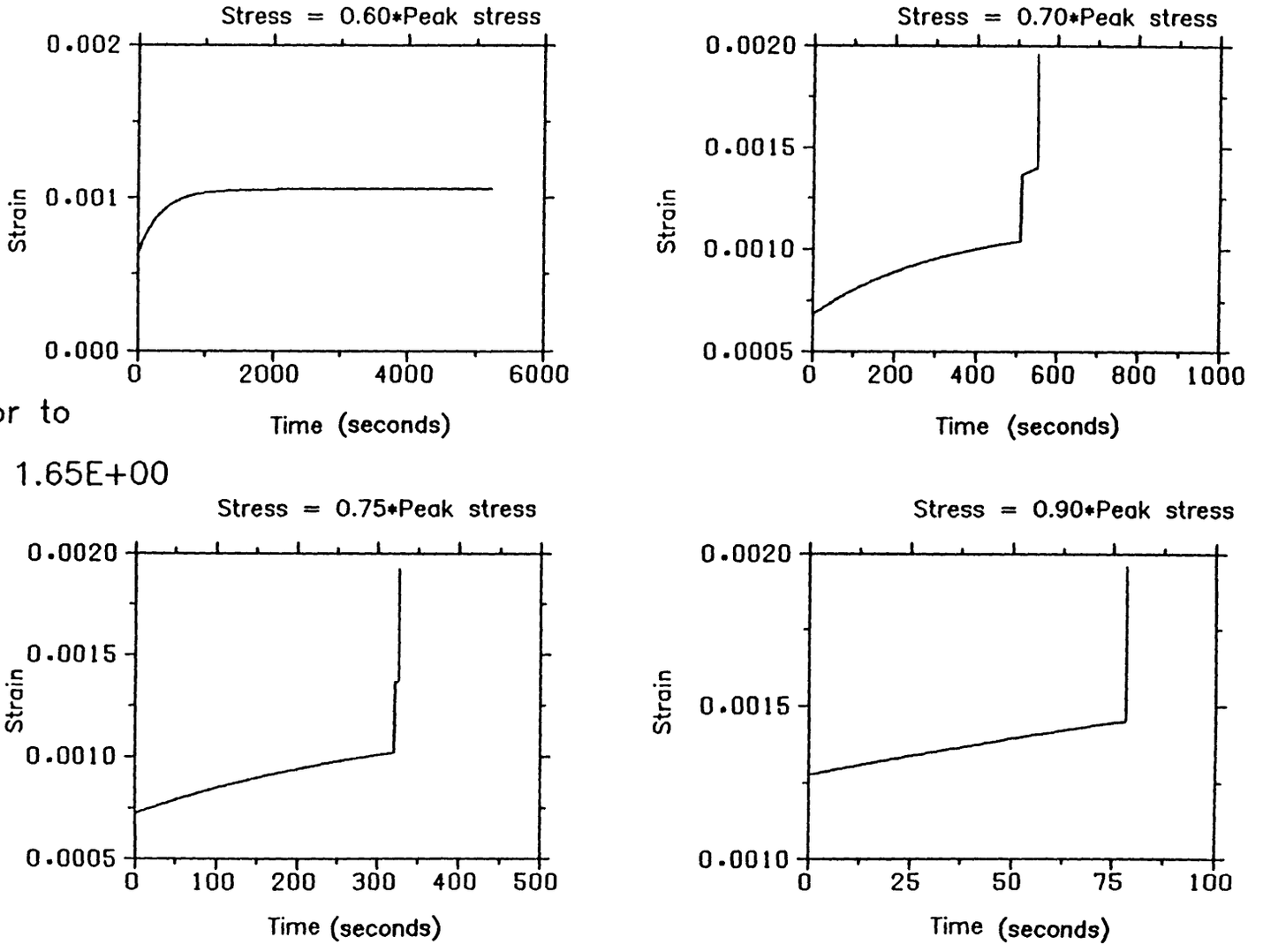

Strain rate prior to creep tests = 1.65E+00

Fig. 7.13 Strain time curves of the network model under creep tests

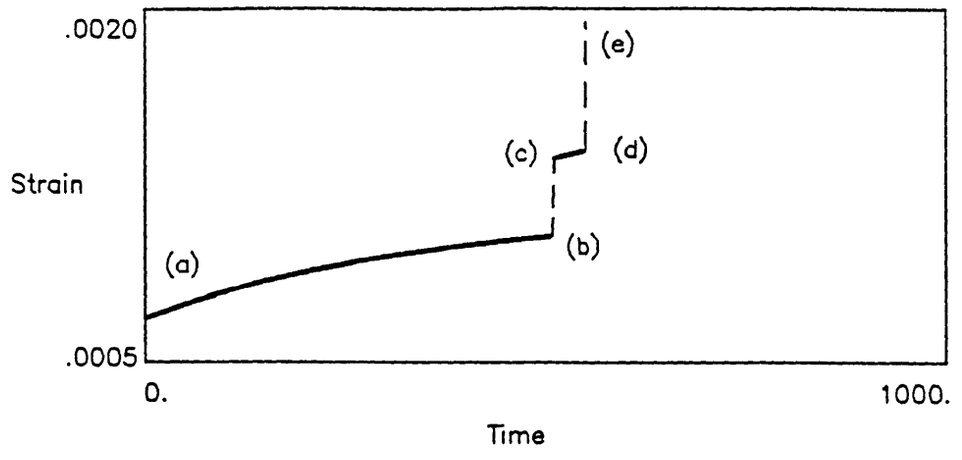

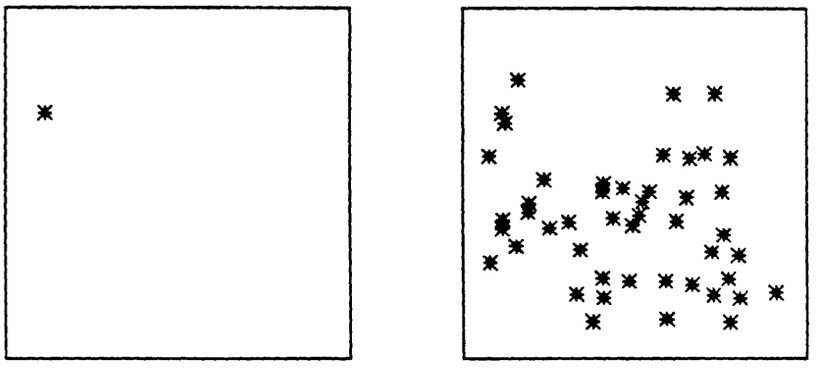

State of sample between a and b

Distribution at seperation i.e. d to e

Strain rate prior to test = 1.65E+00

Stress = 0.7 of peak stress

Fig. 7.14 Increase of strain with time and the distribution of failed members of a typical network model under a creep test

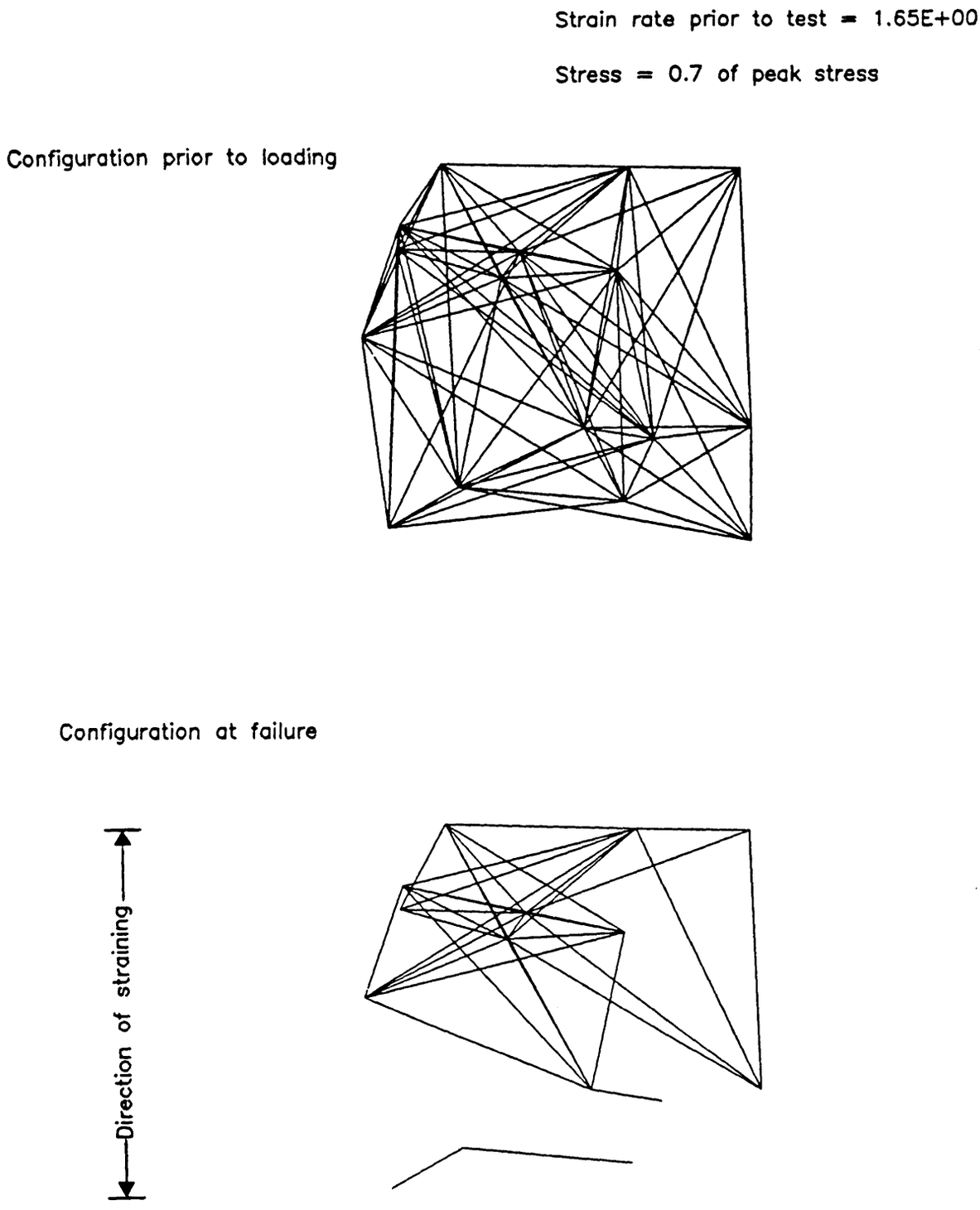

Fig. 7.15 Failure configuration of a typical network model under a creep test

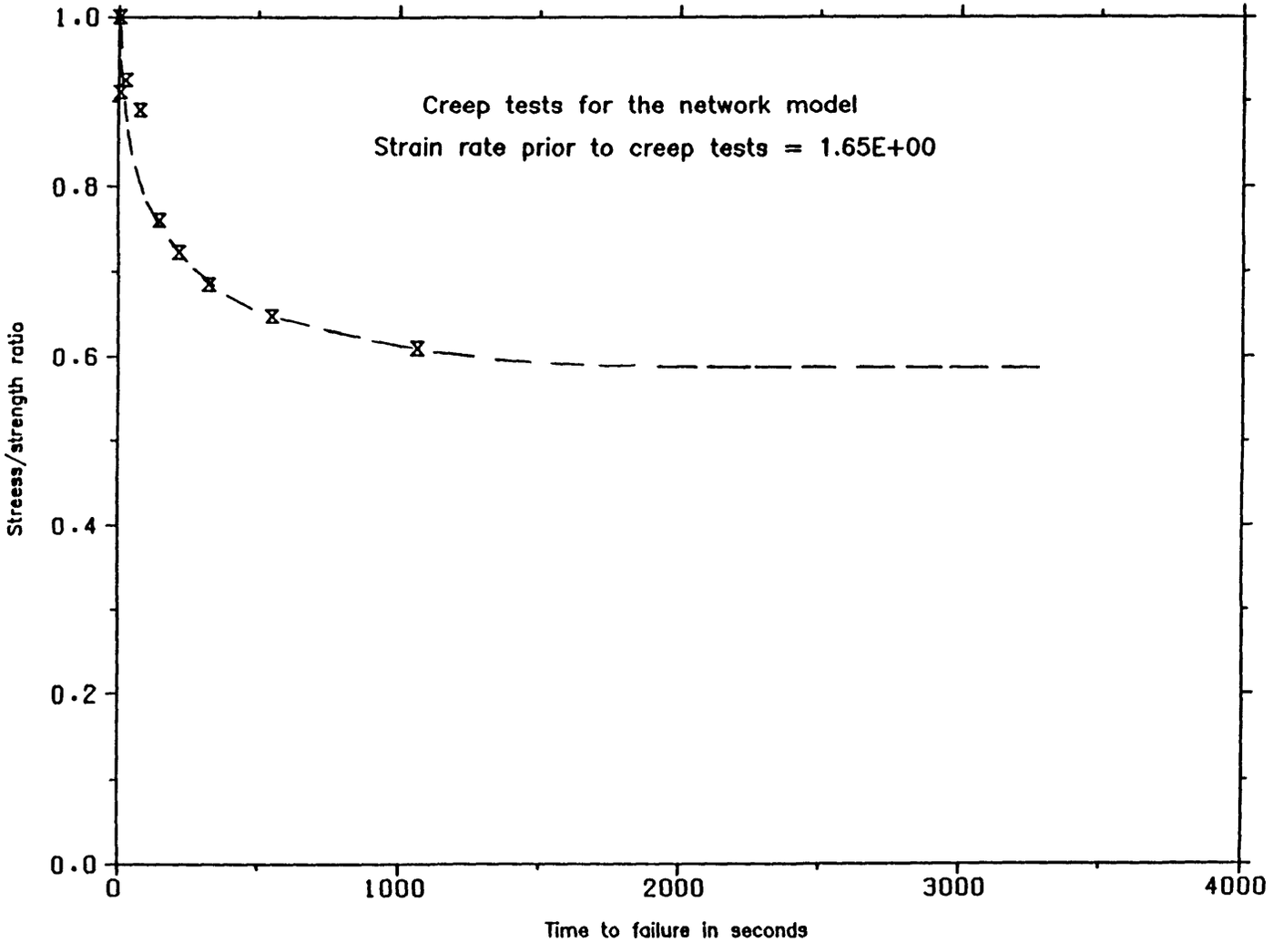

Fig. 7.16 Change of the time to failure with the stress/strength ratio in creep tests

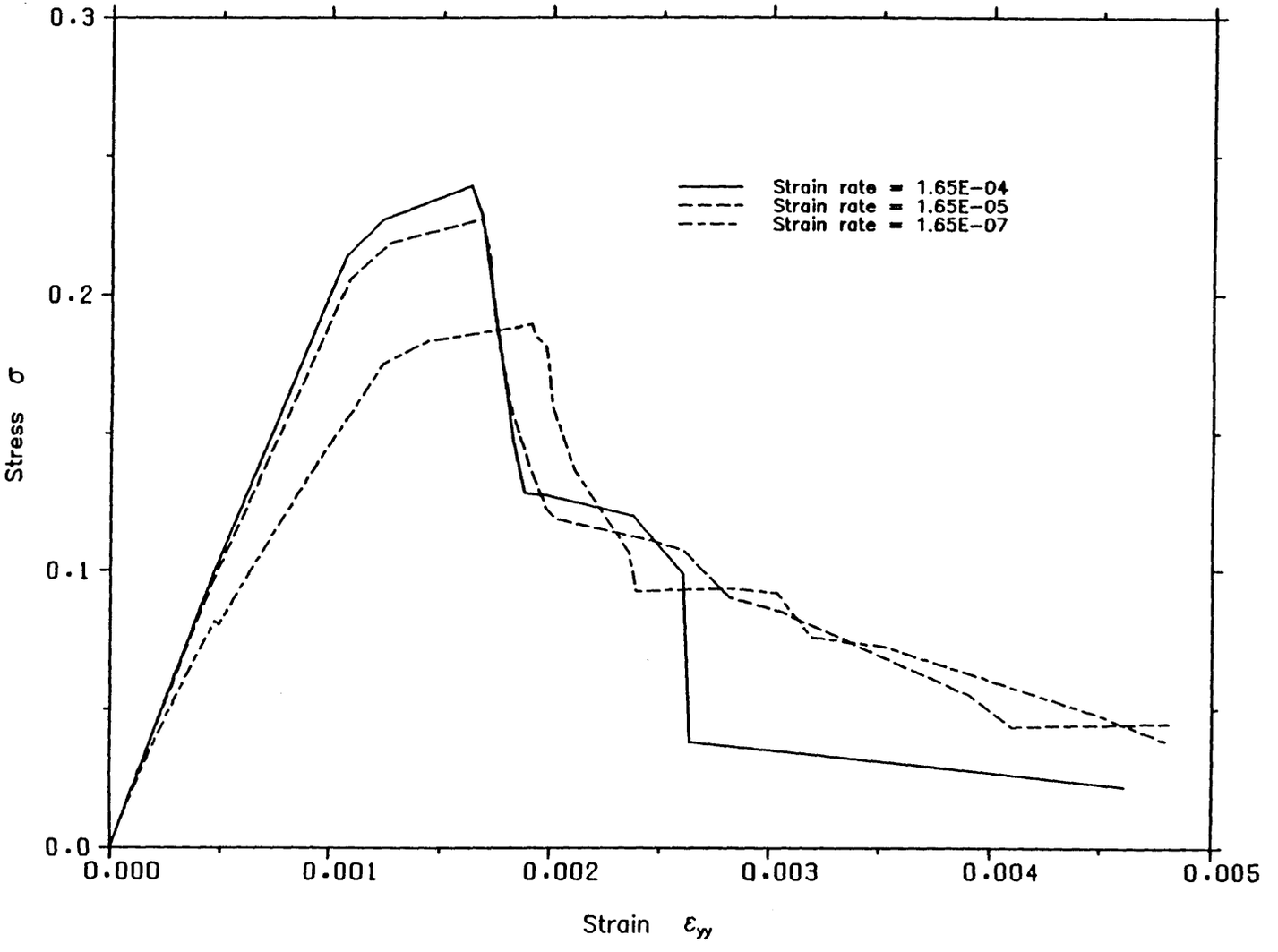

Fig. 7.17 Stress strain curves for the network model at different strain rates – strain rate sensitivity of the instantaneous response ignored

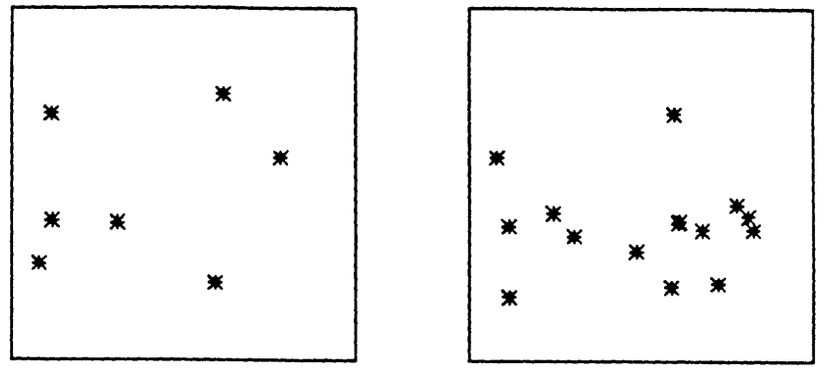

Strain rate = 1.65E−04

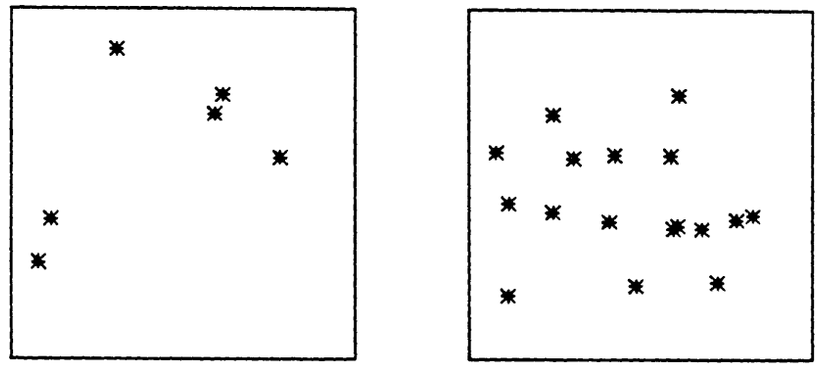

Strain rate = 1.65E−05

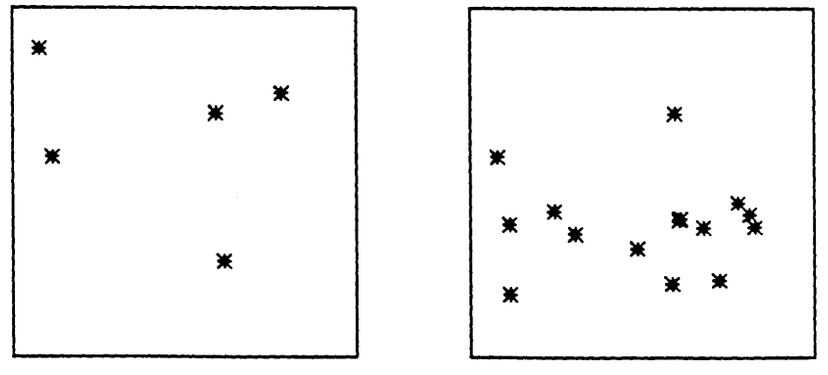

Strain rate = 1.65E−07

Fig. 7.18 Distribution of failed members for a typical network near the peak stress and near complete failure

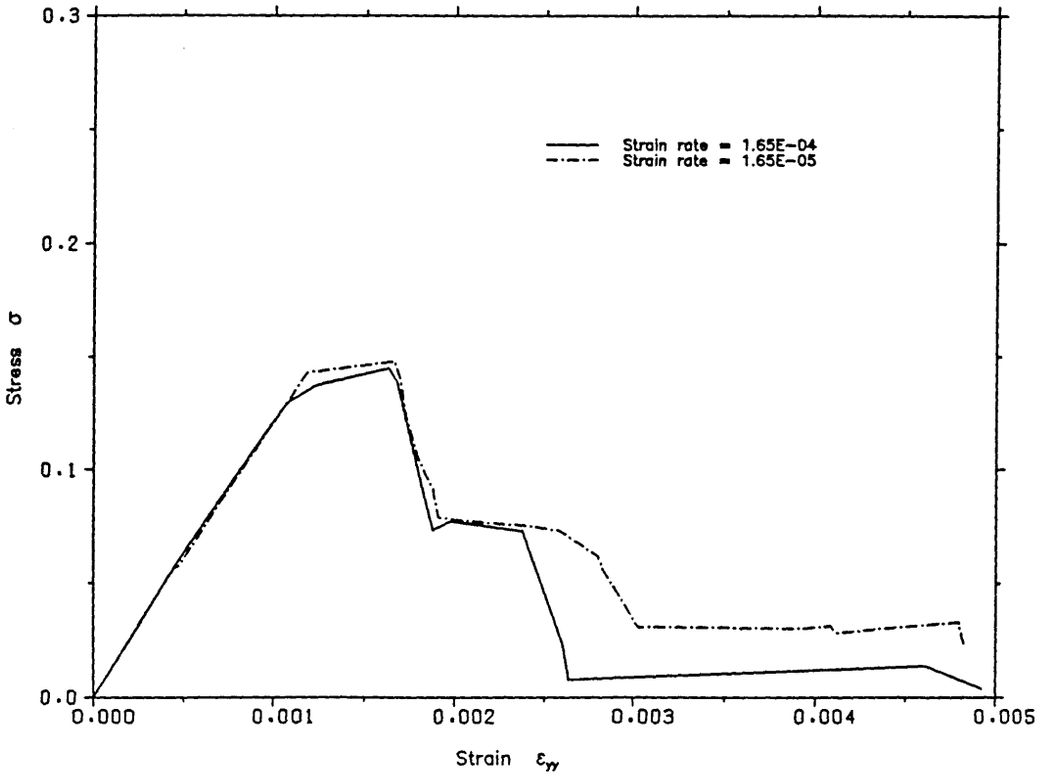

Fig. 7.19 Relaxation loci of the network following two different strain rates

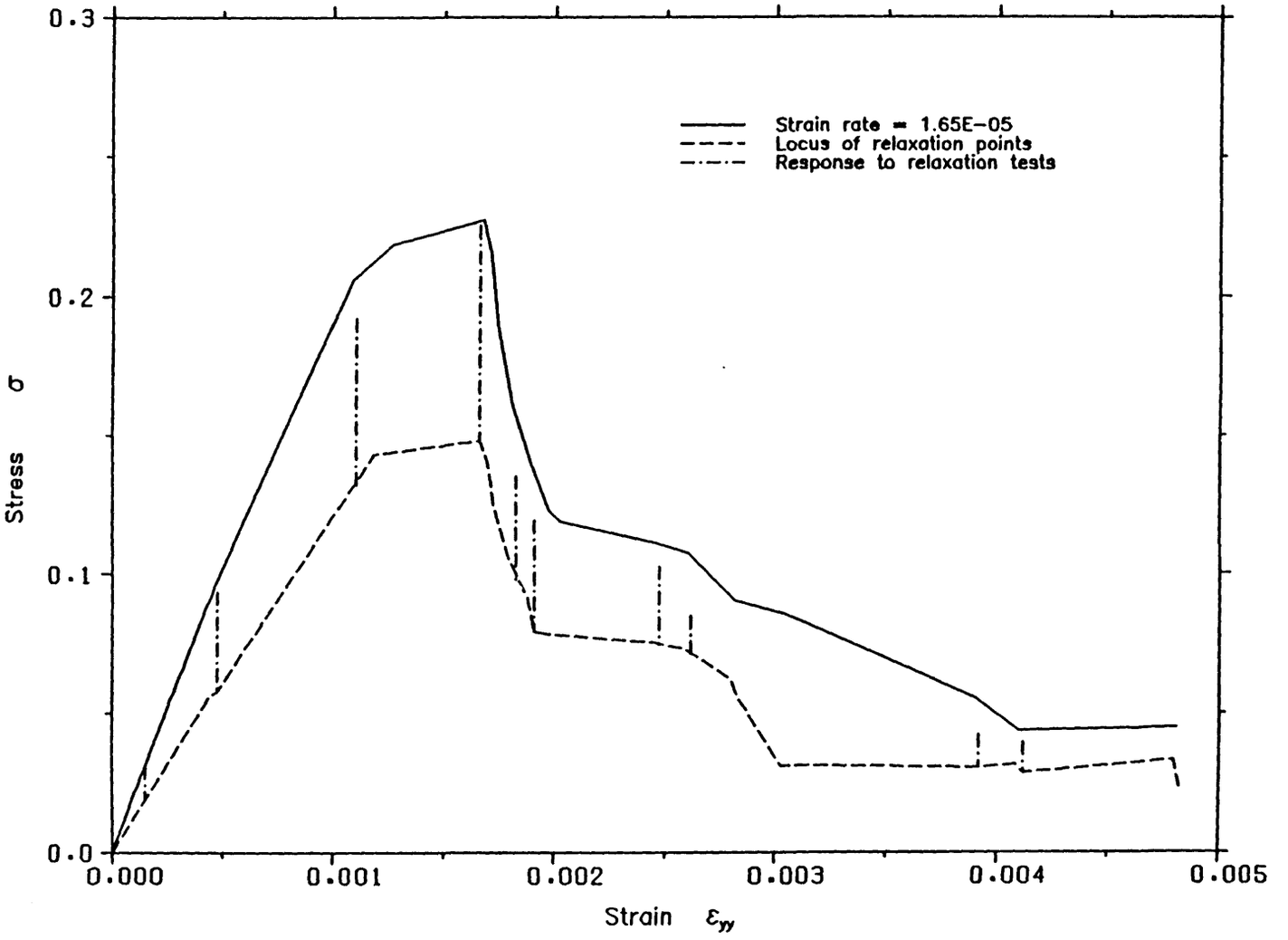

Fig. 7.20 Behaviour of the network model following relaxation tests

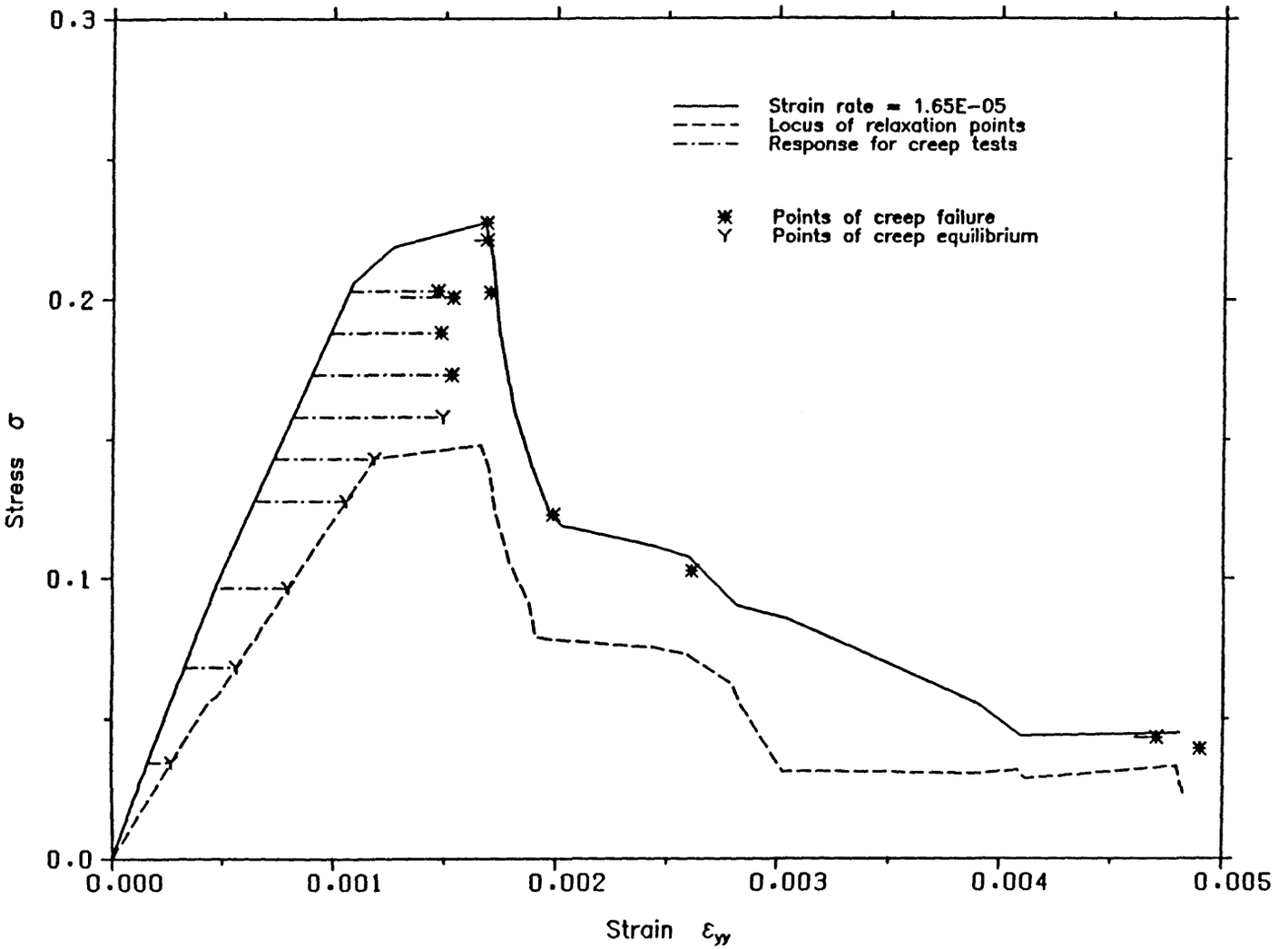

Fig. 7.21 Behaviour of the network model following creep tests

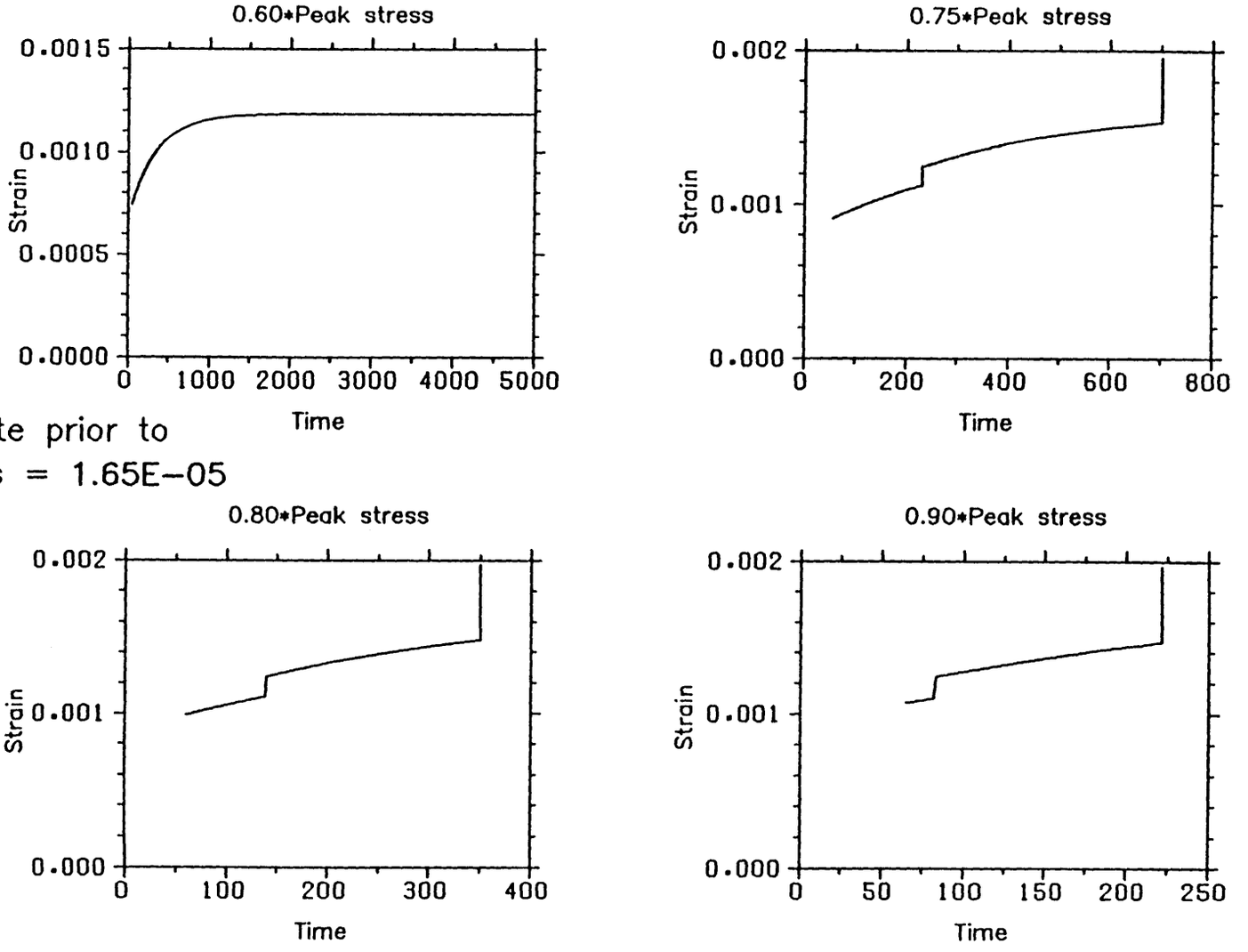

Fig. 7.22 Creep curves of a typical network

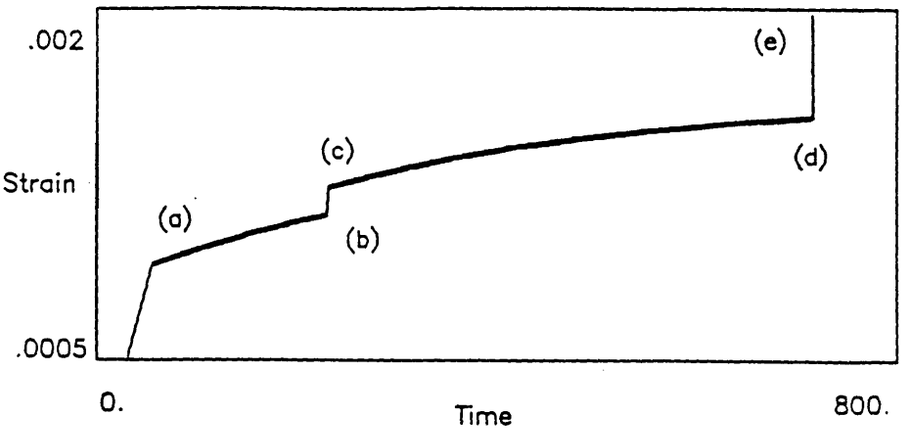

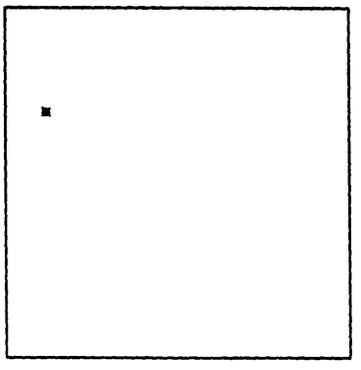

State of sample between a and b

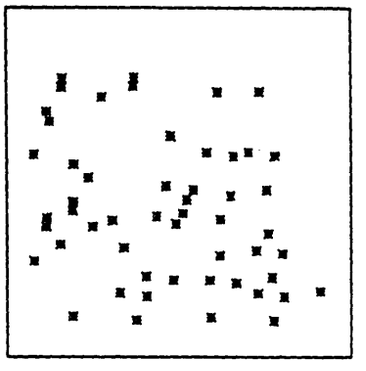

Distribution at seperation i.e. d to e

Strain rate prior to test = 1.65E−05

Stress = 0.7 of peak stress

Fig. 7.23 Increase of strain with time and the distribution of failed members of a typical network model under a creep test

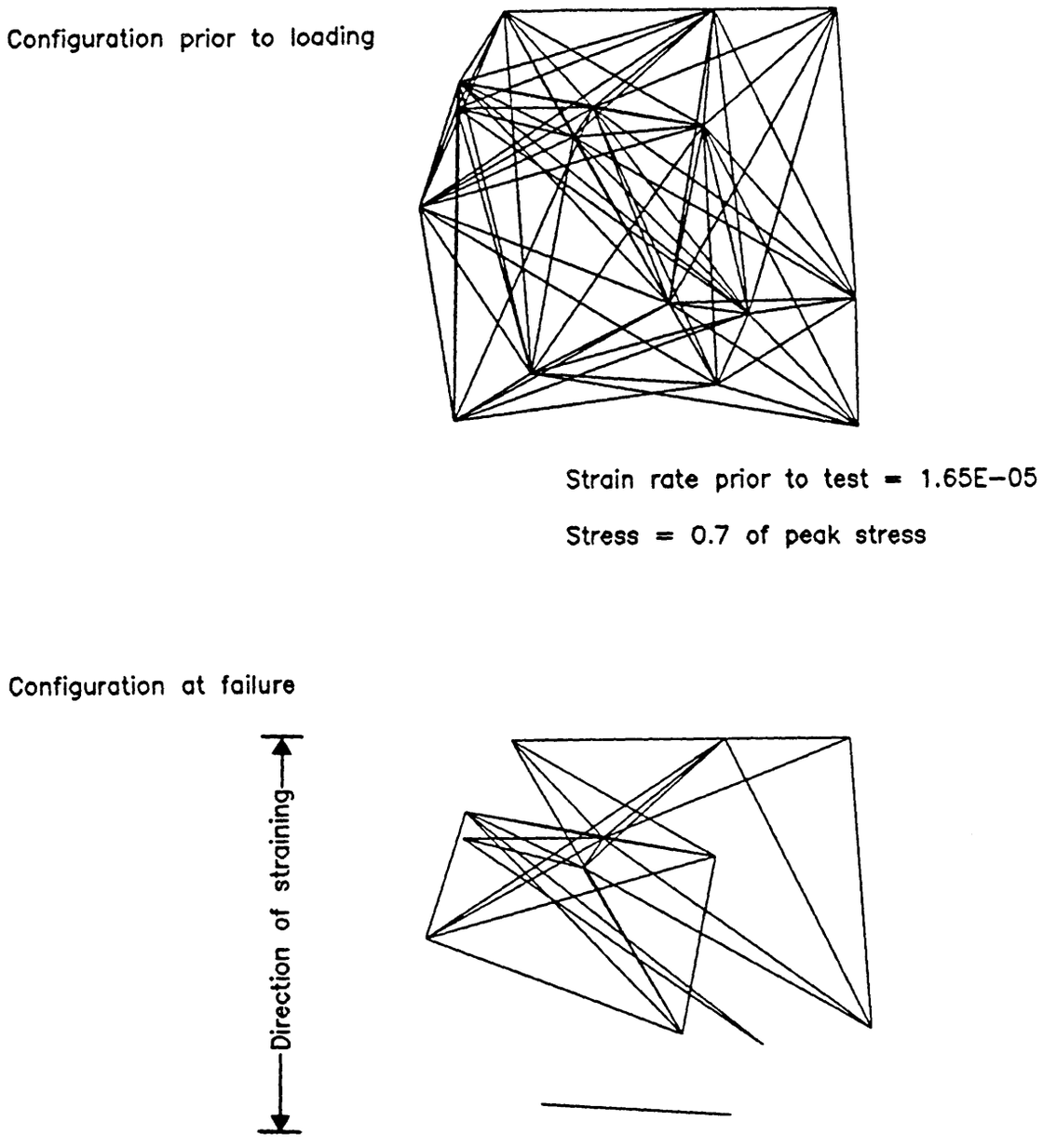

Fig. 7.24 Failure configuration of a typical network model under a creep test

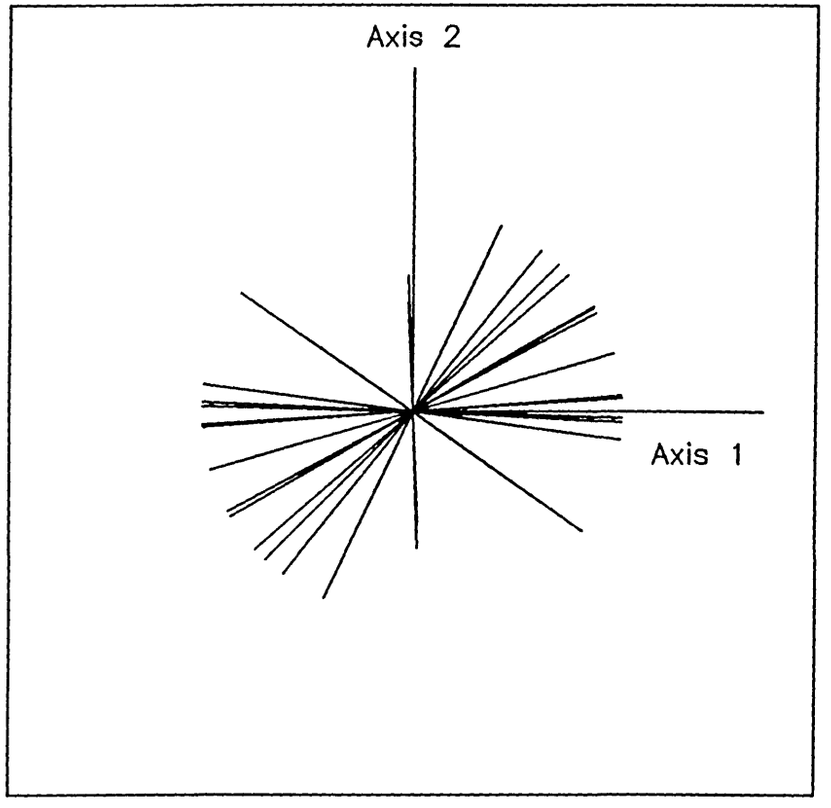

Each line resembles the centre line of a fibre bundle

Fig. 7.25 Orientations of the fibre bundles used in the different tests

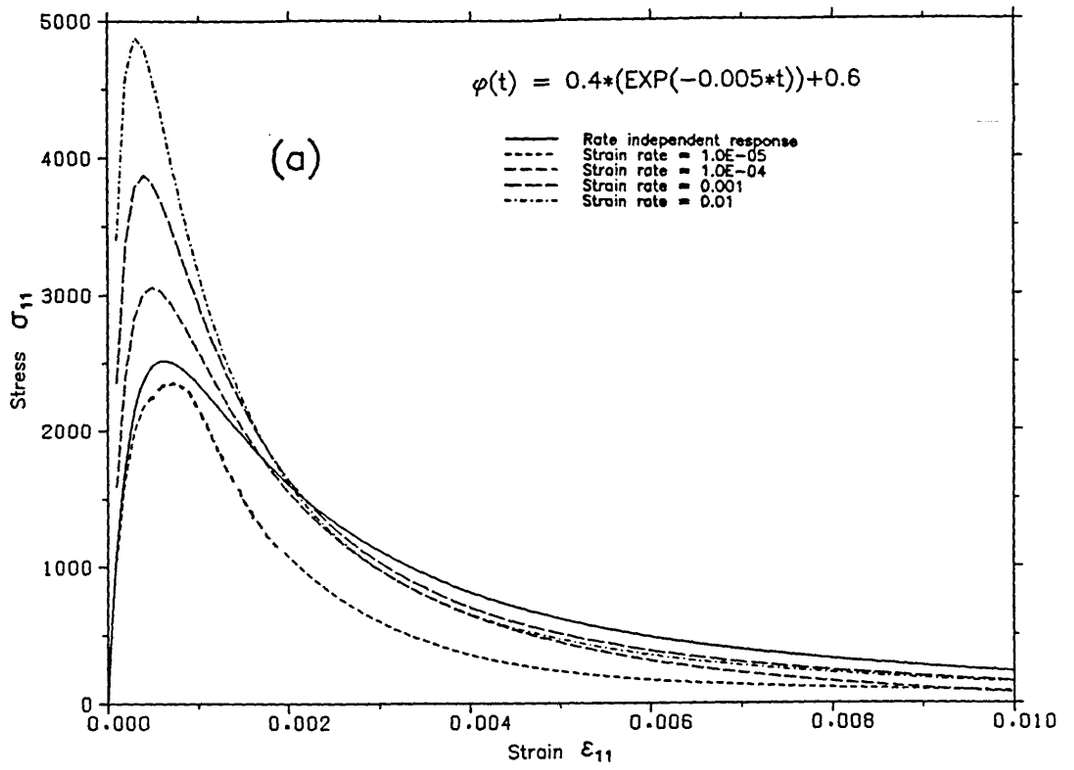

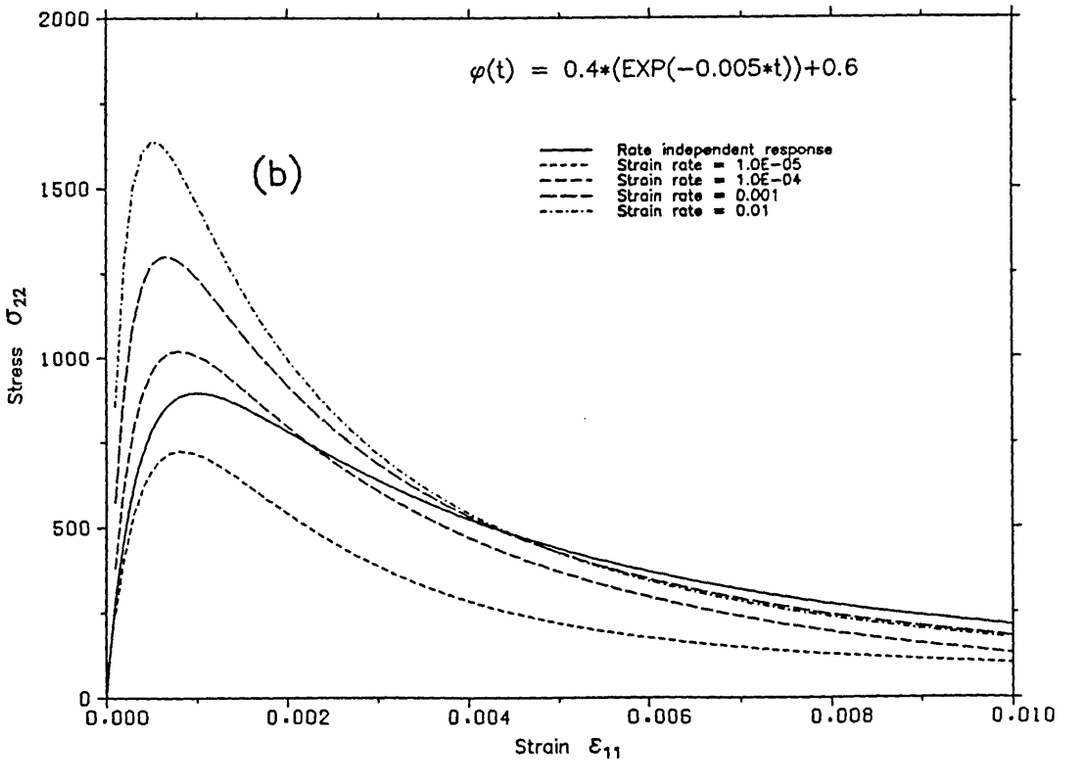

Fig. 7.26

Stress strain curves for a model of fibre bundles whose damage law is rate sensitive . Uniaxial extension tests

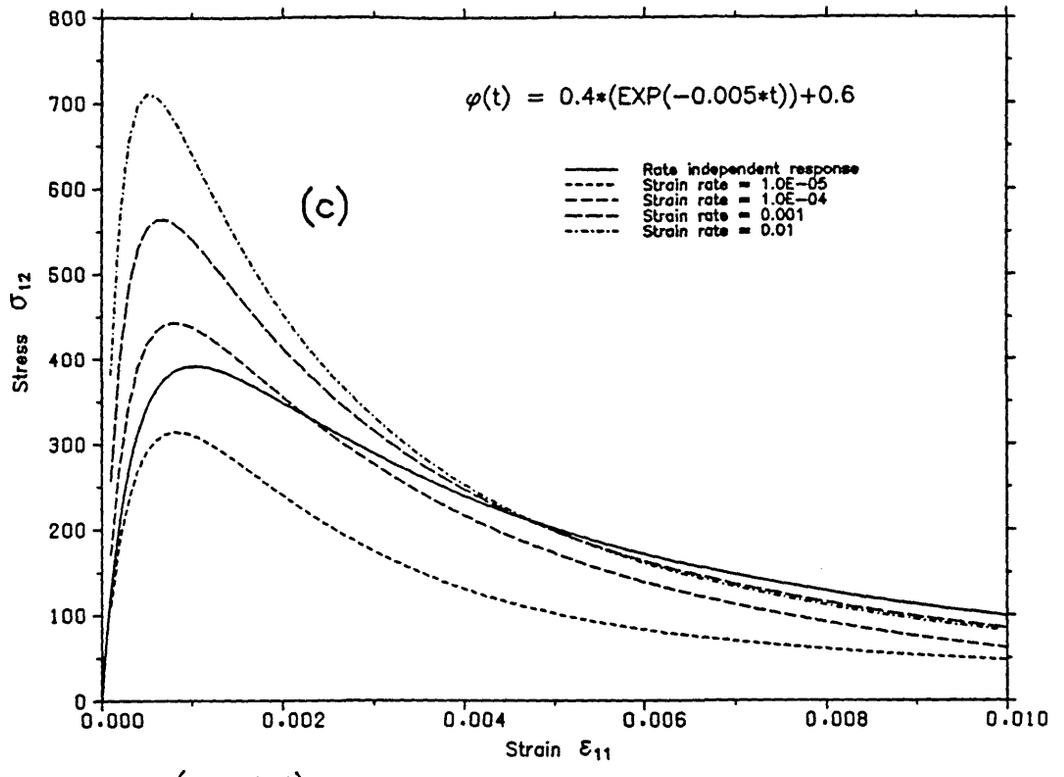

Fig. 7.26 (cont'd)

Stress strain curves for a model of fibre bundles whose damage law is rate sensitive . Uniaxial extension tests

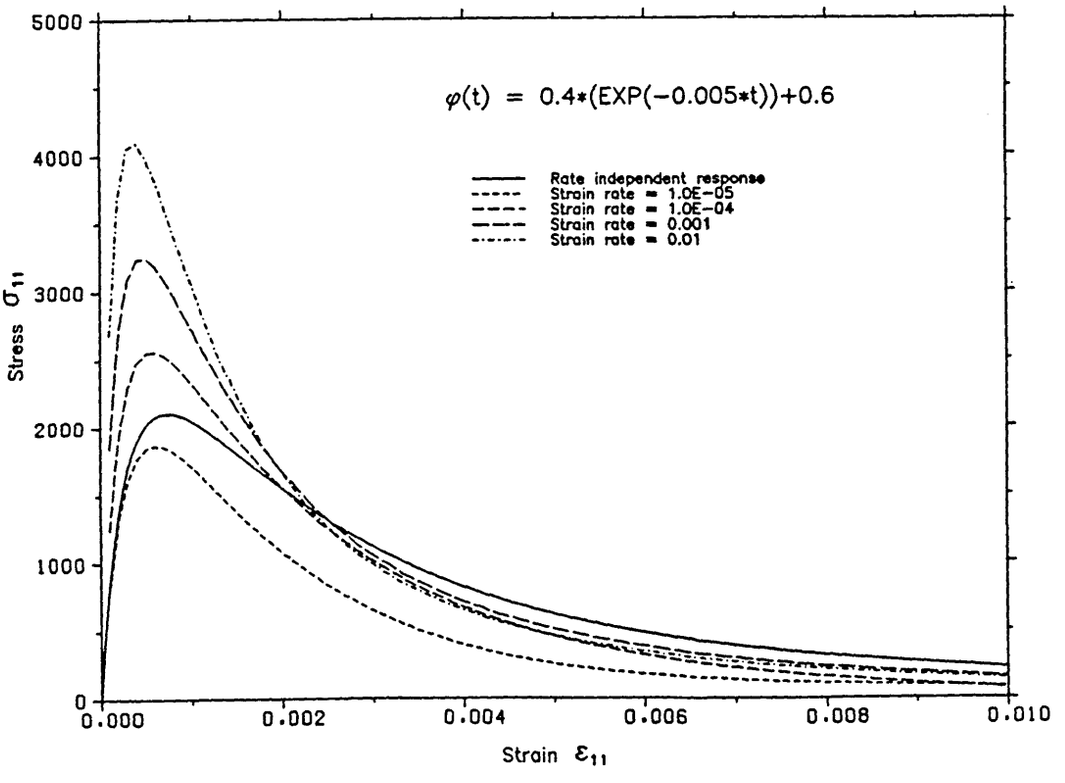

Fig. 7.27

Stress strain curves of a model of fibre bundles whose damage law is rate sensitive . Uniaxial tensile tests

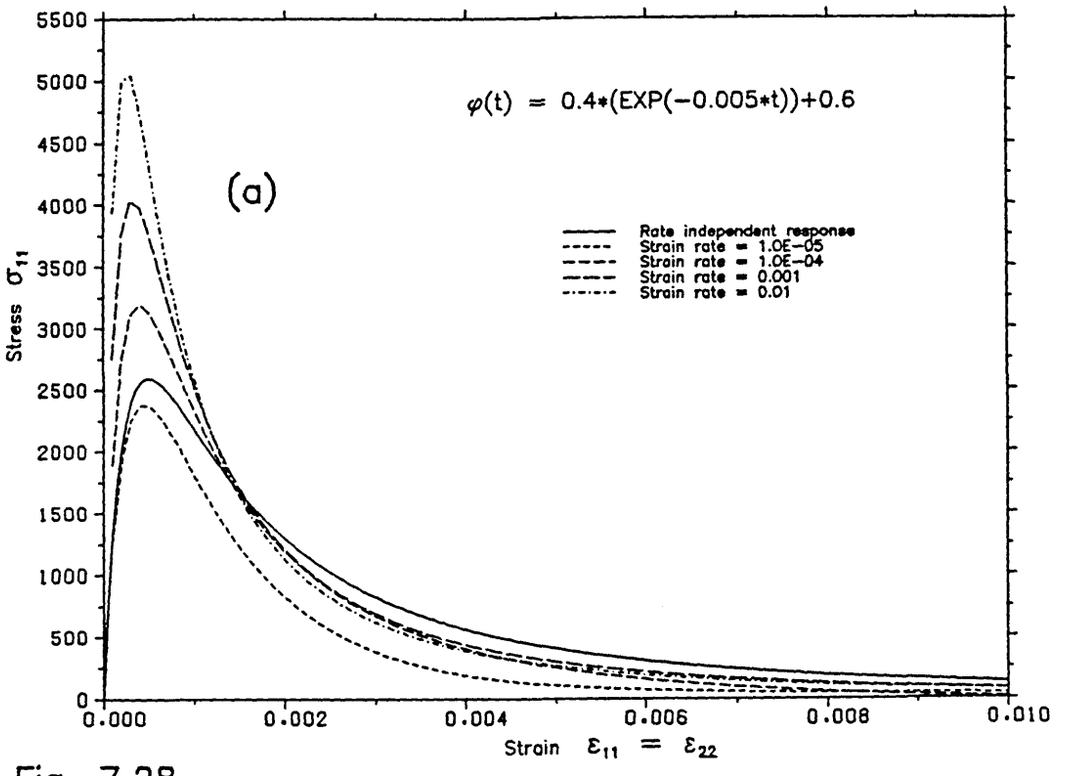

Fig. 7.28

Stress strain curves for a model of fibre bundles whose damage law is rate sensitive . Biaxial extension tests

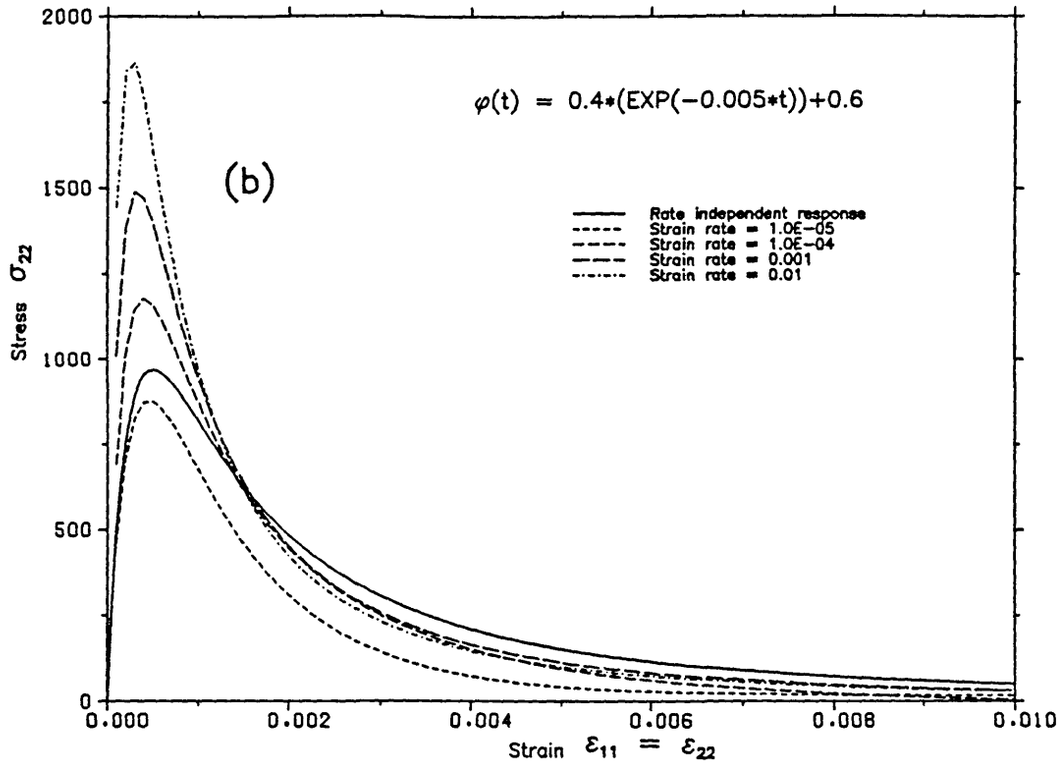

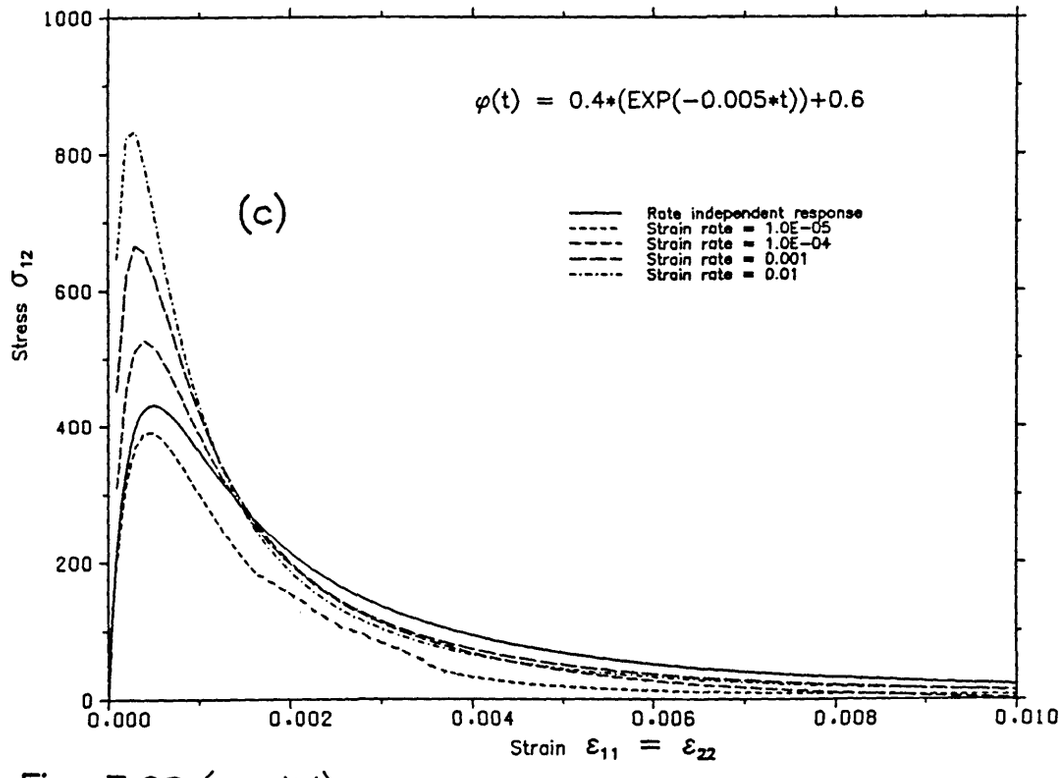

Fig. 7.28 (cont'd)
Stress strain curves for a model of fibre bundles whose damage law is rate sensitive . Biaxial extension tests

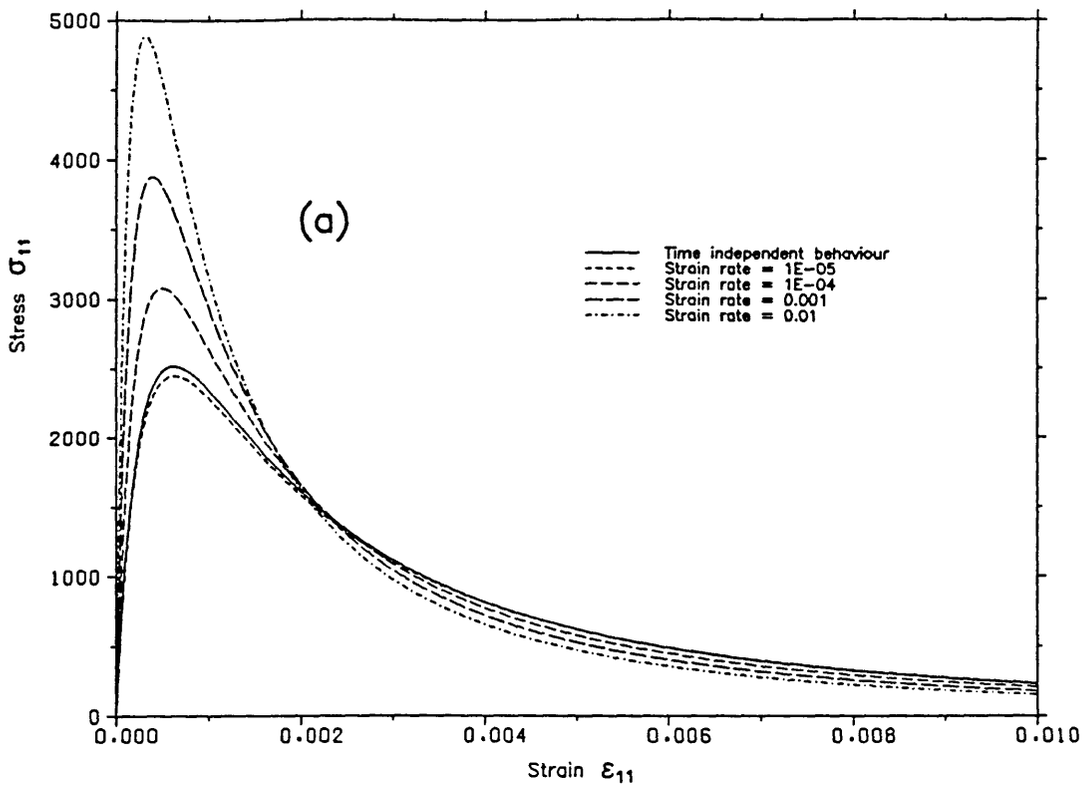

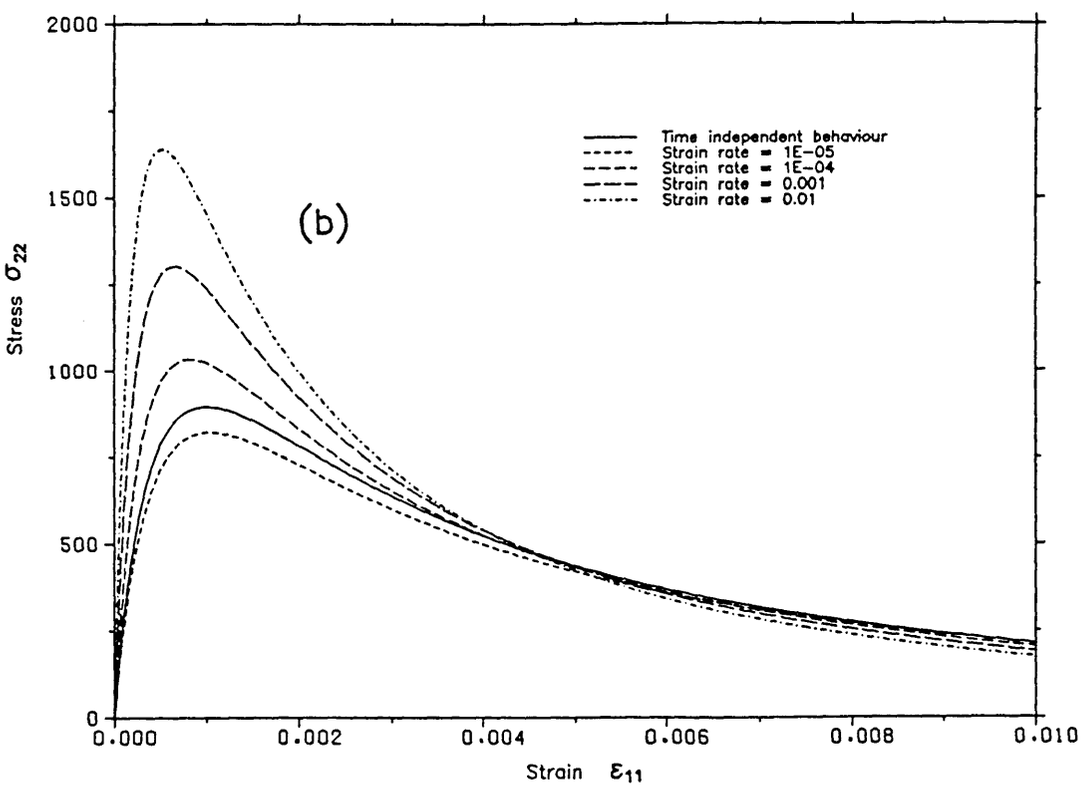

Fig. 7.29
The instantaneous response of a model made of fibre bundles whose damage law is rate sensitive. Uniaxial extension tests

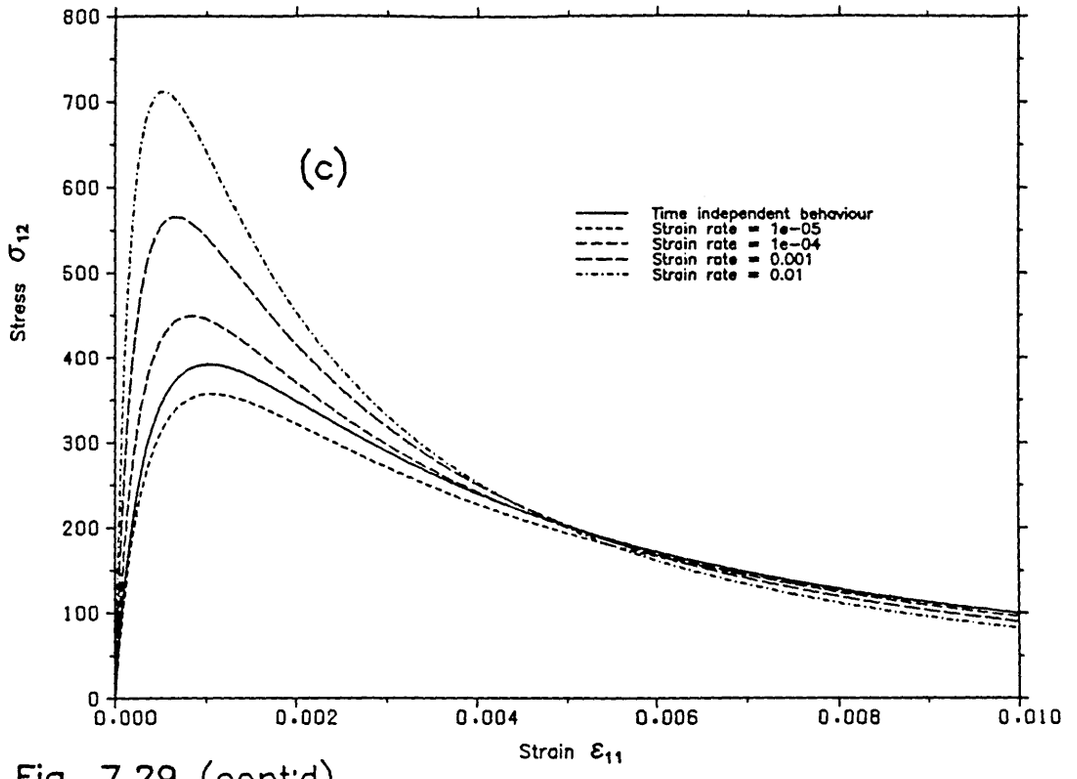

Fig. 7.29 (cont'd)
The instantaneous response of a model made of fibre bundles whose damage law is rate sensitive. Uniaxial extension tests

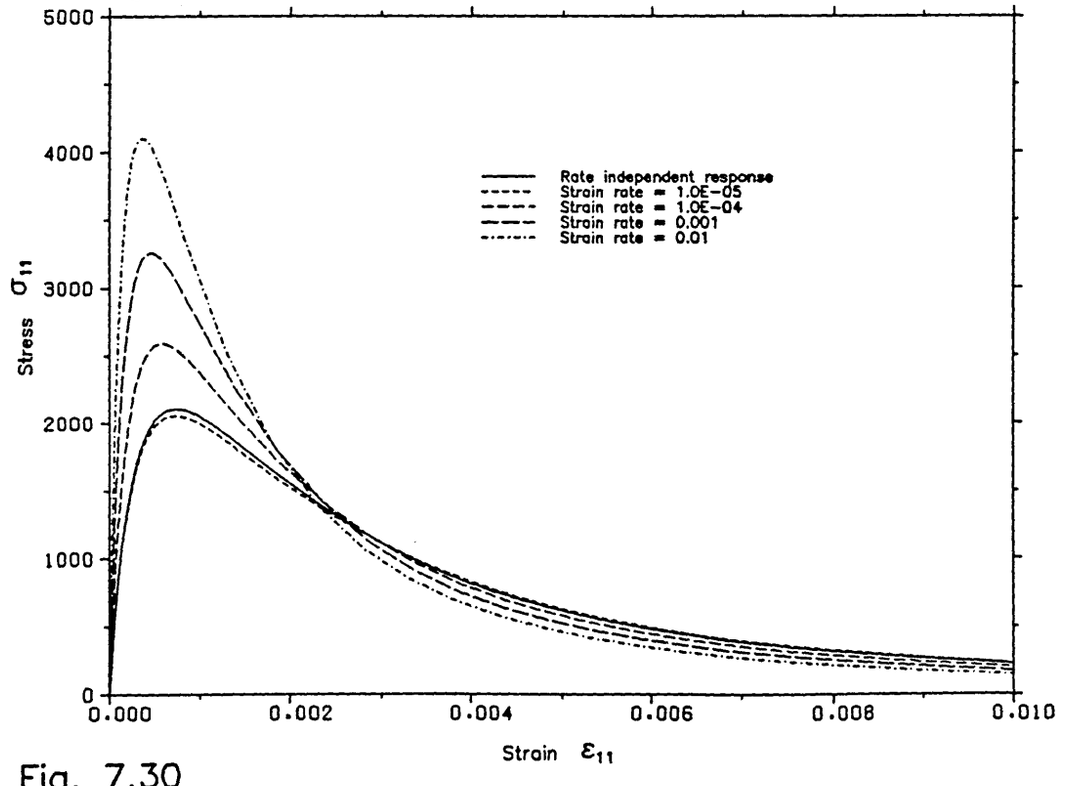

Fig. 7.30
The instantaneous response of a model of fibre bundles whose damage law is rate sensitive. Uniaxial tensile tests

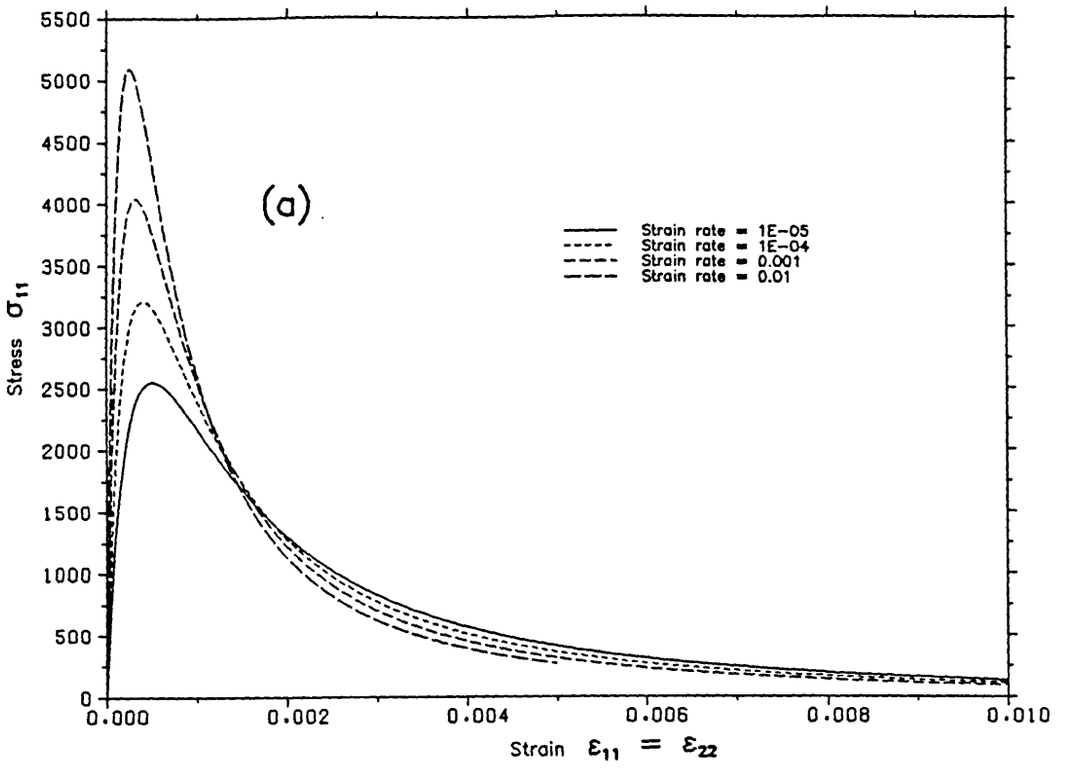

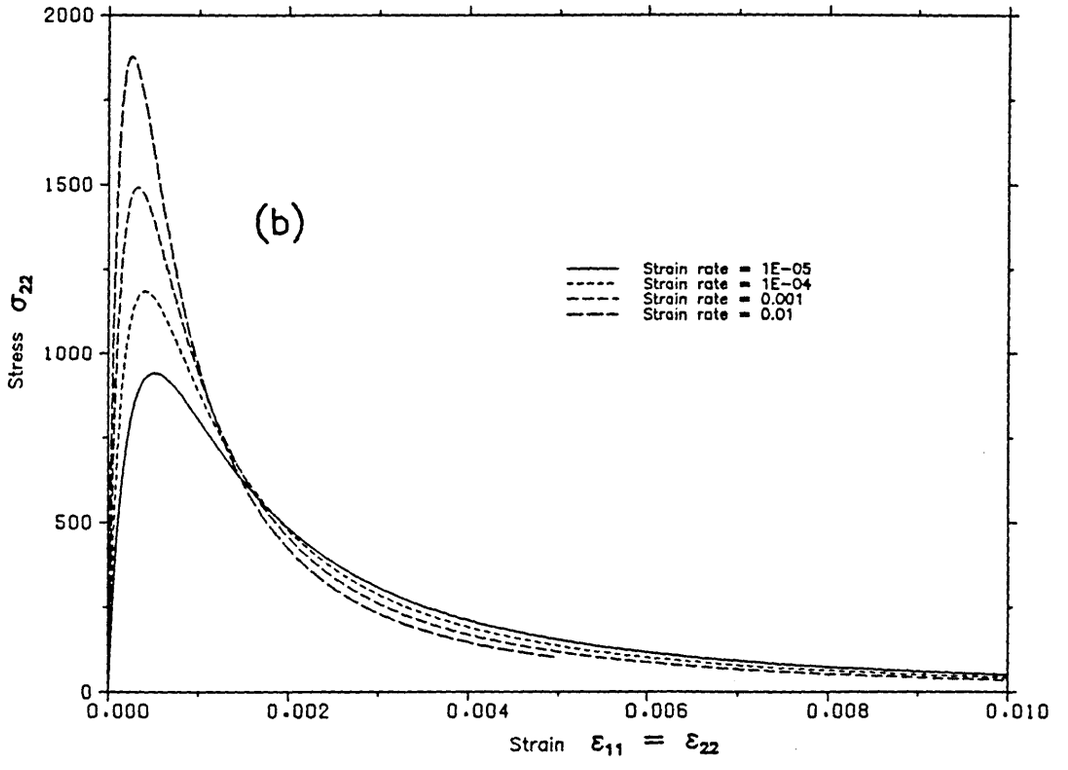

Fig. 7.31
The instantaneous response of a model of fibre bundles whose damage law is rate sensitive. Biaxial extension tests

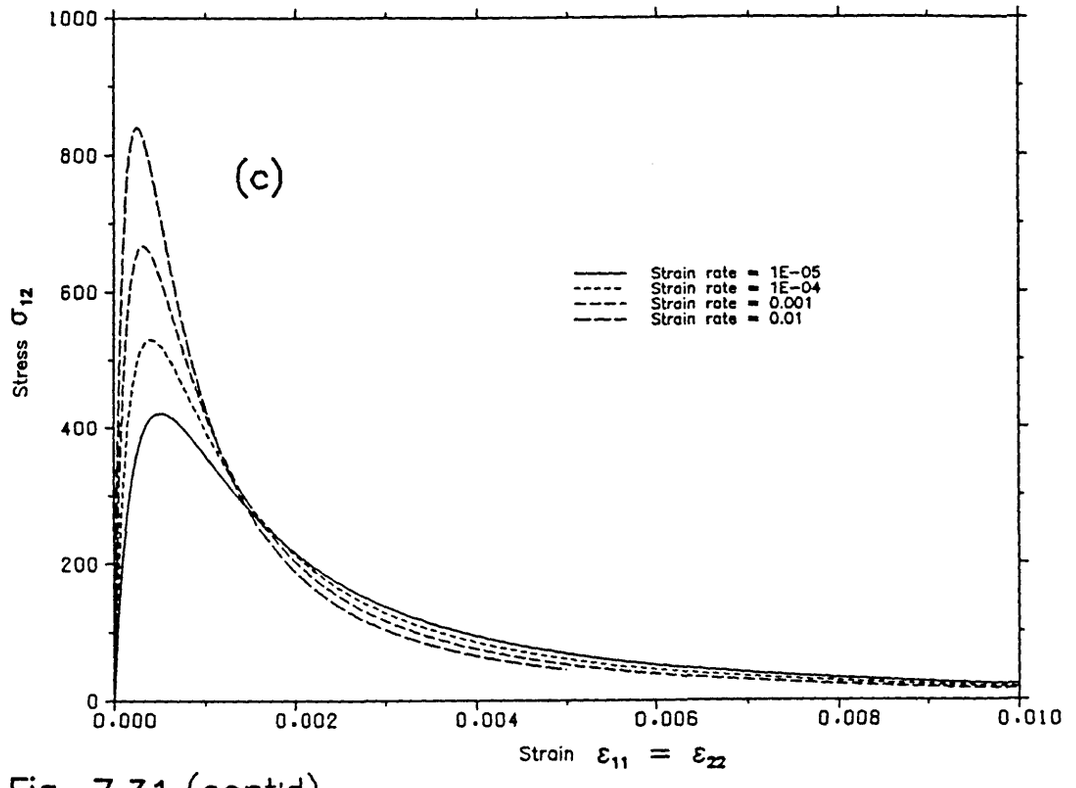

Fig. 7.31 (cont'd)
The instantaneous response of a model of fibre bundles whose damage law is rate sensitive · Biaxial extension tests

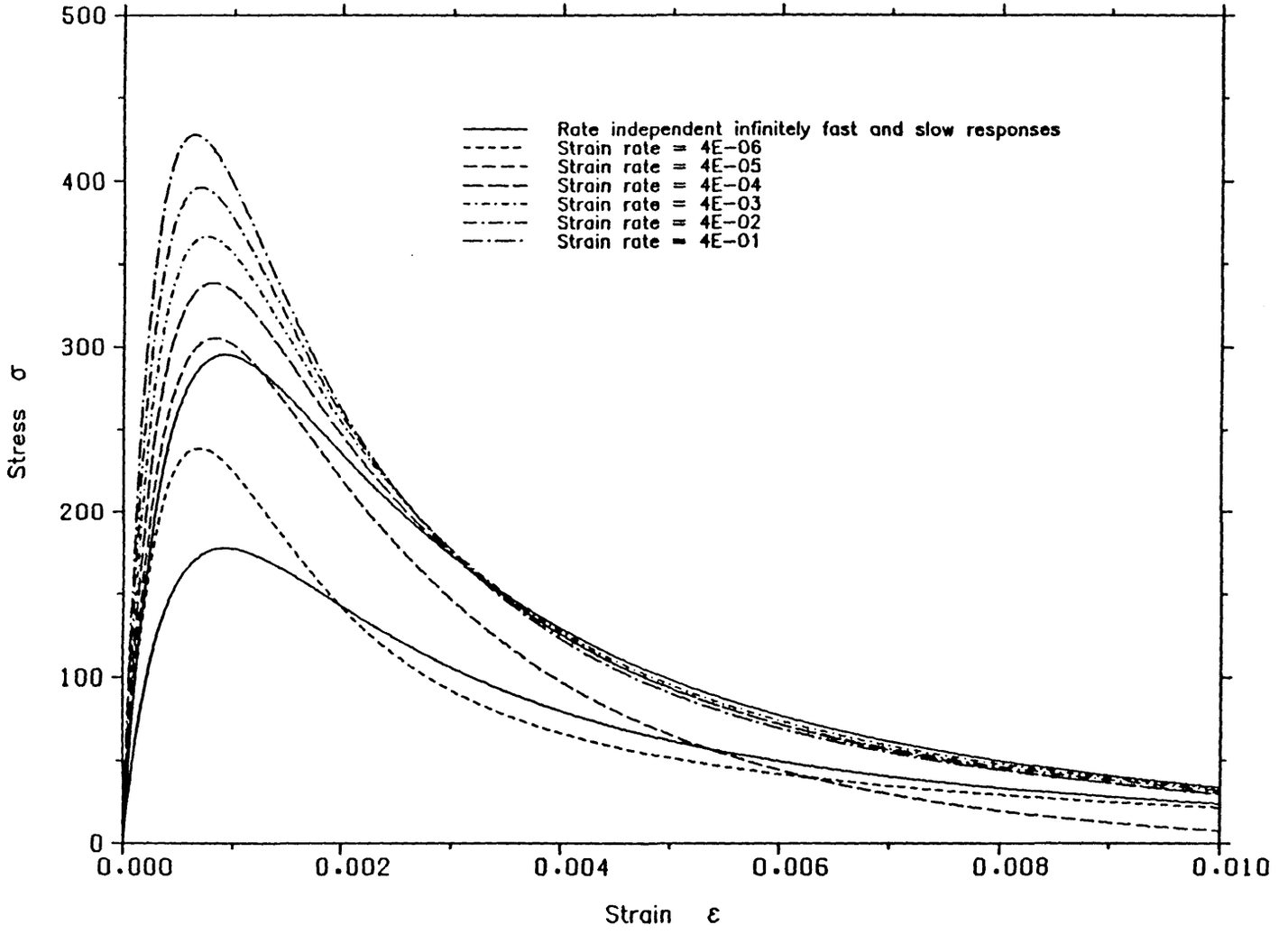

Fig. 7.32 Stress strain curves of a system of two rate sensitive fibre bundles in series

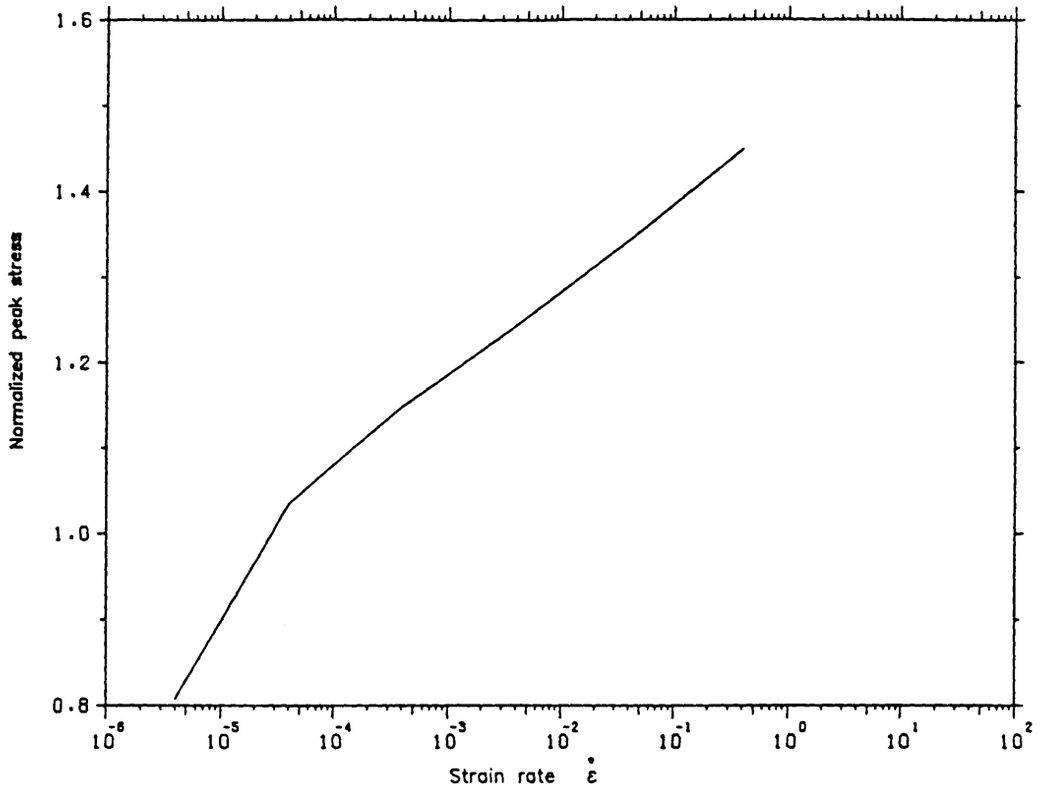

Fig. 7.33 Change of peak stress with strain rate

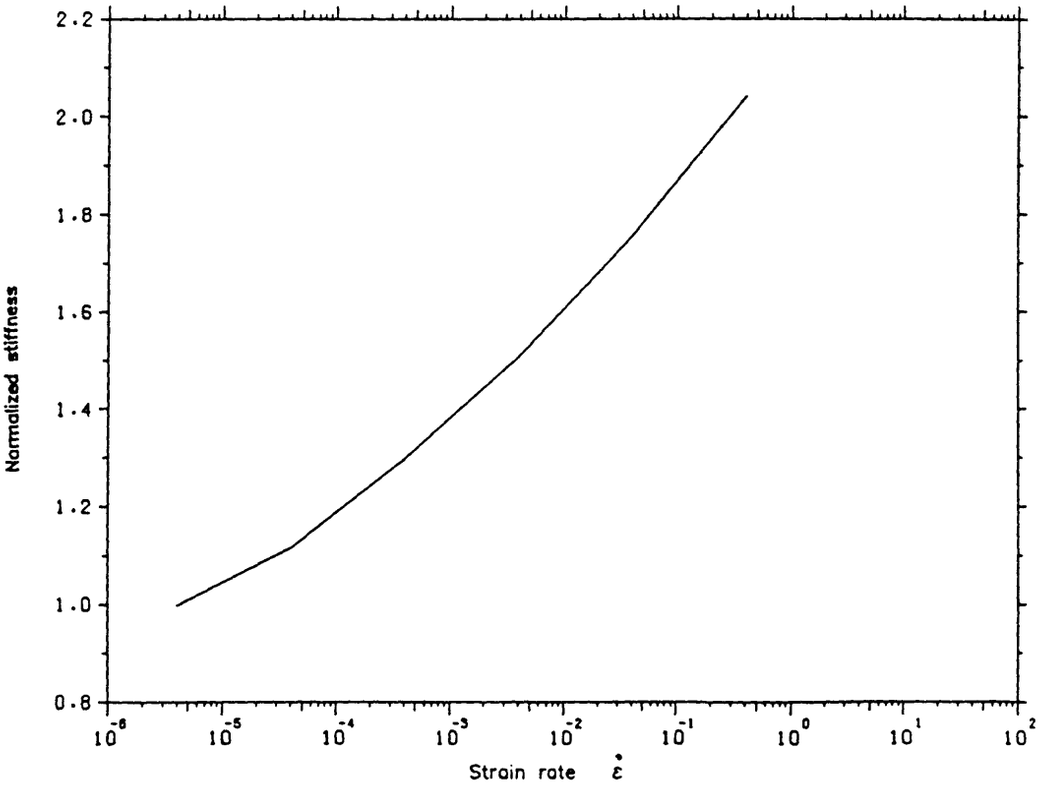

Fig. 7.34 Change of initial tangent stiffness with strain rate

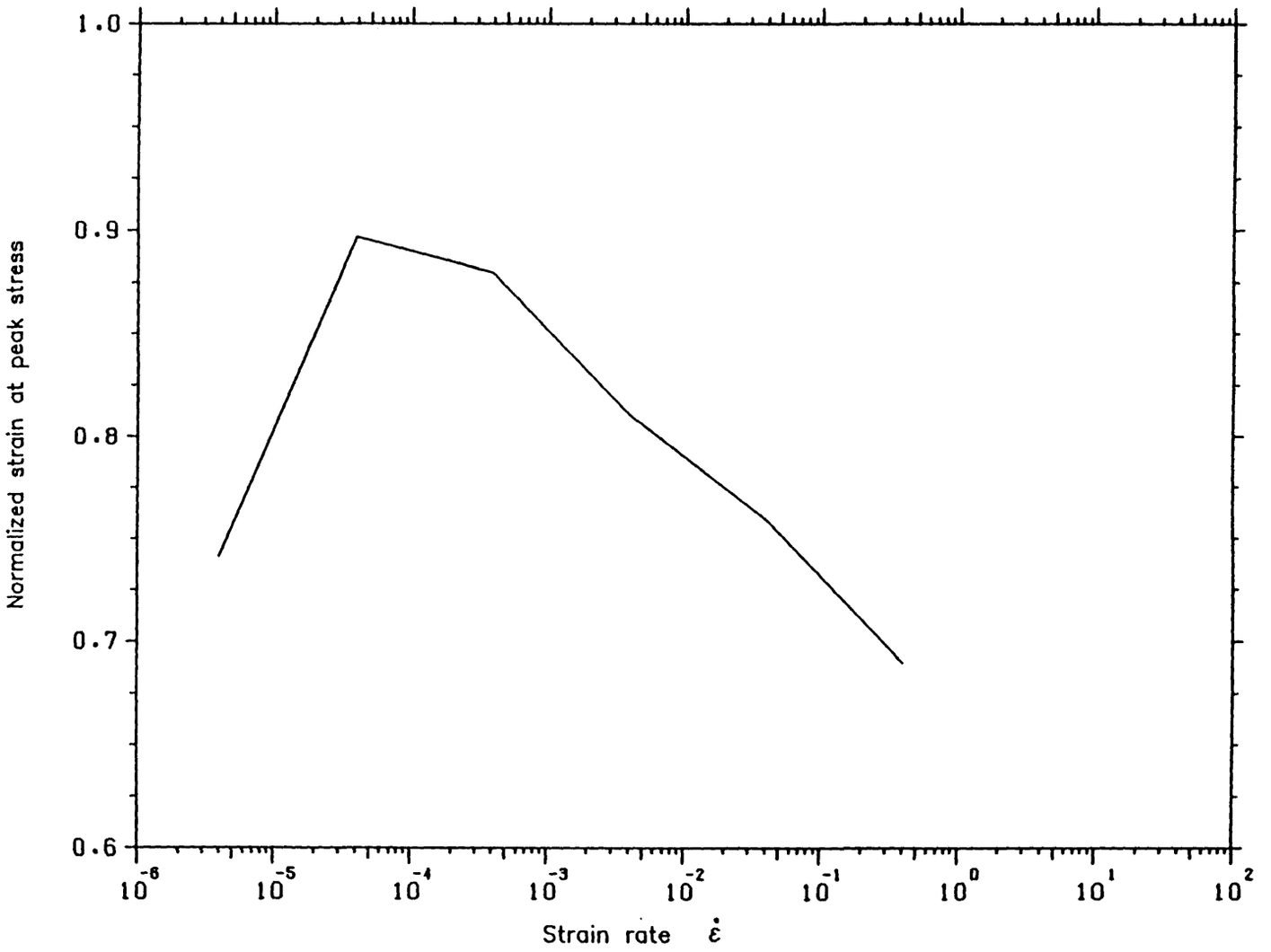

Fig. 7.35 Change of strain at peak stress with strain rate

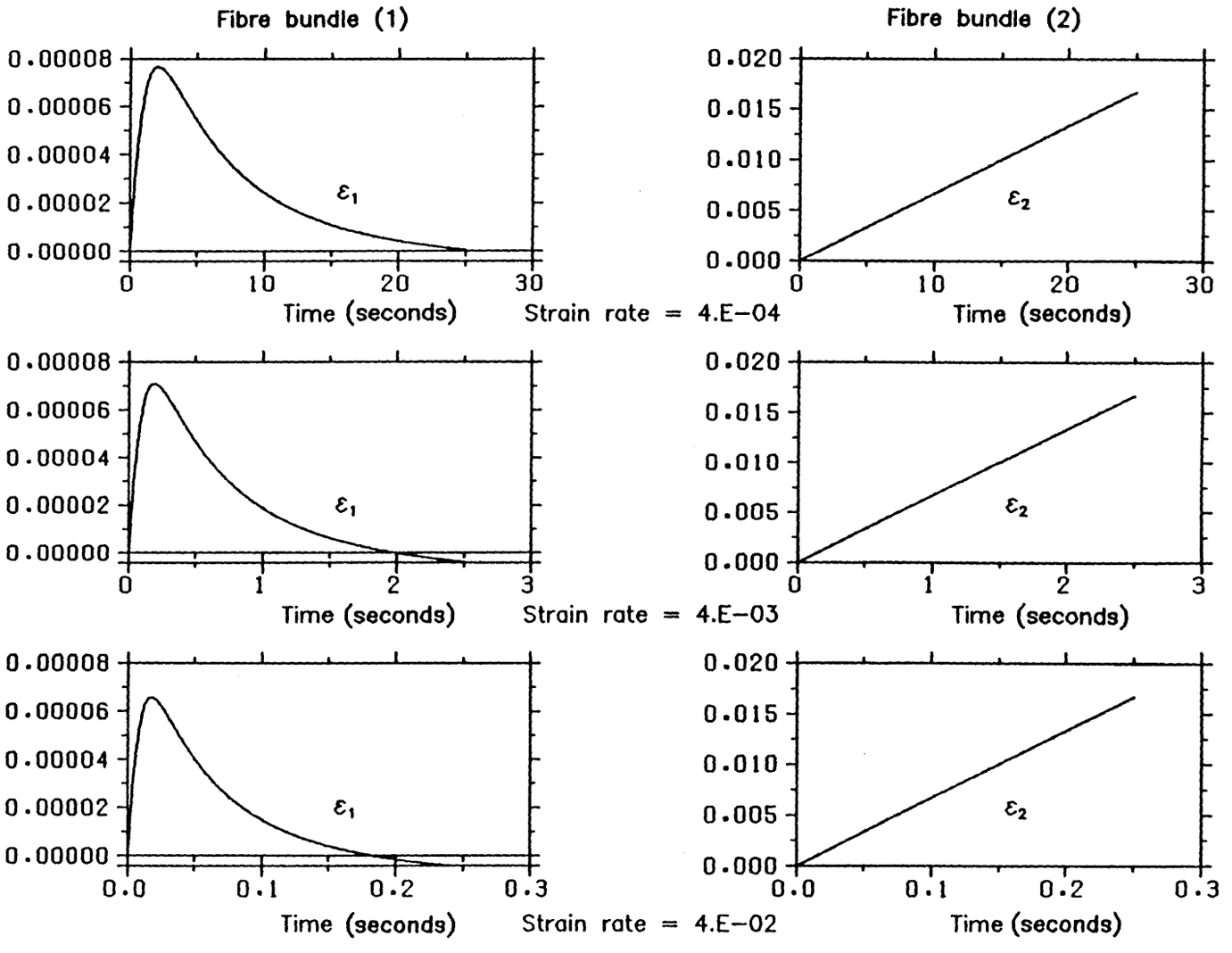

Fig. 7.36 Time histories of strain of individual fibre bundles of the model

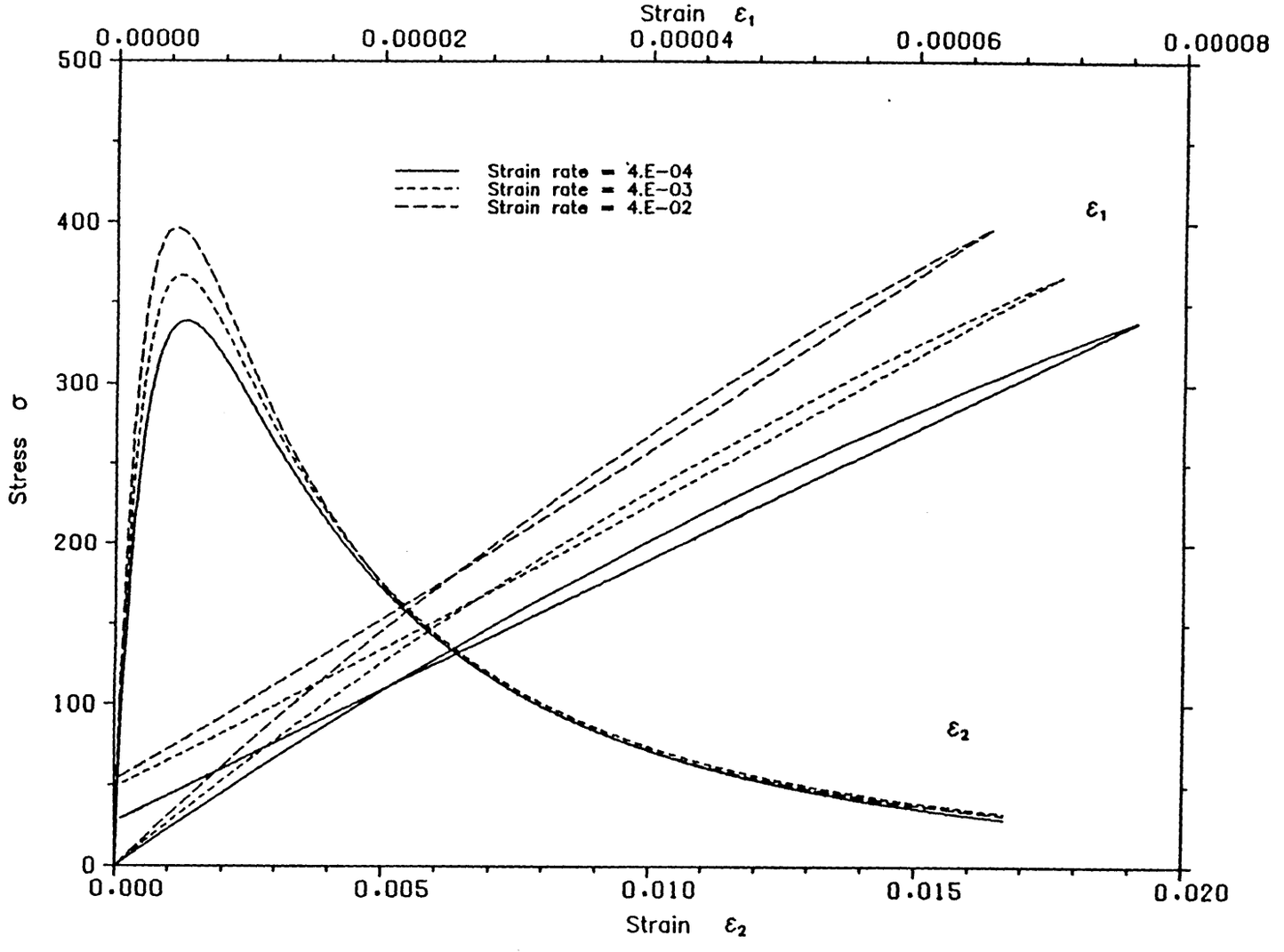

Fig. 7.37 Stress strain curves of individual fibre bundles of the rate dependent model

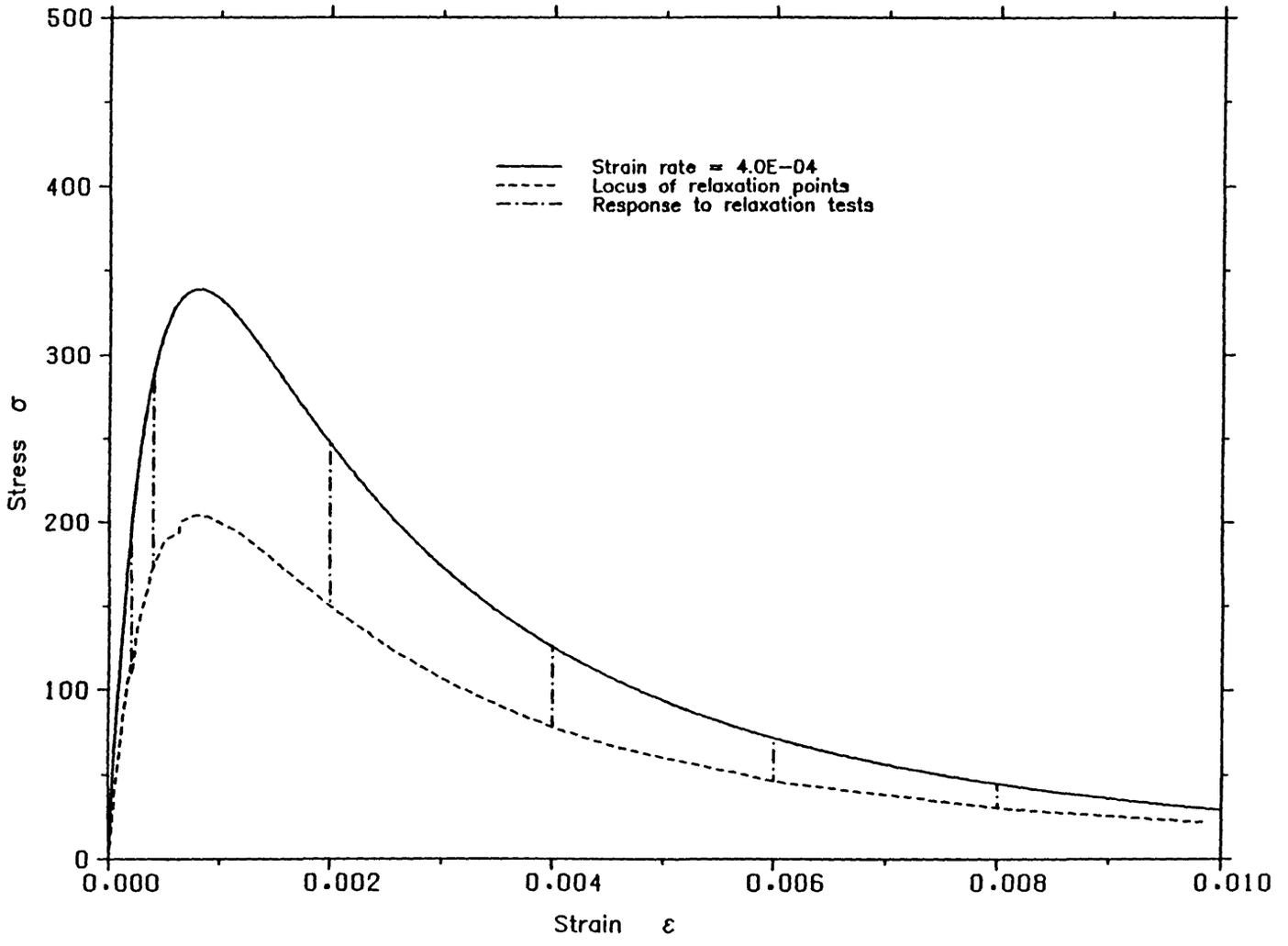

Fig. 7.38 Behaviour of a system of two rate sensitive fibre bundles in series under relaxation tests

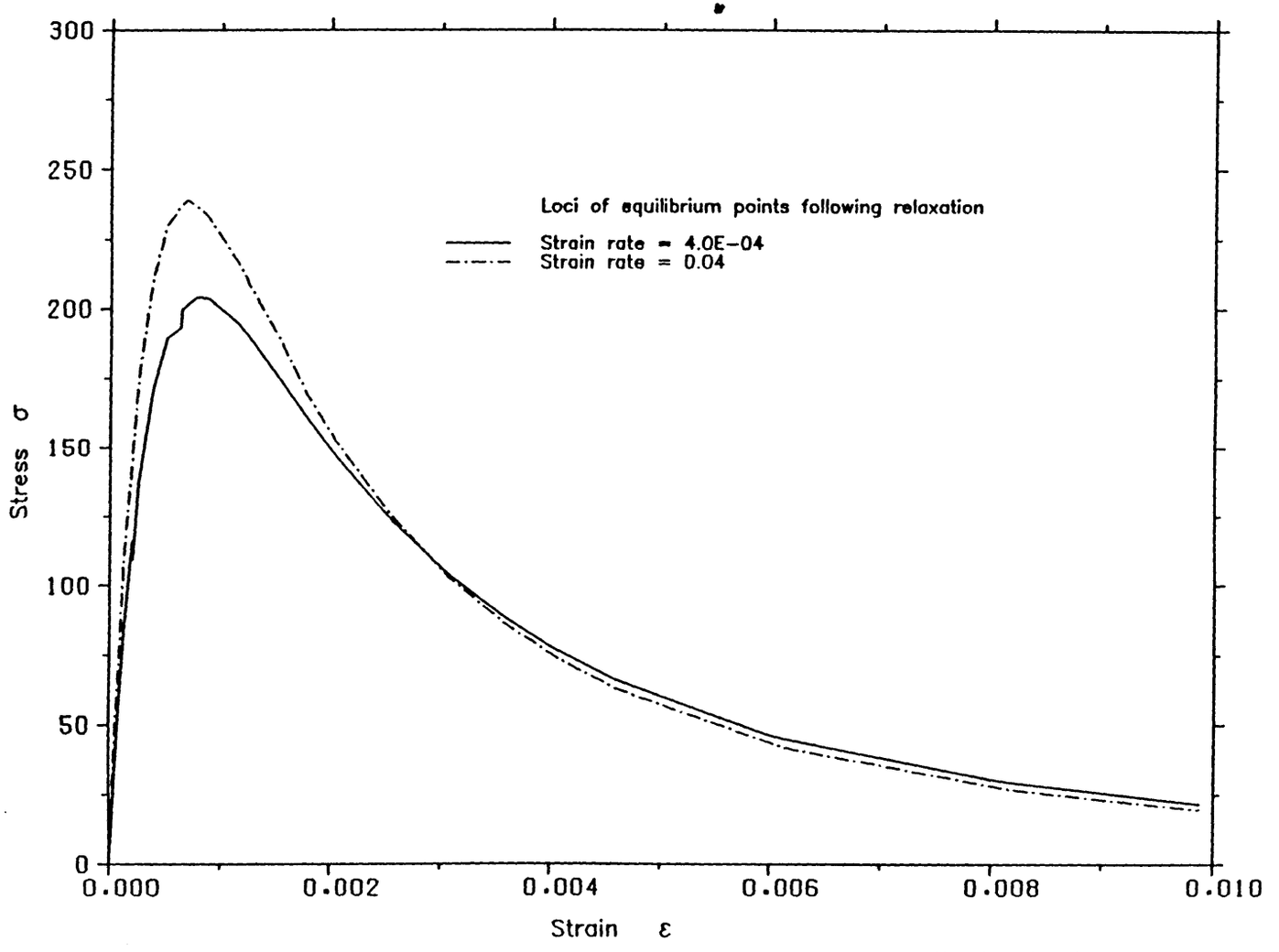

Fig. 7.39 Change of the infinitely slow response with applied strain rate

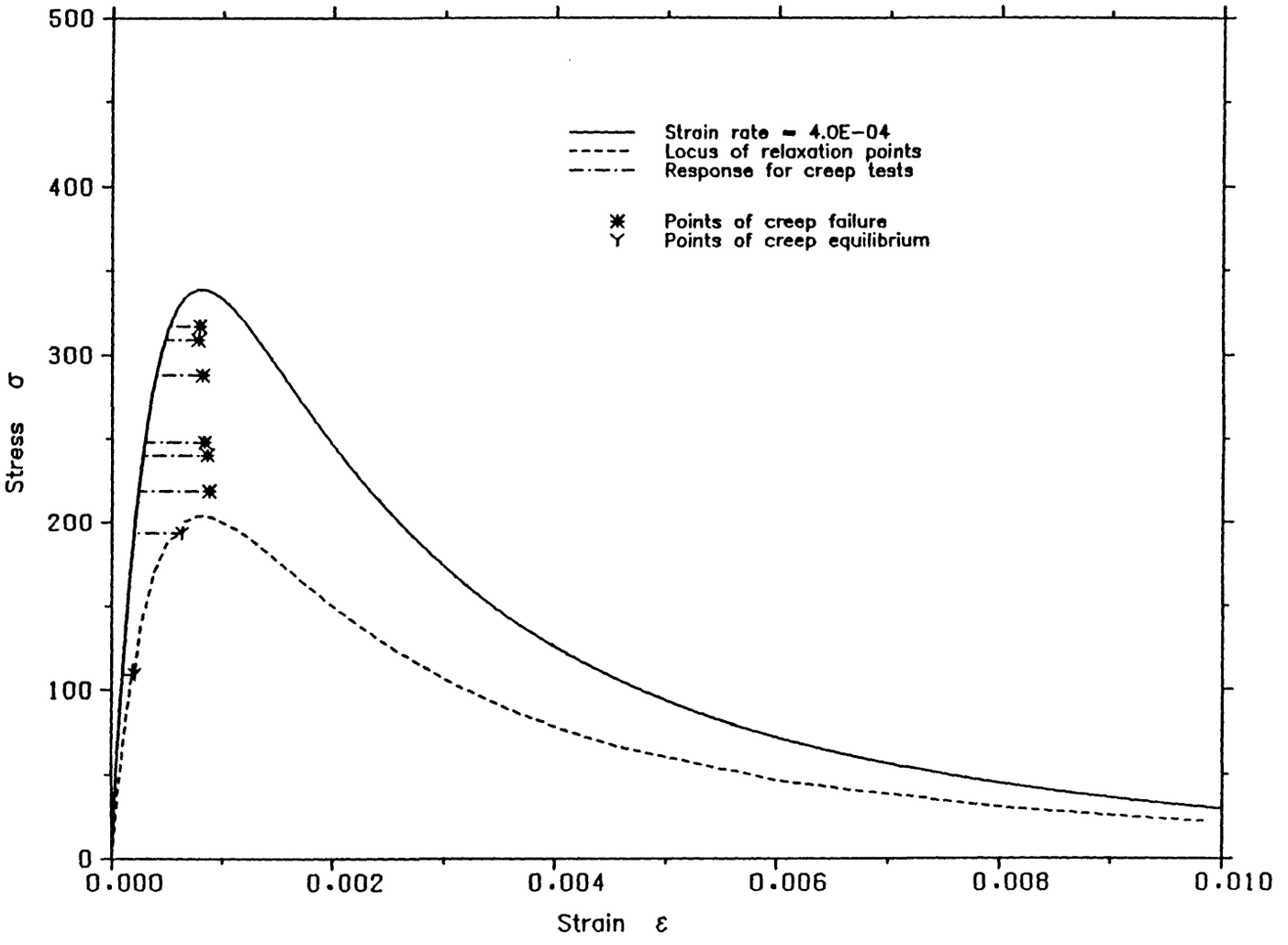

Fig. 7.40 Behaviour of a system of two rate sensitive fibre bundles in series under creep tests

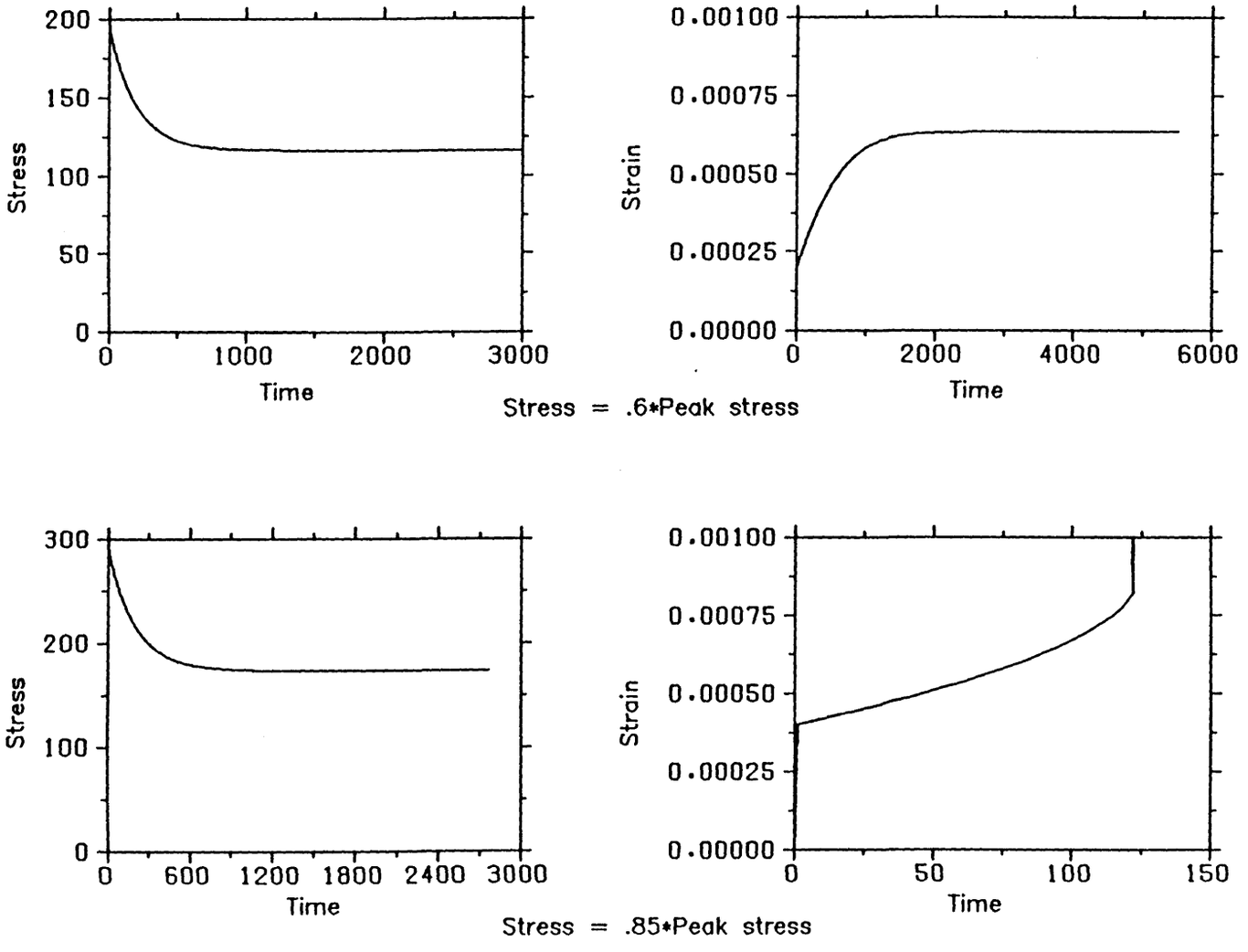

Fig. 7.41 Relaxation and creep curves at two levels of stress
Strain rate prior to test = 4.0E-04

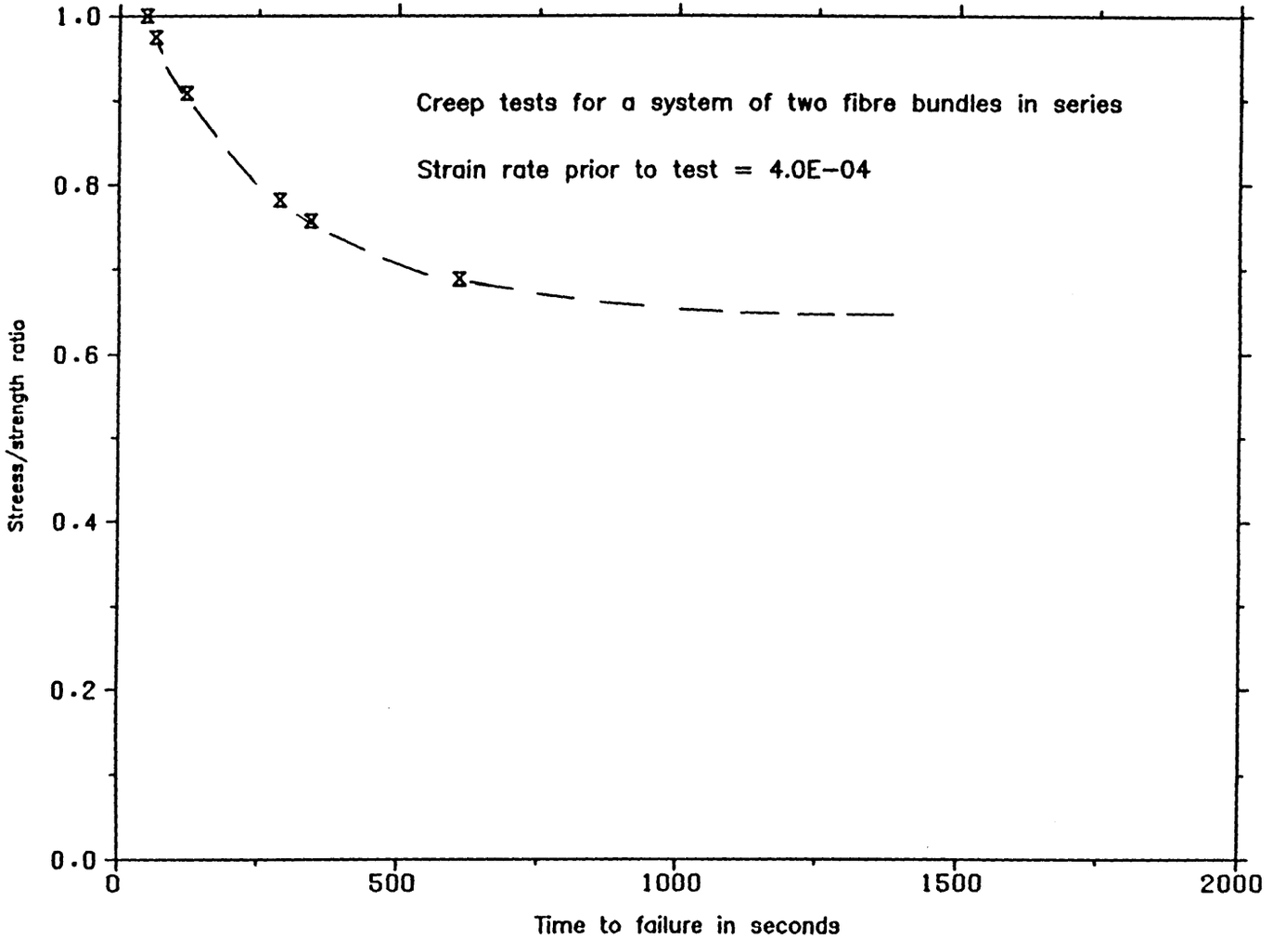

Fig. 7.42 Change of the time to failure with the stress/strength ratio in creep tests

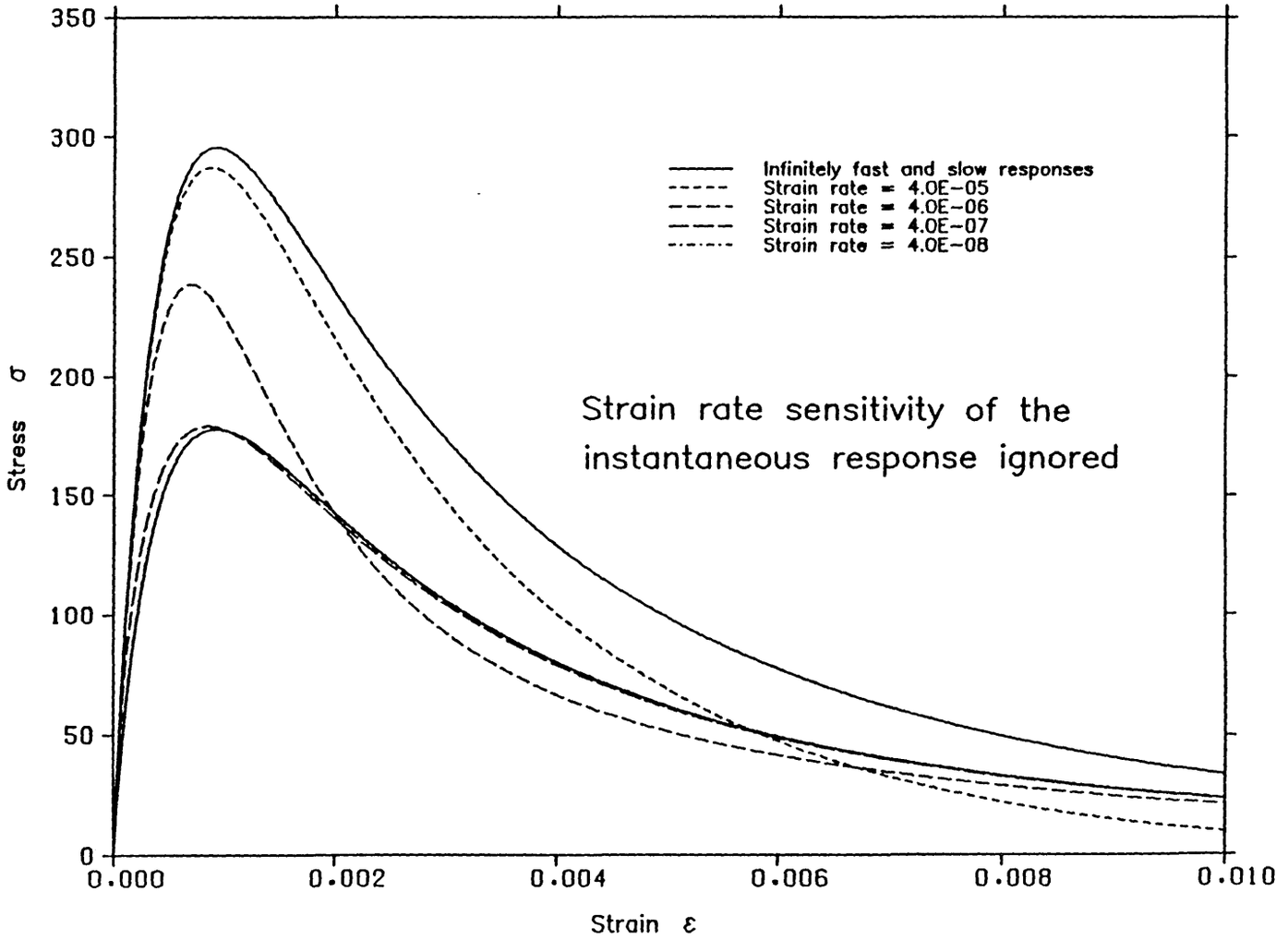

Fig. 7.43 Stress strain curves of the model at different strain rates

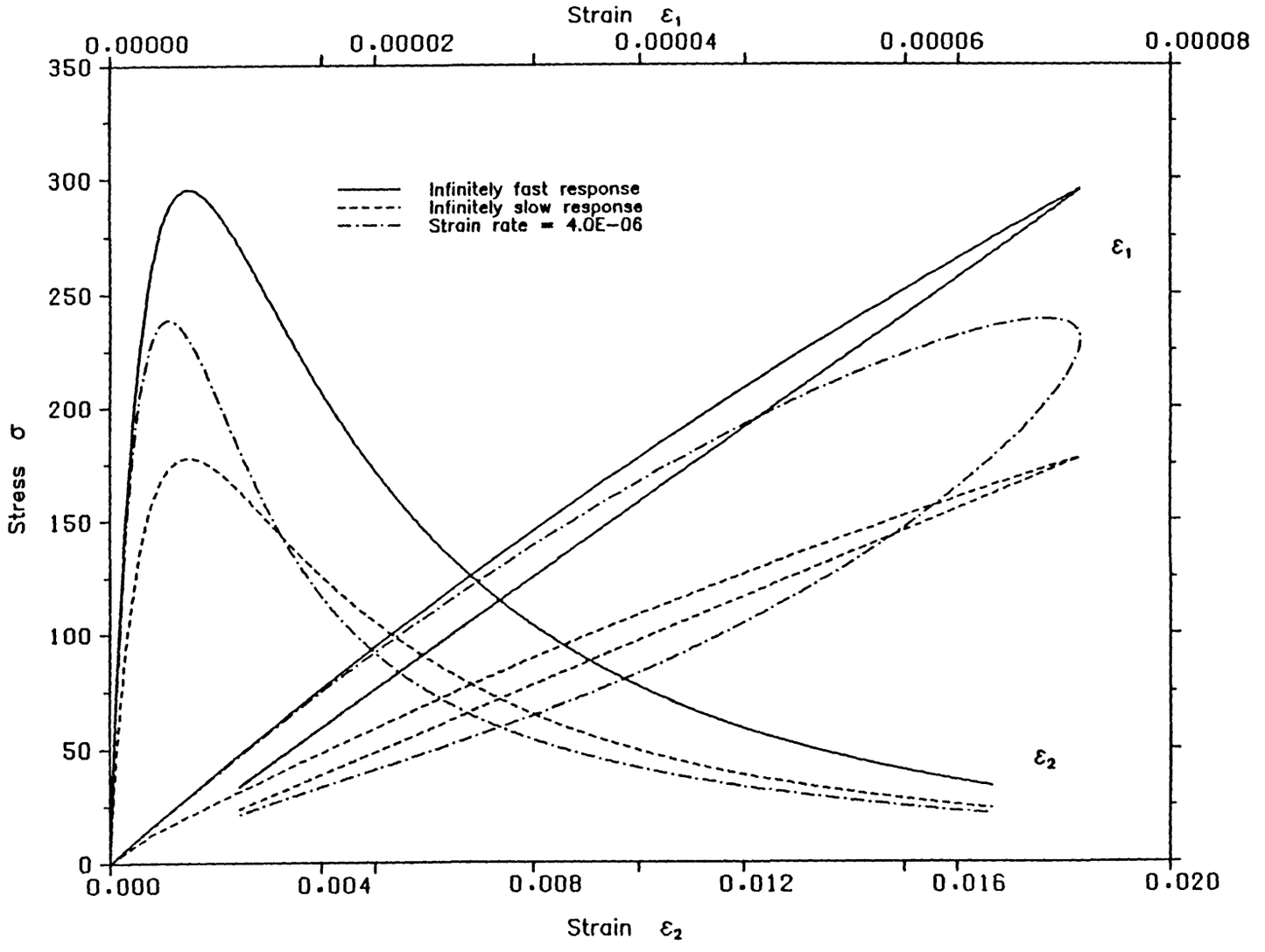

Fig. 7.44 Stress strain curves of individual fibre bundles of the model

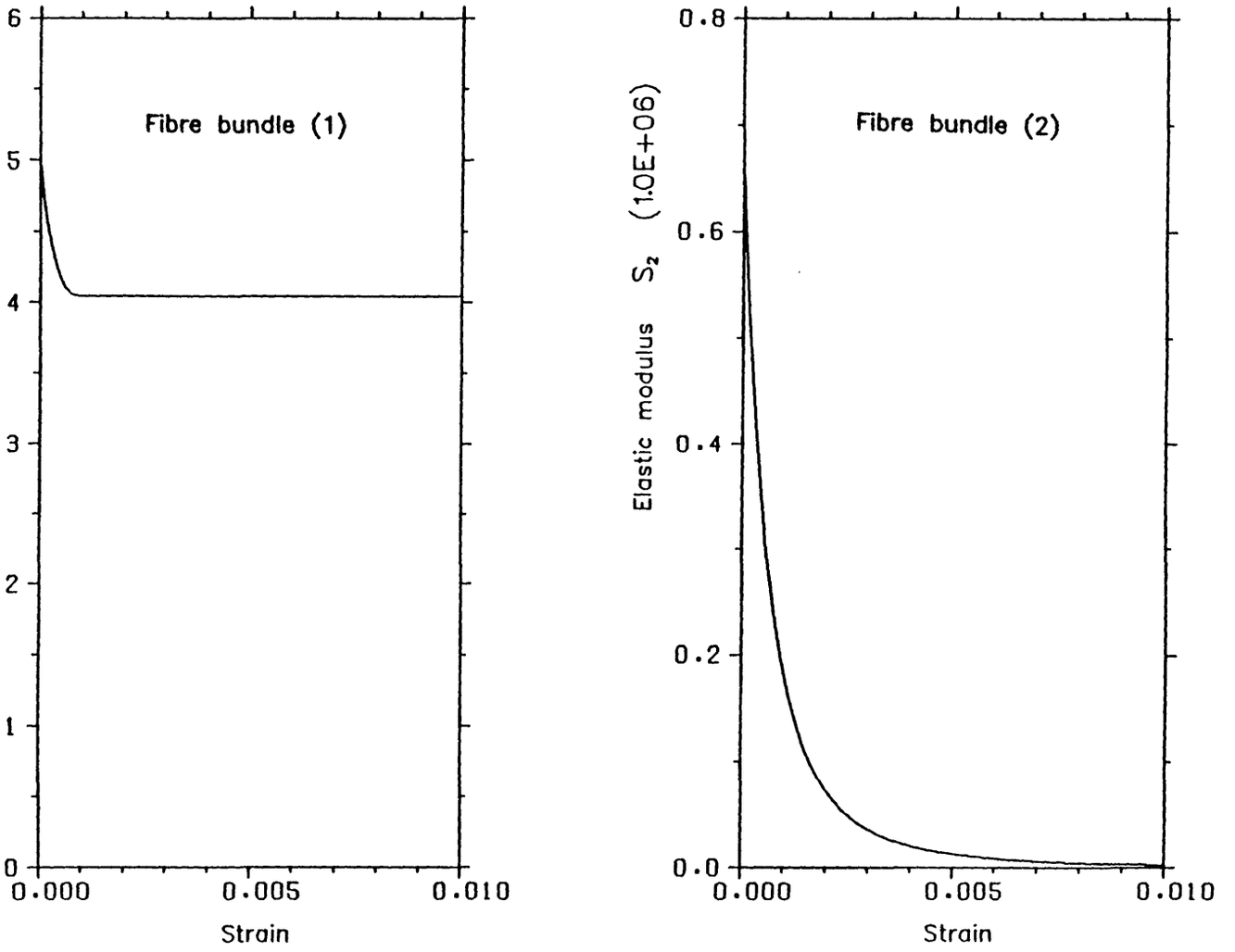

Fig. 7.45 Change of the elastic moduli of the individual fibre bundles of the model

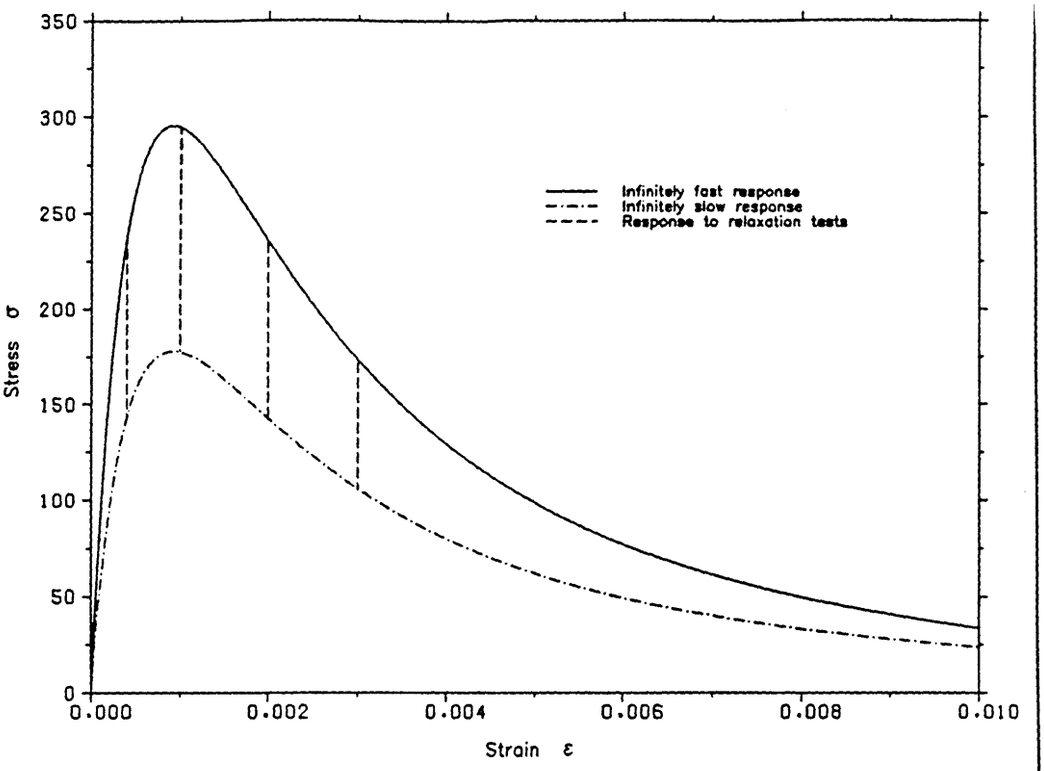

Fig. 7.46 Behaviour of a system of two fibre bundles in series under relaxation tests. Strain rate sensitivity of the instantaneous response ignored

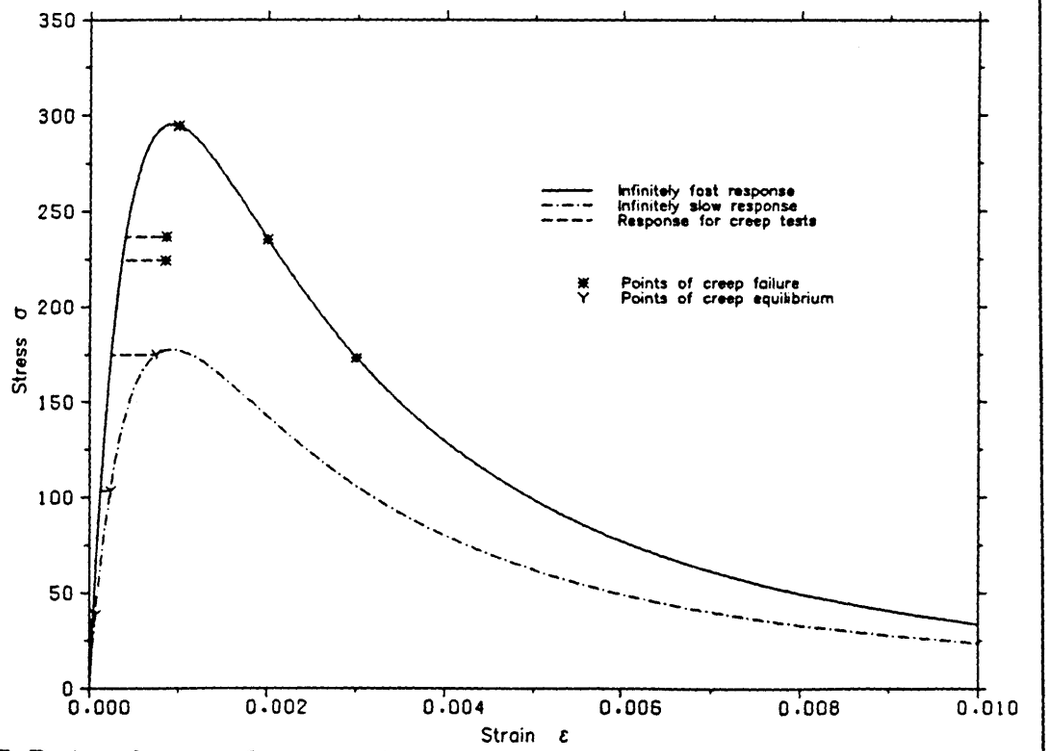

Fig. 7.47 Behaviour of a system of two fibre bundles in series under creep tests. Strain rate sensitivity of the instantaneous response ignored

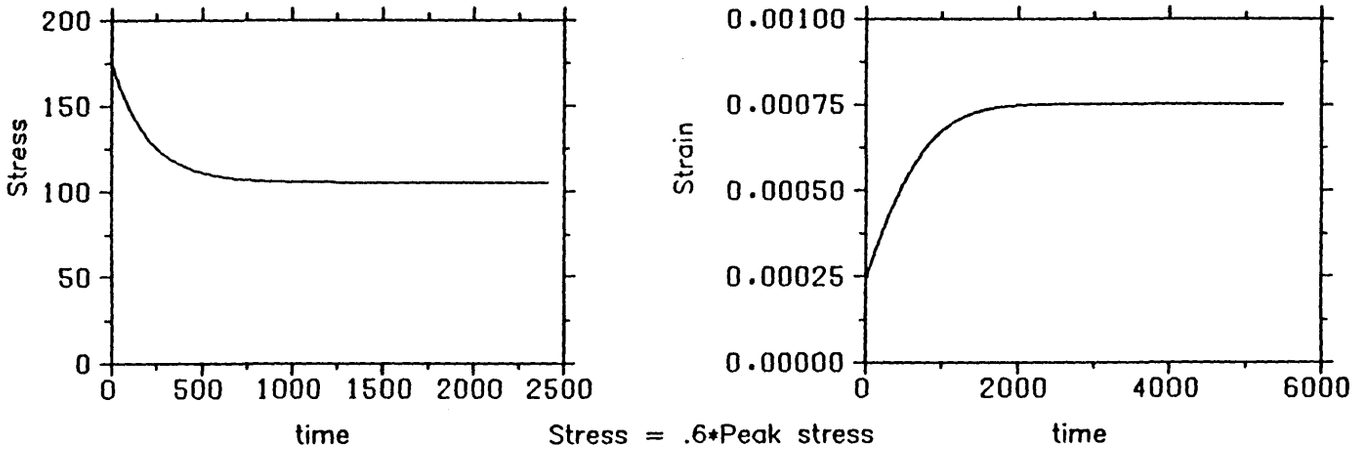

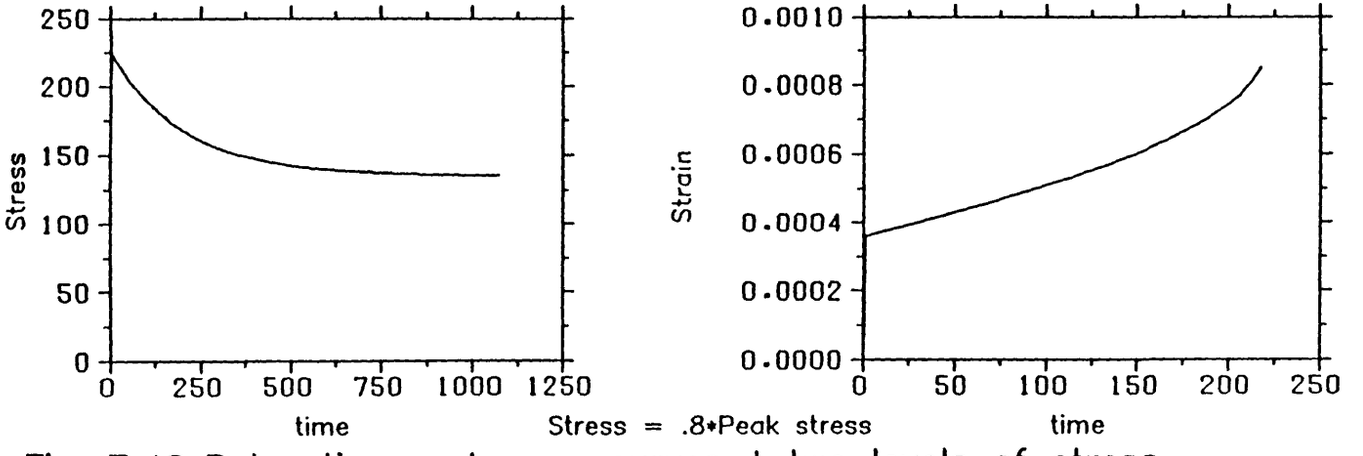

Fig. 7.48 Relaxation and creep curves at two levels of stress

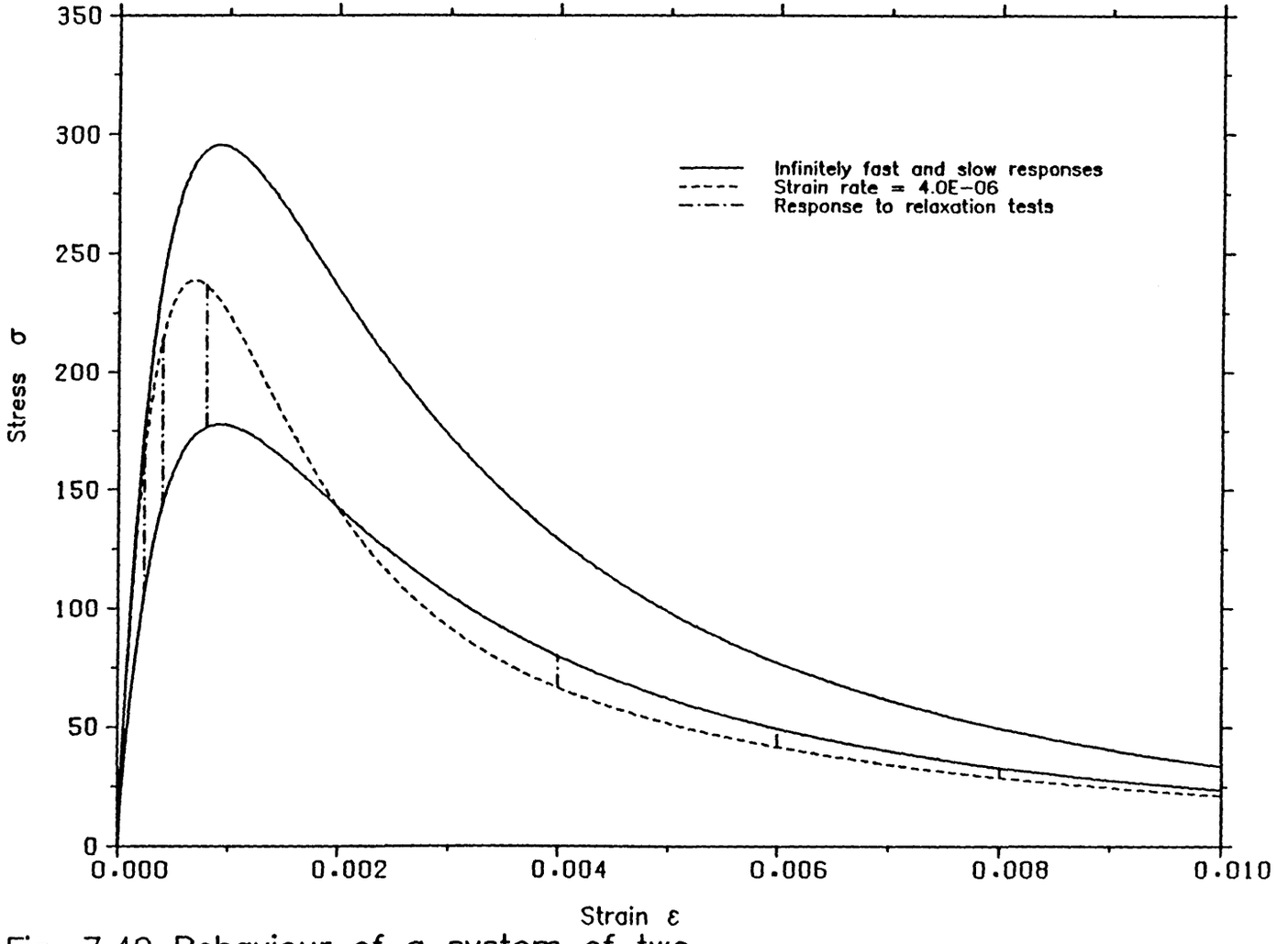

Fig. 7.49 Behaviour of a system of two bundles in series under relaxation tests
Strain rate sensitivity of the instantaneous response ignored

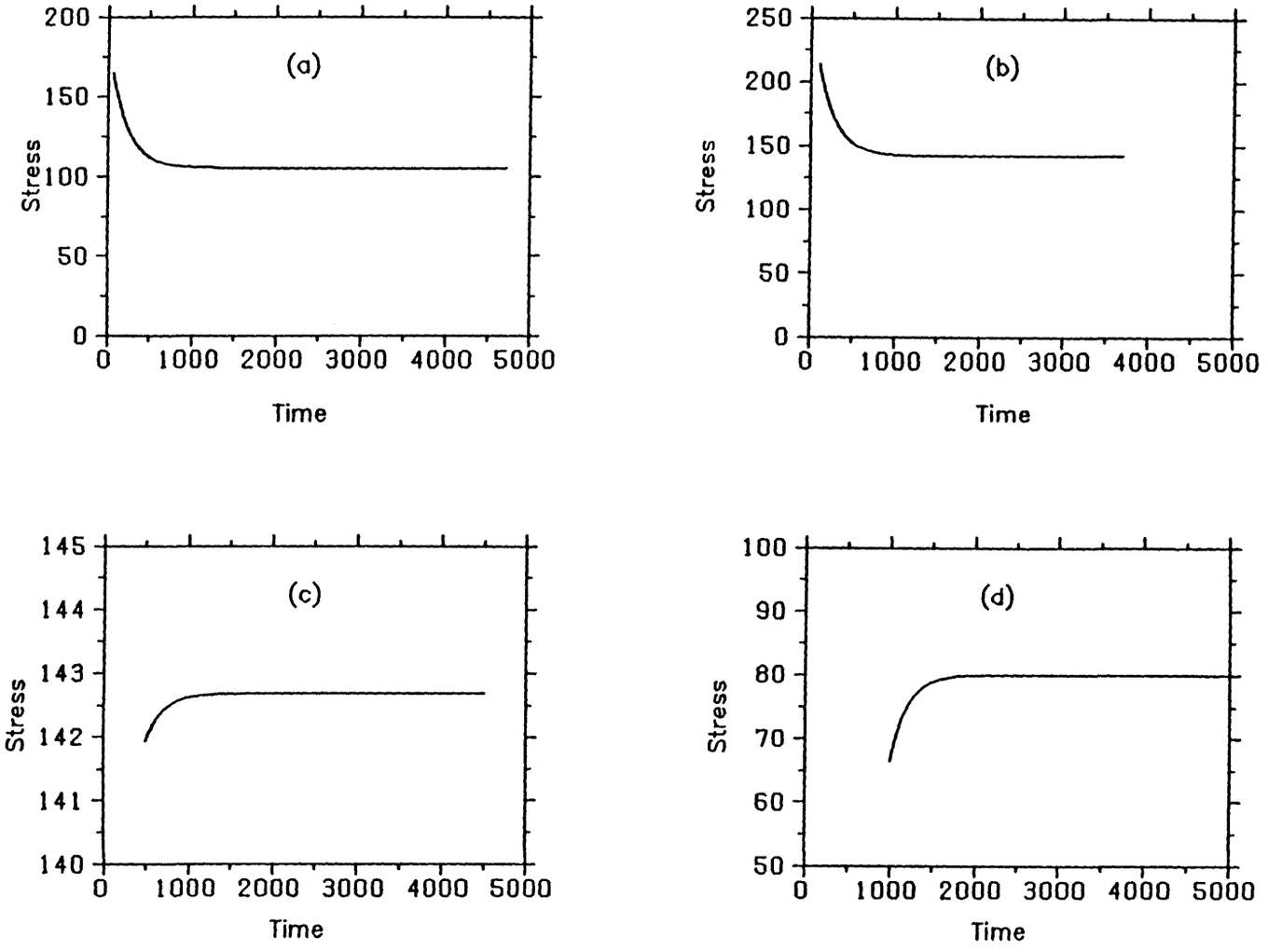

Fig. 7.50 Relaxation curves at different levels of stresses

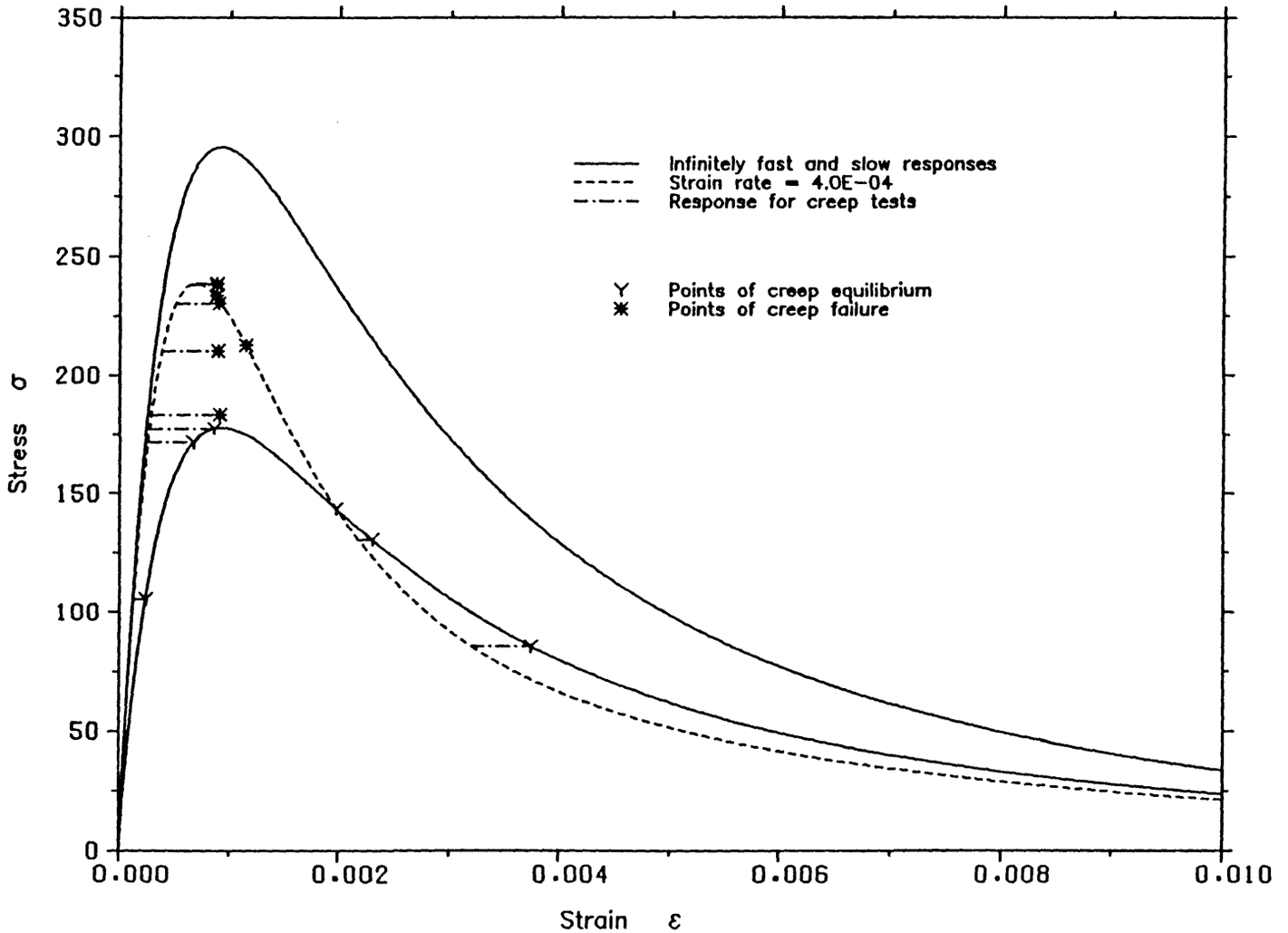

Fig. 7.51 Behaviour of a system of two bundles in series under creep tests
Strain rate sensitivity of the instantaneous response ignored

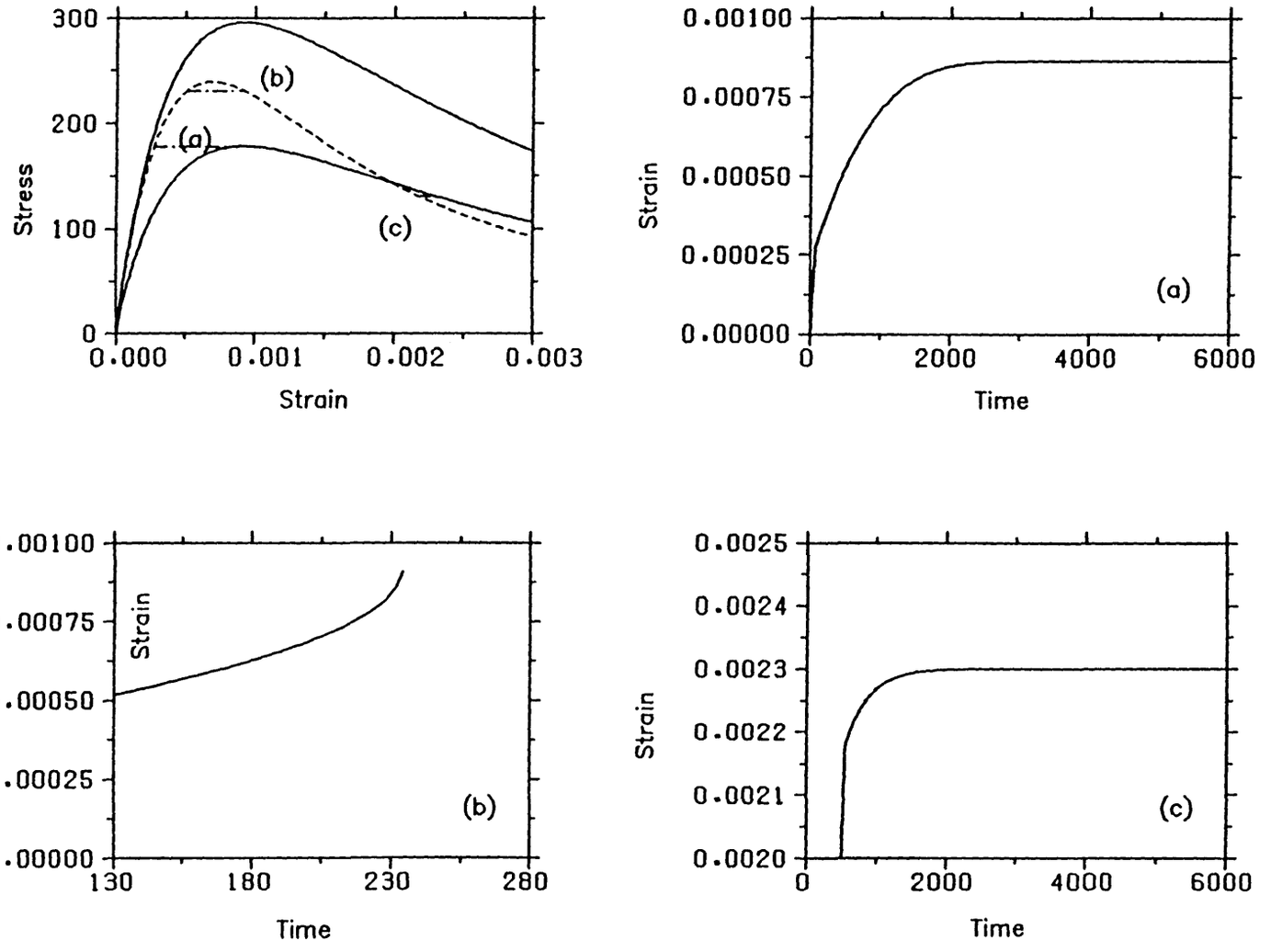

Fig. 7.52 Creep curves at different levels of stress (strain rate = 4.0E−04)

CHAPTER VIII

DISCUSSIONS AND CONCLUSIONS

8–1 Introduction

The principal objective of the work described in this thesis is to extend the theory of progressively fracturing solids [1–6] to include time effects.

Although the theory of progressively fracturing solids has only a limited application to real physical materials, it has been used as a starting point or in conjunction with other idealizations to develop theories describing materials such as concrete, rocks, some clays, and fibrous composites [51,131,133]. These extensions have focused on irrecoverable strains which could be included using plasticity based theories, but have not included time and rate dependent effects which can be important when dealing with problems involving blast, impact, collision, and sustained loading.

In pursuing this objective, an approach similar to that used in developing and exploring the original progressively fracturing solids theory was adopted. This solid has the property that nonlinearity is taken to be entirely due to degradation of stiffness, a form of behaviour that could be reproduced in a simple network model or used as the basic postulate for a continuum theory. The procedure adopted in this thesis was to return to these concepts and introduce time dependence into the network model and use this to explore the effects of introducing time dependence into the continuum description.

In adopting this approach, attention was given to the phenomena involved rather than pursuing the description of any particular real material. Accordingly, in treating time dependence, a description was required which would bring together rate and load history dependence in one model with the prospect of particular behaviour being obtained by an appropriate choice of parameters. This has been achieved in models which take as the primary phenomena time dependence and time–dependent degradation of stiffness. In some applications, the model would have to be combined with other idealizations involving plasticity and irrecoverable deformations.

By exploring the behaviour of a material whose response to loading is governed by stiffness degradation, the following has been achieved:

(a) A more general theory, developed from the progressively fracturing

solids theory, has been formulated. This theory allows the description of a full range of time effects coupled with stiffness degradation.

(b) Particular forms of the theory, namely those incorporating linear loading functions, have been developed and applied to simple loading situations to illustrate the applicability of the theory and the role of the descriptive parameters.

(c) The effects of time dependence have been explored using a network model. These studies provide a greater understanding of the range of applications of the continuum theory and suggest areas where work could be done to extend the theory further.

(d) The network model was used to investigate the effects of heterogeneity and lack of fit which may be considered to occur from loading other than imposed deformations. The results of this investigation provide a particular area where consideration might be given to extending the continuum theory.

(e) The exploration of time dependent behaviour in the network model was undertaken by computer simulation and so was not restricted to phenomena that are already known or understood from the results of physical testing.

(f) It was found that, by the appropriate choice of parameters, the model can provide a description of time dependent behaviour over the range normally covered by experiments. In some instances, these results suggest areas where further experimental studies of real material behaviour would be of particular interest.

Before considering possible applications and further developments in the theory, it is useful to develop these points in some detail.

8–2 The general time–dependent progressively fracturing solids theory

The continuum theory developed by Dougill [1–6] to describe the behaviour of an ideal progressively fracturing solid is based on certain concepts some of which are normally used in the incremental theory of plasticity. As for any other theoretical formulation, the behaviour of a material, whose response to loading is governed by the adopted concepts, is explored within a range of situations.

The theory of progressively fracturing solids does not take into account irrecoverable deformations in the sense that when the solid unloads it returns to a compatible state of zero stress and zero strain. On the other hand, formulations based on the incremental theory of plasticity are limited to a class of ideal materials for which irrecoverable deformations are the only source of nonlinearity and for which degradation of stiffness and strain softening are considered non existent or unstable. A more general approach would be to assume that the material behaviour involves both progressive fracture and irrecoverable deformations at the same time.

The extension of this theory to include time and rate effects coupled with stiffness degradation was presented in chapter V. The concepts adopted in the formulation of this general theory are similar to those adopted in the formulation of the viscoelastic/ plastic theory proposed by Naghdi and Murch [120].

While Naghdi and Murch described the behaviour of a solid whose response is governed by the occurrence of plastic irrecoverable deformations coupled with viscous time effects, the present theory considers a solid whose behaviour is a result of progressive fracture coupled with time and rate effects. Figure 8.1 illustrates the parallelism between these two theories and suggests that a more general description would be attained if both concepts are implemented to formulate one general theory.

The time dependent progressively fracturing solids theory provides a description of time effects over the full range of strain rates. With a particular choice of parameters, the different phenomena associated with time dependence can be explored across the whole range of strain rates, from those for which the long term response of the material is observed up to those for which strain rate sensitivity becomes an important factor in the material response.

Although the proposed theory is applicable over a wide range of strain rates, it is easy to use and can be easily formulated for applications involving finite elements. The parameters involved in the description are easily identified. This has been illustrated by exploring the behaviour of a particular form of the continuum theory, namely that for which linear loading functions are adopted. The resulting model, termed the "fibre bundle model" was tested under a variety of situations and proved to be both easy to handle and very illustrative of the behaviour of an ideal time–dependent progressively fracturing solid.

As an alternative way to illustrate the prediction of the behaviour of an ideal progressively fracturing solid, a network model was devised and tested under different loading conditions. This model provides an ideal material whose response to applied deformations results from the coupled effects of degradation and time dependence. The model proved to be easy to analyse and required moderate time and storage on the computer. Results from these tests are discussed next.

8–2–1 The network model

Burt and Dougill [3] has used the same model, simplified to exclude all time effects, to illustrate the behaviour of an ideal progressively fracturing solid. The behaviour of this model not only illustrates the different phenomena associated with the continuum description but also suggests different aspects where theoretical developments are needed.

The usefulness of the model lies not only in its simplicity but in its flexibility as well. It can be easily adapted to various forms of tests involving different types of loading and boundary conditions.

Tests simulating strain controlled uniaxial tensile conditions at different strain rates were performed. Loading was achieved by applying controlled deformations at a certain rate to boundary zones. Tests, similar to creep and relaxation tests performed on real materials, were also performed.

Results from these tests have shown good qualitative resemblance to those obtained for real materials and are in accordance with predictions from the time–dependent theory of progressively fracturing solids. Failure of the network model is a result of the interrelated effects of degradation resulting from breakage of members, and time dependent damage resulting from the relaxation of stress with time within individual members. The overall process of fracture hence

exhibits time–dependent progressive fracture.

The behaviour of the network model provides good qualitative agreement with that of a class of engineering materials that include concrete and rock. The model did exhibit strain rate sensitivity in a manner similar to that in real materials. It also exhibited the different modes of creep behaviour encountered in physical creep tests. Relaxation of the network model, under constant applied stress, was found to be stable at all stages of loading.

It was noted that the distribution of broken members is well dispersed at early stages of loading but becomes localized at high levels of strains especially when the peak stress is attained. This mode of behaviour, while observed for real materials, is unaccounted for in the continuum idealization.

Another phenomenon observed for the network model which is not directly foreseen from the continuum formulation (chapter V) is that of the unstable instantaneous failure under creep conditions at high levels of sustained stress. This phenomenon is characteristic of real material behaviour under creep tests.

The ease of testing the network model (using the computer) has made possible the investigation of some aspects of material behaviour that have rarely or ever been tackled in physical testing of materials. These aspects include creep and relaxation tests in the strain softening regime as well as strain rate sensitivity in all modes of behaviour (hardening and softening) at a strictly constant strain rate. If these tests are to be possibly performed on real materials, advanced new testing techniques should be used. This suggests devising testing apparatus that can provide a constant strain rate to the sample material as well as the capability of both instantaneously dropping the strain rate to maintain a constant level of strain ($\dot{\epsilon}=0$) and continuously adjusting the strain rate to provide a constant stress ($\dot{\sigma}=0$).

This makes the use of such a model, to investigate other aspects of the time dependent behaviour of real materials, justified.

8–2–2 The fibre bundle model

This model is a particular case of the general continuum theory describing an ideal time–dependent progressively fracturing material. Its response to loading illustrates the applicability of the theory and suggests means

from which the descriptive parameters can be deduced.

As for the network model, the fibre bundle model has been utilized to investigate some modes of behaviour encountered in real materials as well as to assess the predictions expected from the continuum formulation in chapter V. It should be always kept in mind that the fibre bundle idealization is a particular simplified case of the general continuum formulation.

Each individual fibre bundle is treated as a continuum while the overall model is a discrete assembly of these individual continuum units. This makes it easier to implement this model in finite element analysis of real material behaviour because the overall response of the model can always be expressed as a set of constitutive laws the forms of which depend on the form of the assembly adopted.

Since, for this model, it is assumed that degradation and the consequential strain softening are processes that occur at a point, all considerations of localization are unaccounted for. This does not mean that localization is ruled out. If a sample of material is assumed to be formed of points whose mechanical behaviour is idealized by a fibre bundle assembly, then all points on the sample that exhibit strain softening can be thought of as cracks. Localization will follow if size effects are introduced by controlling the size of these units (or points) with respect to the size of the sample. This suggests that further work need to be done to include localization either by the introduction of size effects in the continuum description or by devising means by which a finite element assembly will take such behaviour into account.

In contrast to the network model, the response of an assembly of fibre bundles is a smooth one. No jumps in the stress strain curves were observed.

It is to be noted that the behaviour of the system of fibre bundles in a homogeneous strain field has given an insight on the multidimensional behaviour expected for a time dependent progressively fracturing solid. Tests on such an assembly under different combinations of longitudinal and transverse deformations have shown that strain rate sensitivity encountered in real materials under such conditions can be investigated and simulated to a certain extent.

The simplicity of the system of series fibre bundles has made possible the investigation of not only strain rate sensitivity but the response to creep and

relaxation tests as well.

Results of all these tests have been in satisfactorily qualitative agreement with some aspects of real material behaviour, with those of the network model, and with those expected from the continuum idealization presented in chapter V.

8–2–3 General remarks on the proposed time dependent progressively fracturing description

As in any other continuum formulation, the assumptions about the material behaviour simplify the theory and make its analytical and computational application possible. On the other hand, these simplifying assumptions limit the descriptive capacity of the theory to a particular class of materials.

The ideal model materials presented in chapters VI and VII do not employ the full range of facilities deployed in the continuum formulation. Still, the theory is capable of predicting some aspects of the mechanical behaviour of the model materials. On the other hand, these model materials exhibit some modes of behaviour that are not accounted for in the continuum description but still experience time–dependent progressive fracture.

In the same sense, when using the continuum theory to describe phenomena encountered for physical materials that do not comply precisely with the theoretical assumptions, some deviations from the behaviour predicted by the theory might be encountered. The descriptive capacity of the theory is limited to some aspects of real material behaviour and hence the usefulness of the theory should be assessed by the significance of these modes of behaviour in the particular real situation under consideration.

The behaviour of the model materials, presented in chapter VII, not only simulates some modes of the mechanical behaviour encountered in real materials but also gives an insight on the scope of application of the continuum theory and on the possibility of future extensions.

8–3 Scope of application of the continuum theory

The suitability of the continuum theory for the description of real material behaviour should be appraised in view of past experience of material behaviour and of previous applications of the theory, or other theories, to similar situations.

The assessment of the usefulness of the theory must be based on the actual application under consideration. The theory, being analytically similar to the incremental theory of plasticity, is simple to analyse and apply, especially with the current advancements in numerical and computational techniques. If this or any other theory is to be applied to real materials then the validity of the assumptions behind the theoretical formulation should be assessed. This can be achieved by comparison with results from experimental tests on the behaviour of the particular material under consideration.

The main limitation of the theory is that it considers strain softening as a general continuum behaviour rather than a localized one. Size effects in this class of materials are completely excluded. This exclusion of localized failure and size effects is inherent in the consideration of progressive fracture to be occurring at a point in a continuum.

The theory of progressively fracturing solids considers that stiffness degradation and hence strain softening occur at a point within a continuum. This assumption does not exclude local effects when the continuum theory is applied to a real physical conditions. When a sample of a material is assumed to be composed of points (or units), the behaviour of which is described by the progressively fracturing solids theory, then localized failure might be thought of to happen as a result of strain softening occurring in units within a certain region of the sample with the rest of the sample undergoing elastic unloading. Size effects are hence introduced by the size of this region and the relative size of these units compared to the size of the sample.

As mentioned earlier, the application of this theory, or any other theory, to the behaviour of real materials is faced by some limitations imposed by the assumptions adopted to formulate the theory. Model materials, (like the network model investigated in chapters IV and VII) used to investigate the behaviour of progressively fracturing solids, do not satisfy all the assumptions in the continuum theory and yet provide a description of the behaviour assumed or predicted by the theory. In the same sense, some modes of behaviour of real

physical materials can be predicted by the theory eventhough the material does not fully satisfy the assumptions inherent in the continuum formulation.

Results from experimental testing on real physical materials can hence be used to calibrate the continuum theory (alone or in conjunction with other theories) so that a more practical assessment of the behaviour of real materials becomes possible.

Bazant and Kim [131] proposed a continuum model that combines plasticity and progressive fracture to describe the behaviour of concrete. They based their model on observations that the inelastic behaviour of concrete is a result of both microcracking (resulting in degradation and progressive fracture) and plastic slip (resulting in irrecoverable deformations). They assumed that if the material is subjected to a strain increment $d\epsilon$, the corresponding stress increment comprises three components, an elastic stress increment, a plastic stress increment, and a fracture stress increment. The two inelastic components of the stress are derived from the incremental theory of plasticity and the progressively fracturing solids theory respectively with interdependence between the corresponding loading functions. Calibration of the model was possible and the model's response was found to be in good agreement with experimental results.

Rida [51] suggested an alternative way of using the progressively fracturing solids theory to describe real material behaviour in conjunction with the incremental theory of plasticity. Inspired by the concept of the "overlay" model suggested by Zienkiewicz et al [132], Rida used a parallel arrangement of an elastoplastic material and a progressively fracturing one. The system hence shares the same total strain and its total stress is the combined effect involving the contributions from each material. A weighting factor was introduced to control the ratio by which each constituent model contributes to the total behaviour. The model provides a more realistic description of the behaviour of concrete–like materials than that obtained by each of its constituents alone. This model can hence be easily calibrated against results from experimental tests.

Resende and Martin [133] developed a constitutive model for the description of the mechanical behaviour of granular materials like rock and concrete. Their model is based on Dougill's progressively fracturing theory for the description of shear behaviour and a plasticity model, involving cap yield surfaces, to describe the volumetric response. By expressing progressive fracture and the consequential stiffness degradation in terms of an internal damage

parameter, and by linking the same parameter to the inelastic (or plastic) component of the volumetric strain, coupling between plastic slip and progressive fracture was achieved. Simple tests were suggested to calibrate the proposed constitutive law. Results of numerical tests were in good qualitative agreement with experimental results for cyclic uniaxial compression tests on rocks.

The choice of the theory of progressively fracturing solids, or any other continuum theory, to describe certain modes of real material behaviour should be based on the ease of the parameters involved in the formulation and the correspondence to the range of experiments and problems. A good material model should be both easy to implement and capable of describing the material behaviour with good agreement with experimental results.

The before–mentioned models have combined the continuum progressively fracturing solids theory with plasticity based theories for a more realistic and practical description of material behaviour. Further applications of the theory in conjunction with other existing continuum or damage theories is hence justified and may prove both useful and practical. It should always be kept in mind that the relevance of these applications is dependent on the actual situation under consideration.

As for the time–independent progressively fracturing solids theory, the application of the time–dependent progressively fracturing solids theory to predict the exact behaviour of a certain material is only possible if that material satisfies precisely all the assumptions inherent in the continuum formulation.

The theory provides good predictions for some modes of behaviour in a class of engineering materials whose failure is both time dependent and exhibits progressive fracture as a result of material degradation. This class of materials includes concrete and rock.

For the predictions of these aspects of behaviour to be sound, both qualitatively and quantitatively, the forms of the various laws incorporated in the continuum formulation should be chosen in accordance with experimental evidence and past experience. The forms of these laws might vary depending on the application under consideration. These include the law relating damage to the increments of stress and strain at the time of fracture, and the damage evolution law that incorporates a stress relaxation function.

Because of the concentration on time–dependent progressive fracture in

the continuum idealization and the exclusion of other important aspects of the mechanical behaviour, it might be more realistic to use this theory in conjunction with other theories when real materials are investigated.

One way of achieving this is to extend Bazant and Kim's approach [131] to incorporate time effects. In this case the material description would be based on the assumption that if, a representative sample is subjected to a strain increment then the corresponding stress increment, would comprise three components, a viscoelastic, a fracturing, and a plastic stress increment. The two inelastic stress increments can be derived from the proposed time dependent progressively fracturing solids theory (chapter V) and the viscoelastic/ plastic theory of Naghdi and Murch [120] respectively. Coupling between the two forms of inelastic behaviour can be achieved by choosing the corresponding loading functions to be interdependent or related by some internal variables.

An alternative way of achieving a description incorporating progressive fracture and plastic deformations together with time effects is to adopt an overlay concept in which a viscoelastic/ fracturing solid and a viscoelastic / plastic one are superimposed to occupy the same space. If a representative sample of the solid is subjected to an increment of strain then the response is assumed to be the sum of the two individual responses. The total stress is taken to be the sum of the two components while the strain is assumed to be the same for both constituents. It should be noted that the two modes of behaviour are completely independent of each other. This parallel arrangement in space of two solids can be refined by allocating weighing factors to the different solids when the summation of stresses is performed.

Various combinations between the time–dependent progressively fracturing solids theory and other elastoplastic, viscoelastic/ plastic, elastic/ viscoplastic theories can be performed and calibrated against real material behaviour. The choice of the way to combine these theories, and whether or not coupling between the modes of behaviour that they resemble is assumed to take place, is dependent on the particular material and the particular situation under consideration.

8–4 Possible developments to the idealization of progressively fracturing solids

It was mentioned earlier that the theory of progressively fracturing solids, in its time–independent and time dependent formulations, has limitations in its applicability due to the adoption of particular assumptions on the material behaviour. These limitations can be assessed by exploring the mechanical behaviour of progressively fracturing materials whether these materials are real physical materials or idealized ones. This suggests some areas in the continuum theory as well as the ideal model materials that may need further advancements:

(i) Tests performed on the network model (chapter IV) have shown that the response of this heterogeneous progressively fracturing solid is affected by any type of internal incompatibilities. For this mode of behaviour to simulate real material behaviour, further work is needed regarding the allocation of these incompatibilities to members. For example, if temperature loading, which is an important type of loading that causes such incompatibilities, is to be investigated for a composite material, it might be more profitable to choose the members from more than one set each having a different average value of the coefficient of linear expansion.

(ii) Although internal incompatibilities cause permanent irrecoverable strains in the network model, these are not the only cause of irrecoverable deformations in real materials. Plastic slip is an important cause of these irrecoverable deformations and can be resembled in the behaviour of the network model by assuming, for example, that some members exhibit permanent plastic deformations upon failure. Alternatively, some of the broken members can be assumed to "heal" upon unloading causing an increase in the unloading elastic moduli and consequential permanent overall deformations.

(iii) Tests on the behaviour of the network model under temperature loading, or other loading that causes internal stresses, suggest that the extension of the theory of progressively fracturing solids to include these effects might prove profitable. One way of achieving this is to assume that these effects are measured by some internal variables that are linked to the damage vector which measures the past history of strain. This would require a temperature evolution law that links damage to the past history of temperature (or any other stress inducing load). Alternatively, it can be assumed that the loading function, and hence the material response, can be expressed in terms of strain, strain path history, and temperature history expressed as an individual damage vector. The

interrelation between vectors defining strain history and temperature history should be explored if coupling between the two factors is to be attained.

(iv) It might prove worthwhile to investigate the behaviour of the time–dependent models (chapter VI and VII) with the effects of internal incompatibilities and those due to permanent plastic deformations taken into consideration. This investigation should provide some guide lines to formulate or assess a general time and temperature dependent progressively fracturing solids theory incorporating plastic deformations.

While the effects of plastic deformations can be incorporated in one of many ways discussed in section 8–2–3, those due to temperature or other internal stress inducing factors can be included in fashions similar to those suggested in (iii) above.

(v) Localization of failure has been ignored in the formulation of the continuum theory both in its time independent and time dependent versions. This is an area which requires further investigation because localized failure is a characteristic of real physical materials as well as the proposed network model.

Theoretical work to incorporate localization in the theory of time–dependent progressively fracturing solids can be guided by research done on the localization of failure for solids described by time–dependent plasticity theories. For example the work done to link localization to the neucleation and growth of voids in metals (Needleman and Tvegaard [134], Pan, Serge, and Needleman [135]) can form the basis of possible extensions to the time dependent theory of progressively fracturing solids to include localization and size effects.

(vi) In the study of the application of the continuum theory to real materials or practical situations, there is a need to investigate the possible forms of the loading function F, the damage vector H_k, and the vector describing past time history and rate sensitivity T_q. This investigation should be performed in the light of physical testing on materials to provide appropriate forms for these functions.

(vii) In the theoretical formulation of the continuum theory, expressions describing the instantaneous response of the material rather than its actual response were derived. It was suggested to link the instantaneous response to the actual one by a stress relaxation function. This has resulted in the

formulation of a damage evolution law describing time–delayed damage.

The validity of this theoretical "link" should be investigated in view of real material behaviour. Tests on the network model and the fibre bundle model suggest ways by which the link between the instantaneous response and the actual one can be investigated for real physical materials. Tests on real materials might suggest alternative ways by which this "link" can be achieved and would help to derive appropriate forms for the assumed relaxation moduli and the damage evolution law.

(viii) As an improvement to the descriptive capacity of the network model and the fibre bundle model, limits on the compressive capacity of the individual elements or fibres can be imposed and varied to give a more realistic description. This might suggest the use of different functions (loading functions, relaxation functions, or damage functions) for tensile and compressive behaviour when the continuum theory is used to simulate progressive fracture in real materials.

(ix) It might be useful to study the behaviour of the fibre bundle model with the inclusion of elastoplastic or viscoelastic/plastic fibres. This might suggest alternative ways by which the continuum theory can be extended to describe plastic deformations.

(x) One limitation resulting from the adoption of linear loading functions of the form suggested in chapter VI, is that strain rate sensitivity of the instantaneous behaviour is effective only during loading. During unloading, time dependence is only manifested by the damage evolution law while the instantaneous behaviour is affected by the strain history prior to unloading. This aspect must be investigated in conjunction with results from real material testing involving complex strain histories.

(xi) It would be more convenient, if the continuum theory is to be implemented in finite element studies, to adopt a single loading function rather than using several independent loading functions as in the case of a fibre bundle assembly. This requires some research on the fibre bundle model from which a single non–linear loading function, giving the same or a similar response as that of the various independent ones, can be deduced.

Finally, it should be stressed that the more advanced the theory is the more difficult to implement it becomes. Any developments or advancements in

the descriptive ability of the present theory or the proposed model materials should be sought in light of the need imposed by real physical material behaviour.

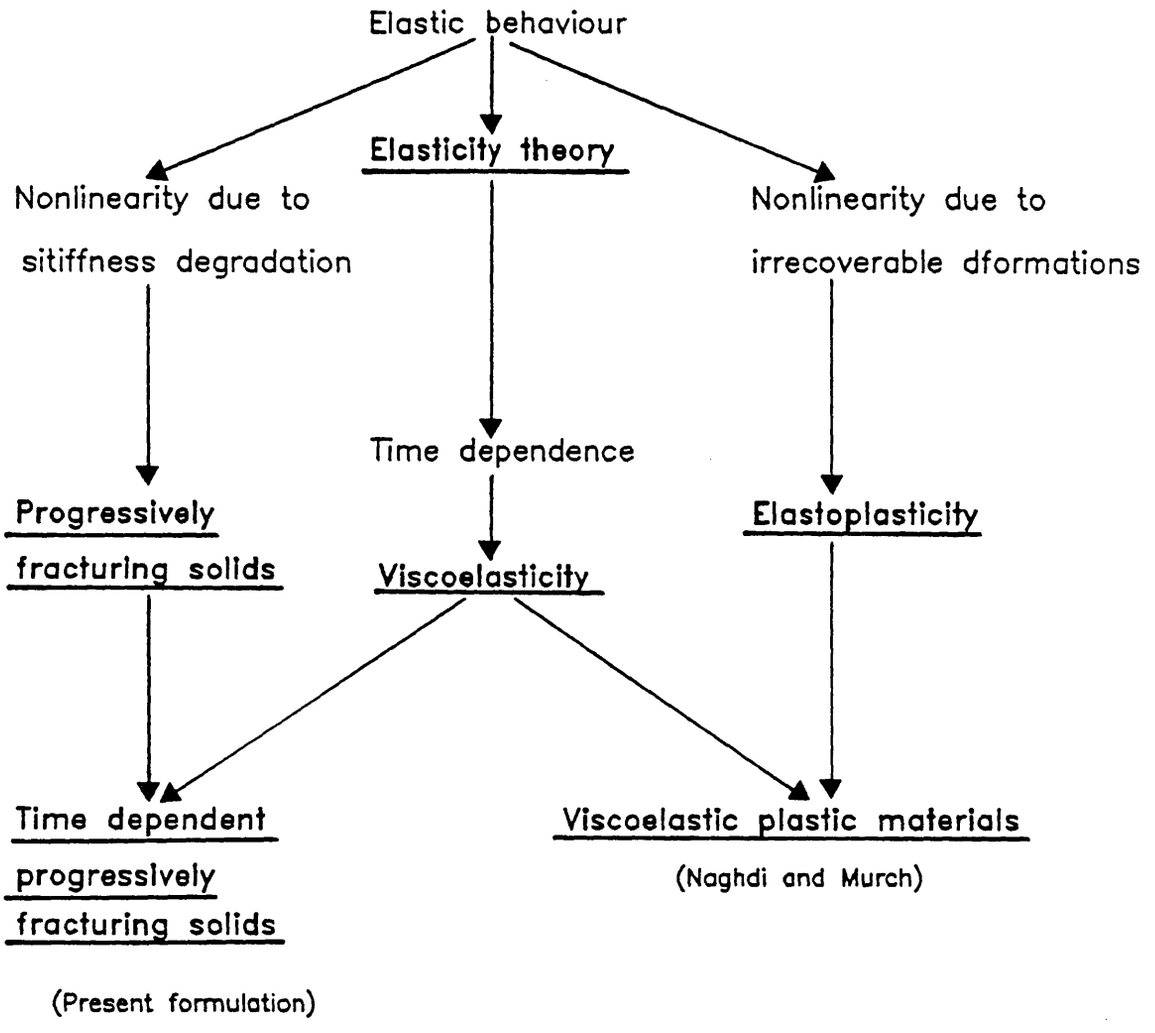

Fig. 8.1 Paths followed in the description of material behaviour

APPENDIX A

BEHAVIOUR OF FIBRE SYSTEMS UNDER TEMPERATURE

Consider an elastic spring with a modulus of elasticity E, area A, and length L. Let its thermal coefficient of expansion be denoted by α. Under a temperature T and deformation u the force in the above fibre is given by

$$F = \frac{A\ E}{L}(u - \alpha L T) \qquad A.1$$

so that the stress becomes

$$\sigma = E(\epsilon - \alpha T) \qquad A.2$$

where F is the force in the spring, σ is the stress given by F/A, and ϵ is the strain given by u/L.

Consider a system of n such fibres in series. The force F in the system due to a deformation u_n and a temperature T is given by

$$F = \frac{A_1 E_1}{L_1}(u_1 - \alpha_1 L_1 T) = \frac{A_2 E_2}{L_2}(u_2 - u_1 - \alpha_2 L_2 T)$$
$$= \frac{A_n E_n}{L_n}(u_n - u_{n-1} - \alpha_n L_n T) \qquad A.3$$

where A_i, E_i, α_i, and L_i represent the area, elastic modulus, coefficient of thermal expansion, and length of the i^{th} fibre. The term $u_i - u_{i-1}$ represent the elongation of the fibre. Thus

$$F \times \left[\frac{L_1}{A_1 E_1} + \frac{L_2}{A_2 E_2} + \ldots + \frac{L_n}{A_n E_n}\right]$$
$$= \left[u_n - T(\alpha_1 L_1 + \alpha_2 L_2 + \alpha_3 L_3 + \ldots + \alpha_n L_n\right] \qquad A.4$$

The system is thus equivalent to one spring with the following constitutive law

$$F = \frac{A\ E}{L}(u_n - \alpha L T) \qquad A.5$$

where

$$AE = LK \qquad A.6$$

$$1/K = 1/k_1 + 1/k_2 + \ldots + 1/k_n \qquad A.7$$

$$k_i = \frac{A_i E_i}{L_i} \qquad A.8$$

$$L = L_1 + L_2 + \ldots + L_n \qquad A.9$$

and
$$\alpha = \frac{\alpha_1 L_1 + \alpha_2 L_2 + \ldots + \alpha_n L_n}{L} \qquad \text{A.10}$$

Consider a system of n fibres in parallel. The force in the assembly F is given by

$$F = \frac{A_1 E_1}{L_1}(u - \alpha_1 LT) + \frac{A_2 E_2}{L_2}(u - \alpha_2 LT) + \ldots + \frac{A_n E_n}{L_n}(u - \alpha_n LT) \qquad \text{A.11}$$

The system is thus equivalent to one spring with the following constitutive law

$$F = \frac{AE}{L}(u - \alpha LT) \qquad \text{A.12}$$

where

$$AE = A_1 E_1 + A_2 E_2 + \ldots + A_n E_n \qquad \text{A.13}$$

and

$$\alpha = \frac{A_1 E_1 \alpha_1 + A_2 E_2 \alpha_2 + \ldots + A_n E_n \alpha_n}{A_1 E_1 + A_2 E_2 + \ldots + A_n E_n} \qquad \text{A.14}$$

It is interesting to note that the equivalent thermal expansion coefficient α of a system of fibres in series is insensitive to changes in the individual fibre's stiffness moduli. Equation A.10 suggests that α is a weighted average of the individual fibres' α_i with the fibres lengths as the weighting factors. As long as no member completely fails, resulting in the complete reduction of its stiffness to zero, any change in the values of the individual member stiffness k_i leaves the value of α unchanged.

The case of parallel arrangement is quite different. Equation A–13 suggests that the average coefficient of thermal expansion α is a weighted average of all the individual values, α_i, with the fibres stiffness moduli as the weighting factors.

Thus a change of the stiffness of an individual fibre might result in a change in the assembly coefficient of thermal expansion α. The complete reduction of a member stiffness to zero is possible here since the assembly will still hold. It should be noted that a change of individual fibre stiffness might result in an increase or decrease in the average value of the assembly's coefficient of linear expansion. It might also have little or no effect on the averaging process. The change is purely statistical and is dependent on the way the averaging

process is altered by the changes of the weighting factors.

APPENDIX B

ANALYSIS STEPS FOR THE NETWORK MODEL –TIME EFFECTS INCLUDED–EDGE DISPLACEMENTS ALWAYS PRESCRIBED

If nodal displacements are prescribed for all nodes within the edge zone (2) (figure 4.2) at all times (section 6–2–9), then the analysis of the behaviour of the network model is performed as follows

(i) For each member, assume that the instantaneous strain rate is identical to that in the previous time step.

(ii) Calculate the assumed value of the instantaneous stiffness $S_i'(t)$, for each member, using the expressions in 6.2.6.

(iii) Assemble the element's stiffness matrix $\underset{\sim}{k}$ (from the matrix equation 6.2.26) in the global network stiffness matrix $\underset{\sim}{K}$.

(iv) Assemble the previous time equivalent nodal force $\underset{\sim}{b}$ (from the matrix equation 6.2.25), in the global force vector, $\underset{\sim}{B}$, of the network.

(v) Repeat (iii) and (iv) for all members.

(vi) Reduce the network's total structural stiffness matrix $\underset{\sim}{K}$ for restrained and prescribed displacements. Transform known incremental nodal displacements into equivalent nodal forces. Assemble these forces into the reduced global force vector $\underset{\sim}{F}$.

(vii) Solve the reduced form of the matrix problem

$$\underset{\sim}{F} - \underset{\sim}{B} = \underset{\sim}{K}\,\underset{\sim}{\Delta u} \qquad \text{B.1}$$

for unknown increments of nodal displacements $\underset{\sim}{\Delta u}$ at time t.

(viii) Using $\underset{\sim}{\Delta u}(t)$, the strain rate in each member can be calculated using expression 6.2.22.

(ix) Calculate the updated value of the instantaneous stiffness $S_i''(t)$, for each member, using expression 6.2.6 and the strain rate calculated in (viii).

(x) Check the convergence by testing that

$$\left| \frac{S_i''(t)}{S_i'(t)} - 1.0 \right| < 0.001 \qquad \text{B.2}$$

If condition B.2 is not satisfied for all members, then replace the assumed values of $S_i'(t)$ by the updated values $S_i''(t)$ and repeat (iii) to (x) until convergence.

(xi) Calculate the stress $\sigma_i(t)$ within the i^{th} member (expression 6.2.29) and the work done by the member during deformation $W_i(t)$ (expression 6.2.28).

(xii) Check failure of the members by ensuring that

$$W_i(t) < W_{if} \qquad \text{B.3}$$

if member has been deforming in tension

or

$$W_i(t) < \beta W_{if} \qquad \text{B.4}$$

if member has been deforming in compression

(xiii) Repeat (xi) and (xii) for all members.

(xiv) If any member has failed (B.3 and B.4 not satisfied) set its instantaneous stiffness modulus $S_i(\tau)$ to zero at all times, $0 \leq \tau \leq t$, and repeat (i) to (xiii) for the same time increment.

(xv) Calculate all nodal forces, at time t, from the unreduced matrix form of B.1.

(xvi) Calculate stress along the network , using the nodal forces calculated in (xv).

(xvii) From the current displacements of the nodes, represented by $u_i(t)$, calculate strain across the network.

(xviii) Calculate the nodal displacements at time $t+\Delta t$ by

$$u_i(t+\Delta t) = u_i(t)+\Delta u_i(t) \qquad \text{B.5}$$

(xix) Repeat (i) to (xviii) for the next increment of time associated with the next boundary displacements.

APPENDIX C

ANALYSIS PROCEDURE FOR THE BEHAVIOUR OF A SYSTEM OF FIBRE BUNDLES IN A HOMOGENEOUS STRAIN FIELD –STRAIN ALWAYS PRESCRIBED

The procedure presented in here describes the steps followed to analyse the behaviour of a system of several fibre bundles held in a homogeneous strain field with strain in all directions prescribed.

At any time t, the values of the instantaneous secant relaxation modulus $\overline{S}^n(\tau)$, the loading function $F^n(\tau)$, the strain tensor $\epsilon_{ij}(\tau)$, and the damage parameter $h^n(\tau)$ are known for all fibre bundles (n=1, N) at all times $\tau \leq t$. The n^{th} fibre bundle is oriented at an angle θ_n with the corresponding directional parameters, given by λ^n_{ij} (expressions 2.4.3). Analysis is followed incrementally along time so that for the next increment of time dt, associated with $d\epsilon_{ij}(t)$, analysis proceeds as follows

(i) Calculate the strain rate $\dot{\epsilon}^n_r(t)$ along the n^{th} fibre bundle (expression 6.3.19).

(ii) Calculate the strain rate parameter $T^n(t)$ using 6.3.18.

(iii) Calculate the change in the strain rate parameter $dT^n(t)$ using 6.3.28.

(iv) Calculate the scalar quantity $\lambda^n_{ij} d\epsilon_{ij}(t)$.

(v) Allocate $C^n(t)=0$ or 1 according to 6.3.24.

(vi) Calculate $dh^n(t)$ and $dF^n(t)$ according to 6.3.25, 6.3.26, and 6.3.27.

(vii) Calculate $dD^n(t)$ by 6.3.22.

(viii) Calculate $d\overline{S}^n(t)$ according to 6.3.51.

(ix) Repeat (i) to (viii) for all N bundles.

(x) Calculate the change in the total instantaneous stiffness of the assembly $dS^T_{ijkm}(t)$ by 6.3.59.

(xi) Calculate the change in the instantaneous response of the assembly $d\sigma^*_{ij}(t)$ by

$$d\sigma^*_{ij}(t) = \left[S^T_{ijkm}(t) + dS^T_{ijkm}(t)\right]\left[\epsilon_{km}(t) + d\epsilon_{km}(t)\right] - S^T_{ijkm}(t)\,\epsilon_{km}(t) \qquad \text{C.1}$$

(xii) Calculate the actual stress $\sigma_{ij}(t)$ at time t by 6.3.56.

(xiii) For each fibre bundle increment the state variables by

$$F^n(t + dt) = F^n(t) + dF^n(t) \qquad C.2$$

and

$$h^n(t + dt) = h^n(t) + dh^n(t) \qquad C.3$$

(xiv) Increment the total strain and total instantaneous stiffness modulus by

$$\epsilon_{ij}(t + dt) = \epsilon_{ij}(t) + d\epsilon_{ij}(t) \qquad C.4$$

and

$$S^T_{ijkm}(t + dt) = S^T_{ijkm}(t) + dS^T_{ijkm}(t) \qquad C.5$$

(xv) Repeat (i) to (xiv) for the next increment of time associated with the next increment of prescribed strains.

APPENDIX D

ANALYSIS PROCEDURE FOR A SYSTEM OF FIBRE BUNDLES HELD IN A HOMOGENEOUS STRAIN FIELD –STRAIN NOT PRESCRIBED AT ALL TIMES

For a system of fibre bundles in a homogeneous strain field when strain in one or more directions is not prescribed but is such that stresses along these directions are always zero, the analysis procedure is different than that described in Appendix C. For such a system the analysis procedure is performed as described in here.

At all times $\tau \leq t$, the values of the instantaneous secant relaxation modulus $\overline{S}^n(\tau)$, the loading function $F^n(\tau)$, and the damage parameter $h^n(\tau)$ are known for all fibre bundles (n=1, N). The strain tensor at time τ, $\epsilon_{ij}(\tau)$, is also known. For the next increment of time dt, the response of the assembly is evaluated as follows

(i) If $F^n(t) < 0$ allocate $C^n(t) = 0$,

If $F^n(t) = 0$ allocate $C^n(t) = 1$.

(ii) Assume that $dT^n(t) = 0$, so that $T^n(t)$ has the same value as $T^n(t-dt)$.

(iii) Calculate $\overline{M}^n(t)$ using 6.3.53 and 6.3.35 and $M^n_{ijkm}(t)$ using 6.3.52.

(iv) Repeat (i) to (iii) for all fibre bundles.

(v) Formulate the system's instantaneous tangential stiffness $M^T_{ijkm}(t)$ using 6.3.60.

(vi) Solve the total equation 6.3.38 in its matrix form

$$d\overset{*}{\sigma}_{ij}(t) = M^T_{ijkm}(t)\, d\epsilon_{km}(t)$$

$$-\left[\sum_{n=1}^{N} \frac{2C^n}{(h^n)^2} \lambda^n_{ij} \lambda^n_{km} \frac{\partial D^n}{\partial T^n} dT^n\right]_t \epsilon_{km}(t) \qquad \text{D.1}$$

for the unknown components of $d\epsilon_{km}(t)$. This can be achieved since the corresponding components of the instantaneous stress increment $d\overset{*}{\sigma}_{ij}(t)$ are all zeros.

(vii) Update the value of $T^n(t)$ using 6.3.19 and 6.3.18.

(viii) Calculate $dT^n(t)$ using 6.3.28.

(ix) Repeat (vii) and (viii) for all fibre bundles.

(x) For each bundle check if

$$\left| r_n - 1.0 \right| \leq 0.001 \qquad \text{D.2}$$

where r_n is the ratio of the updated value of $T^n(t)$ to that assumed. If this condition is not satisfied for each bundle, repeat (i) to (x) with $T^n(t)$ and $dT^n(t)$ in (ii) as those calculated in (viii) of the previous iteration.

(xi) Calculate the scalar quantity $d\bar{\epsilon}^n = \lambda^n_{ij} d\epsilon_{ij}(t)$. Check the validity of the value of $C^n(t)$ allocated in (i) by ensuring that if $C^n(t) = 1$, then the scalar $\lambda^n_{ij} d\epsilon_{ij}(t)$ is greater than zero. If this is satisfied then the allocation in (i) was justified. Otherwise reallocate $C^n(t) = 0$.

(xii) Repeat (xi) for all bundles. If reallocation of $C^n(t)$ was performed for any bundle repeat (i) to (xii), with the reallocated values of $C^n(t)$, until all allocated values are justified.

(xiii) Calculate the approximate value of the change in the instantaneous scalar stress $d\overset{*}{\bar{\sigma}}^n(t)$ by 6.3.54

$$d\overset{*}{\bar{\sigma}}^n(t) = \bar{M}^n(t)\, d\bar{\epsilon}^n(t) - \left[\frac{2C^n}{(h^n)^2} \frac{\partial D^n}{\partial T^n} dT^n\right]_t \bar{\epsilon}^n(t) \qquad \text{D.3}$$

with

$$d\bar{\epsilon}^n(t) = \lambda^n_{ij} d\epsilon_{ij}(t) \qquad \text{D.4}$$

and

$$\bar{\epsilon}^n(t) = \lambda^n_{ij} \epsilon_{ij}(t) \qquad \text{D.5}$$

(xiv) Calculate $dh^n(t)$ and $dF^n(t)$ using 6.3.25, 6.3.26, and 6.3.27.

(xv) Calculate $dD^n(t)$ using 6.3.22.

(xvi) Calculate $d\bar{S}^n(t)$ using 6.3.51.

(xvii) Update the value of the change in the instantaneous scalar stress $d\overset{*}{\bar{\sigma}}^n(t)$ by

$$d\overset{*}{\bar{\sigma}}^n(t) = \left[\bar{S}^n(t) + d\bar{S}^n(t)\right]\left[\bar{\epsilon}^n(t) + d\bar{\epsilon}^n(t)\right] - \bar{S}^n(t)\,\bar{\epsilon}^n(t) \qquad \text{D.6}$$

(xviii) Check that

$$\left| r_n - 1.0 \right| \leq 0.001 \qquad \text{D.7}$$

where r_n is the the ratio of the updated stress increment in D.6 to the approximate one in D.3.

(xix) Repeat (xiii) to (xviii) for all bundles.

(xx) If (xviii) is not satisfied for all fibre bundles, calculate $\bar{M}^n(t)$ by

$$\bar{M}^n(t) = \left[d\overset{*}{\bar{\sigma}}^n(t) + \left[\frac{2C^n}{(h^n)^2} \frac{\partial D^n}{\partial T^n} dT^n\right]_t \bar{\epsilon}^n(t)\right]$$

for all fibre bundles using the updated value of $d\bar{\sigma}^{n*}(t)$ calculated in (xvii). Repeat (v) to (xx) (skipping (xi) and (xii)) until (xviii) is satisfied for all fibre bundles.

(xxi) Calculate the actual stress $\sigma_{ij}(t)$ at time t by 6.3.56.

(xxii) For each fibre bundle increment the state variables F^n and h^n by C.2 and C.3.

(xxiii) Increment the total strain ϵ_{ij} and total instantaneous stiffness modulus S^T_{ijkm} by C.4 and C.5.

(xxiv) Repeat (i) to (xxiii) for the next increment of time dt.

APPENDIX E

A SYSTEM OF TWO FIBRE BUNDLES IN SERIES –TOTAL DEFORMATION ALWAYS PRESCRIBED

The procedure described in this appendix describes the analysis steps followed to evaluate the response of a system of two fibre bundles in series when the total deformation of the assembly is prescribed at all times.

For all times $\tau \leq t$, the values of the instantaneous loading function $F^n(\tau)$, the damage parameter $h^n(\tau)$, strain $\epsilon_n(\tau)$, and the instantaneous stiffness $S^n(\tau)$ for both bundles (n=1, 2) are known. For the calculation of the response in the next increment of time dt associated with $du_2(t)$, analysis proceeds as follows.

(i) Calculate $\int_0^{t-dt}$ by 6.3.69.

(ii) For both bundles assume that $dT^n(t)=0$ and $T^n(t)= T^n(t-dt)$.

(iii) If $F^n(t) < 0$ allocate $C^n(t) = 0$,

If $F^n(t) = 0$ allocate $C^n(t) = 1$.

(iv) Calculate $M^n(t)$ using 6.3.53 and 6.3.35.

(v) Repeat (iii) and (iv) for both bundles.

(vi) Calculate $d\epsilon_1(t)$ and $d\epsilon_2(t)$ by solving the equation

$$M^1(t)d\epsilon_1(t) - M^2(t)d\epsilon_2(t) = \int_0^{t-dt} + \sum_{n=1}^{2} \left[\frac{2C^n}{(h^n)^2}\frac{\partial D^n}{\partial T^n} dT^n \epsilon_n\right]_t \qquad \text{E.1}$$

simultaneously with 6.3.66. It should be noted that E.1 is formulated by substituting 6.3.54 in 6.3.69.

(vii) Calculate the new values of $T^1(t)$ and $T^2(t)$ using 6.3.18 and 6.3.19.

(viii) Calculate the new values $dT^1(t)$ and $dT^2(t)$ using 6.3.28.

(ix) For each bundle check that

$$\left|r_n - 1.0\right| \leq 0.001 \qquad \text{E.2}$$

where r_n is the ratio of the new value of $T^n(t)$ to the old value. If this check fails, use the new values of $T^n(t)$ and $dT^n(t)$ and repeat (iii) to (ix).

(x) Check the validity of the allocated value of $C^n(t)$ by ensuring that if $C^n(t) = 1$, then $d\epsilon_n(t)$ is greater than zero. If this is satisfied, then the allocation in (iii) was justified. Otherwise, reallocate $C^n(t) = 0$.

(xi) Repeat (x) for both fibre bundles.

(xii) If reallocation of $C^n(t)$ was performed for any bundle then repeat (ii) to (xii) using new allocated values of $C^n(t)$.

(xiii) For each fibre bundle find $dF^n(t)$ and $dh^n(t)$ using 6.3.25, 6.3.26, and 6.3.27.

(xiv) Calculate $dD^n(t)$ using 6.3.22 for both bundles.

(xv) Calculate $dS^n(t)$ using 6.3.51 for both bundles.

(xvi) For each bundle calculate the approximate value of $d\overset{*}{\sigma}^n(t)$ by 6.3.54 using the value of $M^n(t)$ last calculated.

(xvii) For each fibre calculate the exact value of $d\overset{*}{\sigma}^n(t)$ by using

$$d\overset{*}{\sigma}^n(t) = \left[S^n(t) + dS^n(t)\right]\left[\epsilon_n(t) + d\epsilon_n(t)\right] - S^n(t)\,\epsilon_n(t) \qquad \text{E.3}$$

(xviii) Check convergence by ensuring that

$$\left|r_n - 1.0\right| \leq 0.001 \qquad \text{E.4}$$

where r_n is the the ratio of the approximate value of the instantaneous stress increment (in xvi) to the exact value (in xvii).

(xix) Repeat (xviii) for both fibre bundles.

(xx) If E.4 is not satisfied for both fibre bundles then update the values of $M^n(t)$ by using 6.3.54 with the updated value of $d\overset{*}{\sigma}^n(\tau)$ calculated in (xvii). Hence,

$$M^n(t) = \left[d\overset{*}{\sigma}^n(t) + \left[\frac{2C^n}{(h^n)^2}\,\epsilon_n\,\frac{\partial D^n}{\partial T^n}\,dT^n\right]_t\right] / d\epsilon_n(t) \qquad \text{E.5}$$

Repeat (vi) to (xx) until (xviii) is satisfied for both bundles.

(xxi) Increment $F^n(t)$, $h^n(t)$, $\epsilon_n(t)$, and $S^n(t)$ by

$$\begin{aligned} F^n(t + dt) &= F^n(t) + dF^n(t) \\ h^n(t + dt) &= h^n(t) + dh^n(t) \\ S^n(t + dt) &= S^n(t) + dS^n(t) \\ \epsilon_n(t + dt) &= \epsilon_n(t) + d\epsilon_n(t) \end{aligned} \qquad \text{E.6}$$

(xxii) Calculate the total stress in the assembly by 6.3.67.

(xxiii) Calculate the total strain in the assembly by

$$\epsilon^T(t + dt) = \frac{u_2(t) + du_2(t)}{L_1 + L_2} \qquad \text{E.7}$$

(xxiv) Repeat (i) to (xxiii) for the next increment of time.

APPENDIX F

A SYSTEM OF TWO FIBRE BUNDLES IN SERIES –TOTAL DEFORMATION PRESCRIBED UP TO TIME t_c

For a system of two fibre bundles in series when, after a time t_c, stress is held constant across the assembly, the analysis procedure follows a different path than that prescribed in Appendix E.

For all times $\tau \leq t$, the values of the instantaneous loading function $F^n(\tau)$, the damage parameter $h^n(\tau)$, strain $\epsilon_n(\tau)$, and the instantaneous stiffness $S^n(\tau)$ for both bundles (n=1, 2) are known. For all times less that t_c the analysis procedure is the same as that given in Appendix E. For all times $t>t_c$ analysis proceeds as follows.

(i) For each bundle assume $dT^n(t) = 0$ and $T^n(t) = T^n(t-dt)$.

(ii) Calculate $d\overset{*}{\sigma}_1(t)$ and $d\overset{*}{\sigma}_2(t)$ by 6.3.70 and 6.3.71.

(iii) Allocate $C^n(t) = 0$ if $F^n(t) < 0$

and $C^n(t) = 1$ if $F^n(t) = 1$.

(iv) Calculate $M^n(t)$ using 6.3.53 and 6.3.35.

(v) Repeat (iii) and (iv) for both bundles.

(vi) Calculate $d\epsilon_n(t)$ by

$$d\epsilon_n(t) = \left[d\overset{*}{\sigma}_n(t) + \left[\frac{2C^n}{(h^n)^2} \epsilon_n \frac{\partial D^n}{\partial T^n} dT^n \right]_t \right] / M^n(t) \qquad \text{F.1}$$

(vii) Repeat vi for both bundles.

(viii) Calculate the new value of $T^n(t)$ and $dT^n(t)$, using 6.3.18, 6.3.19, and 6.3.28, for both bundles.

(ix) Check that

$$|r_n - 1| \leq 0.001 \qquad \text{F.2}$$

where r_n is the ratio of the new value of $T^n(\tau)$ to the old value.

(x) Repeat (ix) for both bundles.

(xi) If (ix) is not satisfied for both bundles repeat (iii) to (x) with the new values of $T^n(t)$ and $dT^n(t)$ for both bundles.

(xii) If $d\epsilon_n(t) > 0$ and $C^n(t) = 1$ then the allocation in (iii) is justified. Otherwise, allocate $C^n(t) = 0$. Repeat for both bundles.

(xiii) If allocation of $C^n(t)$ is not justified, repeat (iii) to (xii) with the new allocated values of $C^n(t)$ until all allocations are justified.

(xiv) For each bundle calculate $dF^n(t)$, $dh^n(t)$, $dD^n(t)$, and $dS^n(t)$ using 6.3.25, 6.3.26, 6.3.27, 6.3.22,and 6.3.51.

(xv) Update the values of $d\epsilon_n(t)$ to

$$d\epsilon_n(t) = \left[d\overset{*}{\sigma}_n(t) - dS^n(t)\,\epsilon_n(t)\right] / \left[S^n(t) + dS^n(t)\right] \qquad \text{F.3}$$

(xvi) For each bundle calculate r_n the ratio of the new value of $\epsilon_n(t)$ to the old value. Convergence is tested by

$$|r_n - 1| \leq 0.001 \qquad \text{F.4}$$

(xvii) If F.4 is not satisfied for both bundles then do steps (xviii) to (xix). Otherwise do steps (xx) onward.

(xviii) Calculate $T^n(t)$ and $dT^n(\tau)$ using the new values of $d\epsilon_n(t)$ 6.3.18, 6.3.19, 6.3.28. Repeat for both fibre bundles.

(xix) Repeat (xiv) to (xvi) until F.4 is satisfied for both bundles.

(xx) Increment F^n, h^n, ϵ_n, $\overset{*}{\sigma}_n$ and S^n by

$$\begin{aligned} F^n(t+dt) &= F^n(t) + dF^n(t) \\ h^n(t+dt) &= h^n(t) + dh^n(t) \\ \epsilon_n(t+dt) &= \epsilon_n(t) + d\epsilon_n(t) \\ \overset{*}{\sigma}_n(t+dt) &= \overset{*}{\sigma}_n(t) + d\overset{*}{\sigma}_n(t) \\ S^n(t+dt) &= S^n(t) + dS^n(t) \end{aligned} \qquad \text{F.5}$$

with

$$d\overset{*}{\sigma}_n(t) = \left[S^n(t) + dS^n(t)\right]\left[\epsilon_n(t) + d\epsilon_n(t)\right] - S^n(t)\,\epsilon_n(t) \qquad \text{F.6}$$

(xxi) Calculate $du_2(t)$ bu 6.3.66 and increment u_2 by

$$u_2(t+dt) = u_2(t) + du_2(t) \qquad \text{F.7}$$

Calculate the total strain $\epsilon^T(t+dt)$ by

$$\epsilon^T(t+dt) = \frac{u_2(t+dt)}{L_1 + L_2} \qquad \text{F.8}$$

(xxii) Repeat (i) to (xxi) for next time increment.

REFERENCES

[1] **Dougill, J.W.,** "Some Remarks on Path Independence in the Small in Plasticity". Quarterly of Applied Mathematics, October 1975, pp 233–243.

[2] **Dougill, J.W.,** "On Stable Progressively Fracturing Solids". Journal of Applied Mathematics and Physics, ZAMP, Vol. 27, 1976, pp 423–437.

[3] **Burt, N.J. and Dougill, J.W.,** "Progressive Failure in a Model Heterogeneous Medium". Journal of the Engineering Mechanics Division, Proceeding of the American Society of Civil Engineers, Vol. 103, No. EM3, 1976, pp 365–376.

[4] **Dougill, J.W.,** "Path Dependence and a General Theory for the Progressively Fracturing Solids". Proceeding of the Royal Society, London, A390, 1983, pp 341–351.

[5] **Dougill, J.W.,** "Constitutive Relations for Concrete and Rock". Applications and Extensions of Elasticity and Plasticity Theory". William Prager Symposium on Mechanics of Geomaterials: Rocks, Concrete, Soils, September 11–15th 1983.

[6] **Dougill, J.W.,** "Structural and Continuum Aspects of Fracture in Brittle Matrix Composites". Paper for Euromech 204 Colloquium and Structure and Crack Propagation in Brittle Matrix Composite Materials, Warsaw, November 1985.

[7] **Swanson, S.R., and Christoforou, A.P.,** "Progressive Failure in Carbon/Epoxy Laminates Under Biaxial Stress". Transaction of the ASME, Vol 109, January 1987, pp 12–16.

[8] **Hahn, H.T., and Tsai, S.W.,** "On the Behaviour of Composite Laminates After Initial Failures". Journal of Composite Materials, Vol. 8, 1974, pp 288–305.

[9] **Labuz, J.F., Shah, S.P., and Dowding, C.H.,** "The Fracture Process Zone in Granite: Evidence and Effect". International Journal of Rock Mechanics and Mineral Sciences of Geomechanics, Abstract Vol. 24, No. 4, 1987, pp 235–246.

[10] **Bieniawski, Z.T., Denkhaus, H.G., and Vogler, U.W.,** "Failure of Fractured Rock". International Journal of Rock Mechanics and Mineral Sciences, Vol. 6, 1970, pp 323–346.

[11] **Yamatomi, J., and Kotake, Y.,** "Pillar Control and the Effects of Back–Filling Support at Kosaka Mine". International Journal of Rock Mechanics and Mineral Sciences of Geomechanics, Abstract Vol. 23, No. 1, 1986, pp 41–53.

[12] **Skempton, A.W.,** "Long Term Stability of Clay Slopes". Geotechnique, Vol 14, No. 2, 1964, pp 77–101.

[13] **Arey, D.W. and Wood, D.M.,** "An Evaluation of Direct Simple Shear Tests on Clay". Geotechnique, Vol. 37, No. 1, 1987, pp 25–35.

[14] **Jewell, R.A. and Wroth, C.P.,** "Direct Shear Tests on Reinforced Sand". Geotechnique, Vol. 37, No. 1, 1987, pp 53–68.

[15] **Scott, R.F.,** "Failure". Geotechnique, Vol. 37, No. 4, 1987, pp 423–466.

[16] **Hvorslev, Dr. M. Jull,** "Physical Properties of Remolded Cohesive Soils". U.S. Army Engineer Waterways Experiment Station, June 1969, pp 114–116.

[17] **Law, K.T.**, "A Servo System for Controlled Stress Path Tests". Laboratory Shear Strength of Soils. ASTM STP 740, R.N. Yong and F.C. Townsend Eds., 1981, pp 164–179.

[18] **Hughes, B.P. and Chapman, G.P.**, "The Deformation of Concrete and Microconcrete in Compression and Tension with Particular Reference to Aggregate Size". Magazine of Concrete Research, Vol. 18, 1966, pp 19–24.

[19] **Evans, R.H. and Marathe, M.S.**, "Microcracking and Stress Strain Curves for Concrete in Tension". Materials and Structures, No.1 , January–February 1968.

[20] **Spooner, D.C.**, "Progressive Damage and Energy Dissipation in Concrete in Uniaxial Compression". A Thesis Submitted to the University of London for the Degree of Doctor of Philosophy, 1974.

[21] **Spooner, D.C. and Dougill, J.W.**, "A Quantitative Assessment of Damage Sustained in Concrete During Compressive Loading". Magazine of Concrete Research, Vol. 27, No. 92, September 1975, pp 151–160.

[22] **Reinhardt, H.W. and Comelissen, H.A.W.**, "Post–Peak Cyclic Behaviour of Concrete in Uniaxial Tensile and Alternating Tensile and Compressive Loading". Cement and Concrete Research, Vol. 14, 1984, pp 263–270.

[23] **Gopalaratnam, V.S., and Shah, S.P.**, "Softening Response of Plain Concrete in Direct Tension". ACI Journal–Proceeding, Vol. 82, 1985, pp 310–323.

[24] **Attiogbe, E.K. and Darwin, D.**, "Strain Due to Sub–Microcracking in Cement Paste and Mortar". ACI Material Journal, Vol. 85, No. 1, 1988, pp 3–11.

[25] **Otter, D.E. and Naaman, H.E.**, "Properties of Steel Fiber Reinforced Concrete Under Cyclic Loading". ACI Material Journal, Vol. 85, No. 4, 1988, pp 254–261.

[26] **Raiss, M.E.**, "Observation of the Development of Fracture Process Zones in Concrete Under Tension". PhD Thesis, University of London, 1986, pp 369–370.

[27] **Maiu, G. and Huckel, T.**, "Non–Associated and Coupled Flow Rules of Elastoplasticity for Rock–Like Materials". International Journal of Rock Mechanics and Mineral Sciences of Geomechanics, Abstract Vol. 16, 1979, pp 77–92.

[28] **Drucker, D.C.**, "On the Postulate of Stability of Material in the Mechanics of Continua". Journal de Mecanique, Vol. 3, No. 2, June 1964.

[29] **Hill, R.**, "A General Theory of Uniqueness and Stability in Elastic–Plastic Solids". Journal of Mechanics and Physics of Solids, Vol. 6, 1985, pp 236–249.

[30] **Il'ushin, A.A.**, "On the Increments of Plastic Deformations and the Yield Surface". Applied Mathematics and Mechanics, Vol. 24, No. 4, 1960, pp 663–668.

[31] **Il'ushin, A.A.**, "On the Postulate of Plasticity". Applied Mathematics and Mechanics, Vol. 25, No. 3, 1961, pp 503–507.

[32] **Casey, J. and Naghdi, P.M.**, "Strain–Hardening Response of Elastic Plastic Materials". Mechanics of Engineering Materials, Edited by Desai and Gallagher, 1984, John Wiley and Sons Ltd, Chapter 4, pp 61–89.

[33] **Chen, W.F. and McCarron, W.O.**, "Modelling of Soils and Rocks Based on the Concepts of Plasticity". Recent Developments in Laboratory and Field Tests and Analysis of Geotechnical Problems, Bangkok, 1983.

[34] **Bazant, Z.P.,** "Instability, Ductility, and Size Effect in Strain–Softening Concrete". Journal of the EM Division, ASCE, Vol. 102, No. EM2, April 1976, pp 331–344.

[35] **Bazant, Z.P. and Panula L.,** "Statistical Stability Effects in Concrete Failure". Journal of the EM Division, ASCE, Vol. 104, No. EM5, October 1978, pp 1195–1212.

[36] **Schreyer, H.L.,** "One Dimensional Softening With Localization". Journal of Applied Mechanics, Transaction of the ASME, December 1986, Vol. 53, pp 791–797.

[37] **Torrenti, J.M.,** "Some Remarks Upon Concrete Softening". Materials and Structures, Vol. 19, No. 113, pp 391–394.

[38] **Ottosen, N.S.,** "Thermodynamic Consequences of Strain–Softening in Tension". Journal of Engineering Mechanics, ASCE, Vol. 112, No. 11, November 1986, pp 1152–1164.

[39] **Palmer, A.C., Maier, G., and Drucker, D.C..** "Normality relations and convexity of yield surfaces for unstable materials or structural elements". Journal of Applied Mechanics, ASME, Vol. 34, 1967, pp 464–470.

[40] **Wecharatana, M. and Shah, S.P.,** "Experimental Methods to Determine Fracture Parameter in Concrete". Technical Report, Technological Institute, Northwestern University, Evanston, Illinois, 1982.

[41] **Kachanov, L.M.,** "Time to Rupture Under Conditions of Creep" (in Russian). IZW, Ak. Nauk SSSr, Otd, Tekh Nark, Vol. 8, 1958, pp 26–31.

[42] **Krajcinovic, D. and Fonseka, G.U.,** "The Continuous Damage Theory of Brittle Materials, Part 1, General Theory". Journal of Applied Mechanics, Transactions of the ASME, Vol. 48, December 1981, pp 809–815.

[43] **Mazars, J.,** "Application de la Mechanique de L'endommagement au Comportement Non Linier et la Rapture du Buton de Structure". PhD Thesis (in French), L'universite Pierre et Marrie Currie, 1984.

[44] **Krajcinovic, D.,** "Distributed Damage Theory of Beams in Pure Bending", Journal of Applied Mechanics, Transaction of the ASME, Paper No. 79–WA/A PM–1, May 1978.

[45] **Fonseka, G.U. and Krajcinovic, D.,** "The Continuous Damage Theory of Brittle Materials, Part 2, Uniaxial and Plane Response Modes". Journal of Applied Mechanics, Transaction of the ASME, Vol. 48, December 1981, pp 816–824.

[46] **Krajcinovic, D. and Selvaraj, S.,** "Constitutive Equations for Concrete". Proceedings on the International Conference on the Constitutive Laws for Engineering Materials, Edited by C.S. Desai, R.H. Gullagher, Tueson, January 1983, pp 399–406.

[47] **Krajcinovic, D.,** "Constitutive Equation for Damaging Materials". Journal of Applied Mechanics, ASME, January 1982.

[48] **Hegencier, G.A., Read, H.E., Valanis, K.C. and Murakami, H.,** "Development of Advanced Constitutive Models for Plain and Reinforced Concrete". S–Cubed Report SSS–R–86–7914 (1986).

[49] **Dougill, J.W.,** "A Mathematical Model for the Failure of Cement Paste and

Mortars". Magazine of Concrete Research, Vol.19, No. 60, September 1967, pp 135–142.

[50] **Dougill, J.W.,** "Further Consideration of a Mathematical Model for Progressive Fracture of a Heterogeneous Material". Magazine of Concrete Research, Vol. 23, No. 74, March 1971, pp 5–10.

[51] **RIDA, M.,** "The Use of Linear Loading Functions in Progressive Fracture, Plasticity and Combined Behaviour". A Thesis Submitted to the University of London for the Degree of Doctor of Philosophy, King's College, June 1981.

[52] **Kormeling, H.A, Zielinski, A.J and Reinhardt, H.W.,** "Experiments on Concrete Under Single and Repeated Uniaxial Impact Tensile Loading". Stevin Report 5–80–3, Delft, 1980.

[53] **Zielinski, A.J. and Reinhardt, H.W.,** "Stress–Strain Behaviour of Concrete and Mortar at High Rates of Tensile Loading". Cement and Concrete Research. Vol. 12, 1982, pp 309–319.

[54] **Zielinski, A.J., Reinhardt, H.W. and Kormeling, H.A.**"Experiments on Concrete Under Uniaxial Impact Tensile Loading". Materials and Structures, Vol. 14, No. 80, 1981, pp 103–112.

[55] **Kormeling, H.A.,** "Experimental Results of Plain and Steel Fibre Reinforced Concrete Under Uniaxial Impact Tensile Loading". Stevin Report, No. 5–84–8, DELFT, 1984.

[56] **Zielinski, A.J.,** "Concrete Under Biaxial Loading: Static Compression, Impact Tension". Stevin Report 5–85–1, DELFT, 1985.

[57] **Evans, R.H.,** "Effect of Loading on the Mechanical Properties of Some Materials". Journal of the Institute of Civil Engineering, Vol. 18, 1942, pp 296–306.

[58] **Watstein, D.,** "Effect of Straining Rate on the Compressive Strength and Elastic Properties of Concrete". Journal of the American Concrete Institute, Vol. 24, No. 8, April 1953, pp 729–744.

[59] **Atchley, B.L. and Furi, H.L.,** "Strength and Energy Absorption Capabilities of Plain Concrete Under Dynamic and Static Loading". Journal of ACI, Vol. 164, November 1967, pp 745–756.

[60] **Hughes, B.P. and Gregory, R.,** "Concrete Subjected to High Rates of Loading in Compression". Magazine of Concrete Research, Vol. 24, No. 78, March 1972, pp 25–36.

[61] **Sparks, P.R. and Menzies, J.B.,** "The Effect of Loading Upon the Static and Fatigue Strengths of Plain Concrete in Compression". Magazine of Concrete Research, Vol. 25, No. 83, June 1973, pp 73–80.

[62] **Kaplan, A.S.,** "Factors Affecting the Relationship Between Rate of Loading and Measured Compressive Strength of Concrete". Magazine of Concrete Research, Vol. 32, No. 111, June 1980, pp 79–88.

[63] **Dilger, W.H., Koch, R. and Kowalczyk, R.,** "Ductility of Plain Concrete and Confined Concrete Under Different Strain Rates". ACI Journal, January–February 1984, pp 73–81.

[64] **Scott, Park, Priestly,** "Stress–Strain Behaviour of Concrete Confined by Overlapping Hoops at Low and High Strain Rates". ACI Journal, Vol. 79, pp

13–27.

[65] **Bischuff, P.H.**, "Compressive Response of Concrete to Hard Impact". A PhD Thesis, Imperial College, University of London, April 1988.

[66] **Mainstone, R.J.**, "Properties of Materials at High Rates of Straining or Loading". Materials and Structures, Vol. 8, No. 44, March–April 1975.

[67] **Zielinski, A.J.**, "Concrete Structures Under Impact Loading, Rate Effects". Stevin Report 5–84–14, DELFT, December 1984.

[68] **Sauris, W. and Shah, S.P.**, "A Strain Rate Dependent Damage Model for Concrete". ASCE–EMD Specialty Conference, Purdue University, May 1983.

[69] **Hughes, B.P. and Watson, A.J.**, "Compressive Strength and Ultimate Strain of Concrete Under Impact Loading". Magazine of Concrete Research, Vol. 30, No. 105, December 1978, pp 189–197.

[70] **Ahmad, S.H. and Shah, S.P.**, "Behaviour of Hoop Confined Concrete Under High Strain Rates". ACI Journal, September–October 1985, pp 634–647.

[71] **Suaris, W. and Shah, S.P.**, "Properties of Concrete Subjected to Impact". Journal of Structural Engineering, ASCE, Vol. 109, No. 7, July 1983, pp 1727–1741.

[72] **Suaris, W. and Shah, S.P.**, "Strain Rate Effects in Fibre–Reinforced Concrete Subjected to Impact and Impulsive Loading". Composites, April 1982, pp 153–159.

[73] **Shah, S.P., Fafitis, A. and Arnold, R.**, "Cyclic Loading of Spirally Reinforced Concrete". Journal of Structural Engineering, ASCE, Vol. 109, No. 7, July 1983, pp 1695–1710.

[74] **Bieniawski, Z.T.**, "Time–Dependent Behaviour of Fractured Rock". Rock Mechanics, Vol. 2, 1970, pp 123–137.

[75] **Rogers, C.O., Pany, S.S., Kumano, A. and Goldsmill, W.**, "Response of Dry and Liquid Filled Porous Rocks to Static and Dynamic Loading by Variously–Shaped Projectiles". Rock Mechanics and Rock Engineering, Vol. 19, 1986, pp 235–260.

[76] **Graham, J., Crooks, J.H.A. and Bell, A.L.**, "Time Effects on the Stress–Strain Behaviour of Natural Soft Clays". Geotechnique, Vol. 33, No. 3, 1983, pp 327–340.

[77] **Schmertmann, J.H., Brand, E.W., Mesri, G., Choi, Y.K., Graham, J., Crooks, J.J.A. and Bell, A.L.**, "Time Effects on the Stress–Strain Behaviour of Natural Soft Clays". Geotechnique, Vol. 34, 1983, pp 433–444.

[78] **Leroueil, S., Kabbaj, M., Tavenas, F. and Bouchard, R.**, "Stress–Strain–Strain Rate Relation for the Compressibility of Sensitive Natural Clays". Geotechnique, Vol. 135, No. 2, 1984, pp 159–180.

[79] **Atkinson, J.H. and Richardson, D.**, "The Effect of Local Drainage in Shear Zones on the Undrained Strength of Overconsolidated Clays". Geotechnique, Vol. 137, No. 3, 1986, pp 393–404.

[80] **Feldman, R.F.**, "Mechanism of Creep of Hydrated Portland Cement Paste". Cement and Concrete Research, Vol. 2, 1972, pp 521–540.

[81] **Hannant, D.J.**, "The Mechanism of Creep in Concrete". Materials and Structures, Vol. 1, No. 5, 1968, pp 403–411.

[82] **Illston, J.M. and Jordaan, I.J.**, "Three–Dimensional Creep Measurements in Young Concrete". Materials and Structures, Vol. 4, No. 24, 1971, pp 371–377.

[83] **Bazant, Z.P., Asghari, A.A. and Schmidt, J.**, "Experimental Study of Creep of Hardened Portland Cement Paste at Variable Water Content". Materials and Structures, Vol. 9, No. 52, 1976, pp 279–290.

[84] **Brown, N.H.**, "The Creep of Hydrated Cement Paste". Cement and Concrete Research, Vol. 6, 1976, pp 475–486.

[85] **Mangat, P.S. and Azari, M.M.**, "Compression Creep Behaviour of Steel Fibre Reinforced Cement Composites". Materials and Structures, Vol. 19, No. 113, 1986, pp 361–369.

[86] **Smadi, M.M., Slate, F.O. and Nilson, A.H.**, "Shrinkage and Creep of High, Medium, and Low Strength Concretes, Including Overloads". ACI Material Journal, May–June 1987, pp 224–234.

[87] **Ward, M.A. and Cook D.J.**, "The Mechanism of Tensile Creep in Concrete". Magazine of Concrete Research, Vol. 21, No. 68, September 1969, pp 151–158.

[88] **Domone, P.L.**, "Uniaxial Tensile Creep and Failure of Concrete". Magazine of Concrete Research, Vol. 26, No. 88, September 1974, pp 144–152.

[89] **Al–Kubaisy, M.A. and Young, A.G.**, "Failure of Concrete Under Sustained Tension". Magazine of Concrete Research, Vol. 27, No. 92, September 1975, pp 171–178.

[90] **Christiansen, K.**, "Eight–Year Deformation Tests on Reinforced Concrete Beams". Materials and Structures, Vol. 21, 1988, pp 172–178.

[91] **Neville, A.M.**, "Properties of Concrete". Longman Scientific and Technical, pp 395–425.

[92] **Illston, J.M.**, "Creep of Concrete". Creep of Engineering Materials, A Journal of Strain Analysis Monogram, Edited by C.D. Pomeroy, Mechanical Engineering Publications Limited, London, 1987, pp 47–66.

[93] **Taylor, M.A. and Mauru, G.C.**, "Short Term Stress Relaxation of Concrete". Magazine of Concrete Research, Vol. 25, No. 84, September 1973, pp 123–135.

[94] **Pirtz, D., Thomas, K. and Monteiro, P.J.M.**, "Stress Relaxation: Comparison of Measured and Computed Values". ACI Journal, May–June 1986, pp 432–437.

[95] **Chosh, R.S. and Timusk, J.**, "Effect of Sustained Loading at Early Ages on the Modulus of Elasticity of Cement Paste". Materials and Structures, Vol. 7, No. 41, 1974, pp 335–339.

[96] **Cook, D.J. and Chindaprasirt, K.**, "Influence of Loading History Upon the Compressive Properties of Concrete". Magazine of Concrete Research, Vol. 132, No. 11, June 1980, pp 89–100.

[97] **Cook, D.J. and Chindaprasirt, K.**, "Influence of Loading History Upon the Tensile Properties of Concrete". Magazine of Concrete Research, Vol. 133, No. 116, September 1981, pp 154–160.

[98] **Pomeroy, C.D.**, "Time–Dependent Deformation of Rocks". Creep of Engineering Materials, A Journal of Strain Analysis Monograph, Edited by C.D. Pomeroy, Mechanical Engineering Publications, London, 1978, pp 1–10.

[99] **Park, D.W. and Juny, J.O.**, "Application of Holographic Interferometry to the Study of Time–Dependent Behavior of Rock and Coal". Rock Mechanics and Rock Engineering, Vol. 21, 1988, pp 259–270, 1988.

[100] **Mesri, G., Febres–Cordeg, E. and Shieldo, D.R.**, "Shear Stress–Strain–Time Behaviour of Clays". Geotechnique, Vol. 31, No. 4, 1981, pp 537–552.

[101] **Soroushian, P., Choi, K–B. and Alhamad, A.**, "Dynamic Constitutive Behaviour of Concrete". ACI Journal, March/April 1986, pp 251–259.

[102] **Mihashi, H. and Izumi, M.**, "A Stochastic Theory for Concrete Fracture". Cement and Concrete Research, Vol. 7, No. 4, 1977, pp 411–422.

[103] **Bazant, Z.P. and Oh, B.H.**, "Strain–Rate Effect in Rapid Triaxial Loading of Concrete". Proc, of the ASCE, Journal of EM division, Vol. 108, No. EM5, October 1982, pp 764–782.

[104] **Bazant, Z.P. and Osman,E.**, "Double Power Law for Basic Creep of Concrete". Materials and Structures, Vol. 9, No. 49, 1976, pp 3–11.

[105] **Bazant, Z.P., Osman, E. and Thonguthai, W.**, "Practical Formulation of Shrinkage and Creep of Concrete". Materials and Structures, Vol. 9, No. 54, 1976, pp 395–406.

[106] **Bazant, Z.P. and Panula, L.**, "Practical Prediction of Time–Dependent Deformation of Concrete". Materials and Structures, Vol. 11, No. 65, 1978, pp 307–328.

[107] **Bazant, Z.P. and Chan, J.C.**, "Double–Power Logarithmic Law for Concrete Creep". Cement and Concrete Research, Vol. 14, 1984, pp 793–806.

[108] **Bazant, Z.P.**, "Numerical Determination of Long–Range Stress History From Strain History in Concrete". Materials and Structures, Vol. 5, No. 27, 1972, pp 135–141.

[109] **Zielinski, A.J.**, "Model for Tensile Fracture of Concrete at High Rates of Loading". Cement and Concrete Research, Vol. 14, 1984, pp 215–224.

[110] **Ishai, O.**, "The Time–Dependent Deformational Behaviour of Cement Paste, Mortar and Concrete". International Conference on the Structure of Concrete, Imperial College, London, September 1965, pp 345–364.

[111] **Beretz, W.**, "A Hypothesis for the Creep of Hardened Cement Paste and the Influence of Simultaneous Shrinkage". International Conference on the Structure of Concrete, Imperial College, London, September 1965, pp 365–387.

[112] **Rossi, P. and Acker, P.**, "A New Approach to the Basic Creep and Relaxation of Concrete". Cement and Concrete Research, Vol. 18, 1988, pp 799–803.

[113] **Hallesland, J.**, "A Stress and Time Independent Strength Law for Concrete". Cement and Concrete Research, Vol. 2, 1972, pp 261–275.

[114] **Gurtin, M.E. and Sternberg, E.**, "On the Linear Theory of Viscoelasticity". Technical Report No. 6, Contract Nonr 562(30), Brown University, June 1962.

[115] **Drucker, D.C.,** "A Definition of Stable Inelastic Material". Journal of Applied Mechanics, ASME, March 1959, pp 101–106.

[116] **Valanis, K.C.,** "A Theory of Viscoplasticity Without a Yield Surface". Archives of Mechanics, Vol. 23, 1971, pp 517–551.

[117] **Valanis, K.C., and Read, H.E.,** "Endochronic Plasticity : Physical Basis and Applications". Mechanics of Engineering Materials, John Willey and Sons Chapter 30, edited by C.S. Desai and K.H. Gallagher, 1984.

[118] **Valanis, K.C., and Read, H.E.,** " An Endochronic Plasticity Theory for Concrete". International Journal of Mechanics of Materials, 1986.

[119] **Sauris, W. and Shah, S.P.,** "A Constitutive Model for Concrete Under Dynamic Loading". A Progress Report, SMIRT7 Conference, Chicago, August 1983.

[120] **Naghdi, P.M. and Murch, S.A.,**"On the Mechanical Behaviour of Viscoelastic/Plastic Solids". Journal of Applied Mechanics, September 1963, pp 321–328.

[121] **Perzyna, P.,** "Fundamental Problems in Viscoplasticity". Advances in Applied Mechanics, Vol. 9, 1966, pp 243–377.

[122] **Zienkiewicz, O.C. and Cormear, I.C.,** "Viscoplasticity–Plasticity and Creep in Elastic Solids– A Unified Numerical Solution Approach". International Journal for Numerical Methods in Engineering, Vol. 8, 1974, pp 821–845.

[123] **Baladi, G.Y. and Rohani, B.,** "Development of an Elastic Viscoplastic Constitutive Relationship for Earth Materials". Chapter 2, Mechanics of Engineering Materials. Edited by C.S. Desai and R.H. Gallagher, 1984.

[124] **Bicanic, N. and Zienkiewicz, O.C.,** "Constitutive Model for Concrete Under Dynamic Loading". Earthquake Engineering and Structural Dynamics, Vol. 11, 1984, pp 689–710.

[125] **Browning, R.V., Gurtin, M.E. and Williams, W.O.,** "A Viscoplastic Constitutive Theory for Filled Polymers". Los Almos National Laboratory, Report No. LA–UR–83–457, Submitted to the International Journal of Solids and Structures, 1983.

[126] **Burt, N.J.,** "Progressive Failure in a Model Heterogeneous Material". A Thesis Submitted to the University of London for the Degree of Dr. of Philosophy, 1975.

[127] **Wittman, F.H., and Knappe, O.W.,** "Temperature Induced Stresses in Concrete". Cement and Concrete Research, Vol. 8, 1978, pp 703–710.

[128] **Prager, W.,** "Non–Isothermal Plastic Deformations". Proceeding of the Konnikle Nederl Akad Van Wetenschappen, Series B, Vol. 61, No. 3, 1958, pp 176–182.

[129a] **Williams, J.G.,** "Fracture Mechanics of Polymers". Ellis Horwood Limited, 1987.

[130] **Sanders, J.L.,** "Plastic Stress Strain Relations Based on Infinitely Many Plane Loading Surfaces". Proc. of the 2nd U.S. National Congress for Applied Mechanics, An Arbor, Michigan, 1954, pp 455–460.

[131] **Bazant, Z.P., and Kim, S.S.**, "Plastic–Fracturing Theory for Concrete". Journal of the EMD, Proceeding of the American Society of Civil Engineers, Vol 105, No EMZ, June 1979, pp 407–428.

[132] **Zienkiewicz, O.C., Najak, G.C., Owen, D.R.J.** " Composite and Overlay Models in Numerical Analysis of Elasto–Plastic Continua". Proceedings Int. Symposium on Foundations of Plasticity, Warsaw, Edited by Sawczuk, Noordhoff, and Groningen, August 30–Sept. 2, 1972, pp 107–132.

[133] **Resende, L. and Martin, J.B.**, "A progressive Damage Continuum Model for Granular Materials". Computer Methods in Applied Mechanics and Engineering, Vol. 42, 1984, pp 1–18.

[134] **Needleman, A. and Tvegaard, V.**, "Limits to Formability in Rate–Sensitive Metal Sheets". Mechanical Behaviour of Materials IV, Edited by J. Carlsson and N.G. Ohlsow, Pergamon Press, Oxford, 1984, pp 51–65.

[135] **Pan, J., Sage, M., Needleman, A.**, " Localization of Deformation in Rate Sensitive Porous Plastic Solids". Int. Journal of Fracture, Vol. 21, 1983, pp 261–278.